Quantum Theory of Multimode Exciton-Polariton Bose-Einstein Condensation

David Racine

School of Physics

Trinity College Dublin

A thesis submitted for the degree of

Doctor of Philosophy

December 2013

Declaration of originality

I, David Racine, hereby declare that this dissertation has not been submitted as an exercise for a degree at this or any other University.

It comprises work performed entirely by myself during the course of my Ph.D. studies at Trinity College Dublin.

A copy of this thesis may be lended or copied by the Trinity College Library upon request by a third party provided it spans single copies made for study purposes only, subject to normal conditions of acknowledgement.

_____

David Racine
December, 2013

Part of this dissertation has been submitted for publication as follows:

D. Racine , P. R. Eastham, "Quantum theory of multimode polariton condensation". *Submitted to Phys. Rev. B.*, Preprint arXiv:1310.3641, 2013

Abstract

This thesis studies Bose-Einstein condensation (BEC) of microcavity exciton-polaritons. BEC is a quantum phase transition, whereby a system spontaneously develops coherence, allowing quantum mechanical effects to be visible on macroscopic scales. Excitons are the bound states of an electron and a hole in a semiconductor. Microcavity polaritons are quasiparticle arising from the strong coupling of excitons to radiation modes confined in a microcavity – a cavity on the scale of the wavelength of light.

Microcavity polaritons decay into external photons, typically in a few picoseconds. Thus, the polariton condensate is a nonequilibrium steady state, maintained by a balance between radiative decay and external pumping. One consequence of this nonequilibrium nature is that, whereas in equilibrium only the lowest energy single-particle state can be macroscopically occupied, for polaritons large occupations can build up in other orbitals. Furthermore, the condensation can occur in several orbitals simultaneously, enabling the study of interacting macroscopic quantum states.

In this thesis, we build a theory for the dynamics of the density matrix describing a multimode polariton condensate. We develop the theory of saturable pumping which we supplement with standard open quantum system decay. Our theory also includes resonant polariton-polariton interactions within the condensate modes. Our generic few-parameter model for the system leads to a Lindblad equation which we use to obtain the steady-state population distributions, and the time-dependent first and second-order coherence functions, in such a multimode condensate. We solve the population distribution detailed balance forms either directly or with approximate analytical solutions. The first-order coherence functions are obtained either directly, with numericals, or with an approximate linearized Fokker-Planck approach and a simpler static limit expression. Among the second-order coherence functions, we consider the dephasing in the intensity oscillations caused by beating between the emission from different condensate modes. Such oscillations are a form of Josephson oscillations.

As a specific application, we consider a polaritonic Josephson junction, formed from a double-well potential, in the Rabi regime. We obtain the population distributions, emission lineshapes and widths (first-order coherence functions) and predict the dephasing time of the Josephson oscillations. Our theory predicts new multimode effects in the linewidth which are due to cross-correlations in the fluctuations of the population distribution.

Acknowledgments

My first thanks go to my supervisor Prof. Paul R. Eastham for having instilled in me an enormous amount of physics knowledge through our numerous and animated discussions. I would also like to acknowledge Prof. Rajendra P. Bajpai for his continuous support and encouragement throughout the years. This thesis would not have been possible without the support of Prof. John F. Donegan, a good man.

Around me, this difficult time in Dublin, was made easier by a few people. Dr Nadjib Baadji, Dr Neal Lemon, Dr Marian Tsanov and Dr Andrey Turchinovich were among them.

I would also like to thank Sonia Durand-Parfait for her support and encouragement and my family back in Québec.

Contents

List of Figures

List of Symbols

$\alpha_{1,2}$	Normalized coupling strength, one reservoir, two modes.
α_{ij}	Normalized coupling strength of reservoir i to mode j.
$\beta_{o,1}$	Reduced coupling strength notation, $\beta_j = \alpha_{ii+j}$.
$g^{(1)}(\tau)$	First-order coherence function.
$g_s^{(1)}(\tau)$	First-order coherence function in the static limit.
γ	Condensate common decay parameter.
$g^J(\tau)$	Coherence decay function of Josephson oscillations.
$g_s^J(\tau)$	Coherence decay function of Josephson oscillations in the static limit.
H	Condensate Hamiltonian (in Ch. 2-6).
η	Condensate intermode interaction strength.
κ	Condensate mode self-interaction strength.
$k_\parallel$	In-plane wavevector component of the light exiting a microcavity.
$\mathcal{L}_d$	Decay superoperator.
$\mathcal{L}_p$	Pumping superoperator.
n_c	Pumping strength, one reservoir.
n_i^c	Pumping strength, multiple reservoirs.
n_s	Saturation parameter, one reservoir.
n_i^s	Saturation parameter, multiple reservoirs.
P_{np}	Population distribution of a two-mode condensate.
$P_{(n,p)}$	Population distribution of a two-mode condensate, with n, p continuous.
$P_{n_1 n_2 ..}$	Population distribution of a multimode condensate.

$P_{(n_1,n_2,..)}$	Population distribution of a multimode condensate, with n_i continuous.
ρ_{nmpq}	Matrix elements of the two-mode condensate density matrix where n, m (p, q) refer to the first (second) condensate.
$\rho^{m_1 m_2}_{n_1\ n_2}$	Matrix elements of the multimode condensate density matrix where n_i, m_i refer to the i^{th} condensate.
$t_c, (t_c)^J$	First-order and Josephson coherence decay times.
$\frac{t}{\Delta\epsilon}$	Control parameter in a double well tight-binding model, where t is the hopping between left and right wells and $\Delta\epsilon$ is the detuning between them.
u_{np}, u^J_{np}	Distributions used to calculate coherence decays, with two modes.
$u_{(n,p)}$	Distribution used to calculate first-order coherence decays, with two modes and n, p continuous.
$u_{n_1 n_2..}$	Distribution used to calculate first-order coherence decays, with many modes.
$u_{(n_1,n_2..)}$	Distribution used to calculate first-order coherence decays, with many modes and n_i continuous.

Chapter 1

Introduction

The pursuit and description [Alle38, Penr51] of macroscopic quantum phenomena has captured the interest of generations of physicists. Beyond the traditional models of superfluidity and Bose-Einstein condensation (BEC) in cold atomic gases, condensation in other, more subtle, quasiparticle systems [Mosk62, Demo06] presents a rich panel of theoretical challenges and phenomena. Among those are *microcavity polaritons*. These quasi-particles, first described by Hopfield [Hopf58] in the context of bulk semiconductors, are eigenstates of the light-crystal Hamiltonian, combining a mixture of photons and excitons – a bound state of an electron in the conduction band and a hole in the valence band, the quanta of excitation in semiconductors. Polaritons were made more readily observable and manipulable through the perfection of molecular beam epitaxy techniques leading to the observation by Weisbuch and co-workers [Weis92] of the splitting of two polariton modes for a two-dimensional quantum well inside a planar microcavity.

Microcavity polaritons, maintaining integral total spin from their two counterparts' bosonic origin, as well as inheriting a very low mass ($\sim 10^{-4} m_e$) from their photonic component, have arisen as a strong model for Bose-Einstein condensation. Although the textbook concept of BEC (Appendix A.1) had to be broadened to consider particles with lifetimes much shorter than their thermal relaxation time, the signature of a macroscopic occupancy of the lowest energy state ($k_{\|} \approx 0$) in the light escaping the cavity is now commonly recognized [Dang98, Love08] (Fig. 1.1).

The new condensate presents a critical temperature much higher than in the alkali atoms' condensate. It requires pumping and exhibits decay, and the large excitonic Bohr radius results in interparticle interactions playing an important role in the physics of polariton condensates. These three effects, pumping, decay, and interactions, have

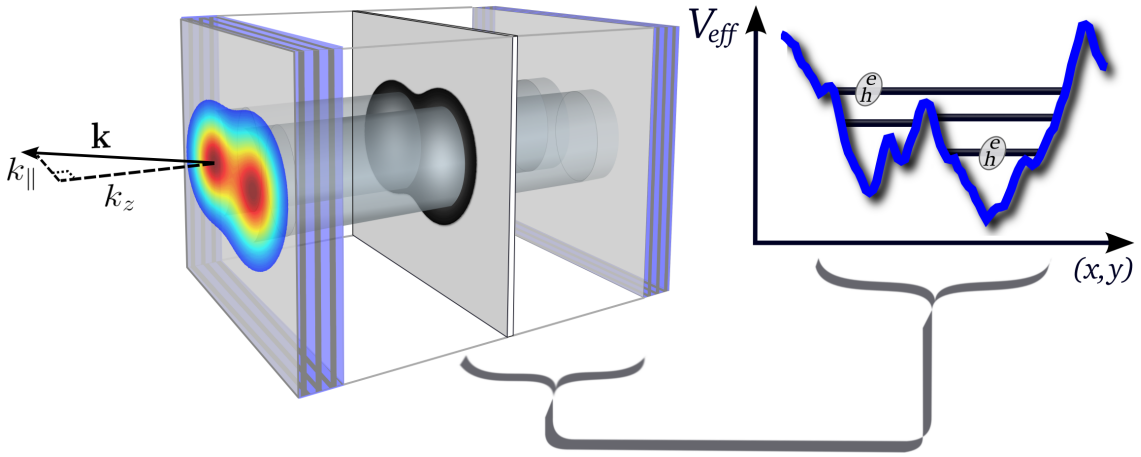

Figure 1.1: Schematic drawing of multimode microcavity polariton condensation. Excitons reside in a quantum well (the planar structure in the center), at the antinode of a light standing wave formed by two distributed Bragg mirrors (on both sides). Excitons and photons couple and hybridize to form light mass polaritons. These can condense, through stimulated scattering, into single particle orbitals formed by disorder in the cavity. The signature of condensation is seen though the intensity of the light exiting the cavity near normal incidence. The polariton condensate is a nonequilibrium steady-state, maintained by a balance between the radiative decay and the external pumping. Because of their nonequilibrium nature multimode condensates can occur (a two modes condensate is depicted here).

been used to make predictions of the linewidth of the coherent light emitted from the cavity[Porr 03, Whit 09]. This linewidth is predominantly caused by the fluctuations in the number of polaritons in the condensate which, through particle interactions, causes the energy of the line to fluctuate[Whit 09].

One further consequence of the nonequilibrium nature of polariton condensates is that, whereas in equilibrium only the lowest energy single-particle state can be macroscopically occupied, for polaritons large occupations can build up in other orbitals. Furthermore, the condensation can occur in several orbitals simultaneously, enabling the study of interacting macroscopic quantum states. The presence of several highly occupied states of a trapping potential can be seen directly in optical emission spectra[Tosi 12, Galb 12], and inferred from the presence of Josephson oscillations[Lago 10, Abba 13]. Such multimode condensation can also occur in spatially extended states, in particular in the Bloch states of one[Lai 07] and two[Masu 12] dimensional lattices. The in-plane potentials that control these condensates can arise from growth induced disorder in the Bragg mirrors[Lang 99, Love 08, Lago 10] , metal-film patterning of the mirror surfaces[Lai 07, Masu 12], and interaction effects[Tosi 12], as well as from the use of non-planar structures such as micropillars and photonic molecules[Galb 12].

The theoretical modeling of these nonequilibrium condensates has been performed

quite extensively within the mean-field approximation, using an augmented Gross-Pitaevskii description[Wout 07, Keel 08, East 08, Rodr 13] to treat the dynamics of the highly occupied orbitals, and to obtain the excitation spectra. Mean field solutions of microscopic models using the nonequilibrium Green's function formalism[Szym 07] have also been developed. The Langevin[Tass 00, Haug 12, Wout 09], Fokker-Planck[Whit 09, Schw 10] and density matrix[Laus 04, Verg 06, Schw 08] frameworks have been used to derive the quantum statistics of the condensate, and hence the first and second-order coherence functions of the optical emission[Porr 03]. While mean field theories are already able to treat several highly occupied orbitals[East 08, Wout 08a], full quantum treatments of this regime have yet to be formulated.

In this thesis we develop a density matrix approach for multimode polariton condensates, in which several single-particle orbitals are driven by several reservoirs. This theory treats both quantum and nonequilibrium fluctuations, and allows photon statistics and emission spectra to be calculated. We first derive a Lindblad equation for two condensate modes (highly occupied orbitals) pumped by a single reservoir of higher energy particles, using a treatment similar to that of a two-mode laser[Sing 80], and then extend the result to treat several reservoirs pumping several condensates. This gives a generic model for the quantum dynamics of a nonequilibrium polariton condensate, with the complexity of the reservoirs captured in a few known parameters. We show how the theory can be used to obtain the population distribution of the condensate orbitals, both numerically and analytically. We also show how it may be used to calculate both first-order and second-order coherence functions. The first-order coherence function, $\langle a_1^\dagger(\tau)a_1\rangle$, is the Fourier transform of the emission spectrum from one condensate orbital. We obtain it in three different ways: (i) direct numerical solution of the Lindblad form, (ii) making a continuum approximation to obtain a soluble partial differential equation, related to the Fokker-Planck equation[Kamp 07, Whit 09], and (iii) a cruder static limit approximation, which neglects the dynamics of the populations, but is generally valid near threshold[Love 08, Whit 09]. Among higher order correlation functions we consider those of the form $\langle a_1^\dagger(\tau)a_2(\tau)a_2^\dagger a_1\rangle$, which relate to the dephasing in the intensity oscillations caused by beating between the emission from different condensate modes. Such oscillations are a form of Josephson oscillations, which have been observed experimentally[Lago 10, Abba 13]. We analyze their dephasing both numerically and in the static limit.

As a specific application of our theory, we study fluctuations in a polariton Josephson junction, formed in a double-well potential[Lago 10], using a tight-binding model in which each well is pumped by a corresponding reservoir. Diagonalizing the Hamilto-

nian leads to symmetric and antisymmetric orbitals when the wells are degenerate. We obtain the population distribution in these orbitals, calculate the emission lineshapes and widths, and predict the dephasing time of the Josephson oscillations in the quasi-linear, strong trapping regime. We predict large fluctuations in the populations when the wells are tuned to resonance, due to the presence of a soft density mode, and show how the emission is broadened by intermode and intramode interactions.

In the remainder of this chapter we cover the context and the essential background of microcavity polariton condensation. We then establish some of the theoretical base from which the thesis develops. Finally we draw links to other theoretical approaches which are being used to treat polariton condensation and we close the chapter by detailing the layout of the remainder of the thesis.

1.1 General Context and Essential Background

Here we cover the general relevance of this work and we review the subjects of quantum microcavities, microcavity polaritons, condensation in general and polariton condensation in particular. This will provide us with the context and essential background before starting to engage with the theory.

1.1.1 Relevance of the Work in this Thesis

This work on multimode polarition condensates registers within a broader context of studying and manipulating strongly correlated many-bodies. On a fundamental level, polariton condensation can be traced back to the first proposition for Bose-Einstein condensation of quasiparticles in the 1960's when Moskalenko proposed that excitons could occupy a much reduced phase space and launched the pursuit of exciton condensation at the experimental level [Mosk62]. The large effective mass of excitons has made this pursuit very difficult and to this day there is no clear demonstration of exciton condensation [Mosk00]. In the meantime, remarkable strides had been make with the trapping and cooling of atomic alkali species and the first Bose-Einstein condensate of cold atom was demonstrated in 1995, earning the 2001 Nobel prize to its discoverers [Kett08]. By then, the solid state physics community had turned to polaritons, due its much lower effective mass, to demonstrate BEC in solids. The first example of polariton condensation can arguably be dated back to the experiments performed by Dang et al in 1998, [Dang98, Keel07], although some prefer to point to a 2006 article in Nature [Kasp06] for

an early example of polariton condensation. During the early years of polariton condensation, researchers in the field had to measure up with colleagues working with cold atoms by demonstrating that they were indeed studying a macroscopic quantum phenomenon and the early literature is reminiscent of this desire of the community to cast itself within the realm of equilibrium physics[East 01, Kasp 06]. Now, the relevance of working far from equilibrium can be fully exploited. The polariton system also presents the advantage of being easily observable through the light exiting a microcavity whereas the measurement process destroys the cold atom condensate. The nonequilibrium nature of polariton condensates adds a whole new portfolio of dynamical phenomena[Caru 13], out of which the formation of multimode condensates occupies center stage. This work embraces fully the nonequilibrium nature of polariton condensation and builds upon it the first quantum theory of multimode polariton condensation.

From a practical point of view, polariton condensation experiments are conducted in the same quantum microcavities structure as vertical cavity surface emitting lasers (VCSEL); the later were first developped in the late 1970's and demonstrated at room temperature in 1988 [Koya88, Skol98]. It is therefore no surprise that the first idea which comes to mind when asked about applications for polariton condensation is a new source of coherent light. Indeed reports of room temperature polariton condensation are steadily appearing in the literature[Chri 07, Lu 12, Li 12] and it is probably safe to say that it won't be long before commercial products based on electrically pumped polariton condensates become available. The appeal for polariton condensation as a coherent light source is due to the fact that stimulated scattering occurs between higher energy polaritons and condensate polaritons instead of electrons recombining with holes and generating laser photons. Through this, lower thresholds can be achieved, enabling devices with lower power consumption. Another application for polariton condensates, this time within the umbrella of quantum information processing, is through the manipulation of the condensates. The fast switching properties of polaritons and their large nonlinear response makes them good candidates for the realization of many algorithms in quantum information science[Ball 13] and in particular continuous variable quantum computation[Brau 05]. Although the realizations which have been proposed so far for such computations involve the use of the upper and lower branches of the polariton dispersion[Liew 11, Demi 14], operations can also be envisaged by using multimode condensates. The work in the thesis can therefore become a useful tool for the development of such theories and applications.

Having discussed the general context of this work, we now continue with a review of underlying physics of polariton condensation.

1.1.2 Quantum Microcavities

Quantum microcavities provide the trapping of light and the control of its coupling with electronic transitions in matter[Vaha03, Kavo07]. They consist of a quantum confinement structure where the excitons reside, and of a cavity which traps light (Fig. 1.1). Of the different confinement methods available, the planar semiconductor microcavities around which our model is developed employ distributed Bragg reflectors (DBR). The matter component consists of quantum wells embedded in the region where the field intensity is the highest in the cavity.

Distributed Bragg reflectors are formed by multiple repeats of high, n_H, and low, n_L, refractive index layers, each of thickness $\lambda/4$, grown on either side of a cavity[Skol98]. The interference of reflected and refracted waves across the structure creates a spectral region where light is reflected across a range of frequencies, known as the stop band. This traps the light into standing wave modes inside the cavity. Appendix A.2 determines the position of the stop band and its reflectivity, $|r| = 1$, in semi-infinite DBRs. Thin, two-dimensional, smaller bandgap, regions are placed at the antinode of the cavity mode. They form the quantum wells where excitonic – Coulomb bound electron-hole states – excitations occur. The cavity resonance matches the energy of an exciton in the quantum wells.

There are two main types of semiconductors microcavities used in experiments. One is grown out of type III-V semiconductors, e.g. $Al_{0.13}Ga_{0.87}As/AlAs$ (n_H/n_L) mirrors, $In_{0.13}Ga_{0.87}As$ QWs and a GaAs cavity[Skol98]. The other uses II-VI semiconductors, e.g. $Cd_{0.75}Mn_{0.25}Te/Cd_{0.40}Mg_{0.60}Te$ (n_H/n_L) mirrors, CdTe QWs, $Cd_{0.80}Mn_{0.20}Te$ cavity and $Cd_{0.88}Zn_{0.12}Te$ substrate[Dang98]. Type II-VI cavities possess stronger exciton binding energy and therefore show a larger Rabi splitting than type III-V cavities (see Sec. 1.1.3). CdTe-based microcavities tend however to have higher lattice-mismatch stress which increases the occurrence of misfit dislocations and leads to higher photonic disorder[Lang02, Keel07]. Typically a large number of quantum wells ($\gtrsim 15$) are embedded in the cavity.

1.1.3 Microcavity Polaritons

Having seen how microcavities are made, we now seek a model description of the quasiparticles they harbour – polaritons. As a first step, we examine their two components separately – quantum well excitons and cavity photons. Then we bring in the coupling between them and derive the polariton dispersion relations. Finally we discuss the

transition from strong coupling to weak coupling regime by introducing phenomenologically the decay of polaritons. For simplicity, the formalism is developed for an infinitely extended uniform system, i.e. in the thermodynamic limit. We set $\hbar = 1$.

Exciton Component

Excitons are the lowest energy excited state of semiconductors. They consist of an electron in the conduction band bound to a hole in the valence band, and are created by optical excitation slightly below the bandgap energy. In deriving a field operator and dispersion relation for them, in the envelope approximation[Corz93], we use the following Hamiltonian, along with the electron and hole Bloch functions,

$$H = \underbrace{\frac{\mathbf{P}^2}{2M}}_{H_M} + \underbrace{\frac{\mathbf{p}^2}{2\mu} - \frac{e^2}{4\pi\epsilon_o\epsilon_r|\mathbb{r}|}}_{H_\mu}, \tag{1.1}$$

$$\frac{1}{\sqrt{V}} e^{i\mathbf{k_e}\cdot\mathbf{r_e}} u_{\mathbf{k_e}}(\mathbf{r_e}), \quad \frac{1}{\sqrt{V}} e^{-i\mathbf{k_h}\cdot\mathbf{r_h}} u^*_{\mathbf{k_h}}(\mathbf{r_h}), \tag{1.2}$$

and the bandgap energy, E_g. The presence and effect of all the other electrons and cores in the system is taken into the dielectric constant, ϵ_r, and the electron and hole effective masses, m_e, m_h. The excitonic envelope makes use of a canonical set of variables, and combinations of electron and hole effective masses[Gasi74],

$\mathbf{r'} = \frac{m_e\mathbf{r_e}+m_h\mathbf{r_h}}{m_e+m_h}$	center of mass	$\mathbb{r} = \mathbf{r_e} - \mathbf{r_h}$	relative distance
$M = m_e + m_h$	total mass	$\mu = \frac{m_e m_h}{m_e+m_h}$	reduced mass
$\mathbf{k} = \mathbf{k_e} + \mathbf{k_h}$	total momentum	$\mathbb{k} = \frac{m_h\mathbf{k_e}-m_e\mathbf{k_h}}{m_e+m_h}$	relative momentum
		$= \alpha_h\mathbf{k_e} - \alpha_e\mathbf{k_h}$	.

The existence of bound states, i.e. excitons, is due to the Coulomb potential of the Hamiltonian (1.1). This gives rise to the hydrogen-like exciton (envelope) wavefunction, and Bohr radius, given by,

$$(H_\mu - E_n)\phi_n(\mathbb{r}) = 0, \qquad a_o = \frac{4\pi\epsilon_o\epsilon_r\hbar^2}{e^2\mu}. \tag{1.3}$$

The ratio ϵ_r/μ makes the exciton Bohr radius much larger ($\sim 10/0.05 \sim 100$) than that of the hydrogen atom. We can associate an exciton, of center-of-mass wavevector,

$\mathbf{k}$, with the state vector, $|D_{\mathbf{k}}\rangle$,

$$\langle \mathbf{r}|D_{\mathbf{k}}\rangle = \int \delta_{\mathbf{r},\mathbf{r}'}\delta_{\mathbb{r},\,\mathbf{r_e}-\mathbf{r_h}}\left[\frac{1}{V}e^{i\mathbf{k}\cdot\mathbf{r}'}\phi_n(\mathbb{r})u_o(\mathbf{r_e})u_o^*(\mathbf{r_h})\right]\mathrm{d}\mathbf{r}'\,\mathbb{r}\,\mathbf{r_e}\,\mathbf{r_h} \tag{1.4}$$

or, with respect to unbound electron and hole state vectors,

$$\langle \mathbf{k_e},\mathbf{k_h}|D_{\mathbf{k}}\rangle = \delta_{\mathbf{k_e}+\mathbf{k_h},\mathbf{k}}\langle \alpha_{\mathbf{h}}\mathbf{k_e} - \alpha_{\mathbf{e}}\mathbf{k_h}|\phi_n\rangle \tag{1.5}$$

where $|\phi_n\rangle$, $\langle \mathbf{r}|\phi_n\rangle = \int \delta_{\mathbf{r},\mathbb{r}}\phi_n(\mathbb{r})\mathrm{d}\mathbb{r}$, is the state vector associated with the internal structure of the exciton. We have used the lattice functions (1.2) at band edge, $\mathbf{k_e} = \mathbf{k_h} = 0$, valid for Wannier excitons, where a_o is much larger than the lattice constant. The Bloch functions, containing the unit cell's electronic structure, provide the magnitude of excitonic coupling with light.

The rest energy associated with excitons in semiconductors is $\varepsilon_o = E_g - E_n$ where $E_n = \frac{e^2}{8\pi\epsilon_r\epsilon_o a_o n^2}$ is the binding energy. This is supplemented by the standard kinetic energy term in their dispersion relation,

$$\varepsilon_{\mathbf{k}} = \varepsilon_o + \mathbf{k}^2/2M, \tag{1.6}$$

with $\mathbf{k}$ describing the in-plane wavevector of the center-of-mass of our quantum well exciton. This is shown as the blue dotted line in Figure 1.2.

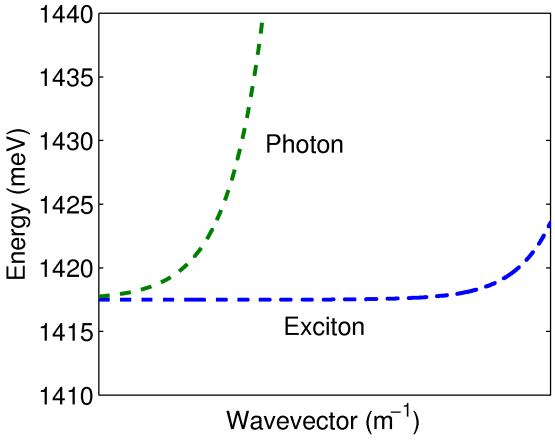

Figure 1.2: Photon (green) and exciton (blue) dispersion relations with $M = 0.25\,m_e$ $m = 2.5 \times 10^{-5}\,m_e$, $\varepsilon_o = \omega_o = 1417.5$meV (values taken from [Skol98]).

Since an exciton is a bound pair of fermions, it can be treated approximately as a boson. To see this, we define a creation operator, $D^\dagger_{\mathbf{k}}|0\rangle = |D_{\mathbf{k}}\rangle$, based on free

electron-hole pair operators, $c^\dagger_{\mathbf{k_e}}, d^\dagger_{\mathbf{k_h}}$,

$$D^\dagger_{\mathbf{k}}\, e^{-i\varepsilon_{\mathbf{k}}t} = \left[\sum_{\mathbf{k_e},\mathbf{k_h}} \langle \mathbf{k_e},\mathbf{k_h}|D_{\mathbf{k}}\rangle c^\dagger_{\mathbf{k_e}} d^\dagger_{\mathbf{k_h}}\right] e^{-i\varepsilon_{\mathbf{k}}t}. \tag{1.7}$$

We then determine the commutation relation of exciton operators from the anticommutation relations of the electron and hole (fermionic) annihilation and creation operators, e.g. $\{c_{\mathbf{k_e}}, c^\dagger_{\mathbf{k'_e}}\} = \delta_{\mathbf{k_e},\mathbf{k'_e}}$:

$$\begin{aligned}
[D_{\mathbf{k}}, D^\dagger_{\mathbf{k'}}]_n &= \delta_{\mathbf{k},\mathbf{k'}} \sum_{\mathbf{k_e},\mathbf{k_h}} \delta_{\mathbf{k},\mathbf{k_h}+\mathbf{k_e}} |\langle \alpha_{\mathbf{h}}\mathbf{k_e} - \alpha_{\mathbf{h}}\mathbf{k_e}|\phi_n\rangle|^2 \Big(c_{\mathbf{k_e}} d_{\mathbf{k_h}} c^\dagger_{\mathbf{k_e}} d^\dagger_{\mathbf{k_h}} - c^\dagger_{\mathbf{k_e}} d^\dagger_{\mathbf{k_h}} c_{\mathbf{k_e}} d_{\mathbf{k_h}}\Big) \\
&= \delta_{\mathbf{k},\mathbf{k'}} \sum_{\mathbf{k_e},\mathbf{k_h}} \delta_{\mathbf{k},\mathbf{k_h}+\mathbf{k_e}} |\langle \alpha_{\mathbf{h}}\mathbf{k_e} - \alpha_{\mathbf{h}}\mathbf{k_e}|\phi_n\rangle|^2 \Big((1 - c^\dagger_{\mathbf{k_e}} c_{\mathbf{k_e}})(1 - d^\dagger_{\mathbf{k_h}} d_{\mathbf{k_h}}) - c^\dagger_{\mathbf{k_e}} c_{\mathbf{k_e}} d^\dagger_{\mathbf{k_h}} d_{\mathbf{k_h}}\Big) \\
&= \delta_{\mathbf{k},\mathbf{k'}} \Big(1 - \sum_{\mathbf{k_e},\mathbf{k_h}} \delta_{\mathbf{k},\mathbf{k_h}+\mathbf{k_e}} |\langle \alpha_{\mathbf{h}}\mathbf{k_e} - \alpha_{\mathbf{h}}\mathbf{k_e}|\phi_n\rangle|^2 \big(c^\dagger_{\mathbf{k_e}} c_{\mathbf{k_e}} + d^\dagger_{\mathbf{k_h}} d_{\mathbf{k_h}}\big)\Big) \\
&= \delta_{\mathbf{k},\mathbf{k'}} \big(1 - \mathcal{O}(\tfrac{N_k\, a_o^3}{V})\big).
\end{aligned} \tag{1.8}$$

The first term samples the entire normalized volume whereas the second one samples the excitonic component of it. At low densities, excitons obey bosonic commutation rules, $[D_{\mathbf{k}}, D^\dagger_{\mathbf{k'}}] = \delta_{\mathbf{k},\mathbf{k'}}$, i.e. are composite bosons.

Photon Component

We now obtain a similar, second quantized form and dispersion relation for cavity photons. As seen in Appendix A.2, the trapped mode inside the cavity penetrates the distributed Bragg reflector (DBR) with decay constant $L_{DBR}/2 \propto -d/\log|\lambda_1|$. The cavity length, L_c, therefore takes an effective length, $L_{eff} = L_c + L_{DBR}$. In a typical GaAs/AlAs structures, $L_c = \lambda$, and $L_{DBR} \sim (3-4)L_c$, [Skol98]. The light mode is therefore more distributed than one would tell by looking at cavity drawings (e.g. Fig. 1.1).

The continuous in-plane wavevector, $\mathbf{k}_\parallel$, adds to the normal wavevector ($L_{\omega_o} = \lambda$) and gives photon energy,

$$\omega_{\mathbf{k}_\parallel} = \frac{\hbar c}{n}\sqrt{(2\pi/L_{w_o})^2 + |\mathbf{k}_\parallel|^2} \tag{1.9}$$

which, with a Taylor expansion and the grouping of the "mass" terms, $m = (n/\hbar c)(2\pi/L_{w_o})$,

provides a quadratic dispersion relationship,

$$\begin{aligned}\omega_{\mathbf{k}_\parallel} &\approx \frac{c}{n}\frac{2\pi}{L_{w_o}}\big(1+\tfrac{1}{2}|\mathbf{k}_\parallel|^2\big)\\ &\approx \omega_o + \frac{|\mathbf{k}_\parallel|^2}{2m}.\end{aligned} \tag{1.10}$$

This is shown as the green dotted line in Figure 1.2.

To describe the electromagnetic field quantum mechanically, we use the radiation gauge, where the vector potential, $\mathbf{A}$, and the scalar potential, U, are

$$\nabla\cdot\mathbf{A} = 0 \text{ (Coulomb gauge) and } U = 0. \tag{1.11}$$

We also use the dipole approximation, $\mathbf{A}(\mathbf{r},t) = \mathbf{A}(\mathbf{r}_o,t) \equiv \mathbf{A}(t)$, since the Bohr radius of the exciton is much smaller than the wavelength of light. We therefore have,

$$\begin{aligned}&\mathbf{A}(\mathbf{r},t) \equiv \mathbf{A}(t),\\ &U(\mathbf{r},t) \equiv 0.\end{aligned} \tag{1.12}$$

The field is quantized[Scul97] and the expression for the vector potential operator becomes,

$$\mathbf{A}(t) = \sum_{\mathbf{k}_\parallel,\lambda} e^{i\mathbf{k}_\parallel\cdot\mathbf{r}}\mathcal{A}_{\mathbf{k}_\parallel}\hat{\mathbf{e}}_\lambda\big(\psi_{\mathbf{k}_\parallel,\lambda}\,e^{i\omega_{\mathbf{k}_\parallel}t} + \psi^\dagger_{\mathbf{k}_\parallel,\lambda}\,e^{-i\omega_{\mathbf{k}_\parallel}t}\big), \tag{1.13}$$

with $\mathcal{A}_{\mathbf{k}_\parallel} = \sqrt{\frac{c^2\hbar}{2\epsilon_o V\omega_{\mathbf{k}_\parallel}}}$, and $\hat{\mathbf{e}}_\lambda$ being the unit polarization vector. We shall be working with matrix elements, and the photon creation and annihilation operators which obey bosonic commutation relations, $[\psi_{\mathbf{k}_\parallel,\lambda}, \psi^\dagger_{\mathbf{k}_\parallel,\lambda}] = 1$.

Exciton-Photon Interaction

The interaction between excitons and photons is now included[Elli57]. In the radiation gauge, the minimal-coupling Hamiltonian satisfies local gauge invariance with the modification

$$\mathbf{p^2} \to (\mathbf{p} - e\mathbf{A})^2 \approx \mathbf{p}^2 - 2e\mathbf{A}\cdot\mathbf{p}. \tag{1.14}$$

Here we have used the commutation relation, $[\mathbf{p},\mathbf{A}] = 0$ since $\nabla\cdot\mathbf{A} = 0$, and neglected the two-photon term, $\mathbf{A}^2$, on the basis of it having different time dependencies, $\psi^\dagger\psi^\dagger, \psi\psi$, or being small, $\psi^\dagger\psi, \psi\psi^\dagger$. The matrix elements for this additional $\mathbf{A}\cdot\mathbf{p}$ term are calculated pertubatively and give the following matrix element for the coupling be-

tween the ground state and a single exciton state

$$g_{\mathbf{k}} = \frac{e\mathcal{A}_{\mathbf{k}}}{m^*\Omega}\delta_{\mathbf{k}\mathbf{k}_\parallel}\langle u_c \mid \hat{\mathbf{e}}_\lambda \cdot \mathbf{p} \mid u_v\rangle, \tag{1.15}$$

where Ω is the unit cell volume and $m^* = \mu$ is the reduced exciton mass (since we used the lattice functions at band edge, (1.4)). While the lattice function provides the strength of the matrix element, momentum conservation rules arise from the envelope function. The delta function, emerging in (1.15) from the calculation of the matrix element, is in fact a conservation of in-plane momentum in the energy transfer between photons and excitons. In-plane momentum conservation also translates in a one-to-one correspondence between the polariton states and the angle at which photons escape the cavity (see Sec. 1.1.5). In addition to enhancing the field intensity, this is another advantage provided by the use of semiconductor microcavities over bulk systems.

Polaritons

Grouping excitons, photons and their interaction together, letting $\mathbf{k}$ be short for $\mathbf{k}_\parallel, \lambda$ and making use of the rotating wave approximation[Scul97], the complete field, exciton and interaction Hamiltonian we shall be using can now be compactly expressed as

$$\mathcal{H} = \sum_{\mathbf{k}} \Big[\omega_{\mathbf{k}}\psi^\dagger_{\mathbf{k}}\psi_{\mathbf{k}} + \varepsilon_{\mathbf{k}}D^\dagger_{\mathbf{k}}D_{\mathbf{k}} + g_{\mathbf{k}}(D^\dagger_{\mathbf{k}}\psi_{\mathbf{k}} + H.c.)\Big], \tag{1.16}$$

where the first term is the photon energy, the second term is the exciton energy and the term proportional to $g_{\mathbf{k}}$ is the coupling between photons and excitons. We observe that excitons and photons are not eigenstates of the Hamiltonian derived so far. We therefore proceed to diagonalize it and determine its eigenvalues based on the dispersion relations presented above (1.6, 1.10). Upper and lower polariton operators are introduced

$$\begin{pmatrix} p^1_{\mathbf{k}} \\ p^2_{\mathbf{k}} \end{pmatrix} = \begin{pmatrix} \cos(\theta_{\mathbf{k}}) & -\sin(\theta_{\mathbf{k}}) \\ \sin(\theta_{\mathbf{k}}) & \cos(\theta_{\mathbf{k}}) \end{pmatrix} \begin{pmatrix} \psi_{\mathbf{k}} \\ D_{\mathbf{k}} \end{pmatrix}, \tag{1.17}$$

where one must choose

$$\tan(2\theta_{\mathbf{k}}) = \frac{2g_{\mathbf{k}}}{\omega_{\mathbf{k}} - \varepsilon_{\mathbf{k}}}, \tag{1.18}$$

for the Hamiltonian to become diagonal. The upper and lower polariton dispersion relations are then found to be

$$E^{1,2}_{\mathbf{k}} = \frac{1}{2}\big[(\omega_{\mathbf{k}} + \varepsilon_{\mathbf{k}}) \pm \sqrt{(\omega_{\mathbf{k}} - \varepsilon_{\mathbf{k}})^2 + 4g^2_{\mathbf{k}}}\,\big]. \tag{1.19}$$

These are plotted with solid lines in Figure 1.3. The shift in energy between the upper and the lower branch at zero wavevector, $\omega_o = \varepsilon_o$ in (1.19), is called the Rabi splitting, $\Omega = 2g$.

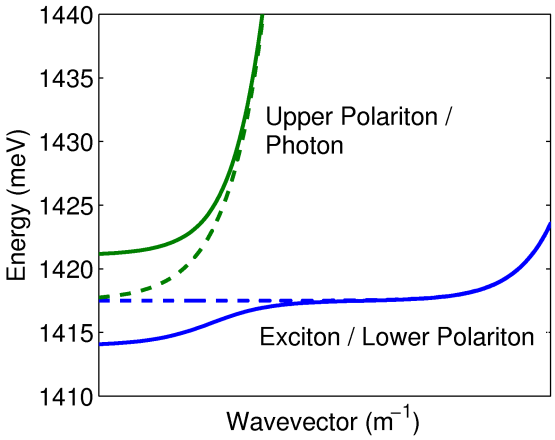

Figure 1.3: Solid lines: Upper and lower cavity polariton dispersion relations with $M = 0.25\,m_e$ $m = 2.5 \times 10^{-5}\,m_e$, $\varepsilon_o = \omega_o = 1417.5$meV, $g = \Omega/2 = 3.5$meV (values taken from [Skol98]). Dotted lines: Photon (green) and exciton (blue) dispersion relations in the absence of coupling.

The Hamiltonian (1.16) is now diagonalized with upper and lower polariton modes,

$$\mathcal{H} = \sum_{\mathbf{k}} \left[E^1_{\mathbf{k}}\, p^{1\dagger}_{\mathbf{k}} p^1_{\mathbf{k}} + E^2_{\mathbf{k}}\, p^{2\dagger}_{\mathbf{k}} p^2_{\mathbf{k}} \right]. \tag{1.20}$$

In this thesis, we work solely with lower branch polaritons. The upper branch lies far above all the experiment energies that are employed and exhibits lifetimes that are much shorter due to the photon component within it being larger.

Strong Coupling

We developed the theory so far without considering the role of decay outside the cavity, i.e. the escape of photons, and therefore polaritons, due to the finite reflectivity of the mirrors. Having a high Q-factor (see Appendix A.3) enables the system to be in a strong coupling regime and to have two polariton branches, as shown in Figure 1.3. From a phenomenological perspective, strong coupling manifests itself by two dips in the reflectivity spectra of the microcavities, as shown in Figure 1.4a. It is seen in multiple optical systems, for example with single quantum dots embedded in Fabry-Perrot micropillars[Vaha 03] and in photonic crystals[Thon 09]. It has also been observed in the radiative coupling of dilute vapor with the external evanescent field of whispering cavity mode in fused silica microspheres[Vern 98]. In the types of systems we are using, strong

coupling can also be observed in an "unfolded microcavity" where the quantum wells are embedded along the DBRs[Aski11], and in bulk microcavities[Tred95, Faur08], where the active medium is the whole cavity and the exciton center of mass motion, $\mathbf{k}$, acquires an additional, quantized degree of freedom in the growth direction.

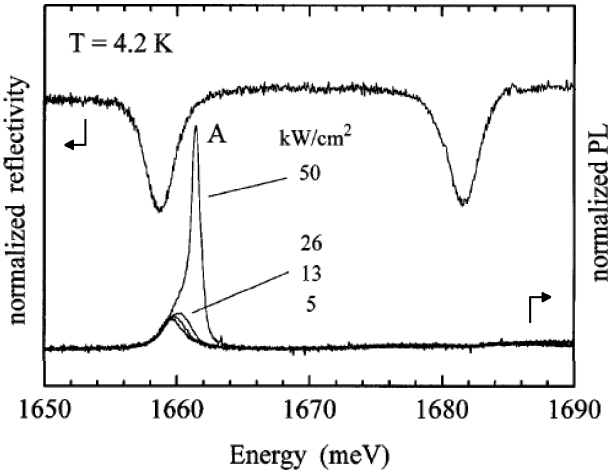

Figure 1.4: (a) The strong coupling between microcavity photons and quantum well excitons is shown in the two polariton absorption dips in the reflectivity spectrum. (b) (see Sec. 1.1.5) The large polariton ground state occupancy above threshold (50kW/cm^2) is seen in the photoluminescence spectrum (from [Dang98]).

The strong coupling regime[Savo95], where polaritons form, takes place when the exciton and cavity linewidths are smaller than the Rabi splitting, Ω. In other words, strong coupling occurs when the decay of polaritons into the continuum outside the cavity and the dephasing due to photonic and excitonic inhomogeneities are smaller than the coupling[Skol98, Keel07, Deng10]. The transition from strong coupling to weak coupling can be observed phenomenologically by introducing a damping term, $i\gamma$, to the photon energy in (1.19), $\omega_{\mathbf{k}} \to \omega_{\mathbf{k}} + i\gamma$, and taking $\mathrm{Re}(E^{1,2}_{\mathbf{k}=0})$. As seen in Figure 1.5, when γ reaches the Rabi splitting energy, $\Omega = 2g$, the two branches merge together, exemplifying diagrammatically the transition from strong coupling to weak coupling regimes.

A full treatment of the transition from strong to weak coupling[Savo95] can be obtained semiclassically with the use of transfer matrices (see Appendix A.2) where the cavity transmission and reflection coefficients are used in conjunction with a transfer matrix for the quantum wells which includes both the nonradiative exciton broadening and radiative decay of excitons. A full quantum treatment is also possible[Savo95]. In this case, a Hamiltonian similar to (1.16) is used, with the light modes expressed as left and right traveling waves, rather then standing waves, and transmission and reflection coefficients for them also obtained form transfer matrices.

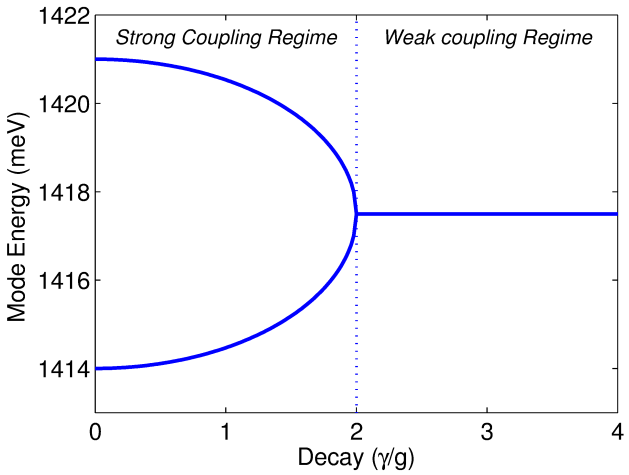

Figure 1.5: Transition of the normal, $\mathbf{k} = 0$, cavity modes from the strong coupling regime, where the spectrum is split due to the interaction, to the weak coupling regime, with $\gamma = [0 \cdot g, 4 \cdot g]$ and $g = 3.5$meV. When γ reaches $2g$, the system enters the weak coupling regime.

1.1.4 Quantum Condensation

The statistics of bosons is such that degenerate conditions carry higher relative statistical weight than in the classical and fermionic cases. In certain situations, this is so dominant that a break of symmetry occurs and a very large number of particles end up in a single particular state; in other words the system "condenses". While condensation is primarily a statistically driven effect, interactions also play a role[Legg 01]. Thermal BEC of the ideal Bose gas in 3D is derived in Appendix A.1; from the derivation we retain that for a given temperature,

$$T_c = \frac{2\pi\hbar^2}{k_B m}\left(\frac{n}{g_{3/2}(1)}\right)^{2/3}, \quad g_{3/2}(1) = 2.612, \tag{1.21}$$

the Bose distribution can only accommodate a finite density, $n \to n_{sat}$. Once the saturation density has been reached, all the exceeding particles end up in the ground state. They form a large occupancy coherent state. In the thermal case, the only property that influences the density of states, once dimensionality has been fixed, is the mass, m, which then appears in the critical temperature, T_c. Figure 1.6 features the phase diagram of thermal BEC.

In one and two-dimensions, the density of states in the thermodynamic limit or hard-wall continuum is such that the Bose distribution diverges as $\mu \to 0$ (1D) or only becomes finite with both $T_c, \mu \to 0$ (2D), and any density can be accommodated within it (expressed in different form in [Hohe67]). Thus the non-interacting gas never

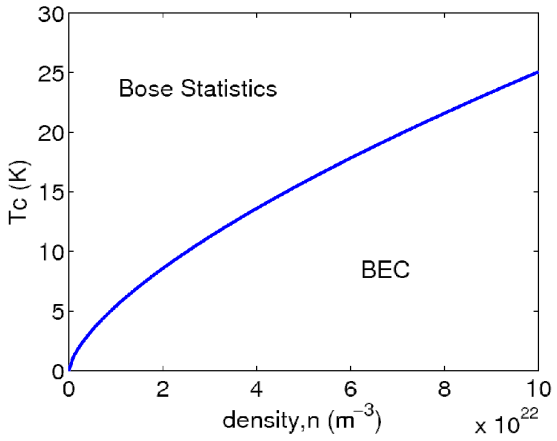

Figure 1.6: Phase diagram of Bose-Einstein condensation occurring in 3D. For densities which are on the right of the blue line a condensate forms.

condenses (1D) or only condenses at $T = 0$ (2D). This is not the case however for a gas of Bose particles confined in a power-law potential[Bagn91]. The one dimensional ideal Bose gas can condense with a potential up to harmonic power. The 2D Bose gas can condense for any finite potential power, as shown in Figure 1.7.

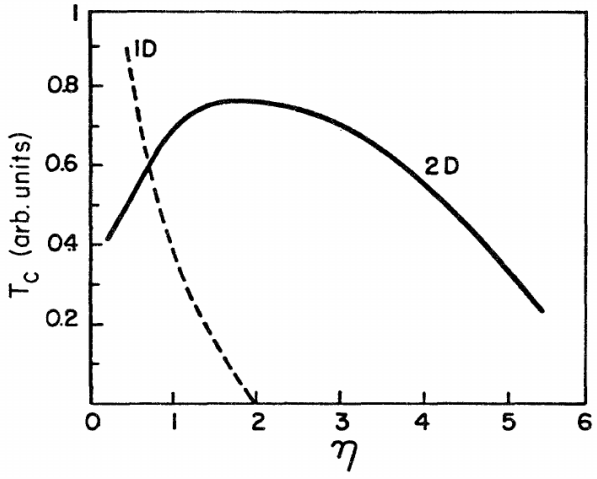

Figure 1.7: Condensation in one and two dimensions of an ideal Bose gas confined in a power-law potential with power η. In one dimension, condensation is possible up to a harmonic potential, $\eta = 2$. In two dimensions, condensation is possible for any finite power potential, with the zero temperature thermodynamic limit being recovered at $\eta \to \infty$ (from [Bagn91]).

We now introduce the concept of off-diagonal long range order, ODLRO, arguably the most important property of macroscopic quantum objects[Penr51, Yang62]. We follow Pitaevkii and Stringari in this derivation[Pita03]. We seize the opportunity to also

introduce density matrices. Let the one-body field density matrix be defined as

$$n(\boldsymbol{r},\boldsymbol{r}') = N\int \mathrm{d}\boldsymbol{r}_2...\mathrm{d}\boldsymbol{r}_N \Psi^*(\boldsymbol{r},\boldsymbol{r}_2,...\boldsymbol{r}_N)\Psi(\boldsymbol{r}',\boldsymbol{r}_2,...\boldsymbol{r}_N) \tag{1.22}$$

where $\Psi(\boldsymbol{r},\boldsymbol{r}_2,...\boldsymbol{r}_N)$ is the N-body wavefunction which is appropriately symmetrized to take into account the indistinguishability of Bose particles. The integration is carried over $N-1$ variables. The one-body density matrix can also be written with Heisenberg picture field operators,

$$n(\boldsymbol{r},\boldsymbol{r}') = \langle\hat{\Psi}^\dagger(\boldsymbol{r})\hat{\Psi}(\boldsymbol{r})\rangle \tag{1.23}$$

which can be expressed as

$$\hat{\Psi}(\boldsymbol{r}) = \sum_i \phi_i a_i. \tag{1.24}$$

Here we used the orthonormal single-particle wavefunctions, ϕ_i, of the system and the annihilation (creation), a_i ($a_i^\dagger$), operators which remove or add particles from these orbitals. This formulation removes the burden of symmetrization in the many-body wavefunction and obeys the commutation relations,

$$[a_i, a_j^\dagger] = \delta_{ij}, \quad [a_i, a_j] = 0. \tag{1.25}$$

The field operator can also express the momentum distribution

$$n(\boldsymbol{p}) = \langle\hat{\Psi}^\dagger(\boldsymbol{p})\hat{\Psi}(\boldsymbol{p})\rangle \tag{1.26}$$

where $\hat{\Psi}(\boldsymbol{p}) = (2\pi\hbar)^{-3/2}\int \mathrm{d}\boldsymbol{r}\exp(i\boldsymbol{p}\cdot\boldsymbol{r}/\hbar)\hat{\Psi}(\boldsymbol{r})$. The momentum space density matrix can therefore be expressed as

$$\begin{aligned} n(\boldsymbol{p}) &= \frac{1}{(2\pi\hbar)^3}\int \mathrm{d}\boldsymbol{r}\mathrm{d}\boldsymbol{r}'\, n(\boldsymbol{r},\boldsymbol{r}')\exp(i\boldsymbol{p}\cdot(\boldsymbol{r}-\boldsymbol{r}')/\hbar) \\ &= \frac{1}{(2\pi\hbar)^3}\int \mathrm{d}\boldsymbol{R}\mathrm{d}\boldsymbol{s}\, n(\boldsymbol{R}+\frac{\boldsymbol{s}}{2},\boldsymbol{R}-\frac{\boldsymbol{s}}{2})\exp(i\boldsymbol{p}\cdot\boldsymbol{s}/\hbar), \end{aligned} \tag{1.27}$$

where $\boldsymbol{s} = \boldsymbol{r}-\boldsymbol{r}'$ and $\boldsymbol{R} = (\boldsymbol{r}+\boldsymbol{r}')/2$. For non-condensed systems, $T > T_c$, the momentum distribution is smooth so $n(\boldsymbol{s})$ vanishes when $\boldsymbol{s}\to\infty$, Figure 1.8. In the case of a condensed system, $T < T_c$, the momentum distribution has a singular behavior

$$n(\boldsymbol{p}) = N_o\delta(\boldsymbol{p}) + \tilde{n}(\boldsymbol{p}) \tag{1.28}$$

where $\tilde{n}(\boldsymbol{p})$ expresses the non-condensed component of the system. The inverse Fourier transform, $n(\boldsymbol{s})$, see (1.27), therefore remains at a finite value at large separations:

$n(\boldsymbol{s})_{\boldsymbol{s}\to\infty} \to n_o$. This feature is called ODLRO[Yang 62]. Every local part of the condensate is linked with every other local part. The one-body density matrix therefore has a non-vanishing off-diagonal value at large separation, Figure 1.8.

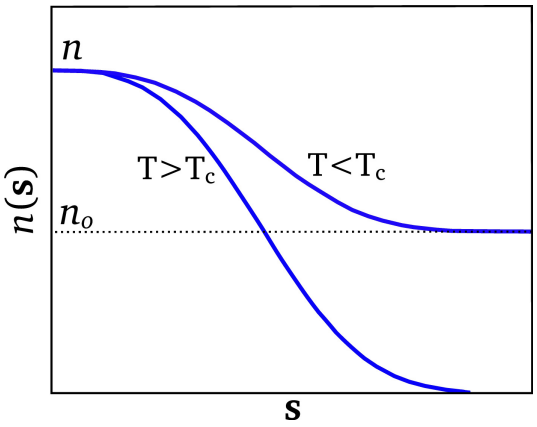

Figure 1.8: Above T_c, the off-diagonal density matrix vanishes at a certain distance, s. Below T_c, the density matrix shows ODLRO and remains at a finite value, n_o, as $\boldsymbol{s} \to \infty$.

Lineshape and coherence functions when treated in the full quantum description appeal to ODLRO through the use of off-diagonal elements.

1.1.5 Polariton Condensation

Polaritons are four orders of magnitude lighter than excitons (twice the photons effective mass) and seven orders of magnitude lighter than hydrogen atoms. This places them in the ideal position to exhibit Bose condensation. The polariton system is not thermal however; it is a steady state pumped and decaying system (see Sec. 1.2.3). Nevertheless polariton condensation has been demonstrated in multiple types of quantum microcavities[Dang 98, Bali 07, Love 08], as shown in Figures 1.4b,1.9A, and is now showing promising prospects as a new source of low threshold coherent radiation[Lu 12, Li 12], Figure 1.9B.

In the experiments on which our model is based[Love 08, Kasp 08, Deng 10], a laser is shone on the cavity at high incidence angle ($\mathbf{k}_{\|} \gg 0$) and with energy much higher ($\sim$ 100meV) than the lower polariton ground state ($\hbar\omega \gg \hbar(\omega_{\mathbf{k}} - g_{\mathbf{k}})$), creating high $\mathbf{k}$ polaritons. These injected polaritons relax by phonon emission and thermalize by polariton-polariton scattering to lower energy and wavevector, $\mathbf{k}$, and loose the laser coherence in the process[Deng 10]. They then start to experience strong coupling, thereby gaining lower mass and occupying a reduced density of states. At this point, spontaneous symmetry breaking occurs, as stimulated polariton-polariton scattering induces

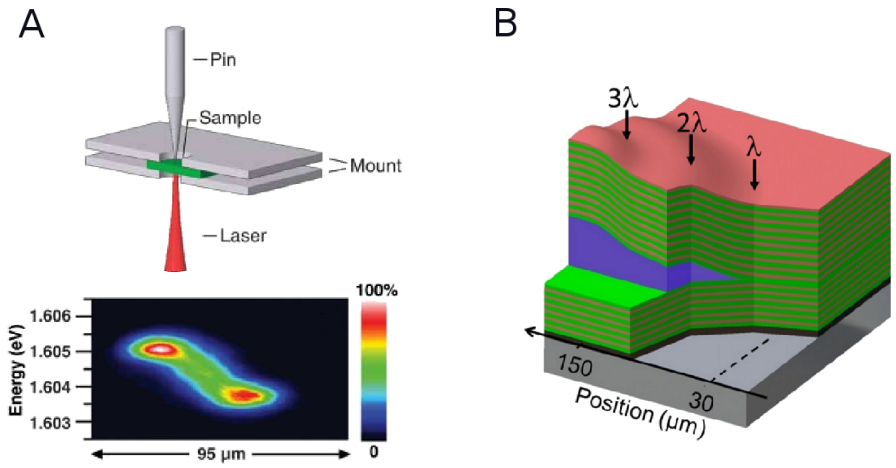

Figure 1.9: A - In stress induced experiments, a pin exerts pressure on the cavity which diminishes the bandgap and therefore lowers the polariton ground state energy at that position. The condensate is shown to move from the region where it is created (left on the contour plot) to the bottom of the stress induced trap (right on the contour plot) demonstrating that the condensate coherence is spontaneous and independent of laser coherence (from [Bali07]). B - Polariton lasing has been observed at room temperature in large (~ 60 meV) exciton oscillator strength ZnO bulk microcavities (from [Li12]).

a macroscopic occupation of the ground state, $\mathbf{k} \approx 0$, of the cavity. Condensate particles will then decay into radiation escaping at near normal incidence from the cavity, $\mathbf{k}_{\parallel} \approx 0$, in a narrow range of energies. Such emission is observed above a threshold pump power, analogous to the critical density in the equilibrium case [Deng03].

The stimulated scattering into, and decay out of, the condensate mode need to balance each other at threshold in order for condensation to occur. The bosonic nature of final state stimulation into the N-polaritons composite object enhances scattering by a factor of $1+N$ ($\sqrt{1+N}$ for amplitude), [Deng10, Keel07]. The scattering term itself is composite, having a Coulomb contribution as well as a subtle Pauli exclusion term arising from the indistinguishability of the electrons and holes within two "separate" excitons [Comb07]. The spin of the polariton also plays a role on the scattering term [Shel10]; parallel spin excitons have an interaction strength one order of magnitude stronger than antiparallel spin excitons [Magn10, Roch00]. A simplified rate equation which includes condensate and reservoir radiative losses as well as scattering rates can be derived, from which the critical pump power for condensation can be estimated [Porr02].

The above picture is based on the dispersion relation, shown in Figure 1.3, from an ideal microcavity with perfect translational symmetry. However in reality, the condensate experiences lateral trapping which gives rise to single particle states, ϕ_j, in the cavity. The potentials which define ϕ_j can stem from (i) cavity-based photonic [Lang02, Savo07] and, to a lesser extent, excitonic [Savo07] disorder in the microcavity, Figure 1.10A, (ii)

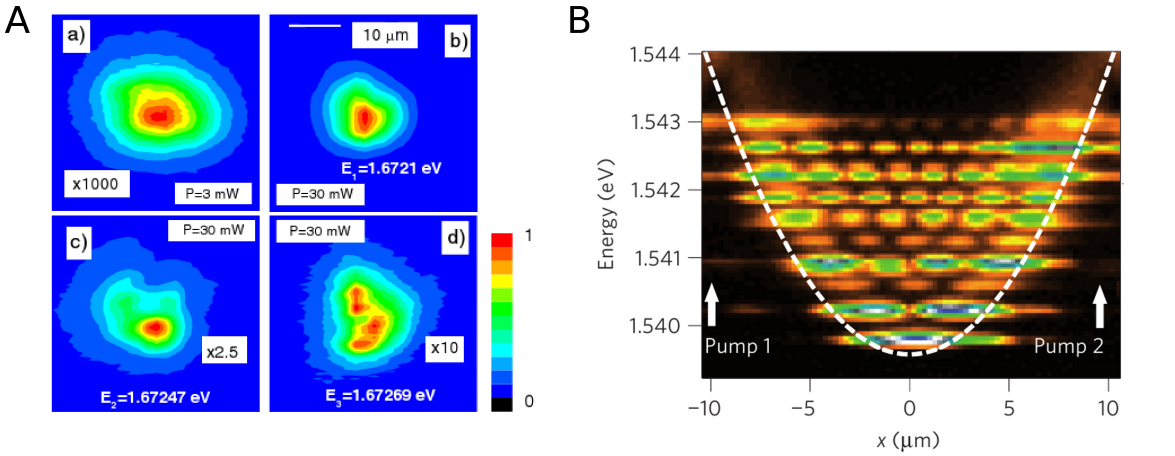

Figure 1.10: A- Multimode polariton condensate arising due to the photonic effective potential caused by defects in the Bragg mirrors. The spectrally and spatially resolved polariton emission is imaged at $k_{\|} \approx 0$ (a) below threshold and (b-d) above threshold (reproduced from [Love08]). B - Multimode Condensate in a harmonic trap formed by repulsive interaction with reservoir polaritons. The two pump beams form reservoirs with a harmonic density profile. The multimode condensate can be resolved both spatially and spectrally (reproduced from [Tosi12]).

photonic[Masu12] and excitonic[Galb12] patterning of the cavity or (iii) reservoir exciton repulsion[Tosi12], Figure 1.10B.

Photonic disorder has been observed to separate the condensate into spatially (and spectrally, the zero of energy varies with the modes) resolvable populations, as depicted in Figure 1.10A. This type of disorder is due to layer width fluctuations in the Bragg mirrors and crystal dislocations[Keel07], as mentioned earlier in Section 1.1.2. These generate an effective potential whose low-energy states will be comparable in size to the wavelength of light, since disorder on shorter scales is averaged away[Lang02]. If the disorder is strong enough, the low-energy states will be spatially and energetically separated.

Our model shall refer to these different condensate populations/modes, and the description of the replenishing of each of them as well as the interaction between them shall be one of the main focuses of this work. The other focus is to determine the population distributions and coherence properties of the modes based on the model.

We highlight that interactions are present within the condensates. They originate from the excitonic component and therefore share the same physical origin as stimulated scattering which forms the condensates. They generate the main source of condensate decoherence[Whit09], i.e., a finite width to the spectral line in experimental data. The first order coherence function, $g^{(1)}(\tau)$, or inverse Fourier transform of the emission linewidth, provides access to it. Figure 1.11a shows the measurement of

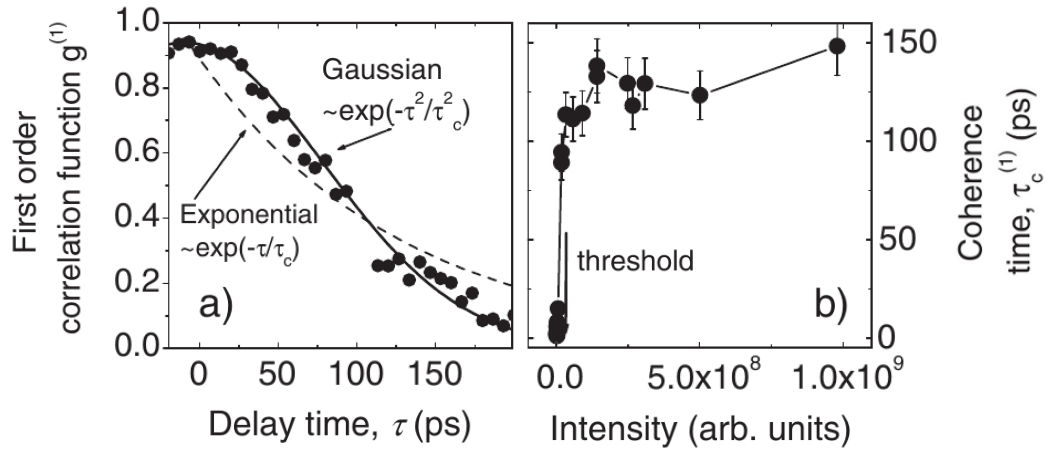

Figure 1.11: a) First order coherence decay of a mode within a multimode polariton condensate. b) Coherence time, t_c, of a mode within a multimode polariton condensate for different pumping powers around and above condensation threshold (reproduced from [Love08]).

$g^{(1)}(\tau)$ performed by Love et al[Love08] on a multimode condensate. They also measured the coherence time, t_c, i.e. the time for which $g^{(1)}(\tau) = e^{-1}$, for different intensities of pumping power, shown in Figure 1.11b. Above threshold, the coherence time of a multimode condensate is of the order of hundreds of picoseconds, much longer than the polariton lifetime (a few picoseconds) and therefore arises from the nonequilibrium nature of the condensate. Our theory will allow to calculate coherence functions and decay times.

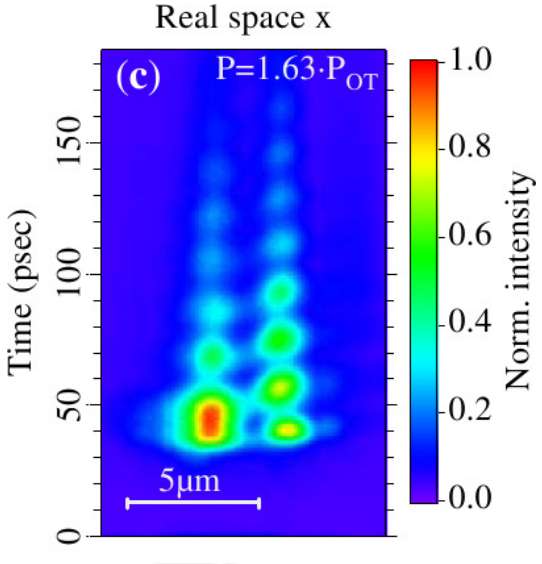

Figure 1.12: Time-resolved measurement of the emission along a line cutting through a two-mode condensate in a double-well. The experiment shows Josephson oscillations (reproduced from [Lago10]).

Lastly we mention Josephson oscillations, one of the most striking effects which arises from multimode polariton condensation. Josephson oscillations occur when two

macroscopically occupied states are separated by a tunneling junction and have a potential difference between them. An oscillating current between the two states can then be observed. These oscillations have indeed been observed in a multimode polariton condensate[Lago 10], as shown in Figure 1.12. As an example of second order coherence, we will calculate the coherence decay of Josephson oscillations in a double well.

1.2 Theoretical Base

Having established the physical context for multimode microcavity polariton condensation, we now form the theoretical basis we will use to describe it. We start by presenting the formalism of density matrices in number states and in the interaction picture. We then derive the Lindblad superoperator for open quantum systems. This will lead us to the description of how pumping and decay, and interactions appear in our model. Finally we discuss linewidth.

1.2.1 Formalism

The fundamental components of our description are orthonormal Fock states or number states, $|n\rangle$, which are acted upon by number operators, $a, a^\dagger$. These states correspond the symmetrized representation of n bosons in a single-particle orbital. Number operators act on them as follow: $a|n\rangle = \sqrt{n}|n-1\rangle$ and $a^\dagger|n\rangle = \sqrt{n+1}|n+1\rangle$. Using this formalism, we can write a many body density matrix

$$\begin{aligned}\rho &= \sum_i P_i \left[\sum_{nm} c_n c_m^* |n\rangle\langle m| \right] \\ &= \sum_{nm} \rho_{nm} |n\rangle\langle m|,\end{aligned} \tag{1.29}$$

which in the most general case is a sum, $\sum_i P_i = 1$, over pure states. In the case of a pure quantum state, $P_i = \delta_{i1}$, the density matrix is idempotent, $\rho^2 = \rho$. Expectation values are obtained by performing the trace over the density acted upon by the operator of interest

$$\begin{aligned}\langle A \rangle &= \mathrm{Tr}(A\rho) \\ &= \sum_{nm} \rho_{nm} A_{mn},\end{aligned} \tag{1.30}$$

where $A_{nm} = \langle n|A|m\rangle$. Density matrices evolve according to

$$\dot{\rho} = -i[H, \rho] \tag{1.31}$$

and, for independent systems, can be combined with the tensor product, $\rho = \rho_1 \otimes \rho_2$. A combined density matrix can be reduced to either density by performing the trace over the one to be left out, e.g. $\rho_1 = \mathrm{Tr}_2[\,\rho\,]$.

For most of this thesis, we shall be using the interaction picture as opposed to the Schrödinger picture. Our equations of motion will be obtained perturbatively. Perturbations are introduced through interactions, either within the condensate or with other systems, i.e. reservoirs. In the interaction picture, the unperturbed time evolution of the condensate, e.g. $H_s = \omega\, a^\dagger a$, is placed in the operators while the interactions either within the condensate or with other systems, here given by H, remain assigned to the state vectors of the condensate density matrix, ρ. To go from the interaction picture, ρ, to the Schrödinger representation, ρ_S, where the whole time evolution is in the density matrix, one can simply provide the density matrix the time dependence that was taken away in the interaction picture,

$$\begin{aligned}
\dot{\rho}_S &= \frac{\mathrm{d}}{\mathrm{d}t} e^{-iH_s t}\, \rho e^{iH_s t} \\
&= -iH_s\rho_S + i\rho_S H_s + e^{-iH_s t}\big(\ \dot{\rho}\ \big)e^{iH_s t} \\
&= -i[H_s, \rho_S] \quad + \qquad e^{-iH_s t}\big(\text{-}i[H, \rho]\big)e^{iH_s t}.
\end{aligned} \tag{1.32}$$

The full Schrödinger evolution is restored.

The evolution of the system (1.31) can also be written with Liouville superoperators, $\dot{\rho} = \mathcal{L}\rho$ or $\rho = e^{\mathcal{L}t}\rho_o$. The Liouville form is a more general object than commutators since it can also accommodate evolutions which are non-unitary, as in open quantum systems.

1.2.2 Open Quantum Systems

In this section we derive the many mode density matrix for quantum decay. The treatment of open quantum systems will provide us with the Lindblad superoperator, $\mathcal{L}_d$, [Lind83, Scul97]. Our system of interest will be coupled weakly to a larger system, a reservoir, which possesses a very large number of degrees of freedom. The system will lose into it both its population and its coherence. The expansion will be done with two modes, which may or may not be independent, i.e. factorizes or not as

$\rho \equiv \rho_s = \rho_1 \otimes \rho_2$. We will generalize the end result to many modes. We combine the density matrix of the two modes with that of two large mode density reservoirs, $\rho_r = \rho_{r_1} \otimes \rho_{r_2}$, which for our purposes are at zero temperature, e.g. $n_{\boldsymbol{k_1}} = \langle b^\dagger_{\boldsymbol{k_1}} b_{\boldsymbol{k_1}} \rangle = 0$. We assume that the initial system-reservoir density factorizes, $\rho_{sr,o} = \rho_o \otimes \rho_{r_o}$. We employ one reservoir per mode in order to avoid having to worry about cross-talk/feedback through the reservoir[Alei 12], e.g. $\langle a_2^\dagger \, b_{\boldsymbol{k_1}} \, b^\dagger_{\boldsymbol{k_1}} a_1 \rangle$. Since the entire theory is constructed in a perturbative manner, we work with the unperturbed states of the system; any two system and reservoir operators commute. Other perturbative terms will be added as we construct the theory.

The system-reservoir Hamiltonian, in the interaction picture[1] and the rotating wave approximation is

$$H = \sum_{\boldsymbol{k_1},\boldsymbol{k_2}} \Big[g_{\boldsymbol{k_1}} \big(b^\dagger_{\boldsymbol{k_1}} a_1 + a_1^\dagger b_{\boldsymbol{k_1}} \big) + g_{\boldsymbol{k_2}} \big(b^\dagger_{\boldsymbol{k_2}} a_2 + a_2^\dagger b_{\boldsymbol{k_2}} \big) \Big]. \tag{1.33}$$

The solution of the system-reservoir density matrix, $\rho_{sr} = \rho_{sr,o} e^{\mathcal{L}t}$, evolves as

$$\rho_{sr} = \rho_{sr,o} + \sum_{n=1}^{\infty} (-i)^n \int_{t_o}^{t} \mathrm{d}\tau_n \int_{t_o}^{\tau_n} \mathrm{d}\tau_{n-1} ... \int_{t_o}^{\tau_2} \mathrm{d}\tau_1 [H, [H, ..[H, \rho_{s'r_o}]..]], \tag{1.34}$$

where the prime in $\rho_{s'r_o}$ denotes the dependence of the system on past history, e.i. $\rho_s(\tau_1)$. Given that $\langle b_{\boldsymbol{k_{1,2}}} \rangle = \langle b^\dagger_{\boldsymbol{k_{1,2}}} \rangle = 0$, the expansion has to be taken to second order, and we neglect the higher order terms based on the coupling interactions being weak. Our equation of motion therefore reads,

$$\dot{\rho}_{sr} = - \int_{t_o}^{t} [H, [H, \rho_{s'r_o}] \,], \tag{1.35}$$

where at this point the time dependence is due to both the interactions and the evolution of the operators. This type of expansion, taken up to second order that also assumes that the system-reservoir density matrix, $\rho_{s'r}$, factorizes at t_o is called the Born approximation. This is borrowed from scattering theory[Gasi 74]. Next we also use $\langle b_{\boldsymbol{k_{1,2}}} b_{\boldsymbol{k_{1,2}}} \rangle = \langle b^\dagger_{\boldsymbol{k_{1,2}}} b^\dagger_{\boldsymbol{k_{1,2}}} \rangle = 0$, and since $\langle b^\dagger_{\boldsymbol{k_{1,2}}} b_{\boldsymbol{k_{1,2}}} \rangle = 0$, $\langle b_{\boldsymbol{k_{1,2}}} b^\dagger_{\boldsymbol{k'_{1,2}}} \rangle = \delta_{\boldsymbol{k_{1,2}} \boldsymbol{k'_{1,2}}}$ to keep

[1] The relation between Schrödinger, $a_{1S}, b_{\boldsymbol{k_1}S}$ and interaction pictures, $a_1, b_{\boldsymbol{k_1}}$, operators is given by $a_1 = e^{iH_1 t} a_{1S} \, e^{-iH_1 t} = a_{1S} e^{-i\omega_1 t}$, $\quad b_{\boldsymbol{k_1}} = e^{iH_{\boldsymbol{k_1}} t} b_{\boldsymbol{k_1}S} \, e^{-ie^{iH_{\boldsymbol{k_1}}{}^t} t} = b_{\boldsymbol{k_1}S} e^{-i\nu_{\boldsymbol{k_1}} t}$, etc.
Where $H_1 = \omega_1 a^\dagger_{1S} a_{1S}$, $H_{\boldsymbol{k_1}} = \nu_{\boldsymbol{k_1}} b^\dagger_{\boldsymbol{k_1}} b_{\boldsymbol{k_1}}$, see also (1.32).

only the terms which will survive the trace below. We are left with eight terms,

$$\begin{aligned}\dot{\rho}_{sr} = -\int_{t_o}^{t} \Big[\sum_{\boldsymbol{k}_1} g_{\boldsymbol{k_1}}^2 \big(a_1^\dagger b_{\boldsymbol{k_1}} b_{\boldsymbol{k_1}}'^\dagger a_{1'} \rho_{s'r_o} - b_{\boldsymbol{k_1}}^\dagger a_1 \rho_{s'r_o} a_{1'}^\dagger b_{\boldsymbol{k_1}}' \big) + H.c. \\ + \sum_{\boldsymbol{k}_2} g_{\boldsymbol{k}_2}^2 \big(a_2^\dagger b_{\boldsymbol{k}_2} b_{\boldsymbol{k}_2}'^\dagger a_{2'} \rho_{s'r_o} - b_{\boldsymbol{k}_2}^\dagger a_2 \rho_{s'r_o} a_{2'}^\dagger b_{\boldsymbol{k}_2}' \big) + H.c. \Big] dt'.\end{aligned} \tag{1.36}$$

The primes, $b'_{\boldsymbol{k}_{1,2}}, a_{1'}, a_{2'}$, denote dependence on the past history, $b_{\boldsymbol{k}_{1,2}}(t'), a_1(t'), a_2(t')$.

We then make the interaction picture time-dependence explicit in the operators, $b_{\boldsymbol{k_{1,2}}} \to b_{\boldsymbol{k_{1,2}}} e^{-i\nu_{\boldsymbol{k}} t}$, $a_{1,2} \to a_{1,2} e^{-i\omega_{1,2} t}$. We also take the trace over the reservoirs, reminding ourselves of the invariance of the trace under cyclic permutation, $\mathrm{Tr}[b_r^\dagger \rho_{r_o} b_r] = \mathrm{Tr}[b_r b_r^\dagger \rho_{r_o}]$; we let $g_{\boldsymbol{k}} = g_{\boldsymbol{k_{1,2}}}$,

$$\begin{aligned}\dot{\rho} = -\int_{t_o}^{t} \Big[\sum_{\boldsymbol{k}} g_{\boldsymbol{k}}^2 e^{i(\omega_1 - \nu_{\boldsymbol{k}})(t-t')} \big(a_1^\dagger a_1 \rho(t') - a_1 \rho(t') a_1^\dagger \big) + H.c. \\ + \sum_{\boldsymbol{k}} g_{\boldsymbol{k}}^2 e^{i(\omega_2 - \nu_{\boldsymbol{k}})(t-t')} \big(a_2^\dagger a_2 \rho(t') - a_2 \rho(t') a_2^\dagger \big) + H.c. \Big] dt',\end{aligned} \tag{1.37}$$

where we used, e.g. $\langle b_{\boldsymbol{k_1}} b_{\boldsymbol{k_1}}^\dagger \rangle = 1$. We use the fact that the reservoir degrees of freedom are dense and smooth to let

$$\sum_{\boldsymbol{k}} g_{\boldsymbol{k}}^2 \to \int \mathrm{d}\nu_{\boldsymbol{k}} D(\nu_{\boldsymbol{k}}) g_{\boldsymbol{k}}^2. \tag{1.38}$$

We are therefore left with the integration $\int_{t_o}^{t} \mathrm{d}t' \int \mathrm{d}\nu_{\boldsymbol{k}}$ which can be rewritten as $\int_0^\infty \mathrm{d}t' \int \mathrm{d}\nu_{\boldsymbol{k}}$. The integration in time being over half space provides a Cauchy principal value, $\mathsf{P}\Big(\frac{1}{\omega_{1,2} - \nu_{\boldsymbol{k}}}\Big)$, which corresponds to the celebrated Lamb shift [Wall 10]. The shift can be interpreted by the fact that in perturbation theory levels tend to repel each other, and since there are more vacuum levels above, $]w_{1,2}, \infty]$ than below, $[0, \omega_{1,2}[$, the transition of interest, there therefore is a net shift in energy. This energy renormalization has already been accounted for in the exciton energy and we choose in our calculation to neglect the phenomenon, and to first perform the integration with respect to frequency. This will provide us with a delta-correlation in the reservoir fluctuations. To do this, we assume the density of state of the reservoir to take a constant value given by $2\pi D(\nu_{\boldsymbol{k}}) g_{\boldsymbol{k}}^2|_{\omega_{1,2}} = \gamma/2$ and we lower the integration limit to $-\infty$. This leads to the Weisskopf-Wigner approximation

$$\int_{-\infty}^{\infty} \mathrm{d}\nu_{\boldsymbol{k}} e^{i(\omega_1 - \nu_{\boldsymbol{k}})(t-t')} = 2\pi\delta(t-t'). \tag{1.39}$$

which generates the Markov approximation. In it, the dense number of degrees freedom of the reservoir over a large range of $\boldsymbol{k}_{1,2}$ absorbs any dependence on the past history of the system $\delta(t-t')$ such that $\rho(t')$ in (1.37) turns into $\rho(t)$; such processes are said to be Markovian. The reservoir has no memory, an excitation within it instantaneously relaxes towards equilibrium, and it is thus said to be "delta-correlated".

The equation of motion is now time-local and the reservoir degrees of freedom have been eliminated,

$$\dot{\rho} = -\frac{\gamma}{2}\Big[\big(a_1^\dagger a_1\rho - 2a_1\rho a_1^\dagger + \rho a_1^\dagger a_1\big) + \big(a_2^\dagger a_2\rho - 2a_2\rho a_2^\dagger + \rho a_2^\dagger a_2\big)\Big], \tag{1.40}$$

We extract the matrix elements from the density matrix equation of motion. The density matrix form is

$$\rho = \sum_{nmpq} \rho_{nmpq}\,|\,n\rangle\langle m\,|\otimes|\,p\rangle\langle q\,|, \tag{1.41}$$

where n,m (p,q) refer to matrix elements of the first (second) mode. We perform the manipulation leading to matrix elements in length for one of the terms, $-2a_1\rho a_1^\dagger$, in (1.40),

$$\begin{aligned}\dot{\rho}_{nmpq} &= \ldots\ -2\sum_{n'm'p'q'}\langle n,p|a_1\rho_{n'm'p'q'}|n',p'\rangle\langle m',q'|a_1^\dagger|m,q\rangle\ \ldots\\ &= \ldots\ -2\sum_{n'm'p'q'}\langle n+1,p|\sqrt{n+1}\rho_{n'm'p'q'}|n',p'\rangle\langle m',q'|\sqrt{m+1}|m+1,q\rangle\ \ldots\\ &= \ldots\ -2\sqrt{n+1}\rho_{n+1m+1pq}\sqrt{m+1}\ \ldots\end{aligned} \tag{1.42}$$

The complete form reads,

$$\begin{aligned}\mathcal{L}_d\rho_{nmpq} = -\frac{\gamma}{2}\Big[&(n+m+p+q)\rho_{nmpq}\\ &-2\big((n+1)(m+1)\big)^{\frac{1}{2}}\rho_{n+1m+1pq} - 2\big((p+1)(q+1)\big)^{\frac{1}{2}}\rho_{nmp+1q+1}\Big],\end{aligned} \tag{1.43}$$

where we also begun to use the superoperator notation, $\mathcal{L}_d$. For many modes, this generalizes to,

$$\mathcal{L}_d\rho^{m_1m_2\cdot\cdot}_{n_1\ n_2\cdot\cdot} = -\frac{\gamma}{2}\sum_i\Big[(n_i+m_i)\rho^{m_1m_2\cdot\cdot}_{n_1\ n_2\cdot\cdot} - 2\big((n_i+1)(m_i+1)\big)^{\frac{1}{2}}\rho^{m_1\ldots m_i+1\cdot\cdot}_{n_1\ \ldots n_i+1\cdot\cdot}\Big], \tag{1.44}$$

where n_i and m_i refer to the matrix elements of i^{th} mode. The damping $(n_i=m_i)$ and decoherence $(n_i\neq m_i)$ action can be seen in (1.44); the occupation of $\rho^{m_1\ldots m_i+1\cdot\cdot}_{n_1\ \ldots n_i+1\cdot\cdot}$ falls into $\rho^{m_1m_2\cdot\cdot}_{n_1\ n_2\cdot\cdot}$, inducing growth. The occupation of level $\rho^{m_1m_2\cdot\cdot}_{n_1\ n_2\cdot\cdot}$ itself falls into the level below, hence the negative rate associated with it.

1.2.3 Pumping and Decay, Interactions

The condensate formation considerations discussed in Section 1.1.5 are included here within the scope of our pumping and decay model, illustrated in Figure A.1. The polariton population is divided into two groups; one is the higher energy polariton reservoirs and the other consists of the condensate modes. Stimulated scattering from the reservoir populates the condensate modes. The process through which this occurs is called pumping and in the density matrix model will involve a superoperator, $\mathcal{L}_p$. We derive the form of $\mathcal{L}_p$ in Chapter 2. The condensate emits coherent photons outside the microcavity in a process which we call decay and in the evolution of the density matrix takes the form of the superoperator we derived above, $\mathcal{L}_d$. We also mentioned in Section 1.1.5 that condensate modes interact together. This interaction is given the unitary Hamiltonian, H, which can remain in commutator form and will also be further elaborated upon in Chapter 2.

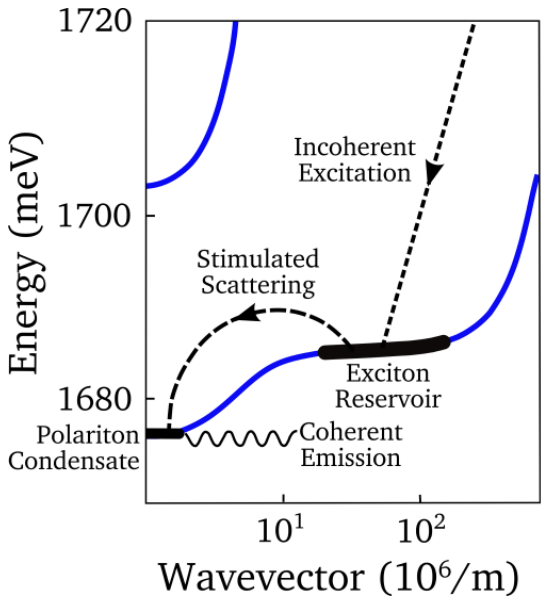

Figure 1.13: Pumping into and decay from the polariton condensate. A reservoir of higher energy polariton (Exciton Reservoir) is created by shining the cavity with a laser at higher energy and at high incidence angle. The quasi-particles introduced by the laser relax and loose their coherence via multiple scattering until they reach the region above the bottleneck region of the dispersion relation and form the reservoir. Polaritons then enter the condensate via stimulated scattering. Condensate polaritons decay outside the cavity through the emission of coherent photons.

Our model is inspired by laser theory[Scul97], since a laser also consists of a large, nonequilibrium occupation of bosons in a single mode. Overall, we shall obtain an

equation of motion which only contains the condensate modes degrees of freedom,

$$\dot{\rho} = \mathcal{L}_p\rho + \mathcal{L}_d\rho - i[H, \rho], \tag{1.45}$$

where ρ is the reduced density matrix for the low-energy polariton states. From this, we will be able to extract physics such as the linewidth of the condensate emission.

1.2.4 Linewidth

The early theory of the linewidth ($\delta\omega$, see Appendix A.3 for general damping theory) of polariton condensate emission was presented by Porras and Tejedor[Porr 03]. They coupled the condensate to a thermal reservoir and obtained Lindblad terms for pumping and decay. They also included a term, κ, for the two-body interactions within the condensate and determined the cross-over for the emission linewidth to be determined by Schawlow-Townes ($\delta\omega \propto 1/N$, see below) or by interactions ($\delta\omega \propto \kappa N$). For atomic condensates, similar theories are described by Gardiner and Zoller[Gard 98] and Thomson and Wiseman[Thom 02].

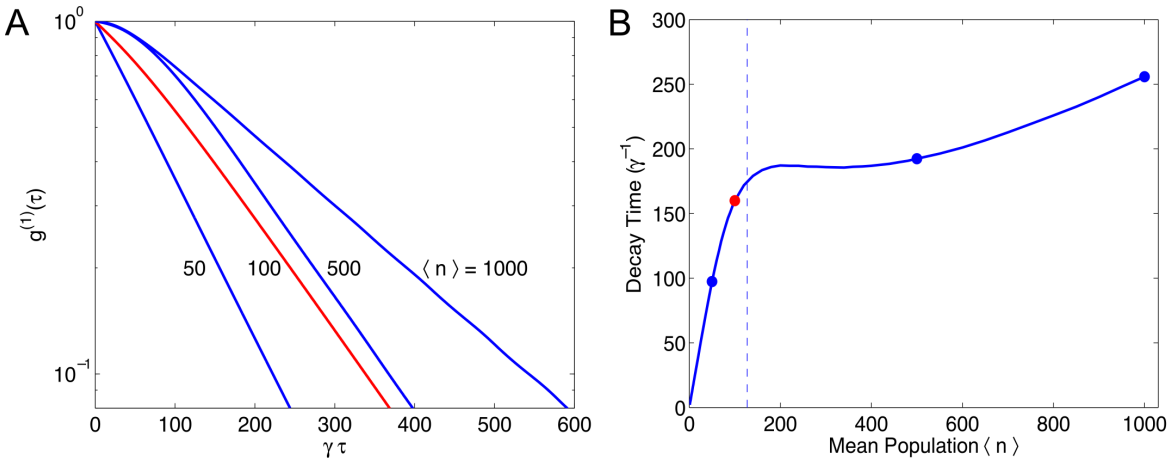

Figure 1.14: A- Coherence decay, $g^{(1)}(\tau)$, of the single mode density matrix equation based on laser theory with added polariton-polariton interactions, for populations $\langle n\rangle = 50, 100, 500, 1000$. B- Coherence time, τ_c, obtained for the intercept of $g^{(1)}(\tau_c) = 1/e$ for population $\langle n\rangle$ varying from 1 to 1000. The coherence time first increases, then plateaus near field threshold (dotted vertical line) and starts increasing again. (recalculation based of [Whit 09])

Whittaker and Eastham, in 2009, revisited the theory of polariton emission linewidth[Whit 09]. Rather than coupling the condensate to a thermal reservoir, they used laser theory in density matrix form[Scul 97]. To account for interactions within the condensate, they added an anharmonic term, $\kappa(a^\dagger a)^2$, to their Hamiltonian. The coherence decay, $g^{(1)}(\tau) \propto \langle a^\dagger(\tau)a\rangle$, they obtained is shown in Figure 1.14A, for different single

mode populations, $\langle n \rangle$. The inverse Fourier transform of the coherence function gives the emission lineshape. Figure 1.14B shows the decay time, $g^{(1)}(\tau_c) = 1/e,\ \tau_c = 2/\delta\omega$, for populations going from 1 to 1000. From the linewidth form they obtained from density matrices, they reached simple, experimentally parametrized expressions for both first, $g^{(1)}(\tau)$, and second, $g^{(2)}(\tau)$, order coherence functions. While $g^{(2)}(\tau)$ does not depend on κ and standard laser expressions could be used directly, their expression for $g^{(1)}(\tau)$ includes the dependence on κ. The theory recovers the generic Kubo lineshape form[Kubo54], which we derive below. The body of the thesis will make extensive use of the treatment of Whittaker and Eastham.

In the remainder of this section we develop the Kubo lineshape theory from linear response theory[Hamm05] and place the results in [Whit09] within this context. We also point out the occurrence of motional narrowing and of slow modulation which we shall refer to as the static limit. We start with a quantity commonly used to discuss linear response theory, the polarization, given by the dipole operator

$$P(t) = \mathrm{Tr}[\mu\rho] \equiv \langle \mu\rho \rangle. \tag{1.46}$$

The unperturbed density matrix, ρ, generally do not have polarization; the perturbation terms generate it. The infinite order perturbation (equiv. to 1.34) reads

$$\rho(t) = \rho^{(0)} + \sum_{n=1}^{\infty} \rho^{(n)}(t), \tag{1.47}$$

where each term can be written in a form involving the commutator of the dipole operator, $\boldsymbol{E} \cdot \boldsymbol{r} \propto \boldsymbol{r} = \mu$,

$$\rho^{(n)}(t) = -i^n \int_{-\infty}^{t} d\tau_n \int_{-\infty}^{\tau_n} d\tau_{n-1} ... \int_{-\infty}^{\tau_2} d\tau_1 [\mu(\tau_n), [\mu(\tau_{n-1}), ...[\mu(\tau_1), \rho(-\infty)]. \tag{1.48}$$

The expectation value of polarization due to the linear response therefore is

$$P(t) = -i \int_{-\infty}^{t} \langle \mu(t) [\mu(\tau_1, \rho(-\infty)] \rangle d\tau_1. \tag{1.49}$$

We use $t_1 = t - \tau_1$, set $\tau_1 = 0$ and change the integration limits of (1.49) accordingly,

$$P(t) = -i \int_{0}^{\infty} \langle \mu(t_1) [\mu(0), \rho(-\infty)] \rangle dt_1 \tag{1.50}$$

The time variable has been eliminated from the equation and we can combine the integration with the ensemble average. The integrand is the linear response function

which we manipulate as follows,

$$S(t) = -i\langle\mu(t)[\mu(0),\rho(-\infty)]\rangle \tag{1.51}$$
$$= -i\langle\mu(t)\mu(0)\rho(-\infty)\rangle + i\langle\mu(t)\rho(-\infty)\mu(0)\rangle \tag{1.52}$$
$$= -i\langle\mu(t)\mu(0)\rho(-\infty)\rangle + i\langle\rho(-\infty)\mu(0)\mu(t)\rangle \tag{1.53}$$
$$= -i\langle\mu(t)\mu(0)\rho(-\infty)\rangle + i\langle\mu(t)\mu(0)\rho(-\infty)\rangle^*. \tag{1.54}$$

We have made use of the invariance of the trace under cyclic permutation (1.53) and the Hermiticity of operators (1.54). The absorption spectrum

$$A(\omega) = 2\mathrm{Re}\int_0^\infty dt e^{i\omega t} i\langle\mu(t)\mu(0)\rho(-\infty)\rangle \tag{1.55}$$

provides the equivalent of the lineshape. To move towards Kubo theory, we now let the dipole operator be expressed as a classical observable with gap energy frequency $\omega(\tau)$,

$$\mu(t) \propto e^{-i\int_0^t d\tau\omega(\tau)}. \tag{1.56}$$

and we separate the frequency into its time average and a fluctuating part,

$$\omega(\tau) = \omega + \delta\omega(\tau), \quad \langle\delta\omega(\tau)\rangle = 0\,. \tag{1.57}$$

We then perform a cumulant expansion [Mand 95] of $S(t)$ and retain only the leading order term,

$$\begin{aligned} S(t) &= e^{-i\omega t}\left\langle \exp\left(-i\int_0^t d\tau\delta\omega(\tau)\right)\right\rangle \\ &= e^{-i\omega t}\left[1 - i\int_0^t d\tau\langle\delta\omega(\tau)\rangle - \frac{1}{2}\int_0^t\int_0^t d\tau d\tau'\langle\delta\omega(\tau)\omega(\tau')\rangle \;\; ...\;\right] \\ &\approx e^{-i\omega t}\left[e^{-\frac{1}{2}\int_0^t\int_0^t d\tau d\tau'\langle\delta\omega(\tau)\delta\omega(\tau')\rangle}\right] \equiv e^{-i\omega t}e^{-g(t)}. \end{aligned} \tag{1.58}$$

In generic processes (and in Kubo's derivation), the correlation function $\langle\delta\omega(\tau)\delta\omega(\tau')\rangle$ decays exponentially, $\Delta^2 e^{-\frac{|\tau'|}{\tau_c}}$, where our generic exponential decay function is parametrized

with amplitude, Δ^2, and decay time, τ_c. The exponent in (1.58) then becomes,

$$\begin{aligned} g(t) &= \frac{1}{2}\int_0^t \int_0^t d\tau d\tau' \langle \delta\omega(\tau)\omega(\tau')\rangle \\ &= \int_0^t \int_0^\tau d\tau d\tau' \langle \delta\omega(\tau')\delta\omega(0)\rangle \\ &= \int_0^t \int_0^\tau d\tau d\tau' \Delta^2 e^{-\frac{|\tau'|}{\tau_c}} \\ &= \Delta^2 \int_0^t d\tau(-\tau_c e^{-\frac{\tau}{\tau_c}} + \tau_c) \\ &= \Delta^2\tau_c^2(e^{-\frac{t}{\tau_c}} + \frac{t}{\tau_c} - 1). \end{aligned} \tag{1.59}$$

In the second step, we performed time-ordering [Hamm 05, Maha 00] through which the factor one-half was eliminated. We are therefore left with the standard Kubo form

$$S(t) = \exp\left[\Delta^2\tau_c^2(e^{-\frac{t}{\tau_c}} + \frac{t}{\tau_c} - 1)\right]. \tag{1.60}$$

There are two limits to this expression. One is the fast modulation, motional narrowing or homogeneous limit,

$\Delta\tau_c \ll 1$; $e^{-t/\tau_c} \to 0$, $t/\tau_c \gg 1$

$$\begin{aligned} g(t) &\approx \Delta^2\tau_c^2\left(\frac{t}{\tau_c}\right) \\ &= \Delta^2\tau_c\, t \end{aligned} \tag{1.61}$$

which leads to a Lorentzian lineshape (cf. 1.55),

$$\begin{aligned} A(\omega) &= 2\mathrm{Re}\int_0^\infty e^{i\omega t}e^{-\Delta^2\tau_c t}dt \\ &= 2\mathrm{Re}\frac{1}{\Delta^2\tau_c + i\omega} \\ &= 2\frac{\Delta^2\tau_c}{(\Delta^2\tau_c)^2 + \omega^2} \propto \frac{1}{1 + (\frac{\omega}{\Delta^2\tau_c})^2}. \end{aligned} \tag{1.62}$$

The other limit is the slow modulation, static limit or inhomogeneous limit,

$\Delta\tau_c \gg 1$; $e^{-t/\tau_c} \to 1 - t/\tau_c + t^2/2\tau_c^2$

$$\begin{aligned} g(t) &\approx \Delta^2\tau_c^2\left(\frac{t^2}{2\tau_c^2}\right) \\ &= \frac{\Delta^2 t^2}{2} \end{aligned} \tag{1.63}$$

which leads to a Gaussian lineshape,

$$\begin{aligned} A(\omega) &= 2\mathrm{Re}\int_0^\infty e^{i\omega t}e^{-\frac{\Delta^2 t^2}{2}}dt \\ &= 2\sqrt{2\pi}\Delta e^{-\frac{\omega^2}{2\Delta^2}} \propto e^{-\frac{\omega^2}{2\Delta^2}}. \end{aligned} \tag{1.64}$$

In [Whit09], the Kubo form that was obtained, $2\mathrm{Re}S(\tau) = e^{-g(\tau)} \equiv g^{(1)}(\tau)$, is

$$g^{(1)}(\tau) = \exp\left[-\frac{4n_c\kappa^2}{\bar{\gamma}^2}(e^{-\bar{\gamma}\tau} + \bar{\gamma}\tau - 1)\right] \cdot \exp\left[\frac{n_c}{4\bar{n}^2}(e^{-\bar{\gamma}\tau} - \bar{\gamma}\tau - 1)\right] \tag{1.65}$$

$$= \exp\left[-\frac{4n_c\kappa^2}{\bar{\gamma}^2}(e^{-\bar{\gamma}\tau} + \bar{\gamma}\tau - 1)\right] \cdot \exp\left[-\frac{n_c}{4\bar{n}^2}(e^{-\bar{\gamma}\tau} + \bar{\gamma}\tau - 1) + \frac{n_c}{2\bar{n}^2}(e^{-\bar{\gamma}\tau} - 1)\right], \tag{1.66}$$

where, in addition to κ, $\bar{n}$ is the mean field population of the condensate, n_c is the pumping strength and $\bar{\gamma} = \bar{n}\gamma/n_c$ is the exponential decay rate of $g^{(2)}(\tau)$. The first exponential accounts for the interaction induced decay while the second one is Schawlow-Townes, enhanced by additional terms which often occur in semiconductor systems[Henr82].

The physical origin of the Schawlow-Townes is the spontaneous emission which occurs while polaritons both enter the condensate and are emitted into photons outside the cavity. This process generates amplitude variations with variance, $\sigma^2 \propto 2\cdot\omega\gamma^2$. The random walk phase variation subtended by this process, $\delta\phi = \delta A_q/A$, is the quadrature component perpendicular to the amplitude divided by the amplitude, A or $\sqrt{N}$. The variance of spectral density induced along the soft mode is therefore given by $\omega\gamma^2/N$, the Schawlow-Townes linewidth[Pasc13, Scha58].

1.3 Relation to Other Theoretical Approaches

Other than the density matrix formalism, several other theoretical tools are being used to describe the physics of polariton condensation. In this section, we provide a survey

of them and discuss each one based on criteria such as the use of first principles, the physics that they capture, and the types of quantities that can be obtained from them.

We start with the Boltzmann rate equations which describes nonequilibrium kinetics[Tass 97, Bany 00]. This equation employs densities as main variables and the transition rates can be parametrized with matrix elements obtained from first principles[Deng 10]. There are usually one set of equations for the occupation of reservoir states

$$\partial_t n_k = P(t) - \frac{n}{\gamma_k} - \sum_{k'} W^{ph}_{kk'}\big(n_{k'}(n_k+1) - n_k(n_{k'}+1)\big) - \sum_{k'k_1k_2} W^{PP}_{k\,k'k_1k_2}\big(n_k n'_k(n_{k_1}+1)(n_{k_2}+1) - n_{k_1}n_{k_2}(n_k+1)(n_{k'}+1)\big) \tag{1.67}$$

and one equation for the occupation of the condensate

$$\partial_t n_o = -\frac{n}{\gamma_o} - \sum_{k'} W^{ph}_{o\,k'}\big(n_{k'}(n_o+1) - n_o(n_{k'}+1)\big) - \sum_{k'k_1k_2} W^{PP}_{o\,k'k_1k_2}\big(n_o n'_k(n_{k_1}+1)(n_{k_2}+1) - n_{k_1}n_{k_2}(n_o+1)(n_{k'}+1)\big). \tag{1.68}$$

The term $P(t)$ accounts for the laser induced incoherent pumping of the reservoir. The γ_k, γ_o terms are decay rates of the polaritons. $W^{ph}_{kk'}$ and $W^{PP}_{kk'k_1k_2}$ are for polariton-phonon and polariton-polariton scattering respectively. Notice that the Boltzmann equations account for stimulated scattering with the $(n_{o,k}+1)$ occurring within them. They can be used to determine quantitatively the threshold and obtain nonequilibrium phase diagrams[Malp 03]. The Boltzmann equation do not consider any form of fluctuations (since they treat only an average occupation), ODLRO, exciton disorder and high density (saturation) regime.

The Gross-Pitaevskii equation augmented with pumping and decay terms embraces the physical reality one step further[Wout 07, Keel 08]. The condensate is modeled with a single-particle macroscopic wavefunction, ψ, the order parameter, which is normalized to N. In the standard cold atom Gross-Pitaevskii equation the equation reads as standard Schrödinger kinetic, ∇^2, and potential, V, terms supplemented with a point interaction term, $g|\psi|^2$. For polariton condensates, pumping and decay terms, inspired by classical laser operation, are added. In one instance of the theory, a separate, Boltzmann type equation is added to keep track of the reservoir dynamics, n_R, [Wout 07, Lago 10] while one other [Keel 08, East 08] reservoir saturation is included via a nonlinear

term, Γ, and reservoir interactions appear via a trapping potential, $V(r)$, with one equation being used. The form which includes a reservoirs explicitly is

$$i\hbar\partial_t\psi = \left[-\frac{\hbar^2\nabla^2}{2m} + \frac{i}{2}[R(n_R) - \gamma] + g|\psi|^2 + 2g'n_R\right]\psi \tag{1.69}$$

$$\partial_t n_R = P - \gamma_R n_R - R(n_R)|\psi|^2 + D\nabla^2 n_R, \tag{1.70}$$

whereas the form with nonlinear pumping (and a trapping potential) is

$$i\partial_t\psi = \left[-\frac{\hbar^2\nabla^2}{2m} + V(r) + g|\psi|^2 + i(\gamma_{eff} - \Gamma|\psi|^2)\right]\psi. \tag{1.71}$$

The first set of equations makes use of a analytically more elaborate monotonic function, $R(n_R)$, for the scattering into the condensate as well as diffusion, $D\nabla^2$, of reservoir polaritons. The second form presents the advantage of being contained in a single equation and being more easily manipulable, both analytically and numerically. The Gross Pitaevskii approach allows to determine a number of quantities relating to the order parameter: the elementary excitation spectrum[Wout 07], vortices[Keel 08], superfluidity properties[Caru 13] and multimode dynamics[East 08]. It is a mean field theoretical tool, and does not include fluctuations, the source of coherence decay; although the theory has inspired the use of classical limit Wigner functions to include fluctuations[Wout 09].

The role of exciton disorder and finite excitation/saturation has been studied extensively by Eastham, Littlewood and others by modeling the exciton subsystem as a set of localized two-level systems[East 01]. Their model is a generalization of the Dicke model, which can be solved to determine thermodynamic properties such as the phase diagram as well as response functions including those describing the optical emission. Initial work on a thermodynamic equilibrium condensate has more recently been supplemented by studies of nonequilibrium condensation, i.e. including gain and loss processes using the Keldysh Green's function approach[Szym 07].

The big advantage of the density matrix formalism in this thesis is that it allows to treat the both thermal and quantum fluctuations in the order parameter of an open quantum system. It also treats ODLRO but does not consider the saturation of excitons[Skol 98] in the quantum well. It is parametrized phenomenologically rather than from first principles.

1.4 Layout of the Thesis

Having presented both the background and the theoretical context of this thesis, we are ready to embark into the original component of it. The original work is contained within four chapters (Chapters 2−5). The next chapter builds our density matrix model for many reservoir and many mode condensates and for the treatment of condensate interactions. Chapters 3 and 4 present a general application of the theory while Chapter 5 is a specific one.

In Chapter 3, we lay out how the theory can be used to obtain the population distributions of each mode, both directly and with analytic expressions. Chapter 4 is dedicated to coherence functions which we solve for numerically and approximatively in two ways, a more involved Fokker-Planck scheme and a simpler static limit approximation. The coherence functions that we use are the first order correlation of one mode and the coherence decay of Rabi regime Josephson oscillations between two modes.

In Chapter 5, we apply the theory to the tight-binding model of a double well potential. We extract the population distribution of the symmetric and antisymmetric modes of the double well for different detuning between the wells and we show example calculations of first and second order coherence functions with each to the three approaches mentioned above. Finally we conclude and suggest some future work in Chapter 6.

Chapter 2

Pumping and Interaction Model

This chapter constructs the equation of motion for the reduced density matrix describing Bose Einstein condensates of polaritons [Deng 10, Keel 07, Scul 97], whose general form is, (1.45),

$$\dot{\rho} = \mathcal{L}_p\rho + \mathcal{L}_d\rho - i[H, \rho]. \tag{2.1}$$

Here $\mathcal{L}_p, \mathcal{L}_d$ are the superoperators describing the pumping and damping of the low-energy polariton states. The Hamiltonian, H, is for the dynamics and interactions of the condensate modes. We already reached a form for $\mathcal{L}_d$ in our introduction to open quantum systems (Sec. 1.2.2). While the physics of condensate formation was also described (Sec. 1.1.5), we have yet to obtain an explicit form for the pumping, $\mathcal{L}_p$. This shall be the first goal of this chapter. The second aim is to describe the Hamiltonian, H. We seek throughout to maintain the theory in the most general form possible, such that it can be applied to a wide range of configurations.

Towards reaching $\mathcal{L}_p$, we first describe the characteristics of the reservoirs and condensates which we use onwards to develop our model of the pumping (Sec. 2.1). We then derive a form for $\mathcal{L}_p$ in a simplified pumping model (Sec. 2.2) which is then expanded into the general theory (Sec. 2.3). We also introduce the pumping parametrization we will use throughout the remainder of the thesis (Sec. 2.4).

In the introduction, we explained how condensate polaritons can be trapped in a photonic or excitonic potential and how their excitonic component interacts (Sec. 1.1.5). The second part of the chapter describes how we choose orbitals based on these potentials and how interactions are approximated, leading to soluble form for H, (Sec. 2.5).

2.1 Key Features of the Reservoirs and Condensates

In this section we give a brief description of the essential features of reservoir and condensate polaritons which our model will incorporate. We extract these features from the exposé presented in Chapter 1.

In our model, both for reservoirs and condensate modes, we suppose that polaritons are the elementary excitations of the microcavity system [Hopf58]; their internal structure was introduced and discussed in the introduction (Sec. 1.1.3). Towards condensation, the laser-induced high energy reservoir polaritons have thermalized via polariton-polariton interactions, and cooled down through polariton-phonon interactions [Deng10], near the bottleneck (highly excitonic lower region) of the lower dispersion relation (Sec. 1.1.5); only these reservoir polaritons enter our model. Condensates are trapped (photonic, excitonic disorder; quantum well, cavity patterning; reservoir repulsion) and are separated from one another either because of their spatial profile or the single-particle state energy levels they occupy (Sec. 1.1.5). Their nonequilibrium nature enables BEC to form at energies other than the lowest level [East08] and distinction between spatially superimposed condensates is based on linewidth. Spatial trapping causes the condensates to spread in momentum along the bottom of the lower branch [Kasp06].

Reservoir polaritons are much heavier, $m = \left(\frac{d^2E}{dk^2}\right)^{-1}$, than condensate polaritons, m', and are therefore effectively immobile on the long length scale relevant to the condensate [Wout08b]. The condensate modes densities can overlap with several reservoirs and can thereby be replenished by several distinct sources [Rich05].

Alongside with the condensate formation mechanism, stimulated scattering, its decay outside the cavity and the excitonic-based polariton-polariton interactions (Sec. 1.2.3), these observations are all the essentials that are needed to derive our model.

2.2 One Reservoir Pumping Two Modes

In this section, we first present the general approach to the one-reservoir, two-modes problem. We then detail the two steps which lead up to our model expression.

General Approach to the Problem

As is often done in mesoscopic physics[Altl10], we aim for a pumping model which captures the essential physics leading to the formation of condensates, and can be parameterized with experimental results. Rather than deriving directly a Liouville superoperator for many reservoirs arbitrarily pumping many modes (Sec.2.3), we first solve a simplified model: one reservoir pumping two condensates. This simplified treatment was obtained independently but shows similarity to that in [Sing80]. We use the treatment to generalize towards the many-reservoir, many-mode model.

The one reservoir, two modes problem is analogous to the two-mode laser. This problem has been treated extensively with rate equations and in the semiclassical approximation[Hake75, Puri01]. The Heisenberg-Langevin approach has also been utilized[Hake75, Scul97]. While a full quantum approach was also used, it had to be tailored to a specific problem where each mode is associated with a distinct transition[Sing80]. In the other approaches, the energy detuning between the modes and their different rotating rates could be used to isolate the dynamics of the quantities of interest. All through these approaches, the underlying key principle resides in the fact that the field is the synergetic component of the system, it is responsible for the common phase of the order parameter and the non-locality. The matter component provides the system non-linearities.

In the full quantum two-mode laser[Sing80] a restriction had to be applied in order to make the problem soluble in closed form. Each mode had to be attributed a separate lower level in the transition. This obliged a break in degeneracy at this level with, e.g., Zeeman splitting. This restriction does not apply in the case of a one-reservoir two-mode condensate pumping model. This is because, rather than having discrete transition energies, the polariton dispersion relation is continuous, and the distinct levels appear naturally; transitions occur between any two localized states on the dispersion.

Thus we consider, as shown in Figure 2.1, a reservoir of many, labeled by i, higher-energy, incoherent polariton states above the bottleneck region, $|a\rangle_i$. These are driven through final-state stimulation into the lowest-energy orbitals, $|n\rangle, |p\rangle$, generating the condensates, while by-product states, $|b_1\rangle_i, |b_2\rangle_i$, take up the excess momentum and energy. The by-product states can be polaritons or outgoing phonons. Within our approach, these processes, polariton-polariton scattering and phonon emission, lead to the same form for $\mathcal{L}_p$. This model can be solved in closed form, in the interaction picture, using second-order perturbation theory in the scattering strength[Hamm05] and

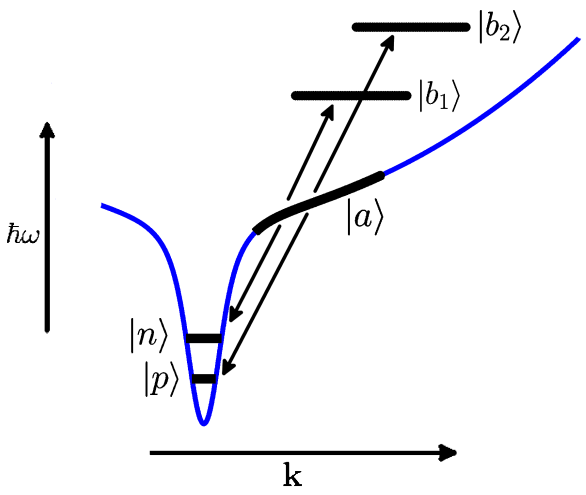

Figure 2.1: Schematic of model of condensate formation. Reservoir polaritons $|a\rangle_i$ enter the condensate modes,$|n\rangle$, $|n\rangle$, through stimulated scattering. By-product polaritons/excitons, $|b_1\rangle_i$, $|b_2\rangle_i$, carry the excess momentum, energy.

an adiabatic elimination procedure[Sing 80]. This provides us with the theoretical bridge towards our many reservoirs pumping many modes derivation (Sec. 2.3).

The interaction picture Hamiltonian describing the scattering from the i^{th} reservoir state, with annihilation operator, $(c_a)_i$, into low-energy polaritons (a_1, a_2), and some by-products $(c_{b_1}, c_{b_2})_i$ is,

$$\mathcal{H}_p = \sum_i g_1 a_1^\dagger (c_{b_1}^\dagger \frac{(c_a)^2}{\sqrt{2}})_i + g_2 a_2^\dagger (c_{b_2}^\dagger \frac{(c_a)^2}{\sqrt{2}})_i + \text{H.c.} \tag{2.2}$$

$\mathcal{H}_p$ is written for the case of polariton-polariton scattering; $\frac{(c_a)^2}{\sqrt{2}} c_{b_1}^\dagger$ acting on a state with two reservoir polaritons and no by-product polariton, $|2,0\rangle$, gives $|0,1\rangle$. The operator $\frac{(c_a)^2}{\sqrt{2}}$ becomes c_a when phonons are the by-products, $c_a c_{b_1}^\dagger |1,0\rangle = |0,1\rangle$. But reservoir levels will be traced over in our expension and the final expression is parameterized from experiments; the form of the reservoir operators do not affect the theory. The scattering matrix elements, g_1, for example, is given by

$$g_1 = \int dr dr' V(r-r') \phi_1^*(r) \phi_{b1,i}^*(r') \phi_{a,i}(r) \phi_{a,i}(r'), \tag{2.3}$$

where $V(r-r')$ is the potential two between excitons at points r and r'. Since reservoir polaritons are much more localized than those of the condensate, $V(r-r')$ can be

approximated by a point interaction given by $V_o\delta(r-r')$, which provides g_1 the form

$$\begin{aligned} g_1 &\approx \int dr V_0 \phi_1^*(r)\phi_{b1,i}^*(r)\phi_{a,i}(r)\phi_{a,i}(r) \\ &\propto \phi_1^*(r_i), \end{aligned} \tag{2.4}$$

where $\phi_1^*(r_i)$ is the amplitude of the condensate orbital at the reservoir location. Matrix elements, $g_1,\ g_2$, are proportional to the condensate amplitude at reservoir location, r_i.

We introduce the projection of the condensate-reservoir density matrix onto the i^{th} reservoir state, $\rho_i = \text{Tr}_{j\neq i}\,\hat{\rho}$, and its matrix elements,

$$\rho_i = \rho_{nmpq}^{\alpha_i\beta_i}\,|\,n\rangle\langle m\,|\otimes|\,p\rangle\langle q\,|\otimes|\,\alpha_i\rangle\langle\beta_i\,|, \tag{2.5}$$

with $\alpha_i, \beta_i \in \{a, b_1, b_2\}$ and n, m (p, q) refering to the matrix elements of the first (second) mode. The sum over i provides the composite density matrix, ρ, with matrix elements $\rho_{nmpq}^{\alpha\beta} = \sum_i \rho_{nmpq}^{\alpha_i\beta_i}$, for which our simplified from for the "density" Hamiltonian, $\mathcal{H}_p$ (2.2), translates into (we use the version of $\mathcal{H}_p$ phonon by-products for notational simplicity),

$$H_p = \sum_{i=1,2} g_i\big(a_i^\dagger c_{b_i}^\dagger c_a + c_a^\dagger c_{b_i} a_i\big), \tag{2.6}$$

and the operators, a_i, c_{b_i}, are now acting on the composite levels, see Fig. 2.2. We have therefore greatly simplified the problem by treating reservoir levels $|a\rangle_i$ with a single upper level $|a\rangle$, and similarly with $|b_1\rangle_i,\ |b_2\rangle_i$ becoming $|b_1\rangle,\ |b_2\rangle$.

The remainder of this section revolves around solving the following schematic relation,

$$\dot{\rho} = -i[H_p, \rho] - \gamma_r\rho_{[a,b_i\to\phi]} + \lambda_r\rho_{[\phi\to a]} + (\mathcal{L}_d\rho). \tag{2.7}$$

The term proportional to λ_r accounts for the replenishing of upper level $|a\rangle$ from an other vacuum state $|\phi\rangle$, which is schematically depicted by the subscript $[\phi\to a]$. This corresponds to the relaxation of laser generated higher energy polaritons into the reservoir. The γ_r term is the decay of $|a\rangle, |b_i\rangle$ levels via channels other than the condensates, e.g., spontaneous emission into outside cavity modes, schematically depicted by $[a, b_i\to\phi]$. Linking these two processes to a common, vacuum level, $|\phi\rangle$, will allow to algebraically manipulate these $\lambda_r,\ \gamma$ terms through rate equations, and eliminate the levels, leaving only the degrees of freedom which pertain to the condensate, $\rho_{nmpq}^{\alpha_i\beta_i}\to\rho_{nmpq}$.

Two different time scales are associated with the processes in (2.7). The replen-

ishing λ_r and the relaxation γ_r are much faster than the dynamics of the condensates, $-i[H_p, \rho]$, $\mathcal{L}_d\rho$ (1.43). The two different time scales involved allow us to make a twofold adiabatic expansion. First we isolate the λ_r dynamics into an effective pumping rate r. We then solve for a traced form, $\mathrm{Tr}_{a,b_i}[\rho]$, of the slow varying processes, $\dot{\rho} \approx -i[H_p, \rho']$, on a time scale for which ρ' appears to be stationary, $\dot{\rho}' \approx 0$, with respect to the γ_r dynamics. The end result is a parametrized equation which only contains the condensate's degrees of freedom.

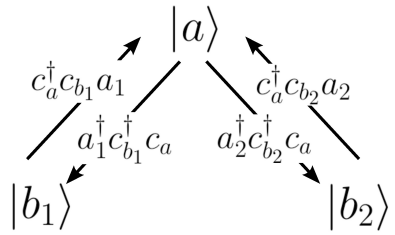

Figure 2.2: Transitions generated by Hamiltonian H_p. This configuration allows the pumping to be solved exactly.

In bosonic systems, Hamiltonian commutators often generate, potentially infinite, recursive sets of equations which all have to be solved in order to reach a solution. The level configuration presented here generates a Hamiltonian which does not have this feature, making our problem soluble in closed form. The three levels make 3×3=9 density matrix elements which need to be visited through the action of the Hamiltonian, H_p, in such a way that the number of particles in the system is conserved. We express this criteria diagrammatically by placing H_p (2.6) in a transition diagram, Fig. 2.2. The diagram should not possess any loops where we can pass through a transition, in the same direction, more than once, i.e. every transition between two levels should only be paired with its Hermitian conjugate. The general pumping problem discussed below, Section 2.3 (2.51), also has this feature. Two quanta (one for bra, the other for ket) are being passed between the condensate and the levels, allowing to survey the 9 matrix elements in closed form.

Eliminating the Non-Condensate Degrees of Freedom from the Replenishing Component of the Model

We now perform the first manipulation highlighted above and in (2.7). We eliminate the reservoir levels degrees of freedom in the λ_r term of Eq. (2.7). We do so by introducing the density matrix for our reservoir vacuum level, $\Phi = \rho^{\phi\phi}|\phi\rangle\langle\phi|$, writing

the equation of motion for $\rho \otimes \Phi$, projected onto $|\phi\rangle$, i.e. the population of $|\phi\rangle$,

$$\langle\phi|\frac{d(\rho\otimes\Phi)}{dt}|\phi\rangle = \cancelto{0}{-i\langle\phi|[H_p,\rho\otimes\Phi]|\phi\rangle} - \lambda_r\langle\phi|\rho\otimes\Phi|\phi\rangle + \gamma_r\sum_{\alpha=a,b_i}\langle\alpha|\rho\otimes\Phi|\alpha\rangle. \quad (2.8)$$

Notice the sign changes in front of λ_r, γ_r with respect to Eq. (2.7). On the r.h.s., the H_p term vanishes identically, $[H_p, \Phi] = 0$. The l.h.s. is also zero,

$$\langle\phi|\frac{d(\rho\otimes\Phi)}{dt}|\phi\rangle = \langle\phi|\dot{\rho}'\otimes\Phi|\phi\rangle + \langle\phi|\rho\otimes\dot{\Phi}|\phi\rangle = 0, \quad (2.9)$$

since the condensate is assumed to appear stationary and the level $|\phi\rangle$ is considered stationary. We can therefore read from (2.8) the steady-state matrix elements equation

$$0 = -\lambda_r\rho^{\phi\phi}_{nmpq} + \gamma_r(\rho^{aa}_{nmpq} + \rho^{b_1b_1}_{nmpq} + \rho^{b_2b_2}_{nmpq}), \quad (2.10)$$

or

$$\lambda_r\rho^{\phi\phi}_{nmpq} = \gamma_r(\rho^{aa}_{nmpq} + \rho^{b_1b_1}_{nmpq} + \rho^{b_2b_2}_{nmpq}), \quad (2.11)$$

which we use in conjunction with the trace over all the levels, $\mathrm{Tr}_{a,b_i,\phi}[\rho\otimes\Phi]$,

$$\rho_{nmpq} = \rho^{\phi\phi}_{nmpq} + \rho^{aa}_{nmpq} + \rho^{b_1b_1}_{nmpq} + \rho^{b_2b_2}_{nmpq} \quad (2.12)$$

or

$$\rho^{aa}_{nmpq} + \rho^{b_1b_1}_{nmpq} + \rho^{b_2b_2}_{nmpq} = \rho_{nmpq} - \rho^{\phi\phi}_{nmpq}. \quad (2.13)$$

Placing (2.13) into (2.11) and solving for $\rho^{\phi\phi}_{nmpq}$ gives

$$\lambda_r\rho^{\phi\phi}_{nmpq} = \gamma_r(\rho_{nmpq} - \rho^{\phi\phi}_{nmpq}) \quad (2.14)$$

$$\rho^{\phi\phi}_{nmpq} = \frac{\gamma_r}{\lambda_r+\gamma_r}\rho_{nmpq}. \quad (2.15)$$

Hence

$$\lambda_r\rho^{\phi\phi}_{nmpq} = \frac{\lambda_r\gamma_r}{\lambda_r+\gamma_r}\rho_{nmpq} = r\rho_{nmpq}, \quad (2.16)$$

and our schematic relation (2.7) now becomes

$$\dot{\rho} = -i[H_p,\rho] - \gamma_r\rho_{[a,b_i\to\phi]} + r\rho. \quad (2.17)$$

We obtained an effective pumping rate, r, which does away with external degrees of freedom [Scul 97]. Expressions for the term proportional to γ_r involves levels $|a\rangle, |b_i\rangle$,

which will be eliminated in the trace process below.

Performing the Adiabatic Expansion to Isolate the Condensate Dynamics.

Next we write the contribution to the equation of motion for the scattering into the condensate, $\dot{\rho} = -i[H_p, \rho]$, the slowly varying processes of (2.17) (the polarization, e.g. $\rho^{\alpha\beta}_{nmpq}, \alpha \neq \beta$, do not exhibit fast oscillation in the interaction picture). These will generate the traced form, $\dot{\rho}^{aa}_{nmpq} + \dot{\rho}^{b_1b_1}_{nmpq} + \dot{\rho}^{b_2b_2}_{nmpq}$, mentioned above. The components of $-i[H_p, \rho]$, are

$$\dot{\rho}^{aa}_{nmpq} = -i\big[g_1\sqrt{n+1}\rho^{b_1a}_{n+1mpq} + g_2\sqrt{p+1}\rho^{b_2a}_{nmp+1q} - g_1\sqrt{m+1}\rho^{ab_1}_{nm+1pq} - g_2\sqrt{q+1}\rho^{ab_2}_{nmpq+1}\big] \tag{2.18}$$

$$\dot{\rho}^{b_1b_1}_{nmpq} = -i\big[g_1\sqrt{n}\rho^{ab_1}_{n-1mpq} - g_1\sqrt{m}\rho^{b_1a}_{nm-1pq}\big] \tag{2.19}$$

$$\dot{\rho}^{b_2b_2}_{nmpq} = -i\big[g_2\sqrt{p}\rho^{ab_2}_{nmp-1q} - g_2\sqrt{q}\rho^{b_2a}_{nmpq-1}\big]. \tag{2.20}$$

We point out the standard form of the prefactors on the r.h.s., such as $\sqrt{n+1}$, which generate the stimulated scattering (amplification) and, along with inversion, the term in r, are responsible for macroscopic occupation of the low-energy modes, i.e., condensation. In total there are 8 matrix elements on the r.h.s. of Eqs. (2.18−2.20) which we need to solve for. We do so with three sets of full pumping equation matrix elements obtained from (2.17). The set we use to solve the aa part, (2.18), is

$$\dot{\rho}^{aa}_{nmpq} = (\text{Eq. 2.18, rhs}) - \gamma_r\rho^{aa}_{nmpq} + r\rho_{nmpq} \tag{2.21}$$

$$\dot{\rho}^{ab_1}_{nm+1pq} = -i\big[g_1\sqrt{n+1}\rho^{b_1b_1}_{n+1m+1pq} + g_2\sqrt{p+1}\rho^{b_2b_1}_{nm+1p+1q} - g_1\sqrt{m+1}\rho^{aa}_{nmpq}\big] - \gamma_r\rho^{ab_1}_{nm+1pq} \tag{2.22}$$

$$\dot{\rho}^{b_1a}_{n+1mpq} = -i\big[g_1\sqrt{n+1}\rho^{aa}_{nmpq} - g_1\sqrt{m+1}\rho^{b_1b_1}_{n+1m+1pq} - g_2\sqrt{q+1}\rho^{b_1b_2}_{n+1mpq+1}\big] - \gamma_r\rho^{b_1a}_{n+1mpq} \tag{2.23}$$

$$\dot{\rho}^{ab_2}_{nmpq+1} = -i\big[g_1\sqrt{n+1}\rho^{b_1b_2}_{n+1mpq+1} + g_2\sqrt{p+1}\rho^{b_2b_2}_{nmp+1q+1} - g_2\sqrt{q+1}\rho^{aa}_{nmpq}\big] - \gamma_r\rho^{ab_2}_{nmpq+1} \tag{2.24}$$

$$\dot{\rho}^{b_2a}_{nmp+1q} = -i\big[g_2\sqrt{p+1}\rho^{aa}_{nmpq} - g_1\sqrt{m+1}\rho^{b_2b_1}_{nm+1p+1q} - g_2\sqrt{q+1}\rho^{b_2b_2}_{nmp+1q+1}\big] - \gamma_r\rho^{b_2a}_{nmp+1q} \tag{2.25}$$

$$\dot{\rho}^{b_1b_2}_{n+1mpq+1} = -i\big[g_1\sqrt{n+1}\rho^{ab_2}_{nmpq+1} - g_2\sqrt{q+1}\rho^{b_1a}_{n+1mpq}\big] - \gamma_r\rho^{b_1b_2}_{n+1mpq+1} \tag{2.26}$$

$$\dot{\rho}^{b_2b_1}_{nm+1p+1q} = -i\big[g_2\sqrt{p+1}\rho^{ab_1}_{nm+1pq} - g_1\sqrt{m+1}\rho^{b_2a}_{nmp+1q}\big] - \gamma_r\rho^{b_2b_1}_{nm+1p+1q} \tag{2.27}$$

$$\dot{\rho}^{b_1b_1}_{n+1m+1pq} = -i\big[g_1\sqrt{n+1}\rho^{ab_1}_{nm+1pq} - g_1\sqrt{m+1}\rho^{b_1a}_{n+1mpq}\big] - \gamma_r\rho^{b_1b_1}_{n+1m+1pq} \tag{2.28}$$

$$\dot{\rho}^{b_2b_2}_{nmp+1q+1} = -i\big[g_2\sqrt{p+1}\rho^{ab_2}_{nmpq+1} - g_2\sqrt{q+1}\rho^{b_2a}_{nmp+1q}\big] - \gamma_r\rho^{b_2b_2}_{nmp+1q+1} \tag{2.29}$$

The sets for b_1b_1, (2.19) and b_2b_2, (2.20), are Eqs. (2.21−2.29) shifted according to : $n, m \to n-1, m-1$ and $p, q \to p-1, q-1$, respectively. Notice that the evolution of all the elements on the r.h.s. of Eqs (2.21−2.29) is contained within the set of equations, i.e. it can be solved in closed form. The natural way to solve a set of coupled equations

is in matrix form; we write Eq. (2.21−2.29) and their shifted version as,

$$\dot{R} = -MR + A \qquad \dot{R}' = -M'R' + A' \qquad \text{and} \qquad \dot{R}'' = -M''R'' + A''. \tag{2.30}$$

The matrix M and each of the R and A vectors are presented on page 46. The matrices M' and M'' are obtained with the shift substitution mentioned above. The R vectors are formed from elements of the density matrix in which two quanta are being passed between the reservoir levels and the condensate modes. The A vectors are the driving terms.

We solve for R adiabatically i.e. assuming A (ρ_{nmpq}) doesn't change over the time scale set by γ_r. Formally ([Scul97], Appendix 11.A), this is performed by using the integrating factor $e^{\int_{-\infty}^{t'} M dt''} = e^{Mt''|_{-\infty}^{t'}} = e^{Mt'}$, giving,

$$e^{Mt'}\dot{R} + e^{Mt'}MR = e^{Mt'}A \tag{2.31}$$

$$\frac{\mathrm{d}(e^{Mt'}R)}{\mathrm{d}t'} = e^{Mt'}A \tag{2.32}$$

$$\int_0^{(e^{Mt}R)} d(e^{Mt'}R) = \int_{-\infty}^{t} e^{Mt'}A dt'. \tag{2.33}$$

We assume that the condensate field term, $e^{Mt}R$, slowly builds up, starting from zero when t is at $-\infty$, and that on this scale the driving term, A, is independent of time. Thus (2.33) solves into

$$e^{Mt}R \simeq e^{Mt}M^{-1}A \tag{2.34}$$

or

$$R \simeq M^{-1}A, \tag{2.35}$$

where the 8 matrix elements we seek are within R, R', R''. We shall obtain the inverse matrices $M^{-1}, M'^{-1}, M''^{-1}$ through the identity $M^{-1} = \frac{C^T}{|M|}$ or $M^{-1} = \frac{C}{|M|}$ since M is symmetric; C is the cofactor matrix. The use of cofactors and determinants will be advantageous in the derivation of the generalized form below (Sec.2.3). Mathematica can provide these terms easily.

Obtaining the Model Expression

At last, we extract the 8 terms needed in (2.18−2.20),

$$\rho^{ab_1}_{nm+1pq} = rM^{-1}_{21}\rho_{nmpq} \tag{2.36}$$
$$\rho^{b_1a}_{n+1mpq} = rM^{-1}_{31}\rho_{nmpq} \tag{2.37}$$
$$\rho^{ab_2}_{nmpq+1} = rM^{-1}_{41}\rho_{nmpq} \tag{2.38}$$
$$\rho^{b_2a}_{nmp+1q} = rM^{-1}_{51}\rho_{nmpq} \tag{2.39}$$

$$\rho^{ab_1}_{n-1mpq} = rM'^{-1}_{21}\rho_{n-1m-1pq} \tag{2.40}$$
$$\rho^{b_1a}_{nm-1pq} = rM'^{-1}_{31}\rho_{n-1m-1pq} \tag{2.41}$$

$$\rho^{ab_2}_{nmp-1q} = rM''^{-1}_{41}\rho_{nmp-1q-1} \tag{2.42}$$
$$\rho^{b_2a}_{nmpq-1} = rM''^{-1}_{51}\rho_{nmp-1q-1}. \tag{2.43}$$

and (2.18−2.20) become

$$\begin{aligned}\dot\rho^{aa}_{nmpq} = &-i\big[g_1\sqrt{n+1}\,M^{-1}_{31} + g_2\sqrt{p+1}\,M^{-1}_{51} \\ &\qquad - g_1\sqrt{m+1}\,M^{-1}_{21} - g_2\sqrt{q+1}\,M^{-1}_{41}\big]r\rho_{nmpq}\end{aligned} \tag{2.44}$$
$$\dot\rho^{b_1b_1}_{nmpq} = -i\big[g_1\sqrt{n}M'^{-1}_{21} - g_1\sqrt{m}M'^{-1}_{31}\big]r\rho_{n-1m-1pq} \tag{2.45}$$
$$\dot\rho^{b_2b_2}_{nmpq} = -i\big[g_2\sqrt{p}M''^{-1}_{41} - g_2\sqrt{q}M''^{-1}_{51}\big]r\rho_{nmp-1q-1}. \tag{2.46}$$

which simplify nicely into the form, $\dot\rho^{aa}_{nmpq} + \dot\rho^{b_1b_1}_{nmpq} + \dot\rho^{b_2b_2}_{nmpq} = \mathcal{L}_p\rho_{nmpq}$,

$$\begin{aligned}\mathcal{L}_p\rho_{nmpq} = &-r\frac{\big(g_1^2(n-m)+g_2^2(p-q)\big)^2 + \gamma_r^2\big(g_1^2(n+m+2)+g_2^2(p+q+2)\big)}{\big(g_1^2(n-m)+g_2^2(p-q)\big)^2 + 2\gamma_r^2\big(g_1^2(n+m+2)+g_2^2(p+q+2)\big)+\gamma_r^4}\rho_{nmpq} \\ &+\frac{2r\gamma_r^2g_1^2\sqrt{nm}}{\big(g_1^2(n-m)+g_2^2(p-q)\big)^2 + 2\gamma_r^2\big(g_1^2(n+m)+g_2^2(p+q+2)\big)+\gamma_r^4}\rho_{n-1m-1pq} \\ &+\frac{2r\gamma_r^2g_2^2\sqrt{pq}}{\big(g_1^2(n-m)+g_2^2(p-q)\big)^2 + 2\gamma_r^2\big(g_1^2(n+m+2)+g_2^2(p+q)\big)+\gamma_r^4}\rho_{nmp-1q-1},\end{aligned} \tag{2.47}$$

We observe that, as in the form for the damping, $\mathcal{L}_d$ (1.44), the expression obtained contains only the condensate degrees of freedom. We shall postpone the parametrization of $\mathcal{L}_p$ in a notation which reflects the pumping physics (Sec.2.4) until a generalized pumping expression is derived below. Here we only point out that the two time scales we exploited in the expansion (2.7) imply that $g_{1,2} \ll \gamma_r$ which in the denominators translates as $g^4_{1,2} \ll \gamma_r^2 g^2_{1,2} \ll \gamma_r^4$. The constant term, γ_r^4, is larger than the others for

small occupation but will inevitably be comparable at large occupations and therefore generates saturation. The denominators generate saturation in the condensation occupation.

We see also that the minus sign in front of the term ρ_{nmpq} means that its occupancy leaves towards higher levels while the levels below, $\rho_{n-1m-1pq}$, $\rho_{nmp-1q-1}$, with their positive signs, replenish it. We have pumping action.

$$R = \begin{pmatrix} \rho^{aa}_{nmpq} \\ \rho^{ab_1}_{nm+1pq} \\ \rho^{b_1a}_{n+1mpq} \\ \rho^{ab_2}_{nmpq+1} \\ \rho^{b_2a}_{nmp+1q} \\ \rho^{b_1b_2}_{n+1mpq+1} \\ \rho^{b_2b_1}_{nm+1p+1q} \\ \rho^{b_1b_1}_{n+1m+1pq} \\ \rho^{b_2b_2}_{nmp+1q+1} \end{pmatrix} \qquad R' = \begin{pmatrix} \rho^{aa}_{n\text{-}1m\text{-}1pq} \\ \rho^{ab_1}_{n\text{-}1mpq} \\ \rho^{b_1a}_{nm\text{-}1pq} \\ \rho^{ab_2}_{n\text{-}1m\text{-}1pq+1} \\ \rho^{b_2a}_{n\text{-}1m\text{-}1p+1q} \\ \rho^{b_1b_2}_{nm\text{-}1pq+1} \\ \rho^{b_2b_1}_{n\text{-}1mp+1q} \\ \rho^{b_1b_1}_{nmpq} \\ \rho^{b_2b_2}_{n\text{-}1m\text{-}1p+1q+1} \end{pmatrix} \qquad R'' = \begin{pmatrix} \rho^{aa}_{nmp\text{-}1q\text{-}1} \\ \rho^{ab_1}_{nm+1p\text{-}1q\text{-}1} \\ \rho^{b_1a}_{n+1mp\text{-}1q\text{-}1} \\ \rho^{ab_2}_{nmp\text{-}1q} \\ \rho^{b_2a}_{nmpq\text{-}1} \\ \rho^{b_1b_2}_{n+1mp\text{-}1q} \\ \rho^{b_2b_1}_{nm+1pq\text{-}1} \\ \rho^{b_1b_1}_{n+1m+1p\text{-}1q\text{-}1} \\ \rho^{b_2b_2}_{nmpq} \end{pmatrix} \tag{2.48}$$

$$M = \begin{pmatrix} \gamma_r & -ig_1\sqrt{m+1} & ig_1\sqrt{n+1} & -ig_2\sqrt{q+1} & ig_2\sqrt{p+1} & 0 & 0 & 0 & 0 \\ -ig_1\sqrt{m+1} & \gamma_r & 0 & 0 & 0 & 0 & ig_2\sqrt{p+1} & ig_1\sqrt{n+1} & 0 \\ ig_1\sqrt{n+1} & 0 & \gamma_r & 0 & 0 & -ig_2\sqrt{q+1} & 0 & -ig_1\sqrt{m+1} & 0 \\ -ig_2\sqrt{q+1} & 0 & 0 & \gamma_r & 0 & ig_1\sqrt{n+1} & 0 & 0 & ig_2\sqrt{p+1} \\ ig_2\sqrt{p+1} & 0 & 0 & 0 & \gamma_r & 0 & -ig_1\sqrt{m+1} & 0 & -ig_2\sqrt{q+1} \\ 0 & 0 & -ig_2\sqrt{q+1} & ig_1\sqrt{n+1} & 0 & \gamma_r & 0 & 0 & 0 \\ 0 & ig_2\sqrt{p+1} & 0 & 0 & -ig_1\sqrt{m+1} & 0 & \gamma_r & 0 & 0 \\ 0 & ig_1\sqrt{n+1} & -ig_1\sqrt{m+1} & 0 & 0 & 0 & 0 & \gamma_r & 0 \\ 0 & 0 & 0 & ig_2\sqrt{p+1} & -ig_2\sqrt{q+1} & 0 & 0 & 0 & \gamma_r \end{pmatrix} \tag{2.49}$$

$$A = r \begin{pmatrix} \rho_{nmpq} \\ 0 \\ 0 \\ 0 \\ 0 \\ 0 \\ 0 \\ 0 \\ 0 \end{pmatrix} \qquad A' = r \begin{pmatrix} \rho_{n\text{-}1m\text{-}1pq} \\ 0 \\ 0 \\ 0 \\ 0 \\ 0 \\ 0 \\ 0 \\ 0 \end{pmatrix} \qquad A'' = r \begin{pmatrix} \rho_{nmp\text{-}1q\text{-}1} \\ 0 \\ 0 \\ 0 \\ 0 \\ 0 \\ 0 \\ 0 \\ 0 \end{pmatrix} \tag{2.50}$$

2.3 Many Reservoirs Pumping Many Modes

We now derive the expression for $\mathcal{L}_p$ in the general case where u reservoirs replenish v condensates. We shall make use of the derivation above and, while still being driven by the physics, draw guidance from algebraic patterns which appear within it.

In deriving $\mathcal{L}_p$ (2.47) above, we made use of brute analytic force. We learned by doing this, that even though the determinant of $|M|$ goes as $\mathcal{O}(\gamma_r^9)$, its inverse, $M^{-1} = \frac{C^T}{|M|}$, simplifies and the form left in the denominator only goes up to $\mathcal{O}(\gamma_r^4)$; the same as in the one-mode problem [Scul97]. There is an algebraic pattern to be exploited in solving the types of many-reservoir pumping many-mode problems which obey the configuration in Fig.2.2. One can think that this pattern should indeed occur when observing that we started with individual reservoir polaritons in our Hamiltonian (2.2) which we then grouped into a single, composite three-level system (2.6).

Indeed, in the single reservoir, two-mode Hamiltonian (2.6), the choice of grouping individual states, $|a\rangle_i$, together to form a single state, $|a\rangle$, was theoretically convenient but should not distract us from the actual physical problem. Here we shall group the individual reservoir polariton states, $|a\rangle_i$, into distinct reservoir states, $|a_i\rangle$, and keep the notation separate for each of them. By doing this, each reservoir obtains its own adiabatic term (2.9) and therefore its own effective pumping rate, r_i.

In order to continue with the second part of our general adiabatic expansion, we recast the one reservoir, two modes notation into the general u-reservoirs, v-modes notation. The composite interaction picture Hamiltonian (2.6) now takes the form,

$$H_p = \sum_{i,j} g_{ij}\big(a_j^\dagger c_{b_{ij}}^\dagger c_{a_i} + c_{a_i}^\dagger c_{b_{ij}} a_j\big), \tag{2.51}$$

with i labeling the reservoirs and j the modes. The v-modes reduced density matrix elements take the form $\rho_{n_1 n_2.. \; n_j..}^{m_1 m_2.. m_j..}$. We see from (2.51) that for each of the u levels, $|a_i\rangle$, there are now v levels, $|b_{ij}\rangle$, therefore making $1+v$ levels per reservoir. The matrix M_i, which associates the i^{th} reservoir with all v condensates, will therefore have $(1+v)^2 \times (1+v)^2$ elements. And the full matrix is a Kronecker sum, $M = \sum_i I \otimes .. \otimes M_i \otimes .. \otimes I$. In taking the adiabatic expansion however, each term of the Kronecker sum gives its own instantaneous change, r_i, to the composite density matrix, $\dot{\rho}_{n_1 n_2..}^{m_1 m_2..}$, and can therefore be solved for independently. Since $(A \otimes B)^{-1} = A^{-1} \otimes B^{-1}$, we can focus on obtaining M_i^{-1}, and the trace over the reservoir levels, $\mathrm{Tr}_{a_i b_{ij}} \rho$, shall provide the summation which is explicit in the Kronecker sum.

For the i^{th} reservoir, the trace is $\dot{\rho}^{m_1 m_2 .., a_i a_i}_{n_1 n_2 ..} + \sum_j \dot{\rho}^{m_1 m_2 .., b_{ij} b_{ij}}_{n_1 n_2 ..}$ with each element given by,

$$\begin{aligned}
\dot{\rho}^{m_1 m_2 .., a_i a_i}_{n_1 n_2 ..} &= \langle a_i | -i[H_p, \rho] | a_i \rangle && (2.52)\\
&= -i \sum_j \Big[g_{ij} \sqrt{n_j + 1} \rho^{m_1 .. m_j .., b_{ij} a_i}_{n_1 .. n_j + 1 ..} - g_{ij} \sqrt{m_j + 1} \rho^{m_1 .. m_j + 1 .., a_i b_{ij}}_{n_1 .. n_j ..} \Big] && (2.53)\\
&= \sum_j \Big[f^{(i)}_{2j} \rho^{m_1 .. m_j .., b_{ij} a_i}_{n_1 .. n_j + 1 ..} + f^{(i)}_{2j+1} \rho^{m_1 .. m_j + 1 .., a_i b_{ij}}_{n_1 .. n_j ..} \Big] && (2.54)\\
\dot{\rho}^{m_1 m_2 .., b_{ij} b_{ij}}_{n_1 n_2 ..} &= \langle b_{ij} | -i[H_p, \rho] | b_{ij} \rangle && (2.55)\\
&= -i \Big[g_{ij} \sqrt{n_j} \rho^{m_1 .. m_j .., a_i b_{ij}}_{n_1 .. n_j - 1 ..} - g_{ij} \sqrt{m_j} \rho^{m_1 .. m_j - 1 .., b_{ij} a_i}_{n_1 .. n_j ..} \Big] && (2.56)\\
&= f^{(ij)}_{2j} \rho^{m_1 .. m_j .., a_i b_{ij}}_{n_1 .. n_j - 1 ..} + f^{(ij)}_{2j+1} \rho^{m_1 .. m_j - 1 .., b_{ij} a_i}_{n_1 .. n_j ..} && (2.57)
\end{aligned}$$

with the first $2v + 1$ elements of $f^{(i)}, f^{(ij)}$ written in vector form,

$$f^{(i)}_{\{1,2v+1\}} = \begin{pmatrix} 0 \\ i g_{i1} \sqrt{m_1 + 1} \\ -i g_{i1} \sqrt{n_1 + 1} \\ .. \\ i g_{ij} \sqrt{m_j + 1} \\ -i g_{ij} \sqrt{n_j + 1} \\ .. \\ i g_{iv} \sqrt{m_v + 1} \\ -i g_{iv} \sqrt{n_v + 1} \end{pmatrix} \quad f^{(ij)}_{\{1,2v+1\}} = \begin{pmatrix} 0 \\ 0 \\ 0 \\ .. \\ -i g_{ij} \sqrt{n_j} \\ i g_{ij} \sqrt{m_j} \\ .. \\ 0 \\ 0 \end{pmatrix} \tag{2.58}$$

In our one reservoir, two modes derivation, we did not need the complete inverse of M. Rather, we only needed elements of the first column M^{-1}_{i1}, (2.36−2.43). Here this is, $(M_{\boldsymbol{i}})^{-1}_{i1} \equiv h^{(\boldsymbol{i})}_i$,

$$h^{(i)}_i = \frac{C^{(i)}_{i1}}{|M_i|} = \frac{C^{(i)}_{i1}}{\sum_j \mathfrak{m}^{(i)}_j C^{(i)}_{j1}}, \tag{2.59}$$

where we also adopted a simplified notation for the elements of the first column of the matrix, $(M_i)_{j1} \equiv \mathfrak{m}^{(i)}_j$. The determinant, $|M_i|$, is written as a column product of matrix and cofactor elements. We observe that all the cofactors in this column, $C^{(i)}_{i1}$, contain terms in the form,

$$\zeta = \gamma_r^{(v-1)^2} \Big(\sum_j g_{ij} (n_j + 1) + \gamma_r^2 \Big)^{(v-1)} \Big(\sum_j g_{ij} (m_j + 1) + \gamma_r^2 \Big)^{(v-1)} \tag{2.60}$$

and they cancel while forming the inverse matrix elements,

$$h_i^{(i)} = \frac{\zeta c_i^{(i)}}{\sum_j \mathfrak{m}_j^{(i)} \zeta c_j^{(i)}} = \frac{c_i^{(i)}}{\sum_j \mathfrak{m}_j^{(i)} c_j^{(i)}}. \tag{2.61}$$

This will indeed make the denominator stay of $\mathcal{O}(\gamma_r^4)$,

$$\log\big(\mathcal{O}(|M_i|)\big) - \log\big(\mathcal{O}(\zeta)\big) = (v+1)^2 - \big((v-1)^2 + 2\cdot 2(v-1)\big) = 4. \tag{2.62}$$

Physically, these terms cancel because when deciding to keep the notation separate for u reservoirs while grouping the $|a\rangle_i$ levels into $|a_i\rangle$ composite level, we also introduced transitions which otherwise would have been accounted for only once. These additional transitions while modifying the algebra do not change the power of the terms involved. They end up in the term ζ and cancel out in the derivation of the matrix element.

The first $2v+1$ terms of the simplified $c^{(i)}$ are

$$c^{(i)}_{\{1,2v+1\}} = \begin{pmatrix} \gamma_r\big(\sum_k g_{ik}^2(n_k+m_k+2) + \gamma_r^2\big) \\ ig_{i1}\sqrt{m_1+1}\big(\sum_k g_{ik}^2(m_k-n_k) + \gamma_r^2\big) \\ ig_{i1}\sqrt{n_1+1}\big(\sum_j g_{ik}^2(m_k-n_k) - \gamma_r^2\big) \\ .. \\ ig_{ij}\sqrt{m_j+1}\big(\sum_k g_{ik}^2(m_k-n_k) + \gamma_r^2\big) \\ ig_{ij}\sqrt{n_j+1}\big(\sum_k g_{ik}^2(m_k-n_k) - \gamma_r^2\big) \\ .. \\ ig_{iv}\sqrt{m_v+1}\big(\sum_k g_{ik}^2(m_k-n_k) + \gamma_r^2\big) \\ ig_{iv}\sqrt{n_v+1}\big(\sum_k g_{ik}^2(m_k-n_k) - \gamma_r^2\big) \end{pmatrix} \tag{2.63}$$

and the ones for $\mathfrak{m}_j^{(i)}$ are

$$\mathfrak{m}^{(i)}_{\{1,2v+1\}} = \begin{pmatrix} \gamma \\ -ig_{i1}\sqrt{m_1+1} \\ ig_{i1}\sqrt{n_1+1} \\ .. \\ -ig_{ij}\sqrt{m_j+1} \\ ig_{ij}\sqrt{n_j+1} \\ .. \\ -ig_{iv}\sqrt{m_v+1} \\ ig_{iv}\sqrt{n_v+1} \end{pmatrix}. \tag{2.64}$$

We note that the first column of M_i multiplies the first element of R_i, i.e. $\rho^{m_1 m_2..m_j.., a_1 a_1}_{n_1 n_2..n_j..}$. Looking back at Eq. (2.17), the first term in (2.64) originates from $\gamma_r\langle a_i|\rho|a_i\rangle$ while the next $2v$ terms originate from, $\langle a_i|-i[H_p,\rho]|a_i\rangle$ and all the other terms in that column

are zero. This explains why we only focused on the first $2v+1$ terms of $c_i^{(i)}$.

We now determine that the generalization of manipulating (2.36−2.43) into (2.18−2.20) to reach $\mathcal{L}_p$ (2.47) is,

$$\begin{aligned}\mathcal{L}_p\rho^{m_1m_2\cdot\cdot}_{n_1n_2\cdot\cdot} &= \sum_i \Big[f^{(i)}\cdot h^{(i)}\, r_i\rho^{m_1m_2\cdot\cdot}_{n_1n_2\cdot\cdot} + \sum_j f^{(ij)}\cdot h^{(ij)}\, r_i\rho^{m_1m_2\cdot\cdot m_j-1\cdot\cdot}_{n_1n_2\cdot\cdot n_j-1\cdot\cdot}\Big] \\ &= \sum_i \Big[\frac{f^{(i)}\cdot c^{(i)}}{\mathfrak{m}^{(i)}\cdot c^{(i)}} r_i\rho^{m_1m_2\cdot\cdot}_{n_1n_2\cdot\cdot} + \sum_j \frac{f^{(ij)}\cdot c^{(ij)}}{\mathfrak{m}^{(ij)}\cdot c^{(ij)}} r_i\rho^{m_1m_2\cdot\cdot m_j-1\cdot\cdot}_{n_1n_2\cdot\cdot n_j-1\cdot\cdot}\Big]\end{aligned} \tag{2.65}$$

where $\mathfrak{m}_i^{(ij)}$, $c_i^{(ij)}$ are the same as (2.64, 2.63) except for $m_j, n_j \to m_j-1, n_j-1$.

Notice in (2.58) that n_j, m_j are inverted in $f^{(ij)}$ with respect to the way they appear in $c^{(ij)}$ (see $c^{(i)}$, (2.63)). This along with the $\pm$ sign in front of γ_r^2 in (2.63) gives

$$\begin{aligned} f^{(ij)}\cdot c^{(ij)} =&\ \big(-ig_{ij}\sqrt{n_j}\big)\Big[ig_{ij}\sqrt{m_j}\big(\textstyle\sum_{k\neq j} g_{ik}^2(m_k-n_k) + g_{ij}^2(m_j-n_j-2)+\gamma_r^2\big)\Big] \\ &+\big(ig_{ij}\sqrt{m_j}\big)\Big[ig_{ij}\sqrt{n_j}\big(\textstyle\sum_{k\neq j} g_{ik}^2(m_k-n_k) + g_{ij}^2(m_j-n_j-2)-\gamma_r^2\big)\Big] \\ =&\ g_{ij}^2\sqrt{n_jm_j}\gamma_r^2 + g_{ij}^2\sqrt{m_jn_j}\gamma_r^2 \\ =&\ 2g_{ij}^2\sqrt{n_jm_j}\gamma_r^2 \end{aligned} \tag{2.66}$$

The product $f^{(i)}\cdot c^{(i)}$ does not have this feature,

$$\begin{aligned} f^{(i)}\cdot c^{(i)} =&\ \textstyle\sum_j\Big[\big[-g_{ij}^2(m_j+1)+g_{ij}^2(n_j+1)\big]\sum_k g_{ik}^2(m_k-n_k)\Big] \\ &+\textstyle\sum_j\Big[-g_{ij}^2(m_j+1)\gamma_r^2 - g_{ij}^2(n_j+1)\gamma_r^2\Big] \\ =&-\big(\textstyle\sum_j g_{ij}^2(m_j-n_j)\big)^2 - \gamma_r^2\sum_j g_{ij}^2(n_j+m_j+2) \end{aligned} \tag{2.67}$$

The product $\mathfrak{m}^{(i)}\cdot c^{(i)}$ differs from $f^{(i)}\cdot c^{(i)}$ only because of the γ_r instead 0 at the top of $\mathfrak{m}^{(i)}$ with respect to $f^{(i)}$ and a sign difference in front of the other elements. This generates a factor of 2 and a γ_r^4 term which make the denominator differ from the numerator in the prefactor for $\rho^{m_1m_2\cdots}_{n_1\,n_2\,\cdots}$. And we obtain,

$$\begin{aligned}\mathcal{L}_p\rho^{m_1m_2\cdots}_{n_1\,n_2\,\cdots} = \sum_i r_i\Bigg[&-\frac{\big(\sum_j g_{ij}^2(n_j-m_j)\big)^2+\gamma_r^2\sum_j g_{ij}^2(n_j+m_j+2)}{\big(\sum_j g_{ij}^2(n_j-m_j)\big)^2+2\gamma_r^2\sum_j g_{ij}^2(n_j+m_j+2)+\gamma_r^4}\rho^{m_1m_2\cdots}_{n_1\,n_2\,\cdots} \\ &+\sum_j\frac{2\gamma_r^2g_{ij}^2\sqrt{n_jm_j}\rho^{m_1m_2\cdot\cdot m_j-1\cdot\cdot}_{n_1\,n_2\,\cdots n_j-1\cdot\cdot}}{\big(\sum_k g_{ik}^2(n_k-m_k)\big)^2+2\gamma_r^2\sum_k g_{ik}^2(n_k+m_k+2)-4\gamma_r^2g_{ij}^2+\gamma_r^4}\Bigg].\end{aligned} \tag{2.68}$$

We have therefore obtained a generalized form for $\mathcal{L}_p$.

2.4 Notation

Until now, we postponed to establish a notation which reflects pumping and damping physics, rather than original Hamiltonian matrix elements. Here we define the parameters which we use throughout; these are a generalization of those used in [Whit09] for the single mode case.

We first define the dimensionless pumping strength, which is the ratio between the pumping parameter and the decay parameter. The factor of 2 gets absorbed when going from amplitude to density (Chapter 3),

$$n_c = \frac{r}{2\gamma} \quad \rightarrow \quad n_i^c = \frac{r_i}{2\gamma}, \tag{2.69}$$

We separate with an arrow the one-reservoir two-modes notation (Sec. 2.2) from the many-reservoir many-mode notation (Sec. 2.3). To simplify the notation, we also assume that the decay rates, γ in the damping $\mathcal{L}_d$ (1.44) and γ_r, are the same.

Next is the saturation parameter, the ratio between decay into other channels and condensate modes scattering coefficients,

$$n_s = \frac{\gamma^2}{4(g_1^2 + g_2^2)} \quad \rightarrow \quad n_i^s = \frac{\gamma^2}{4\sum_j g_{ij}^2}, \tag{2.70}$$

and finally, we use a normalized transition strength for the coupling of the reservoirs to each mode,

$$\alpha_1 = \frac{g_1^2}{g_1^2 + g_2^2}, \quad \alpha_2 = \frac{g_2^2}{g_1^2 + g_2^2} \quad \rightarrow \quad \alpha_{ij} = \frac{g_{ij}^2}{\sum_k g_{ik}^2}. \tag{2.71}$$

In this notation, the pumping superoperators (2.47, 2.68) in the equation of motion read as follows,

$$\begin{aligned}
\mathcal{L}_p\rho_{nmpq} = &-\gamma n_c \frac{\frac{1}{8n_s}\big(\alpha_1(n-m)+\alpha_2(p-q)\big)^2 + \frac{1}{2}\big(\alpha_1(n+m+2)+\alpha_2(p+q+2)\big)}{\frac{1}{16n_s}\big(\alpha_1(n-m)+\alpha_2(p-q)\big)^2 + \frac{1}{2}\big(\alpha_1(n+m+2)+\alpha_2(p+q+2)\big)+n_s}\rho_{nmpq} \\
&+\frac{\gamma n_c\,\alpha_1\sqrt{nm}}{\frac{1}{16n_s}\big(\alpha_1(n-m)+\alpha_2(p-q)\big)^2 + \frac{1}{2}\big(\alpha_1(n+m)+\alpha_2(p+q+2)\big)+n_s}\rho_{n-1m-1pq} \\
&+\frac{\gamma n_c\,\alpha_2\sqrt{pq}}{\frac{1}{16n_s}\big(\alpha_1(n-m)+\alpha_2(p-q)\big)^2 + \frac{1}{2}\big(\alpha_1(n+m+2)+\alpha_2(p+q)\big)+n_s}\rho_{nmp-1q-1},
\end{aligned} \tag{2.72}$$

$$\mathcal{L}_p\rho^{m_1m_2\cdots}_{n_1\,n_2\,\cdots} = \gamma\sum_i n_i^c\Bigg[-\frac{\frac{1}{8n_i^s}\big(\sum_j\alpha_{ij}(n_j-m_j)\big)^2+\frac{1}{2}\sum_j\alpha_{ij}(n_j+m_j+2)}{\frac{1}{16n_i^s}\big(\sum_j\alpha_{ij}(n_j-m_j)\big)^2+\frac{1}{2}\sum_j\alpha_{ij}(n_j+m_j+2)+n_i^s}\rho^{m_1m_2\cdots}_{n_1\,n_2\,\cdots} + \sum_j\frac{\alpha_{ij}\sqrt{n_jm_j}\rho^{m_1m_2..m_j-1..}_{n_1\,n_2\,\ldots n_j-1..}}{\frac{1}{16n_i^s}\big(\sum_k\alpha_{ik}(n_k-m_k)\big)^2+\frac{1}{2}\sum_k\alpha_{ik}(n_k+m_k+2)-\alpha_{ij}+n_i^s}\Bigg]. \tag{2.73}$$

2.5 The Approximative Hamiltonian of the Condensate

In this section we present the Hamiltonian, H, appearing in the equation of motion (2.1), and point out which manipulations and approximations can be exploited to simplify the many-mode condensate problem. While the choice of reservoirs and the choice of Hamiltonian, H_p, allowed us to simplify the problem for the decay and pumping, here we shall resort to choice of basis and rotating wave approximations to achieve that goal. As described in the introduction (Secs. 1.1.5, 1.2.3), condensate interactions stem from electron-electron, hole-hole and election-hole interactions [Comb 07, Roch 00], which are parametrized as exciton-exciton interactions and incorporated as interactions between the elementary excitations of our system, polaritons [Deng 10]. These interactions are treated up to two-body terms, $a_i^\dagger a_j^\dagger a_k a_l$, with matrix elements

$$\mathsf{g}_{ijkl} = V_0\int d^dr\phi_i^*(r)\phi_j(r)\phi_k^*(r)\phi_l(r). \tag{2.74}$$

In the pumping sections above (Secs. 2.2, 2.3), we used the interaction picture to find an exact solution for the pumping superoperator, here we use the Schrödinger picture, in order to make use of the difference in energy between modes (detuning) to build an argument to discard rapidly oscillating terms which remain small upon time integration. The general many-mode Hamiltonian reads,

$$H = \sum_i\Omega_iA_i^\dagger A_i + \sum_{i\neq j}t_{ij}A_i^\dagger A_j + \sum_{ijkl}G_{ijkl}A_i^\dagger A_j^\dagger A_kA_l, \tag{2.75}$$

where we also used a general definition for the operators A_i acting on arbitrary orbitals

for our modes. We shall provide a justification for approximating this Hamiltonian as,

$$H = \sum_i \omega_i a_i^\dagger a_i + \sum_{ij} \mathrm{g}_{ij} a_i^\dagger a_j^\dagger a_i a_j, \tag{2.76}$$

where the operators a_i are associated with a new mode definition and the terms that are non-particle conserving within each mode have been eliminated. The forms for pumping and decay superoperators, $\mathcal{L}_p$, $\mathcal{L}_d$, (2.73, 1.44), are particle conserving as well. This translates into the evolution of the condensate density matrix, $\rho^{m_1 m_2 \cdots}_{n_1 n_2 \ldots}$, necessitating only a subset of the full space it spans. More precisely, having an equation of motion that is particle conserving translates into using $\mathcal{O}(n^N)$ elements of the density matrix rather than its full set of elements, $\mathcal{O}(n^{2N})$; n is the maximum number of particles included in each mode and N is the number of modes.

The operators O, that we apply on ρ to obtain any particular expectation value $\langle O \rangle$ are partly immune to this criterion, given that they operate on a steady state which is diagonal (see Sec. 4.2.3). We shall see in Chapter 4 that the first order coherence and Josephson decay operators that we use are particle conserving within each mode.

With the equation of motion being number conserving, the problem remains numerically tractable up to 2 modes and possibly 3. We therefore focus in showing in which circumstances one can treat the physics of the problem with (2.76) instead of (2.75).

The first step in doing so is to eliminate the hopping term, t_{ij}. This can be done exactly by diagonalizing the quadratic part of H, (2.75), [East08],

$$a_i = \sum_{\mathbf{i}} f_{\mathbf{i}}(\{\Omega_i\}, \{t_{ij}\}) A_{\mathbf{i}} \tag{2.77}$$

$$\omega_i = f_i(\{\Omega_i\}, \{t_{ij}\}) \tag{2.78}$$

$$\mathrm{g}_{ijkl} = f_{ijkl}(\{\Omega_i\}, \{t_{ij}\}, \{G_{ijkl}\}). \tag{2.79}$$

In other words, we rewrite H using a linear combination of operators $A_{\mathbf{i}}$ and we obtain

$$H = \sum_i \omega_i a_i^\dagger a_i + \sum_{ijkl} \mathrm{g}_{ijkl} a_i^\dagger a_j^\dagger a_k a_l. \tag{2.80}$$

A specific example of this procedure is presented in Chapter 5.

It is more difficult to justify $\mathrm{g}_{ijkl}\delta_{ik}\delta_{jl} \to \mathrm{g}_{ij}$. Table 2.1 shows the forms that the interaction terms can have. Our model only allows to solve the forms δ_{ijkl} and

$\delta_{ij}\delta_{kl}$. The other forms are non-particle conserving within each mode and we attempt a justification for neglecting them. This exercise is challenging because we try to contain all the possible scenarios in an situation where the density matrix has potentially infinite number of dimensions.

Form of g_{ijkl}	δ_{ijkl}	$\delta_{ik}\delta_{jl}$ $\delta_{il}\delta_{jk}$	$\delta_{ij}\delta_{kl}$	δ_{ijk} δ_{ikl} δ_{ijl} δ_{jkl}	$i\neq j\neq k\neq l$ $i\neq k, j\neq l$ $i\neq l$	Total
Nb of occurences	N	$2N(N-1)$	$N(N-1)$	$4N(N-1)$	N^4-7N^2+6N	N^4
Number of occurences and operator forms in two modes (with redundancies)	2 $a_0^\dagger a_0^\dagger a_0 a_0$ $a_1^\dagger a_1^\dagger a_1 a_1$	4 $a_0^\dagger a_1^\dagger a_0 a_1$ $a_1^\dagger a_0^\dagger a_1 a_0$ $a_1^\dagger a_0^\dagger a_0 a_1$ $a_0^\dagger a_1^\dagger a_1 a_0$	2 $a_0^\dagger a_0^\dagger a_1 a_1$ $a_1^\dagger a_1^\dagger a_0 a_0$	8 $a_0^\dagger a_0^\dagger a_0 a_1$ $a_1^\dagger a_1^\dagger a_1 a_0$ $a_0^\dagger a_1^\dagger a_0 a_0$ $a_1^\dagger a_0^\dagger a_1 a_1$ $a_0^\dagger a_0^\dagger a_1 a_0$ $a_1^\dagger a_1^\dagger a_0 a_1$ $a_1^\dagger a_0^\dagger a_0 a_0$ $a_0^\dagger a_1^\dagger a_1 a_1$	0	16

Table 2.1: Forms of the two-body interaction operator and occurrence of each type in an N-mode condensate. The two forms on the left of the thick line conserve the number of particle in each mode. The ones one the right do not and cannot be included in our model. The lower part of the table shows how each form occurs in two modes.

To do so, we first write the density matrix in the Schrödinger picture, giving all the time dependence to the density operator, but nonetheless making a distinction between the time evolution due to the linear terms and the interaction term of the Hamiltonian (2.80),

$$\rho = \sum_{n_\mathbf{i}, m_\mathbf{i}} \rho_{n_\mathbf{i}}^{m_\mathbf{i}} e^{-i\omega_\mathbf{i}(n_\mathbf{i}-m_\mathbf{i})t} |n_\mathbf{i}\rangle\langle m_\mathbf{i}|. \tag{2.81}$$

We look at the evolution of ρ, in a perturbative scheme and estimate under which circumstances the non-particle conserving terms provide a transition probability over infinite time that is finite rather the infinite and therefore do not contribute to the dynamics. The evolution $\dot{\rho} = -i[H, \rho]$, with (2.81) on the r.h.s and the commutator of (2.80) on the r.h.s. is,

$$\sum_{n_\mathbf{i}, m_\mathbf{i}} \left[\dot{\rho}_{n_\mathbf{i}}^{m_\mathbf{i}} - i\omega_\mathbf{i}(n_\mathbf{i}-m_\mathbf{i})\rho_{n_\mathbf{i}}^{m_\mathbf{i}}\right] e^{-i\omega_\mathbf{i}(n_\mathbf{i}-m_\mathbf{i})t} |n_\mathbf{i}\rangle\langle m_\mathbf{i}| \; = -i[\sum_i a_i^\dagger a_i, \rho] - i[\sum_{ijkl} \mathrm{g}_{ijkl} a_i^\dagger a_j^\dagger a_k a_l, \rho]. \tag{2.82}$$

The term with $-i\omega_\mathbf{i}(n_\mathbf{i} - m_\mathbf{i})$ cancels with $i[\sum_i a_i^\dagger a_i, \rho]$ on the r.h.s., and we are left

with,

$$\sum_{n_{\mathbf{i}},m_{\mathbf{i}}} \dot{\rho}^{m_{\mathbf{i}}}_{n_{\mathbf{i}}} e^{-i\omega_{\mathbf{i}}(n_{\mathbf{i}}-m_{\mathbf{i}})t} |n_{\mathbf{i}}\rangle\langle m_{\mathbf{i}}| = -i\big[\sum_{ijkl} \mathsf{g}_{ijkl}\, a_i^\dagger a_j^\dagger a_k a_l, \rho\big]. \tag{2.83}$$

We focus on the terms where none of the indices are the same, $\sum_{\neq} \mathsf{g}_{ijkl}$, the second last column of Table 2.1. We then note that in this case the commutator in (2.83) generates states,

$$a_i^\dagger a_j^\dagger a_k a_l\, \rho^{..m_{i,j,k,l}..}_{..n_{i\text{-}1,j\text{-}1,k+1,l+1}..} |..n_{i\text{-}1,j\text{-}1,k+1,l+1}..\rangle\langle..m_{i,j,k,l}..| = \sqrt{n_i}\sqrt{n_j}\sqrt{n_k+1}\sqrt{n_l+1}\rho^{..m_{i,j,k,l}..}_{..n_{i\text{-}1,j\text{-}1,k+1,l+1}..} |..n_{i,j,k,l}..\rangle\langle..m_{i,j,k,l}..| \tag{2.84}$$

with time dependence $e^{-i\sum_{\mathbf{i}}\omega_{\mathbf{i}}(n_{\mathbf{i}}-m_{\mathbf{i}})t} e^{-i(-\omega_i-\omega_j+\omega_k+\omega_l)t}$, and

$$|..n_{i,j,k,l}..\rangle\langle..m_{i+1,j+1,k-1,l-1}..|\rho^{..m_{i+1,j+1,k\text{-}1,l\text{-}1}..}_{..n_{i,j,k,l}..} a_i^\dagger a_j^\dagger a_k a_l = \sqrt{m_i+1}\sqrt{m_j+1}\sqrt{m_k}\sqrt{m_l}\rho^{..m_{i+1,j+1,k-1,l-1}..}_{..n_{i,j,k,l}..} |..n_{i,j,k,l}..\rangle\langle..m_{i,j,k,l}..| \tag{2.85}$$

with the same time dependence $e^{i\sum_{\mathbf{i}}\omega_{\mathbf{i}}(m_{\mathbf{i}}-n_{\mathbf{i}})t} e^{i(\omega_i+\omega_j-\omega_k-\omega_l)t}$.

We can now cancel the state vectors and the linear time dependence on either side of the form $\dot{\rho} = -i[H,\rho]$, reaching,

$$\dot{\rho}^{m_1 m_2..}_{n_1 n_2..} = -i\sum_{\neq} \mathsf{g}_{ijkl} e^{-i(-\omega_i-\omega_j+\omega_k+\omega_l)t}\Big(\sqrt{n_i}\sqrt{n_j}\sqrt{n_k+1}\sqrt{n_l+1}\,\rho^{..m_{i,j,k,l}..}_{..n_{i-1,j-1,k+1,l+1}..} - \sqrt{m_i+1}\sqrt{m_j+1}\sqrt{m_k}\sqrt{m_l}\,\rho^{..m_{i+1,j+1,k-1,l-1}..}_{..n_{i,j,k,l}..}\Big). \tag{2.86}$$

We treat each matrix element of (2.83) individually.

We shall determine if these terms gives a finite change in occupation by examining if the integrate evaluated from minus infinity diverges,

$$\int_{-\infty}^{t} \dot{\rho}^{..m_{i,j,k,l}..}_{..n_{i,j,k,l}..} d\tau_n = -i\sum_{\neq}\int_{-\infty}^{t} d\tau_n\, \mathsf{g}_{ijkl} e^{-i(-\omega_i-\omega_j+\omega_k+\omega_l)\tau_n}\times \Big(\sqrt{n_i}\sqrt{n_j}\sqrt{n_k+1}\sqrt{n_l+1}\int_{-\infty}^{\tau_n} d\tau_{n-1}\,\dot{\rho}^{..m_{i,j,k,l}..}_{..n_{i-1,j-1,k+1,l+1}..} - \sqrt{m_i+1}\sqrt{m_j+1}\sqrt{m_k}\sqrt{m_l}\int_{-\infty}^{\tau_n} d\tau_{n-1}\,\dot{\rho}^{..m_{i+1,j+1,k-1,l-1}..}_{..n_{i,j,k,l}..}\Big). \tag{2.87}$$

This will iteratively provide an integration over the entire Fock space $\int_{-\infty}^{t} d\tau_n \int_{-\infty}^{\tau_n} d\tau_{n-1}.. \int_{-\infty}^{\tau_2} d\tau_1 f(f..(f(\rho^{..}_{..})))$, with each integration giving a factor of order

$$-i\sum_{\neq} \frac{\mathsf{g}_{ijkl}}{-i(-\omega_i-\omega_j+\omega_k+\omega_l)}\Big(\sqrt{n_i}\sqrt{n_j}\sqrt{n_k+1}\sqrt{n_l+1} - \sqrt{m_i+1}\sqrt{m_j+1}\sqrt{m_k}\sqrt{m_l}\Big)(\rho^{..}_{..}). \tag{2.88}$$

We note that $(\rho^{\cdot}_{\cdot\cdot})$ is bounded between $[0,1]$ and are of same magnitude in each iteration since the distribution is either smooth or symmetric on either side of the matrix element being considered. We choose to make $\rho^{\cdot}_{\cdot\cdot}$ equal to one. Since we are mostly concerned with diagonal elements we can pick a set of non-trivial indices $n_{i,j,k,l} = n+1$, $m_{i,j,k,l} = n$. Conservatively, we also let $\sum_{\neq} \mathrm{g}_{ijkl} \approx N^4\mathrm{g}$ (see Table 2.1), and the factor becomes,

$$-\frac{i}{2}\sum_{\neq}\frac{\mathrm{g}_{ijkl}\big((n+1)(n+2)-(n+1)n\big)}{-i(-\omega_i-\omega_j+\omega_k+\omega_l)} \approx \frac{N^4\mathrm{g}\ (n+1)}{(-\omega_i-\omega_j+\omega_k+\omega_l)}. \tag{2.89}$$

When this term is smaller than 1, the integration (2.87) will tend towards zero, $\Pi_n(x_n < 1) \to 0$. Otherwise it may diverge, setting a finite transition rate. The two other forms of the non-resonant scattering processes in Table 2.1 create criteria which scale like,

$$\frac{N^2\mathrm{g}\,n}{\omega_i-\omega_j} \tag{2.90}$$

We have therefore generated a criteria for using $\mathrm{g}_{ijkl}\,\delta_{ik}\delta_{jl} \to \mathrm{g}_{ij}$. When the matrix elements and number of modes, $N^4\mathrm{g}$, times the average occupation of the condensates, $\langle n_{i,j,k,l}\rangle$, is comparable to the difference in energy between them, $(-\omega_i-\omega_j+\omega_k+\omega_l)$, the particle non-conserving interaction terms can be neglected. When these conditions are met, we shall say that we are in the strong trapping regime.

Having set an argument for the neglect of certain terms, we now switch back to the interaction picture and write the Hamiltonian of the condensate as,

$$H = \sum_i \kappa_i a_i^\dagger a_i^\dagger a_i a_i + \frac{1}{2}\sum_{i\neq j}\eta_{ij}a_i^\dagger a_i a_j^\dagger a_j. \tag{2.91}$$

Throughout, we will reserve κ for condensate modes self-interactions and η for energy (density) interactions between condensate modes.

2.6 Discussion

The physics of bosonic systems, when treated quantum mechanically, presents the particular challenge of generating potentially infinite sets of equations. Both for the pumping superoperator and the condensate Hamiltonian, we had to invest significant effort to prevent this from happening. We managed, after selecting the problem adequately and imposing certain quantitative restrictions, to obtain a full equation of motion which we can exploit ($\mathcal{L}_p$, 2.73; $\mathcal{L}_d$, 1.44; H, 2.91).

The questions naturally arise : what interesting physics did we miss by imposing these restrictions? What can this or that term do for our problem? The description that we have at the moment is very near the diagonal. It presents occupation fluctuations, which are absent in mean-field theory, but limits strongly the incorporation of off-diagonal terms. Careful addition of these other interaction terms (see Table 2.1) will mix the Fock states and introduce very rich phenomena (the most obvious here are certain regimes of Josephson oscillation, see Chapter 4). The answer for how to introduce these terms in the Hamiltonian H to obtain new physics is not at the model level, but rather lies within the approximative schemes of the next two chapters. Nonetheless we did not solve for them in this thesis. The conclusion will present some ideas for how to incorporate them.

Chapter 3

Population Distribution Functions

Having obtained our equation of motion for many-mode polariton condensates, and pointed out the physics it captures and the approximations it entails, we now move from theoretical description to extraction of physical information. The first and simplest physical quantity we will seek is the population distribution, i.e. the probability distribution of the occupation numbers for the low-energy polariton modes. It corresponds to the diagonal elements of the reduced density matrix, ρ. We obtain expressions both for one reservoir pumping two modes (Sec. 3.1) and many reservoirs pumping many modes models (Sec. 3.2).

We use two analytical tools to obtain the distributions. The first relies on the detailed balance form [Carm 74, Scul 97] of individual steady-state transitions. This provides two equivalent steady-state subequations, one of which we either use as is to obtain the population distribution directly, or feed in our second analytical tool. In it, we approximate the occupation numbers with continuous variables and turn the transition steps within the detailed balance equations into first-order Taylor expansions (Secs. 3.1.1, 3.2.1). The approximate differential equations we obtain from this process are solved, either exactly (for the one reservoir, two modes case) or approximately (in the many reservoir, many mode case). The solutions are multivariate Gaussians.

Two follow-on sections are added to each main derivation. To the one-reservoir, two-mode section, we add how our solution reduces to the one mode problem [Whit 09] or can be generalized to one reservoir pumping many modes (Sec. 3.1.2). After the multi-reservoir, multi-mode derivation, we show the source of the approximation in the multivariate Gaussian solution (Sec. 3.2.2). We also select example solutions in each model and analytical tool: a mode competition example obtained numerically (Sec. 3.1.3), and an analytical three-mode distribution (Sec. 3.2.3).

3.1 Population – Single Reservoir, Two Modes

We keep a separate section for the special case of one reservoir and two modes, rather than directly presenting the many reservoirs pumping many modes solution, for two reasons. First an analytic solution for the population distribution can be obtained in a controlled way, by approximating the occupation numbers as continuous variables. Second it exemplifies, in a full quantum description, the principle of mode competition, as understood in laser theory [Hake 86].

Population distributions are obtained with the diagonal elements of the density matrix equation of motion,

$$\dot{P}_{np} = \langle n, p|\dot{\rho}|n, p\rangle. \tag{3.1}$$

In other words, we let $m = n$ and $q = p$ in the equation of motion for ρ_{nmpq},

$$\begin{aligned}\dot{P}_{np} = \gamma n_c \Bigg[\frac{\alpha_1 n}{\alpha_1 n + \alpha_2(p+1) + n_s} P_{n-1p} + \frac{\alpha_2 p}{\alpha_1(n+1) + \alpha_2 p + n_s} P_{np-1} - \frac{\alpha_1(n+1) + \alpha_2(p+1)}{\alpha_1(n+1) + \alpha_2(p+1) + n_s} P_{np} \Bigg] \\ + \gamma \Big[(n+1)P_{n+1p} + (p+1)P_{np+1} - (n+p)P_{np} \Big],\end{aligned} \tag{3.2}$$

where the first line corresponds to the pumping term, $\mathcal{L}_p$ (2.72) and the second line is for the Lindblad decay, $\mathcal{L}_d$, (1.43). Notice that the condensate Hamiltonian is seemingly absent in (3.2). This is because the Hamiltonian we approximated, H (2.91), is particle conserving within each mode, and its contribution to the evolution of diagonal elements is therefore zero,

$$\begin{aligned}\sum_{i \neq j} \langle n, p| \text{-}i \big[(a_i^\dagger a_i)^2 + \tfrac{1}{2} a_i^\dagger a_i a_j^\dagger a_j, \rho \big] |n, p\rangle &= \text{-}i \big[(n^2 + p^2 + np)\rho_{nnpp} - (n^2 + p^2 + np)\rho_{nnpp} \big] \\ &= 0\,.\end{aligned} \tag{3.3}$$

Throughout, we will be interested in population distributions in the steady-state, $\dot{P}_{np} = 0$.

3.1.1 Detailed Balance Solution and Analytic Solutions

To solve the population distribution equation and find the steady-state, we use detailed balance. Eq. (3.2) describes the change in the occupation probabilities, due to transitions which increase or decrease the number of particles in each mode, i.e. pumping and decay. The first two terms on the first line correspond to transitions into the state

of n, p particles due to pumping, while the third term describes transitions from the n, p state to higher occupation, also due to pumping. The second line, similarly, gives the dynamics due to loss processes. We can find a steady-state solution by requiring that the growth of an occupation probability due to pumping matches its decay due to loss, and vice versa. This is a form of detailed balance condition [Carm 74]. Specifically in (3.2), this corresponds to the steady-state equation splitting in two equivalent subequations,

$$0 = \gamma n_c \left[\frac{\alpha_1 n}{\alpha_1 n + \alpha_2 (p+1) + n_s} P_{n-1p} + \frac{\alpha_2 p}{\alpha_1 (n+1) + \alpha_2 p + n_s} P_{np-1} \right] - \gamma (n+p) P_{np}, \tag{3.4}$$

$$0 = -\gamma n_c \frac{\alpha_1 (n+1) + \alpha_2 (p+1)}{\alpha_1 (n+1) + \alpha_2 (p+1) + n_s} P_{np} + \gamma \Big[(n+1) P_{n+1p} + (p+1) P_{np+1} \Big]. \tag{3.5}$$

Rearranging (3.4) gives,

$$P_{np} = \begin{cases} P_o & , n, p = 0 \\ \dfrac{n_c \alpha_1 P_{n-1p}}{\alpha_1 n + \alpha_2 + n_s} & , p = 0 \\ \dfrac{n_c \alpha_2 P_{np-1}}{\alpha_1 + \alpha_2 p + n_s} & , n = 0 \\ \dfrac{n_c}{n+p} \left(\dfrac{\alpha_1 n P_{n-1p}}{\alpha_1 n + \alpha_2 (p+1) + n_s} + \dfrac{\alpha_2 p P_{np-1}}{\alpha_1 (n+1) + \alpha_2 p + n_s} \right) & , n, p \neq 0. \end{cases} \tag{3.6}$$

We separated the solution in cases because, by only having matrix elements and no state vectors in the equation, there is no vacuum state to indicate the unphysical states (e.g. $P_{n-1p}|_{n=0} \rightarrow P_{-1p}$) which are otherwise implied in the case $n, p \neq 0$. Repeated application of these forms allows us to develop the full distribution from the probability of the vacuum state, P_o, which is simply a normalization. Using (3.6), it is straightforward to obtain the distribution numerically for a given set of control parameters, $n_c, n_s, \alpha_{1,2}$.

The second analytical tool is to approximate the occupation numbers as continuous variables and to replace index differences in occupation probability elements with first order Taylor expansions,

$$P_{n-1p} \rightarrow P_{(n,p)} - 1 \cdot \partial_n P_{(n,p)} \quad \text{and} \quad P_{np-1} \rightarrow P_{(n,p)} - 1 \cdot \partial_p P_{(n,p)}. \tag{3.7}$$

Doing this, Eq. (3.6) transforms into,

$$P_{(n,p)} = \frac{n_c}{n+p}\left(\frac{\alpha_1 n(1-\partial_n)}{\alpha_1 n+\alpha_2 p+n_s}+\frac{\alpha_2 p(1-\partial_p)}{\alpha_1 n+\alpha_2 p+n_s}\right)P_{(n,p)}. \tag{3.8}$$

The brackets around indices indicate that they are now continuous variables. We simplified the denominators by neglecting the +1s which appear in (3.6), since $n_s \gg 1$. The solution is the multivariate Gaussian

$$P_{(n,p)} = \frac{1}{Z}\cdot\exp\left(-\frac{(n+p)^2}{2n_c}+\frac{\alpha_1 n_c-n_s}{\alpha_1 n_c}n+\frac{\alpha_2 n_c-n_s}{\alpha_2 n_c}p\right). \tag{3.9}$$

This solution can be manipulated into the form (3.8); we postpone the steps until the one reservoir, many modes example below, (3.16).

To demonstrate an important feature which occurs in multimode population distributions, we write (3.9) in matrix form

$$\begin{aligned} P_{(n,p)} &= \frac{1}{Z}\exp\left[-\frac{1}{2n_c}\begin{pmatrix}n & p\end{pmatrix}\cdot\begin{pmatrix}1 & 1\\ 1 & 1\end{pmatrix}\cdot\begin{pmatrix}n\\ p\end{pmatrix}+\begin{pmatrix}\frac{\alpha_1 n_c-n_s}{\alpha_1 n_c} & \frac{\alpha_2 n_c-n_s}{\alpha_2 n_c}\end{pmatrix}\begin{pmatrix}n\\ p\end{pmatrix}\right],\\ &= \frac{1}{Z}\exp\left[-\frac{1}{2}\begin{pmatrix}n & p\end{pmatrix}\cdot A\cdot\begin{pmatrix}n\\ p\end{pmatrix}+B\begin{pmatrix}n\\ p\end{pmatrix}\right], \end{aligned} \tag{3.10}$$

to point out that A is singular and that the variance, A^{-1}, therefore diverges. This is also seen by changing variables according to

$$u = \frac{1}{\sqrt{2}}(n-p) \tag{3.11}$$

$$v = \frac{1}{\sqrt{2}}(n+p) \tag{3.12}$$

and choosing $\alpha_{1,2} = 0.5$. Under these circumstances, Eq. (3.9) becomes

$$P_{(u,v)} = \frac{1}{Z}\cdot\exp\left(-\frac{v^2}{n_c}+\frac{n_c-2n_s}{n_c}\sqrt{2}v\right). \tag{3.13}$$

The equation is satisfied with any value of u. There is a soft mode which occurs along the n+$p = const$ direction. The simplest example of a soft mode is in the relative phase between two oscillators, there is no restoring force associated with this parameter and it is therefore free to take any value. New physics arise along a soft mode when a small pertubation is added to the otherwise free parameter[Piko01]. The population

distribution has large uncertainty along the soft mode, so long as $n, p \geq 0$. The vacuum therefore adds an additional complexity to our description i.e. a cutoff to the distribution. This peculiar soft mode is already present here, in the one reservoir two modes model, but will also occur in the general model. We call this specific distribution by the name "ridge" because of its visual appearance when plotted on a mesh, as in Fig. 3.1.

We also note in Figure 3.1 the depence of the population distribution in the pumping paramaters, n_c, n_s. In Fig. 3.1A-C the effect of increasing n_c is to place the distribution further above threshold. As n_c increases the width of the distribution also increases. In Fig. 3.1D-F, with n_s increasing and $\bar{n} = n_c - n_s$ constant, the spread of the distribution increases but its position above threshold remains constant.

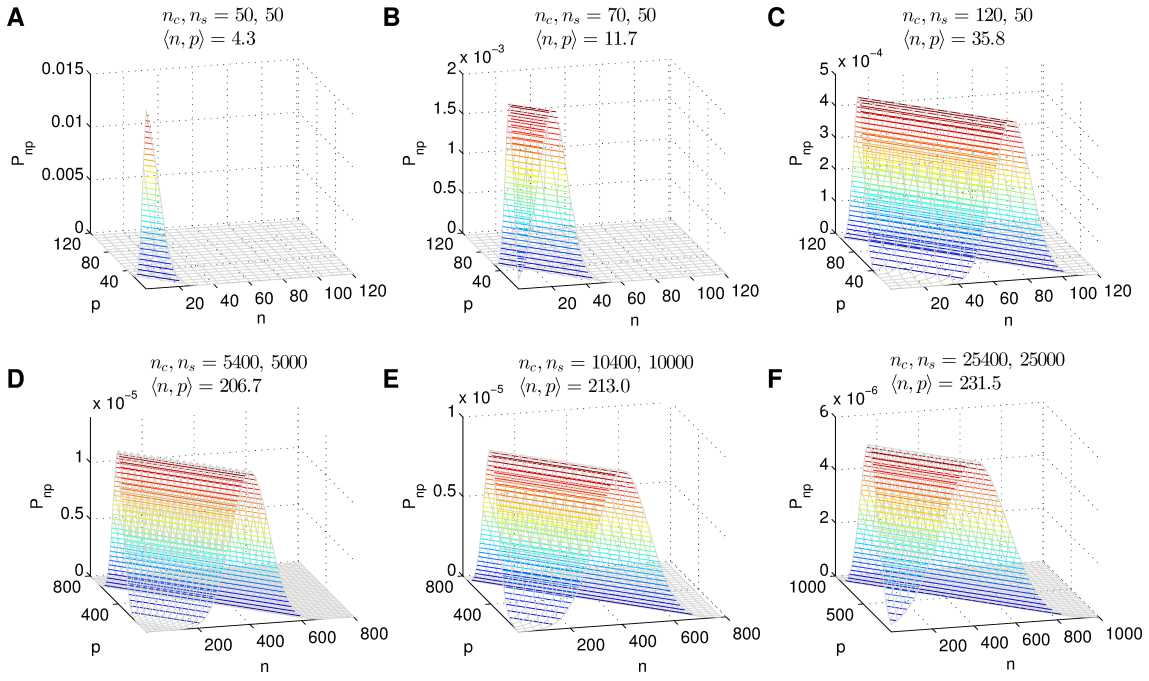

Figure 3.1: Dependence of the ridge population distribution on pumping parameters, n_c, n_s. (A-C) For $n_s = 50$ and increasing n_c, the population goes from threshold, $n_c = 50$, to above threshold, $n_c = 70$, and far above threshold, $n_c = 120$. As n_c increases the spread of the distribution, $\propto \sqrt{n_c}$ in the n+p direction, also increases. (D-F) This is also observed for $n_s = 5000, 10000, 25000$ and constant $\bar{n} = n_c - n_s = 400$. The position of the ridge stays constant, but its spread increases.

3.1.2 Corollaries of the Single Reservoir, Two Modes Solution

The single-reservoir, two-mode solution obtained above, Eq. (3.9), can be used to either recover the known solution for a single-reservoir, single-mode condensate[Whit 09], or

generalized to obtain the solution for a single-reservoir, many-mode condensate[Sing 80]. These two solutions are presented for completeness.

To recover the single reservoir, single mode solution, we set $\alpha_{1,2} = 1, 0$ and Eq. (3.9) is rewritten as

$$P_{(n,p)} = \frac{1}{Z} \cdot \exp\Bigg(- \frac{n^2}{2n_c} + \frac{n_c - n_s}{n_c} n \Bigg) \exp\Bigg(- \frac{2np + p^2}{2n_c} - \frac{n_s}{0 \cdot n_c} p \Bigg). \tag{3.14}$$

The second exponential is either one when $p = 0$, or zero when $p > 0$. We therefore obtain

$$\begin{aligned} P_{(n)} &= \frac{1}{Z} \cdot \exp\Bigg(- \frac{n^2 - 2(n_c - n_s)n + (n_c - n_s)^2}{2n_c} + \frac{(n_c - n_s)^2}{n_c} \Bigg) \\ &= \frac{e^{\frac{\bar{n}^2}{2n_c}}}{Z} \exp\Big(- \frac{(n - \bar{n})^2}{2n_c} \Big), \end{aligned} \tag{3.15}$$

where $\bar{n} = n_c - n_s$. This agrees with the form quoted in [Whit09], as expected.

Our form (3.9) can also be generalized to the general case of one reservoir pumping many modes[Sing 80],

$$P_{(n_1,n_2,n_3 \ldots)} = \frac{1}{Z'} \exp\Big(- \frac{\big(\sum_j n_j\big)^2}{2n_c} + \sum_i \frac{\alpha_i n_c - n_s}{\alpha_i n_c} n_i \Big), \tag{3.16}$$

which we show is the exact solution of the many-mode version of (3.8),

$$\sum_i n_i P = n_c \sum_i \frac{\alpha_i n_i (P - \partial_{n_i} P)}{\sum_j \alpha_j n_j + n_s}, \tag{3.17}$$

by placing the derivatives,

$$\partial_{n_i} P_{(n_1,n_2,n_3 \ldots)} = \Big(- \frac{1}{\alpha_i n_c} \big(\alpha_i \sum_j n_j + n_s\big) + 1 \Big) P_{(n_1,n_2,n_3 \ldots)}, \tag{3.18}$$

into it.

The Ps on either side of (3.16) cancel and we reach

$$\sum_i n_i = n_c \sum_i \frac{\alpha_i n_i \cdot \frac{1}{\alpha_i n_c}\left(\alpha_i \sum_j n_j + n_s\right)}{\sum_j \alpha_j n_j + n_s} \tag{3.19}$$

$$= \sum_i \frac{n_i\left(\alpha_i \sum_j n_j + n_s\right)}{\sum_j \alpha_j n_j + n_s} \tag{3.20}$$

$$= \frac{\sum_j n_j\left(\sum_i \alpha_i n_i + n_s\right)}{\sum_j \alpha_j n_j + n_s} \tag{3.21}$$

$$= \sum_j n_j \ . \tag{3.22}$$

We interchanged the two sums between lines (3.20) and (3.21). The two sides are the same; Eq. (3.16) is the solution of the single-reservoir, many-mode continuous population equation (3.17), so long as the discreteness of the occupation number can be neglected.

3.1.3 Mode Competition Example

While non-equilibrium physics gives rise to stable situations which do not otherwise exist in equilibrium (e.g. multiple BECs, [Tosi12]), it can also give rise to unstable situations, where a minute change in a control parameter generates completely different outputs. One such phenomenon is mode competition[East 08], which is present when one reservoir pumps more than one condensate. Mode competition is well known in laser physics[Hake 86, Sing 80].

The underlying physics of mode competition can be explained quite simply by noting that if the coupling strength, g, of one mode is slightly higher than in the others, it grows more rapidly. Due to stimulated scattering more reservoir polaritons will then enter this mode which will grow even bigger. The other mode will receive gain with much reduced stimulated scattering enhancement, $g\sqrt{n+1}$, and will not be able to compete for the gain medium therefore remaining at low occupancy. In contrast, by having multiple reservoirs, Sec. 3.2, the coupling can be preferentially directed to each mode specifically so that they do not compete for the same medium.

In order to show mode competition, the notation we defined in Sec. 2.4 has to be adapted to the phenomenon. We let g_1 be the strongest coupling that the system can present, g, and g_2 be a fraction of it, αg, with α varying between zero and one. We also define a new saturation parameter, n_s', as the decay strength, γ^2, normalized by

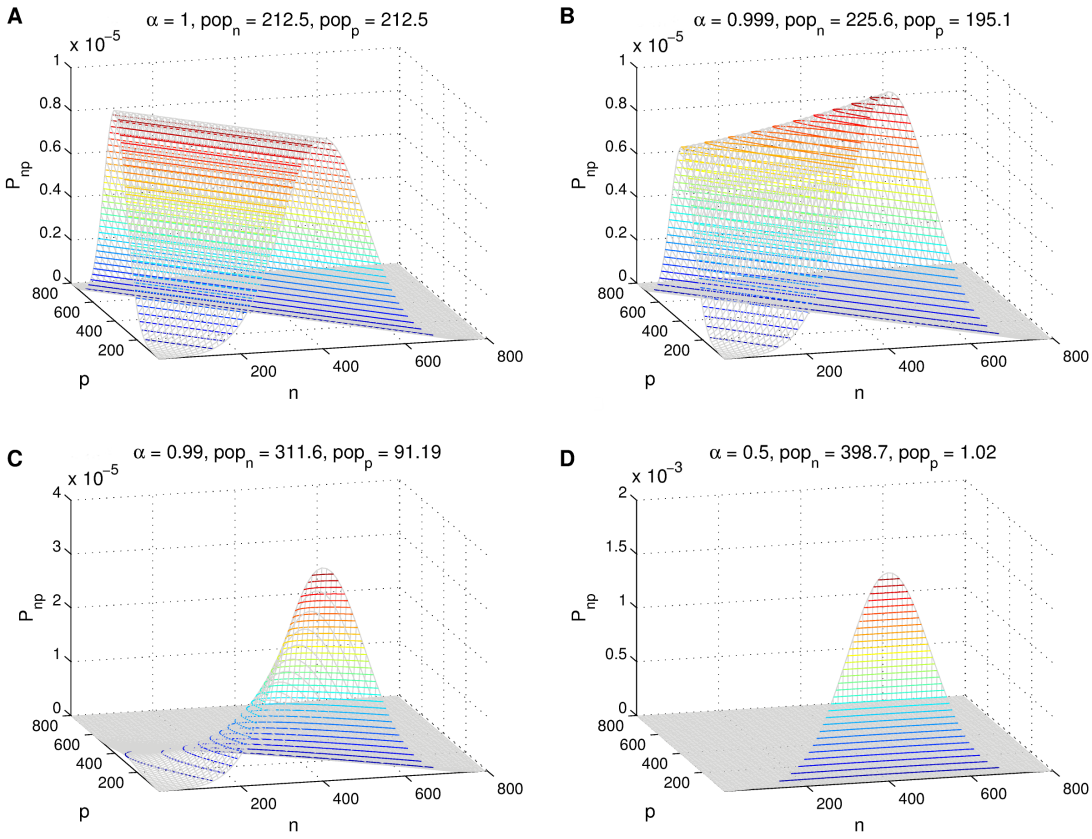

Figure 3.2: Dependence of the population distribution on $\alpha = \frac{\alpha_2}{\alpha_1} = 1,\ 0.999,\ 0.99,\ 0.5$, ($n_s' = 10000$, $n_c = 10400$). The population shows a strong dependence on the α. The two modes both get populated only when they receive the same coupling to the common reservoir. As soon as the coupling to one mode becomes slightly bigger, the population largely ends up in that mode. This exemplifies mode competition.

the maximum coupling, g^2, rather the sum of the couplings. We therefore have

$$\alpha = \frac{g_2^2}{g_1^2} = \frac{\alpha_2}{\alpha_1}, \quad n_s' = \frac{\gamma^2}{4g_1^2} = \frac{n_s}{\alpha_1}, \quad n_c = \frac{r}{2\gamma} = n_c. \tag{3.23}$$

This turns the steady-state population algebraic difference equation (3.6) into

$$P_{np} = \frac{n_c}{n+p} \frac{nP_{n-1p} + \alpha p P_{np-1}}{n + \alpha p + n_s'}, \tag{3.24}$$

where we also dropped the +1s in the denominators, and combined them into a single term. (This can be done since we will not use this distribution as an initial condition in time involving coherence functions (Sec. 4.2.2).) Population distributions obtained from (3.24) are shown in Fig. 3.2 and demonstrate the steep dependence of the popula-

tion distribution on α. We see from it that by changing α by one percent, the solution shifts from being in either mode to being mainly in one mode. The total average population in all cases stays the same, $\langle n\rangle$,$\langle p\rangle \approx 200, 200$ becoming $0, 400$. For this reason, we normalized n_s' by the maximum coupling, g.

3.2 Population – Many Reservoirs, Many Modes

We now move to u reservoirs pumping v modes. We take the Lindblad pumping operator we developed, $\mathcal{L}_p$ (2.73), along with Lindblad decay, $\mathcal{L}_d$ (1.44). Once again, the terms we kept for the Hamiltonian (2.91) mean that the term $-i[H,\rho]$ does not contribute to the population dynamics. We find

$$\begin{aligned}\dot{P}_{n_1 n_2..} = \gamma \sum_i n_i^c \sum_j \Big[\frac{\alpha_{ij} n_j P_{n_1 n_2.. n_j-1..}}{\sum_k \alpha_{ik}(n_k+1) - \alpha_{ij} + n_i^s} - \frac{\alpha_{ij}(n_j+1) P_{n_1 n_2..}}{\sum_k \alpha_{ik}(n_k+1) + n_i^s}\Big] \\ + \gamma \sum_j \Big[(n_j+1) P_{n_1 n_2.. n_j+1..} - n_j P_{n_1 n_2..}\Big].\end{aligned} \tag{3.25}$$

As was emphasized in the mode competition example above (Sec. 3.1.3), we see in the general pumping term, that the growth rate of mode j is reduced by the occupation of all the other modes, giving rise to the sums over modes in the denominators, $\sum_k$. Here however, as long as $u \geq v$, each mode can be preferentially replenished by its own reservoir.

3.2.1 Detailed Balance Solution and Approximate Analytic Solution

Separating Eq. (3.25) using detailed balance, as in Sec. 3.1.1, gives

$$0 = \gamma \sum_i n_i^c \sum_j \frac{\alpha_{ij} n_j P_{n_1 n_2.. n_j-1..}}{\sum_k \alpha_{ik}(n_k+1) - \alpha_{ij} + n_i^s} - \gamma \sum_j n_j P_{n_1 n_2..}, \tag{3.26}$$

$$0 = -\gamma \sum_i n_i^c \sum_j \frac{\alpha_{ij}(n_j+1) P_{n_1 n_2..}}{\sum_k \alpha_{ik}(n_k+1) + n_i^s} + \gamma \sum_j (n_j+1) P_{n_1 n_2.. n_j+1..}, \tag{3.27}$$

and the recursive algebraic difference equations are

$$P_{n_1 n_2 ..} = \begin{cases} P_o & , \, n_{1,2,..} = 0 \\ .. & \\ \frac{1}{\sum_j n_j} \sum_i n_i^c \sum'_{j(n_j \neq 0)} \frac{\alpha_{ij} n_j P_{n_1 n_2 .. n_j - 1 ..}}{\sum_k \alpha_{ik}(n_k+1) - \alpha_{ij} + n_i^s} & , \, \exists \, n_j = 0 \\ .. & \\ \frac{1}{\sum_j n_j} \sum_i n_i^c \sum_j \frac{\alpha_{ij} n_j P_{n_1 n_2 .. n_j - 1 ..}}{\sum_k \alpha_{ik}(n_k+1) - \alpha_{ij} + n_i^s} & , \, n_{1,2,..} \neq 0. \end{cases} \tag{3.28}$$

Again we ascribe the normalization to the vacuum state, P_o. The primed summation, $\sum'_{j(n_j \neq 0)}$, indicates that any term where $n_j = 0$, which connects to unphysical states with negative particle number, is omitted.

The solution to this difference algebraic equation is well approximated, in the special case where $\alpha_{ii+j} = \beta_j, i = 1, 2..u, j = 0, 1, 2, .., v-1$, $i+j$ is circular around v, and n_i^s, n_i^c all the same, by

$$P_{(n_1, n_2, ..)} = \frac{1}{Z} \cdot \exp\left(- \frac{1}{2} \begin{pmatrix} n_1 & n_2 & .. \end{pmatrix} \cdot \mathbb{A} \cdot \begin{pmatrix} n_1 \\ n_2 \\ .. \end{pmatrix} + \mathbb{B} \cdot \begin{pmatrix} n_1 \\ n_2 \\ .. \end{pmatrix} \right) \tag{3.29}$$

with

$$\mathbb{A} = \begin{pmatrix} \frac{\sum_i \beta_i^2}{n_c} & \frac{\sum_{i,j \neq i} \beta_i \beta_j}{n_c} & .. \\ \frac{\sum_{i,j \neq i} \beta_i \beta_j}{n_c} & \frac{\sum_i \beta_i^2}{n_c} & .. \\ .. & .. & .. \end{pmatrix} \tag{3.30}$$

and

$$\mathbb{B} = \begin{pmatrix} \frac{n_c - n_s}{n_c} & \frac{n_c - n_s}{n_c} & .. \end{pmatrix}. \tag{3.31}$$

The off-diagonal terms in $\mathbb{A}$ are all the same. So are the diagonal terms.

Eq. (3.29) can also be written with matrix $\mathbb{A}$ factorized as a sum of v linear terms, squared individually,

$$P_{(n_1, n_2, ..)} = \frac{1}{Z} \cdot \exp\left(\tfrac{1}{2} \sum_{i=0}^{v-1} (\beta_i n_1 + \beta_{\mathrm{mod}_v(i+1)} n_2 + \beta_{\mathrm{mod}_v(i+2)} n_3 + ..)^2 + \tfrac{n_c - n_s}{n_c} \sum_j n_j \right), \tag{3.32}$$

where the index for β is given by the modulus v expression, e.g. $\beta_{\mathrm{mod}_v(v-1+1)} = \beta_o$. We see from this form that even though the number of labels for β_i only depends on the number of modes, v, due the sum $\sum_{i=0}^{v-1}$, the approximation has to have one reservoir associated with each term within it. From this we see that in order for our

approximation to be physically realistic, there needs to be as many reservoirs as there are modes, $u \geq v$.

3.2.2 Approximation Error of the Analytic Expression

To prove the validity of the multivariate Gaussian (3.29) as an approximate, special solution for the population distribution (3.28), we isolate the residual of (3.29) when placed into the continuous version of (3.28), in two modes. The steps illustrate the intricate algebraic interplay in the solution and might be indicative of a way to obtain an exact solution. We start with the two mode version of the last case in (3.28) in the special notation we proposed for the coupling terms, β_o, β_1,

$$P_{np} = \frac{n_c}{n+p}\left(\frac{\beta_o n P_{n-1p} + \beta_1 p P_{np-1}}{\beta_o n + \beta_1 p + n_s} + \frac{\beta_1 n P_{n-1p} + \beta_o p P_{np-1}}{\beta_1 n + \beta_o p + n_s},\right). \tag{3.33}$$

We dropped the ones in the denominators of (3.28), and grouped the resulting expressions together. The approximate solution for it, (3.29), in two modes becomes,

$$P_{(n,p)} = \exp\left(- \begin{pmatrix} n & p \end{pmatrix} \cdot \begin{pmatrix} \frac{\beta_o^2+\beta_1^2}{2n_c} & \frac{\beta_1\beta_o}{n_c} \\ \frac{\beta_1\beta_o}{n_c} & \frac{\beta_o^2+\beta_1^2}{2n_c} \end{pmatrix} \cdot \begin{pmatrix} n \\ p \end{pmatrix} + \begin{pmatrix} \frac{n_c-n_s}{n_c} & \frac{n_c-n_s}{n_c} \end{pmatrix} \begin{pmatrix} n \\ p \end{pmatrix} \right). \tag{3.34}$$

The derivatives of (3.34) are,

$$\partial_n P_{(n,p)} = \frac{1}{n_c}\Big(- (\beta_o^2 + \beta_1^2)n - 2\beta_o\beta_1 p - n_s + 1\Big) P_{(n,p)} \tag{3.35}$$

$$\partial_p P_{(n,p)} = \frac{1}{n_c}\Big(- (\beta_o^2 + \beta_1^2)p - 2\beta_o\beta_1 n - n_s + 1\Big) P_{(n,p)}. \tag{3.36}$$

P_{n-1p} and P_{np-1} in (3.33) are turned into $P_{(n,p)} - 1 \cdot \partial_n P_{(n,p)}$ and $P_{(n,p)} - 1 \cdot \partial_p P_{(n,p)}$. Eqs. (3.35, 3.36) are placed into (3.33), the $P_{(n,p)}$ cancels on either side and we are left with

$$\begin{aligned} 1 \approx \frac{1}{n+p}\Bigg(& \frac{\beta_o n\big((\beta_o^2+\beta_1^2)n + 2\beta_o\beta_1 p + n_s\big) + \beta_1 p\big((\beta_o^2+\beta_1^2)p + 2\beta_o\beta_1 n + n_s\big)}{\beta_o n + \beta_1 p + n_s} \\ & + \frac{\beta_1 n\big((\beta_o^2+\beta_1^2)n + 2\beta_o\beta_1 p + n_s\big) + \beta_o p\big((\beta_o^2+\beta_1^2)p + 2\beta_o\beta_1 n + n_s\big)}{\beta_1 n + \beta_0 p + n_s}\Bigg). \end{aligned} \tag{3.37}$$

We focus on showing the validity of this expression. We first use the identity $\beta_o+\beta_1 = 1$ to manipulate, e.g.,

$$\begin{aligned}\beta_o n\big((\beta_o^2+\beta_1^2)n + 2\beta_o\beta_1 p + n_s\big) &= \beta_o n\big[(1-2\beta_o\beta_1)n + \big(1-(\beta_o^2+\beta_1^2)\big)p\big] + nn_s - \beta_1 nn_s \\ &= \beta_o n[n+p] + nn_s - \beta_o n\big[2\beta_o\beta_1 n + (\beta_o^2+\beta_1^2)p\big] - \beta_1 nn_s\end{aligned}$$

and, focusing on the first line of (3.37), we complete terms which factorize in $(n+p)$,

$$\begin{aligned}\frac{1}{n+p}\Bigg(&\frac{\beta_o n(n+p) + nn_s + \beta_1 p(n+p) + pn_s}{\beta_o n + \beta_1 p + n_s} \\ &+ \frac{-\beta_o n(2\beta_0\beta_1 n + (\beta_o^2+\beta_1^2)p) - \beta_1 nn_s - \beta_1 p(2\beta_o\beta_1 p + (\beta_o^2+\beta_1^2)n) - \beta_o pn_s}{\beta_0 n + \beta_1 p + n_s}\Bigg).\end{aligned} \tag{3.38}$$

The subtle interplay in grouping the terms employed here occurs on three other occasions during the expansion. The first line of (3.38) is 1 and we group terms on the second line,

$$1 + \frac{1}{n+p}\left(\frac{-2\beta_0\beta_1(\beta_o n^2 + \beta_1 p^2) - (\beta_o^2+\beta_1^2)np - (\beta_1 n + \beta_o p)n_s}{\beta_0 n + \beta_1 p + n_s}\right). \tag{3.39}$$

The term $(\beta_o^2+\beta_1^2)np$ had a prefactor $\beta_o+\beta_1$ which simplified to one. We use the same identity once again on one of the term which occurs twice, -2...,

$$\begin{aligned}-\beta_0\beta_1(\beta_o n^2 + \beta_1 p^2) &= -\beta_o\beta_1\big((1-\beta_1)n^2 + (1-\beta_o)p^2\big) \\ &= \beta_o\beta_1(\beta_1 n^2 + \beta_o p^2) - \beta_o\beta_1(n^2+p^2),\end{aligned}$$

to obtain,

$$1 + \frac{1}{n+p}\left(\frac{-\beta_0\beta_1(\beta_o n^2 + \beta_1 p^2) + \beta_0\beta_1(\beta_1 n^2 + \beta_0 p^2) - \beta_0\beta_1(n^2+p^2) - (\beta_o^2+\beta_1^2)np - (\beta_1 n + \beta_o p)n_s}{\beta_0 n + \beta_1 p + n_s}\right). \tag{3.40}$$

We now factorize the first two terms and the last three terms together,

$$1 + \frac{1}{n+p}\left(\frac{\beta_o\beta_1\big((\beta_1-\beta_o)n^2 + (\beta_o-\beta_1)p^2\big)}{\beta_0 n + \beta_1 p + n_s} - \frac{(\beta_o n + \beta_1 p + n_s)(\beta_1 n + \beta_o p)}{\beta_o n + \beta_1 p + n_s}\right) \tag{3.41}$$

or

$$1 + \frac{1}{n+p}\left(\frac{\beta_o\beta_1(\beta_1-\beta_o)(n^2-p^2)}{\beta_0 n + \beta_1 p + n_s} - \big(\beta_1 n + \beta_o p\big)\right). \tag{3.42}$$

The manipulations (3.38–3.42) are also performed with second line of (3.37) which now becomes

$$\begin{aligned} 1 \approx 1 + \frac{1}{n+p}\left(\frac{\beta_o\beta_1(\beta_1-\beta_o)(n^2-p^2)}{\beta_0 n+\beta_1 p+n_s} - \big(\beta_1 n+\beta_o p\big)\right) \\ + 1 + \frac{1}{n+p}\left(\frac{\beta_o\beta_1(\beta_o-\beta_1)(n^2-p^2)}{\beta_1 n+\beta_o p+n_s} - \big(\beta_o n+\beta_1 p\big)\right). \end{aligned} \tag{3.43}$$

This further simplifies as

$$\begin{aligned} 0 \approx & \frac{1}{n+p}\left(\frac{\beta_o\beta_1(\beta_1-\beta_o)(n^2-p^2)}{\beta_0 n+\beta_1 p+n_s} + \frac{\beta_o\beta_1(\beta_o-\beta_1)(n^2-p^2)}{\beta_1 n+\beta_o p+n_s}\right) \\ & + \ 1 + \frac{1}{n+p}\Big(- \big(\beta_1 n+\beta_o p\big) - \big(\beta_o n+\beta_1 p\big)\Big) \end{aligned} \tag{3.44}$$

The $1/(n+p)$ on the first line cancels with $(n^2-p^2) = (n+p)(n-p)$ while the second line vanishes identically. We obtain the residual for (3.37),

$$0 \approx \beta_o\beta_1\left(\frac{(\beta_1-\beta_o)(n-p)}{\beta_0 n+\beta_1 p+n_s} + \frac{(\beta_o-\beta_1)(n-p)}{\beta_1 n+\beta_o p+n_s}\right). \tag{3.45}$$

Our expression (3.34) is therefore exact at $\beta_{o,1} = 1, 0$ or $\beta_{o,1} = 0.5$. We shall see in Chapter 5 that this corresponds to either independent pumping or equal pumping (the ridge). With values of $\beta_{o,1}$ in between (3.34) is approximate. Careful study of this derivation along with the factorized expression (3.32) could lead to the formulation of a fully general analytical expression for the population distribution.

3.2.3 Multivariate Gaussian of a Three-mode Population

The three-mode population distribution has the highest number of modes which can be visualized at once by using the three physical dimensions along with color coding. It is also the highest one for which the full Fock space steady-state solution (3.28) can be easily reached computationally (the three-mode population presented here would have $1500^3 = 3.38 \times 10^9$ elements if obtained computationally). Beyond three modes, one has to rely strictly on the mathematical representation and marginal probability distributions to study population distributions, and the analytical expression (3.29) becomes the primary tool. We therefore use the three-mode analytic solution to show a full size population distribution and to illustrate the relationship of this distribution to the marginal ones.

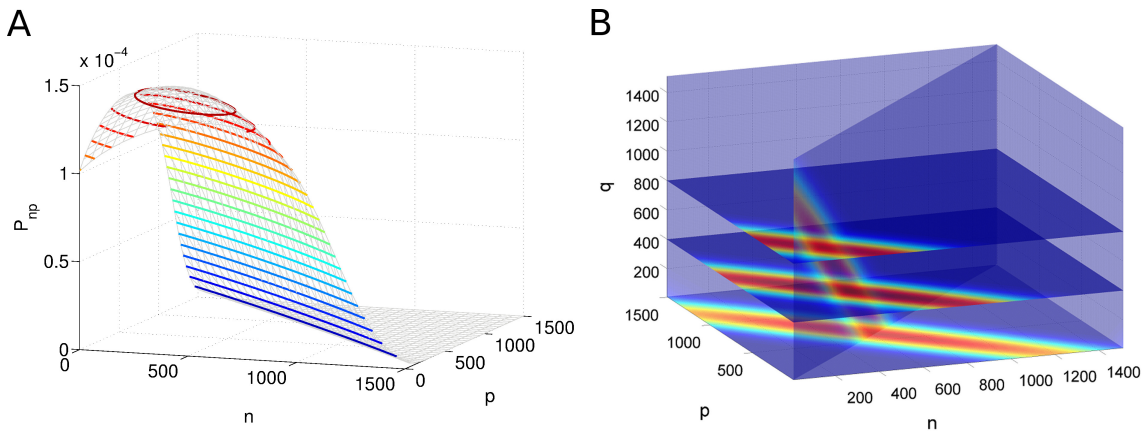

Figure 3.3: (A) Marginal, $P_{(n,p)} = \int P_{(n,p,q)}dq$, and (B) joint, $P_{(n,p,q)}$, population distribution of a 3-mode condensate obtained with the analytical expression (3.29), with $\beta_{o,1,2} = \frac{14}{36}, \frac{11}{36}, \frac{11}{36}$, ($n_s = 10000$, $n_c = 10400$)

The analytical expression we obtained is symmetric in all the modes. One can think of a triangular configuration of three reservoirs and three modes where it is possible, $\beta_o = \alpha_{11}, \alpha_{22}, \alpha_{33}$, $\beta_1 = \alpha_{12}, \alpha_{23}, \alpha_{31}$, $\beta_2 = \alpha_{13}, \alpha_{21}, \alpha_{32}$. We chose values of $\beta_{o,1,2} = \frac{14}{36}, \frac{11}{36}, \frac{11}{36}$. Figure 3.3A shows the marginal population distribution $P_{(n,p)} = \int P_{(n,p,q)}dq$ obtained with (3.29) as well as the full $P_{(n,p,q)}$ representation (Fig.3.3B).

One can see from Figure 3.3B that the probability distribution is concentrated over a plane in the space of occupation numbers, generalizing the near-ridge shape distribution of the two-mode case. The marginal distribution of the two-mode case (Fig. 3.3A), is seen to be a truncated ridge. This quantity describes the probability of a given occupation of the two modes, irrespective of the occupation of the third. Note that although the marginal distribution is non-zero at $n{=}p{=}0$, there is no probability for the vacuum state in the full distribution. This is due to the finite probability of states in which two of the modes are empty, and all the occupation is in the third mode. This should be borne in mind when interpreting marginal distributions for many-mode condensates.

3.3 Discussion

Having a theory which is fully quantum mechanical allows to obtain population distributions of many-mode condensates. Averaging over quantum and thermal fluctuations leads to semiclassical or mean-field theories. Having a distributed value for occupation numbers does however increase substantially the complexity of the problem at hand. In the steady-state and with a particle conserving equation of motion, obtaining the

population directly requires the use of the entire relevant diagonal space of the density matrix. This is done with one of the two detailed balance difference algebraic equations that the model provides. In many modes, this makes the problem intractable quite rapidly. The difference algebraic equation can be manipulated such that only multiple integer of the Fock space need to be visited, but this type of solution loses accuracy very rapidly outside of trivial sets of parameters such as independent pumping and equal pumping (the ridge).

The analytical solutions we developed alleviate this problem. They take the form of multivariate Gaussians which express the population distribution in single-reservoir pumping two (3.8) or several modes (3.9), or many reservoirs pumping many modes (3.29). This type of solution is obtained by observing the patterns in formulas and in plots obtained from them, in combination with formal derivation. The work presented here could only provide an approximate solution for the many-reservoir many-mode model but we have paved the way for more general and accurate solution by pointing out the patterns which occur in the isolation (3.37–3.45) of the residual in the approximation, (3.45).

We shall see in Chapter 5 how population distributions and the way that they describe how fluctuations are correlated play an important role in determining the decoherence of exciton-polariton Bose-Einstein condensates. We also observe in Figs. 3.2A, 3.3B that, while for a single mode condensate[Whit 09] the zero-particle cutoff could be neglected above threshold in order to make the analytical steps simpler, in multi-mode condensates the cutoff continues to plays an important role, even far above threshold. This is because of the occurrence of a soft mode in the population distribution which allows the distribution to reach the zero particle boundary.

Chapter 4

Coherence Functions

We now calculate time-dependent expectation values. The last chapter merely provided us with the steady state reduced density matrix. Here we introduce an extra level of difficulty by considering the action of operators as well as dependence on time. The physical quantities we now extend the theory towards are correlation functions, both first,

$$g^{(1)} = \frac{\langle a^\dagger(t)a(0)\rangle}{\sqrt{\langle a^\dagger(t)a(t)\rangle\langle a^\dagger(0)a(0)\rangle}}, \tag{4.1}$$

and second order, e.g. $g^{(2)} \propto \langle a^\dagger(0)a^\dagger(t)a(t)a(0)\rangle$. The second order function we focus on corresponds to the coherence decay of the intensity oscillations due to beating between the modes. This can be understood as the dephasing of the Josephson oscillations.

As a first step, we shall spend some time looking at the physical grounding for coherence functions (Sec. 4.1), drawing their link to power spectral density, the physical quantity of the system that they describe.

We then move to compute the first order coherence function (4.2) which is the inverse Fourier transform of the emission spectrum; we obtain a matrix equation which allows us to calculate it (Sec. 4.2.1). We show how it is solved numerically for two reservoirs and two modes, and give an example solution which highlights how the correlation of fluctuations between the two modes gives rise to extended coherence times. This is a quantitative manifestation of multimode dynamics (Sec. 4.2.2).

To make it easier to calculate the coherence function, we approximate the matrix equation with a continuous, linearized Fokker-Planck-like equation[Whit 09], and reveal

how it is solved. We show how the solution compares to full numerics (Sec. 4.3.1). As well, we present a simpler approximation scheme, namely the static limit derivation of the linewidth (Sec. 4.3.3).

On Josephson coherence decay (Sec. 4.4), we first explain the origin of the correlation function we calculate (Sec. 4.4.1). We then obtain the matrix equation which describes it and the static limit approximation for it (Sec. 4.4.2). Finally we show how the correlation function for the beating, $g^{(2)}$, can factorize into an absorption and an emission function, $g_a^{(1)} \cdot g_e^{(1)}$, depending on the form of the population distribution (Sec. 4.4.3).

4.1 Physical Interpretation of Coherence Functions

Quantum coherence functions are the expectation value of the two-time correlation of operators, $\langle A^\dagger(\tau)A(0)\rangle$. They serve to describe the wave nature of a system and the random fluctations within it. In quantum optics, coherence functions, along with coherent states, were introduced by Glauber, in relation to the classical limit of quantum electrodynamics[Glau63]. The first order coherence function, $g^{(1)}$, is the Fourier transform of the power spectrum of the system. The visibility in an interferometer gives a measure of it[Scul97]. Second order coherence gives a measure of intensity fluctuations. The Hanbury Brown and Twiss or intensity interferometer provides second order coherence measurements[Brow57].

The link between coherence functions and fluctuations in the system is often drawn in a way that is historically and experimentally relevant but physically obscure. The fact that two time variables appear in them is the result of a mathematical manipulation, which is also mimicked by an interferometer (dividing a signal and imposing a delay). Most importantly, the underlying and intrinsic properties of the system that it describes however, is its power spectrum. We spend a few paragraphs going from spectral density to coherence functions, with the use of little more than the operator version of the Wiener-Khintchin theorem[Weis].

When considered with the theories of thermodynamics, coherence functions can be presented by using the fact that the spectral density has the same form as a linear response function (Sec. 1.2.4). This is used to invoke the fluctuation-dissipation theorem[Call51, Lax60, Lax63] which then prompts the use of a measuring/response element to introduce coherence functions[Scul97]. We shall stay focused on the fluctuations in

our system and show that the inverse transform of our spectral density is indeed the coherence function.

Coherence functions are deep-rooted in the concept of long-range order, ODLRO, [Yang62]. ODLRO is readily seen from the momentum space[Pita03] and Fourier domain (Sec. 1.1.4). We therefore start with the power spectral density of an arbitrary operator, $A(t)$ whose Fourier transform is $\mathcal{A}(\nu)$,

$$\langle \mathcal{A}^\dagger \mathcal{A} \rangle. \tag{4.2}$$

We first need to review the sign convention for i in the Fourier transform of operators. To do this, we start with the Schrödinger equation,

$$\dot{\Psi} = -iH\Psi \quad \Rightarrow \quad \Psi(t) = U\Psi_o,\ U = e^{-iHt}, \tag{4.3}$$

which leads to our standard expression for the evolution of $\rho(t)$,

$$\rho(t) = U\rho_o U^\dagger \Rightarrow \dot{\rho} = -i[H, \rho]. \tag{4.4}$$

Moving from the Schrödinger, A_S, to the Heisenberg, A_H, picture and using an expectation value as a representation invariant reference,

$$\langle A_S \rho(t) \rangle = \langle A_S U \rho_o U^\dagger \rangle = \langle U^\dagger A_S U \rho_o \rangle, \tag{4.5}$$

$$A(t) \equiv A_H = U^\dagger A_S U \quad \Rightarrow \quad \dot{A}_H = i[H, A_H], \tag{4.6}$$

we read the correct sign for i in the evolution of $A(t)$. One has to be careful in determining the sign convention of $A^\dagger(t)$,

$$\dot{A}^\dagger_H = -i[A^\dagger_H, H]. \tag{4.7}$$

We have therefore established the form of the transformation of Heisenberg picture operators from time to frequency domain,

$$\mathcal{A}(\nu) = \int_{-\infty}^{\infty} e^{2\pi i\nu t} A(t) dt \quad \Leftrightarrow \quad A(t) = \int_{-\infty}^{\infty} e^{-2\pi i\nu t} \mathcal{A}(\nu) d\nu \tag{4.8}$$

$$\mathcal{A}^\dagger(\nu) = \int_{-\infty}^{\infty} e^{-2\pi i\nu t} A^\dagger(t) dt \quad \Leftrightarrow \quad A^\dagger(t) = \int_{-\infty}^{\infty} e^{2\pi i\nu t} \mathcal{A}^\dagger(\nu) d\nu. \tag{4.9}$$

Going back to the spectral density of our operator, its inverse Fourier transform is

given by,

$$\begin{aligned}\int_{-\infty}^{\infty} e^{2\pi i\nu\tau}\langle\mathcal{A}^\dagger\mathcal{A}\rangle d\nu &= \int_{-\infty}^{\infty} e^{2\pi i\nu\tau}\mathrm{Tr}\big[\mathcal{A}^\dagger(\nu)\mathcal{A}(\nu)\rho\big]d\nu \\ &= \mathrm{Tr}\Big[\iint_{-\infty}^{\infty} e^{2\pi i\nu\tau}\mathcal{A}^\dagger(\nu)\mathcal{A}(\nu')\delta(\nu'-\nu)d\nu d\nu'\rho\Big].\end{aligned} \tag{4.10}$$

We used the fact that the density operator doesn't have any time (frequency) dependence in the Heisenberg picture to apply the Fourier transform solely on the operators, and added a dummy additional frequency ν' along with a delta function. The delta function is where the second time dependence originates from in the correlation function:

$$\delta(\nu'-\nu) = \int_{-\infty}^{\infty} e^{-2\pi i(\nu'-\nu)t}dt. \tag{4.11}$$

We group the frequencies, ν, ν', and rearrange the integration as follows,

$$\begin{aligned}\int_{-\infty}^{\infty} e^{2\pi i\nu\tau}\langle\mathcal{A}^\dagger\mathcal{A}\rangle d\nu &= \mathrm{Tr}\bigg[\int_{-\infty}^{\infty}\Big[\int_{-\infty}^{\infty} e^{2\pi i\nu(t+\tau)}\mathcal{A}^\dagger(\nu)d\nu\int_{-\infty}^{\infty} e^{-2\pi i\nu' t}\mathcal{A}(\nu')d\nu'\Big]\rho\ dt\bigg] \\ &= \mathrm{Tr}\Big[\int_{-\infty}^{\infty} A^\dagger(t+\tau)A(t)\rho\ dt\Big].\end{aligned} \tag{4.12}$$

We then invoke ergodicity along with the mixed state nature of our density matrix formalism to group the ensemble average provided by the trace with the integration in time. And we thereby reach a coherence function,

$$G(\tau) = \langle A^\dagger(t+\tau)A(t)\rangle. \tag{4.13}$$

At last, the fact that our system is statistically stationary allows to choose any reference time and, in particular, $t = 0$,

$$G(\tau) = \langle A^\dagger(\tau)A(0)\rangle. \tag{4.14}$$

Having obtained the standard form of coherence functions, we revert back to the Schrödinger picture, $A \equiv A_S$,

$$\begin{aligned}G(\tau) &= \langle U^\dagger A^\dagger U A\rho_o\rangle \\ &= \langle A^\dagger U A\rho_o U^\dagger\rangle.\end{aligned} \tag{4.15}$$

And we adopt a Liouville notation, which is more appropriate for open dissipative

systems[Thom02], $\dot{\rho} = \mathcal{L}\rho$, since the time evolution of the reduced system is not unitary, and we write,

$$G(\tau) = \langle A^\dagger e^{\mathcal{L}t} A\rho_o \rangle. \tag{4.16}$$

We note that feedback from the reservoirs, inherent with treating open dissipative systems, is implicitly neglected while transitioning from unitary evolution to Liouville operator. The feedback traces back to the Born and Markov approximations introduced in Section 1.2.2 and the adiabatic elimination in Section 2.2. The short exposé in [Swai81] isolates the term giving rise to this feedback from the Laplace transform of the "unitary" evolution operator of the weak form of the quantum regression theorem. This form of the theorem consists in defining an operator $\rho' = A\rho$ and making use of a single operator form[Swai81],

$$G(\tau) = \langle A^\dagger \rho'(\tau) \rangle. \tag{4.17}$$

As a side note, there also exists a stronger form of the quantum regression theorem, $\langle A^\dagger(\tau)\rangle = c(\tau)\langle A^\dagger\rangle \propto \langle A^\dagger(\tau)A\rangle = c(\tau)\langle A^\dagger A\rangle$, which applies only in linear Markovian systems[Scul97].

Having interpreted the use of coherence functions to describe the condensate order parameter, the remainder of the chapter shall calculate them, in specific first and second order forms.

4.2 First Order Coherence

The first order coherence, $g^{(1)}$, the inverse Fourier transform of the spectral density of the energy fluctuations in the system, also corresponds to the lineshape of the emission from the cavity. In this section, we go through the full derivation of the general first order coherence function and present the numerical solution for it, in two modes. Also we show how, the phase between condensate modes being free, the cross-correlation, $\langle a_1^\dagger(\tau)a_2(0)\rangle$, is zero in our system (Sec. 4.2.3). This will lead us in Section 4.3 to develop approximate solutions for $\langle a_1^\dagger(\tau)a_1(0)\rangle$.

4.2.1 First Order Coherence Function

Based on the equation of motion we obtained for a many-reservoir pumping many-mode condensate (2.1), we shall derive an equation of motion for the field distribution, $u_{n_1 n_2..}$, the magnitude of which shall provide us with $g^{(1)}$. In light of the discussion

held in Sec. 4.1, we start with the power spectral density of the first mode, given by,

$$\hat{g}^{(1)}(\nu) = \langle \hat{a}_1^\dagger \hat{a}_1 \rangle \tag{4.18}$$

where $\hat{a}_1(\nu)$ is the Fourier transform of the operator $a_1(t)$. The choice of the first mode is arbitrary. The corresponding coherence function we shall work with is

$$g^{(1)}(\tau) = \langle a_1^\dagger(\tau) a_1(0) \rangle. \tag{4.19}$$

In superoperator form, it reads,

$$g^{(1)}(\tau) = \langle a_1^\dagger e^{\mathcal{L}\tau} a_1 \rho_o \rangle. \tag{4.20}$$

And we define $\rho'(\tau) = e^{\mathcal{L}\tau} a_1 \rho_o$ such that

$$g^{(1)}(\tau) = \langle a_1^\dagger \rho'(\tau) \rangle. \tag{4.21}$$

Next, we introduce the distribution $u_{n_1 n_2..} = \sqrt{n_1} \rho'^{\,n_1\ n_2..}_{n_1-1 n_2..}$ which provides a convenient way to manipulate the prefactor terms but should not be strictly interpreted as a physical density matrix object since its magnitude is not conserved. Also, as we will see below, the equation of motion of its elements regroups terms which do not have the same physical origin.

We start our expansion with $\dot{u}_{n_1 n_2..} = \sqrt{n_1} \mathcal{L} \rho'^{\,n_1\ n_2..}_{n_1-1 n_2..}$. We consider separately the contribution from the pumping ($\mathcal{L}_p$, 2.47), decay ($\mathcal{L}_d$, 1.44) and condensate Hamiltonian, $-i[H, \rho]$, (2.91). We neglect terms of $\mathcal{O}(n/n_s)$ in the denominator of the pumping component since $n_s \gg \langle n \rangle$ for our system.

$$\begin{aligned}
\sqrt{n_1} \mathcal{L}_p \rho'^{\,n_1\ n_2..}_{n_1-1 n_2..} = \sqrt{n_1} \gamma \sum_i n_i^c \Bigg[& - \frac{\left(\sum_j \alpha_{ij}(n_j+1) - \frac{\alpha_{i1}}{2} \right) \rho'^{\,n_1\ n_2..}_{n_1-1 n_2..}}{\sum_j \alpha_{ij}(n_j+1) - \frac{\alpha_{i1}}{2} + n_i^s} \\
& + \frac{\alpha_{i1} \sqrt{n_1 - 1} \sqrt{n_1} \rho'^{\,n_1-1 n_2..}_{n_1-2 n_2..}}{\sum_k \alpha_{ik}(n_k+1) - \frac{3\alpha_{i1}}{2} + n_i^s} \\
& + \sum_{j \neq 1} \frac{\alpha_{ij} n_j \rho'^{\,n_1\ n_2..n_j-1..}_{n_1-1 n_2..n_j-1..}}{\sum_k \alpha_{ik}(n_k+1) - \alpha_{ij} - \frac{\alpha_{i1}}{2} + n_i^s} \Bigg]
\end{aligned} \tag{4.22}$$

The decay term gives,

$$\sqrt{n_1}\mathcal{L}_d\rho'^{\,n_1\ n_2..}_{n_1-1n_2..} = \sqrt{n_1}\gamma\Bigg[-\Big(\sum_j n_j - \tfrac{1}{2}\Big)\rho'^{\,n_1\ n_2..}_{n_1-1n_2..} + \sqrt{n_1}\sqrt{n_1+1}\rho'^{\,n_1+1n_2..}_{n_1\ \ n_2..} + \sum_{j\neq 1}(n_j+1)\rho'^{\,n_1\ \ n_2..n_j+1..}_{n_1-1n_2..n_j+1..}\Bigg], \tag{4.23}$$

while the condensate modes Hamiltonian gives,

$$\sqrt{n_1}\langle n_1-1, n_{(j\neq 1)}|\ -i[H,\rho']\ |n_{(j)}\rangle = -i\sqrt{n_1}\Bigg[\kappa_1\big((n_1-1)^2-n_1^2\big) + \sum_{j\neq 1}\eta_j\big((n_1-1)n_j - n_1 n_j\big)\Bigg]\rho'^{\,n_1\ n_2..}_{n_1-1n_2..}. \tag{4.24}$$

In the condensate Hamiltonian, H (2.91), we simplified $\eta_{1j} = \eta_{j1} = \eta_j$ and absorbed the factor $\frac{1}{2}$, since the matrix of interaction coefficients is symmetric.

We now come to group the terms in $\sqrt{n_1}$, $\sqrt{n_1 \pm 1}$ to form $u_{..n_i..}, u_{..n_{i\pm1}..}$. One can see in (4.22, 4.23) that the offset factors $\sqrt{n_1 \pm 1}$ originate from inside the square brackets, meaning that they come from the evolution, $\mathcal{L}$, whereas the factors $\sqrt{n_1}$ come from outside and therefore originate from the operator, $\langle a_1^\dagger ...\rangle$. As mentioned above, the evolution of the distribution $u_{n_1n_2..}$ combines terms of different origin. Our manipulations provide the general expression for the evolution of the matrix object $u_{n_1n_2..}$ in our system of many reservoirs pumping many modes,

$$\begin{aligned}\dot{u}_{n_1n_2..} = \gamma\sum_i n_i^c\Bigg[-\frac{\big(\sum_j \alpha_{ij}(n_j+1) - \frac{\alpha_{i1}}{2}\big)u_{n_1n_2..}}{\sum_j \alpha_{ij}(n_j+1) - \frac{\alpha_{i1}}{2} + n_i^s} + \sum_j \frac{\alpha_{ij}n_j u_{n_1n_2..n_j-1..}}{\sum_k \alpha_{ik}(n_k+1) - \alpha_{ij} - \frac{\alpha_{i1}}{2} + n_i^s}\Bigg] \\ +\gamma\Bigg[\Big(\sum_j n_j - \tfrac{1}{2}\Big)u_{n_1n_2..} + n_1 u_{n_1+1n_2..} + \sum_{j\neq 1}(n_j+1)u_{n_1n_2..n_j+1..}\Bigg] \\ +i(\kappa_1(2n_1-1)u_{n_1n_2..} + i\sum_{j\neq 1}\eta_j n_j u_{n_1n_2..}.\end{aligned} \tag{4.25}$$

To write the initial condition for $u_{n_1n_2..}$, we note that at $\tau = 0$ (see (4.20)) we sample the steady state component of the system,

$$u_{n_1n_2..}(0) = \langle n_1, n_2, ...|a_1^\dagger a_1\rho_o|n_1, n_2, ...\rangle = n_1 P_{n_1n_2..}, \tag{4.26}$$

with $P_{n_1n_2..}$ given by (3.28).

Lastly, the magnitude of $\dot{u}_{n_1n_2..}$ gives the coherence function,

$$g^{(1)}(\tau) = \frac{1}{\langle n_1\rangle}\sum_{n_1,n_2..} u_{n_1n_2..}(\tau). \tag{4.27}$$

For up to several hundreds particles and in two modes, (4.25) can be integrated numerically, allowing us to obtain $g^{(1)}(\tau)$ without further approximations.

4.2.2 Numerical Solution for the Coherence Function

We briefly discuss the numerical approach for solving (4.25). The solution was implemented in two modes ($n_1, n_2 \to n, p$; for a two-mode form of (4.25), see (C.1)) using the simplest numerical scheme, forward Euler. The challenge of having to solve in the order a one million coupled equations dissuaded us from investing further effort in developing a code with more elaborate the numerical techniques, e.g. Runge-Kutta[Pres 07], after we obtained reliable numerical solutions. The numerical toolboxes we investigated in Matlab would not support such a large system. We used the code to explore how the linewidth varies with the parameters $\alpha_{ij}, \kappa, \eta$ in a reduced, i.e. smaller n_c, n_s, two-reservoir, two-mode system, out of which we found an interesting multimode feature, also shown here (Fig. 4.1). In Chapter 5, we will present results obtained in a two-reservoir, two-mode system system containing several hundreds particles, as seen in experiments[Tosi 12, Abba 13, Love 08, Whit 09]. These full runs, being quite time consuming, were generated only a small number of times.

The size of the numerical problem is determined by the maximum occupation number which must be considered, in turn depending on the model parameters. In practice we chose p_{max}, n_{max} such that the occupation probability in the steady-state, $P_{n_{max}\, p_{max}}$, is at one-thousandth of its maximum, $(P_{np})_{max}$. The edges of the occupation matrix that we treat form "natural" and "artificial" boundaries[Kamp 07]. The "natural" boundaries occur at $n = 0$, $p = 0$ where, if treated naively, some prefactors would imply unphysical transitions, e.g. $u_{0p} \leftrightarrow u_{-1p}$. We do not need to impose any additional conditions on these boundaries, only pay close attention to the terms which would give rise to these unphysical transitions. They occur in pairs (one linked with $\mathcal{L}_p$ the other with $\mathcal{L}_d$), and we eliminate them appropriately along these boundaries. The "artificial" boundaries occur at p_{max}, n_{max}. The prefactors corresponding to transitions outside these boundaries do not vanish i.e. there is some "probability flow" in and out of the region treated numerically. To deal with these boundaries we set $\dot{u}_{np} = 0$ on them. We found that this procedure, along with the criteria for the size of the region of interest stated above, generates convergent results and reproduces published results for the single-mode case[Whit 09]. We observed that more elaborate schemes such as that used with natural boundaries would introduce mismatch in the complex phase of the elements within the distribution as it evolves and fail to produce converging results.

In implementing the solution, the time steps have to be kept very small, 0.0001γ so that the evolution, produced by the weighted difference between neighbors, remains consistent, i.e. equilibrates, across the distribution. We also note that it is important in defining the coefficients in (4.25) to observe as written the factors ± 0.5, ± 1. Even

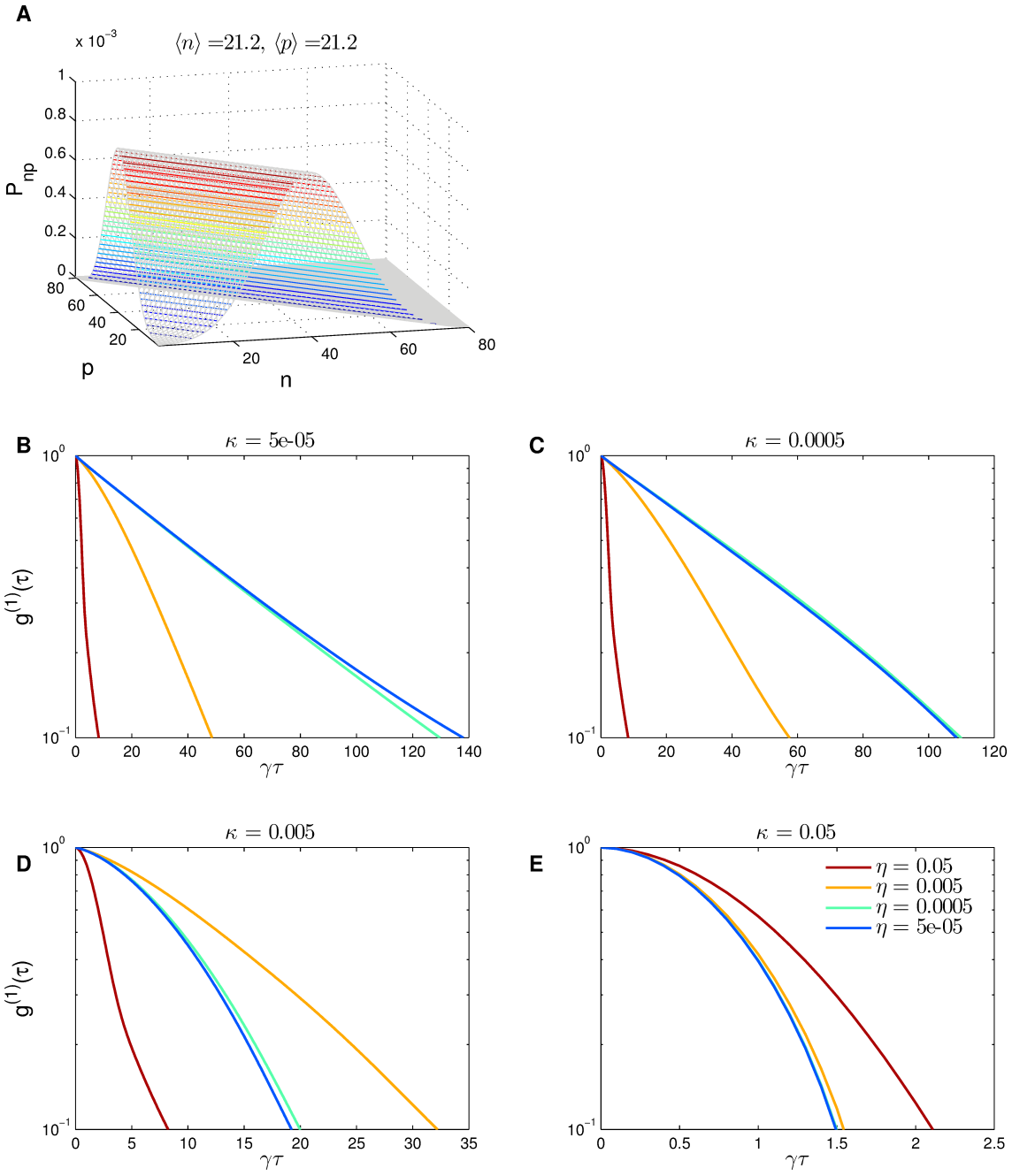

Figure 4.1: Sampling of the parameter space with numerical solutions in a reduced system ($\alpha_{ij} = 0.5$, $n_s = 50$, $n_c = 70$). (A) Population distribution. (B-E) Coherence decay with $\kappa = 5e-5$, 0.0005, 0.005, 0.05 and corresponding values of η in each pane. The coherence time increases for increasing η up to a value of $\eta = \kappa$ and then decreases again.

though they appear small compared with n and p, they are the ones which generate the

difference between two coefficients in (4.25) and are therefore ultimately linked with transition rates. Appendix B gives relevant extracts of the code implementation.

We used a reduced system to explore the parameter space of our model (Sec. 2.4): saturation parameter, $n_s = 50$; pumping strength, $n_c = 70$; reservoir i to condensates j normalized coupling, $\alpha_{ij} = 0.5$ and decay rate $\gamma = 1$, which also sets the unit of time. The ridge-shaped population distribution obtained with these parameters is shown in Fig. 4.1A. Also shown (Fig.4.1B-E) are 16 runs of the code with intra- and inter-mode interactions (Sec. 2.5): $\kappa, \eta = 5e{-}5, 0.0005, 0.005, 0.05$. We notice that, in the ridge case, fluctuations in n and p are anti-correlated[Sing 80]. This translates into energy fluctuations due to κ and η partly canceling each other when both terms are of equal strength. This is observed in Fig.4.1C-E where the coherence time increases until $\eta = \kappa$ and then (Fig.4.1C-D) decreases with η becoming stronger than κ. We will come back to this in a specific example in Chapter 5. We also notice the typical exponential (linear on a semilog plot) decay in Fig.4.1B which gradually becomes Gaussian Fig.4.1E (parabolic on semilog) as the interaction strength increases. The Gaussian decay is characteristic of the static limit, as we shall see in Sec. 4.3.3.

4.2.3 Cross-Correlation Function

Without the non-particle conserving terms in the Hamiltonian (2.91) the phase between any two condensate modes is free. This is shown by the cross-correlation function, $\langle a_1^\dagger(\tau) a_2 \rangle$, being zero. We show it in a two-mode system, where $u^t_{np}(0)$ is zero,

$$\begin{aligned} u^t_{np} &= \langle n, p \mid a_1^\dagger e^{\mathcal{L}t} a_2 \rho \mid n, p \rangle \\ &= \langle n, p \mid a_1^\dagger \rho'(\tau) \mid n, p \rangle \\ &= \sqrt{n}\, \rho'_{n-1npp}(\tau) \end{aligned} \tag{4.28}$$

with

$$\begin{aligned} \rho'_{nnpp} &= \langle n, p \mid a_2 \tilde{\rho} \mid n, p \rangle \\ &= \sqrt{p+1}\, \rho_{nnp+1p} \end{aligned} \tag{4.29}$$

such that

$$u^t_{np}(0) = \sqrt{n}\, \rho'_{n-1npp}(0) = \sqrt{n}\sqrt{p+1}\, \rho_{n-1np+1p,ss} = 0, \tag{4.30}$$

since the steady state, ρ_{ss}, is diagonal in the absence of non-particle conserving terms. Had there been particle exchange induced by the condensate Hamiltonian, the steady

state would not be diagonal, the phase between the modes would be determined and the cross-coherence function would not vanish.

4.3 First Order Coherence – Approximate Solutions

In order to make further headway towards extracting the physics of multi-mode condensates, we need to move beyond the direct numerical solution for the density matrix in Fock space. Here we present two semi-analytic approaches to obtain the first order coherence function. Some computational resources are needed, but in a problem with reduced effective dimensionality.

Analytic work is being made more difficult in this chapter compared with the work on population distributions (Chapter 3) for two reasons. In Chapter 3, it was possible to transform the steady state equation into a differential equation without having to consider the zero-particle cutoff until after an expression is obtained. In contrast, for coherence functions the cutoff enters the problem in the first step, it is part of the initial condition. Also, since we are dealing with off-diagonal terms, the commutator of the condensate Hamiltonian contributes to the equation of motion. These two elements make the solution of multi-mode coherence functions beyond the reach of analytic work.

The first approach we shall present emulates the method of solving the second order continuity equation that is often used to solve for one-step (Poisson), time-local (Markovian) processes, the Fokker-Planck equation [Kamp07, Whit09]; although here additional terms are present to account for decay. The second, and much simpler, approach is to neglect the dynamics due to pumping and decay between the times where the two operators, $a^\dagger(\tau)$ and $a(0)$ in $g^{(1)}(\tau)$, are evaluated. The decay of $g^{(1)}(\tau)$ is then entirely due to the effect of the condensate Hamiltonian. This is the static limit approximation, previously employed in the single-mode case [Love08, Whit09].

4.3.1 Fokker-Planck Approach

The Fokker-Planck approach combines two approximation schemes. First the discrete occupation numbers are treated as continuous and transition operators are approximated by differential operators. This is known as a Kramer-Moyal expansion [Gard98]. This first approximation is done in the same way as we have done to obtain population distributions, in Chapter 3, except here the step operators are turned into derivatives taken up to second order. The resulting equation is a Fokker-Planck form, i.e. a

convection equation, in which the distribution u undergoes drift and diffusion. There are however, additional terms which induce a decay. The second approximation is to expand the prefactors in u into a Taylor series around the maximum of the initial condition, u_o (4.26), and to include all the terms which still allow for an analytic solution to the Fokker-Planck equation i.e. at most a linear drift component and a constant diffusion rate. The solution is obtained by placing the equation thereby obtained in reciprocal space and by solving it with the method of characteristics. We present our solution in the general many-reservoir many-mode formalism. In Appendix C.1, we show a parallel set of equations expressed in a two-reservoir, two-mode formalism.

Kramer-Moyal Expansion and Linearization

We start our Kramer-Moyal expansion by rewriting our distribution function (4.25) with prefactor functions and step operators,

$$\dot{u}_{n_1n_2..} = (\vec{\mathbb{E}}^{-1} - \mathbf{1}) \cdot [\mathbf{q}_{n_1n_2..} u_{n_1n_2..}] + (\vec{\mathbb{E}} - \mathbf{1}) \cdot [\mathbf{r}_{n_1n_2..} u_{n_1n_2..}] + h_{n_1n_2..} u_{n_1n_2..} + s_{n_1n_2..} u_{n_1n_2..}, \tag{4.31}$$

$\vec{\mathbb{E}} = (\mathbb{E}_{n_1}, \mathbb{E}_{n_2}, ..)$ is a step operator vector. The i^{th} step operator, $\mathbb{E}_{n_i}$, acting on the i^{th} element $q_{i,n_1n_2..} u_{n_1n_2..}$ gives $q_{i,n_1n_2..n_i+1..} u_{n_1n_2....n_i+1..}$. The $h_{n_1n_2..}$ term arises from the fact that for mode one, the prefactor of $u_{n_1n_2..}$ (4.25) has an additional $-\frac{1}{2}$ in it, both for pumping and decay. This $-\frac{1}{2}$ component has to be brought out of the step operator expansion; it will give rise to the Shawlow-Townes decay. The term $s_{n_1n_2..}$ carries the interaction induced decay component of u. The exact realizations of $\mathbf{q}_{n_1n_2..}$, $\mathbf{r}_{n_1n_2..}$, $h_{n_1n_2..}$ and $s_{n_1n_2..}$ are not shown; for a two mode version, see Appendix C.1, Equations (C.3−C.8).

We then use the fact that $\dot{u}_{n_1n_2..}$ is smooth with respect to n_i to make it continuous and Taylor expand the step operators into derivatives, $\mathbb{E}_{n_i}^{\pm 1} \to 1 \pm \partial_{n_i} + \frac{1}{2}\partial_{n_i}^2$, up to second order. The step operator distribution function (4.31) takes a Fokker-Planck form,

$$\begin{aligned} \dot{u}_{(n_1n_2..)} = {} & \nabla \cdot [(\mathbf{r}_{(n_1n_2..)} - \mathbf{q}_{(n_1n_2..)}) u_{(n_1n_2..)}] + \tfrac{1}{2}\nabla^2 \cdot [(\mathbf{r}_{(n_1n_2..)} + \mathbf{q}_{(n_1n_2..)}) u_{(n_1n_2..)}] \\ & + h_{(n_1n_2..)} u_{(n_1n_2..)} + s_{(n_1n_2..)} u_{(n_1n_2..)} \end{aligned} \tag{4.32}$$

where $\nabla = (\partial_{n1}, \partial_{n2}, ..)$, $\nabla^2 = (\partial_{n1}^2, \partial_{n2}^2, ..)$. The first order or drift term, ∇, has coefficient, $(\mathbf{r}_{(n_1n_2..)} - \mathbf{q}_{(n_1n_2..)})$, while the second order or diffusion term, ∇^2, has coefficient, $(\mathbf{r}_{(n_1n_2..)} + \mathbf{q}_{(n_1n_2..)})$. The terms in h, s are the ones which make (4.32) differ from being a Fokker-Planck equation. As stated above, because of them the integral of $\dot{u}$ is

non-vanishing, i.e. the integrate of u evaluated at the boundaries is non-zero because of them, causing the magnitude of u to decay, hence the finite linewidth.

In the next steps we will, (i) determine how the coefficients can be Taylor expanded and which terms we can be include towards the solution, (ii) place a general function which reflects these terms in reciprocal space and in a form that can be solved by the method of characteristics, and (iii) show how the coefficients of the transformed equation are obtained.

(i) The partial differential form (4.32) we obtained, like the Fokker-Planck equation, is soluble when h, s and the drift coefficients are at most linear functions, and the diffusion coefficients are constant. We therefore rearrange (4.32) such that these terms are easily read from it

$$\dot{u} = \underbrace{(h+s)}_{\text{linear}} u + \nabla \cdot \Big[\underbrace{\big[\mathbf{r} - \mathbf{p} + \tfrac{1}{2}\nabla \odot (\mathbf{r}+\mathbf{q})\big]}_{\text{at most linear}} u + \tfrac{1}{2} \underbrace{(\mathbf{r}+\mathbf{q})}_{\text{constant}} \odot \nabla u \Big] \tag{4.33}$$

where $\odot$ denotes the element-wise multiplication.

(ii) We now introduce a general form which contains all the terms which appear above,

$$\dot{v} = \alpha v + \sum_i \beta_i n_i' v + \sum_i \gamma_i \partial_{n_i'} v + \sum_{ij} \delta_{ij} \partial_{n_i'} n_j' v + \frac{1}{2} \sum_{ij} \epsilon_{ij} \partial^2_{n_i' n_j'} v, \tag{4.34}$$

where n_i' will become the linearized occupancy (see iii below). This form will allow to keep track of the coefficients while we switch to the (two-sided) Laplace domain. The coefficients will be obtained by linearizing the prefactors. Placing (4.34) in reciprocal space interchanges the partial differentiation operators with multiplication by the conjugate variables, $\partial_{n_i'} \to \mathrm{i}k_i$, and vice versa, $n_i' \to \mathrm{i}\partial_{k_i}$, so that,

$$\alpha \int e^{-\mathrm{i}\sum_i n_i' k_i} v \; d^i n' = \alpha g \tag{4.35}$$

$$\beta_i \int e^{-\mathrm{i}\sum_i n_i' k_i} n_i' v \; d^i n' = \mathrm{i}\beta_i \partial_{k_i} g \tag{4.36}$$

$$\gamma_i \int e^{-\mathrm{i}\sum_i n_i' k_i} \partial_{n_i'} v \; d^i n' = \mathrm{i}\gamma_i k_i g \tag{4.37}$$

$$\begin{aligned} \delta_{ij}' \int e^{-\mathrm{i}\sum_{i,j} n_{i,j}' k_{i,j}} \partial_{n_i'} n_j' v \; d^{i,j} n' &= \mathrm{i}\delta_{ij}' \, k_i \int e^{-\imath \sum_j n_j k_j} n_j' v \; d^j n' \\ &= -\delta_{ij}' k_i \partial_{k_j} g \end{aligned} \tag{4.38}$$

$$\epsilon_{ij} \int e^{-\mathrm{i}\sum_{i,j} n_{i,j}' k_{i,j}} \partial^2_{n_i' n_j'} v \; d^{i,j} n' = -\epsilon_{ij} k_i k_j g. \tag{4.39}$$

Hence instead of being second order, the equation becomes a first order partial differential equation and the linear term (with coefficient δ_{ij}) now appears before the derivative,

$$\dot{g} = \alpha g + \mathrm{i}\sum_i \beta_i \partial_{k_i} g + \mathrm{i}\sum_i \gamma_i k_i g - \sum_{ij} \delta'_{ij} k_i \partial_{k_j} g - \frac{1}{2}\sum_{ij} \epsilon_{ij} k_i k_j g. \tag{4.40}$$

With the method of characteristics[Kamp07], all the derivatives are expressed in terms of differentiation with respect to a single independent variable, t,

$$g(t) \;\rightarrow\; g(t, K(t)) \quad , \quad \frac{\mathrm{d}g}{\mathrm{d}t} = \partial_t g + \sum_j \partial_{k_j} g \, \frac{dk_j}{dt}.$$

We rewrite our partial differential equation (4.40) to reflect this,

$$\dot{g} + \sum_j \big(a_j + \sum_i b_{ij} k_i\big)\partial_{k_j} g = c\, g + \sum_i d_i k_i g + \sum_{ij} e_{ij} k_i k_j g, \tag{4.41}$$

or, in vector form,

$$\dot{g} + \nabla g \cdot (\tilde{A} + \tilde{B}\tilde{K}) = cg + DKg + KE\tilde{K}g, \tag{4.42}$$

where $\tilde{K}$ is the transpose of K, and the final set of coefficients we will use on is,

$$a_j = -(\mathrm{i}\beta_j), \quad b_{ij} = -(-\delta'_{ij}), \quad c = \alpha, \quad d_i = \mathrm{i}\gamma_i, \quad e_{ij} = -\frac{\epsilon_{ij}}{2}. \tag{4.43}$$

(iii) We are now in position to extract the coefficients in (4.42), from (4.33). The linearization point, $\mathbf{n}' = \mathbf{n} - \mathbf{n}^l$, that we use is the maximum of u at $t = 0$, u_o given by (4.26), or (C.2) in two modes. The elements of $\mathbf{n}^l$ are given by,

$$n_i^l = \frac{\langle n_i n_1 P_{(n_1,n_2,..)}\rangle}{\langle n_1 P_{(n_1,n_2,..)}\rangle} = \frac{\langle n_i u_o\rangle}{\langle u_o\rangle}, \tag{4.44}$$

(C.9) in two modes, and the Taylor expansion of the various terms in (4.33, C.3−C.8

in two modes), around $\mathbf{n}_l$ provides us with the coefficients,

$$a_i = -\mathrm{i}\partial_{n_i}(h+s)|_{\mathbf{n}_l} \tag{4.45}$$

$$b_{ij} = \partial_{n_j}(r_{i,n_1n_2..} - q_{i,n_1n_2..})|_{\mathbf{n}_l} \tag{4.46}$$

$$c = h|_{\mathbf{n}_l} \tag{4.47}$$

$$d_i = \mathrm{i}\big(\, r_{i,n_1n_2..} - q_{i,n_1n_2..} + \tfrac{1}{2}\partial_{n_{[j\to i]}}(r_{i,n_1n_2..} + q_{i,n_1n_2..})\,\big)|_{\mathbf{n}_l} \tag{4.48}$$

$$e_{ii} = -\tfrac{1}{2}(r_{i,n_1n_2..} + q_{i,n_1n_2..})|_{\mathbf{n}_l}, \tag{4.49}$$

or (C.10−C.14) in two modes. For simplicity, in the linear drift coefficient B, we neglect the quadratic terms (coefficients for $n_i'^2,\ p_i'^2,\ n_i'p_j'$) in the expansion of $\mathbf{r}+\mathbf{q}$, which our form also allows to treat; they would contribute a small linear term to the drift coefficient. We point out that the subscript i, i.e. $r_i,\ q_i$, in B (and the second terms in D) originate from the subscript in $\mathbb{E}_{n_i}$ while the subscript j, ($[j\to i]$ in D) is linked to n_j' in the linearization of the drift (and diffusion) terms. Also, since the Kramer-Moyal expansion we are using only employs diagonal step operators (in $\mathbb{E}_n, \mathbb{E}_p$ as oppose to a mixture $\mathbb{E}_n\mathbb{E}_p$), the last term, e_{ij}, is diagonal.

Solution of the Linearized Differential Equation

We now provide the solution of the linearized differential equation (4.42), the last step before reaching $g^{(1)}(\tau)$. The remaining steps being in matrix form can be carried either with the general forms above or with the two mode expressions in Appendix C.1. Along the characteristics given by

$$\dot{k_j} = a_j + \sum_i b_{ij}k_i \qquad \text{or} \qquad \dot{K} = A + KB, \tag{4.50}$$

The characteristics equation (4.42) becomes,

$$\frac{\mathrm{d}g\big(K(t),t\big)}{\mathrm{d}t} = \big[c + DK + KE\tilde{K}\big]g, \tag{4.51}$$

and solves into,

$$g = g_o(K_o)\exp\Big[ct + D\int_0^t K\mathrm{d}t' + \int_0^t KE\tilde{K}\mathrm{d}t'\Big]. \tag{4.52}$$

In the next steps, we (i) solve the characteristics, (ii) perform the inner integrals in (4.52), and (iii) provide the full solution and the initial conditions for (4.52).

(i) The characteristics (4.50) have to be solved in the eigenbasis of B. We define the eigenvector matrix P and the relations,

$$\mathbb{B} = P^{-1}BP \tag{4.53}$$

$$\mathbb{A} = AP, \quad \mathbb{K} = KP. \tag{4.54}$$

such that, with $\mathbb{B}$ being diagonal, the characteristic equation (4.50) can be written in the form of uncoupled equations,

$$\dot{\mathbb{K}}P^{-1} = A + \mathbb{K}P^{-1}B \tag{4.55}$$

$$\Rightarrow \dot{\mathbb{K}} = AP + \mathbb{K}P^{-1}BP \tag{4.56}$$

$$= (\mathbb{A}\mathbb{B}^{-1} + \mathbb{K})\mathbb{B} \tag{4.57}$$

$$\Rightarrow \ln(\mathbb{A}\mathbb{B}^{-1} + \mathbb{K}')|_{\mathbb{K}_o}^{\mathbb{K}} = \mathbb{B}t. \tag{4.58}$$

This gives,

$$\mathbb{K} = -\mathbb{A}\mathbb{B}^{-1} + (\mathbb{A}\mathbb{B}^{-1} + \mathbb{K}_o)e^{\mathbb{B}t}, \qquad \mathbb{K}_o = -\mathbb{A}\mathbb{B}^{-1} + (\mathbb{A}\mathbb{B}^{-1} + \mathbb{K})e^{-\mathbb{B}t}. \tag{4.59}$$

Using the eigenvector relations (4.53, 4.54) and $e^{P^{-1}BP} = P^{-1}e^{B}P$, we reach

$$K = -AB^{-1} + (AB^{-1} + K_o)e^{Bt}, \tag{4.60}$$

$$K_o = -AB^{-1} + (AB^{-1} + K)e^{-Bt}. \tag{4.61}$$

It is important that K_o be defined as written here; AB^{-1} cannot be absorbed into its definition. This is because for K and t being zero, K_o also has to be zero if $g_o(K_o)$ in (4.52) is to be consistent with the rest of the solution.

(ii) Next we solve the integral associated with D in (4.52) by making all the time dependence in $K(t)$ explicit, placing the integrand in the eigenbasis of B once again generates a set of uncoupled equations which solve as,

$$\int_0^t K\mathrm{d}t' = \int_0^t \mathrm{d}t'\mathbb{K}P^{-1} \tag{4.62}$$

$$= \Big[-\mathbb{A}\mathbb{B}^{-1}t + \mathbb{K}_o\mathbb{B}^{-1}(e^{\mathbb{B}t} - I)\Big]P^{-1}. \tag{4.63}$$

We then bring the solution back to the original basis

$$\int_0^t K\mathrm{d}t' = -AB^{-1}t + K_oB^{-1}(e^{Bt} - I), \tag{4.64}$$

and substitute K_o (4.61) into the solution,

$$\int_0^t K\mathrm{d}t' = -AB^{-1}t + (AB^{-1} + K)B^{-1}(I - e^{-Bt}). \tag{4.65}$$

The integral associated with E in (4.52) is more involved,

$$\begin{aligned}\int_0^t KE\tilde{K}\mathrm{d}t' =& AB^{-1}E\tilde{B}^{-1}\tilde{A}t \\ &- \int_0^t \Big((AB^{-1} + K_o)e^{Bt}E\tilde{B}^{-1}\tilde{A} + \text{T.c.}\Big)dt' \\ &+ \int_0^t (K_o + AB^{-1})e^{Bt'}Ee^{\tilde{B}t'}(\tilde{K}_o + \tilde{B}^{-1}\tilde{A})dt'.\end{aligned} \tag{4.66}$$

The integral in the second line of (4.66) in performed in the same way as (4.62−4.64), and gives,

$$-\Big((AB^{-1} + K_o)B^{-1}(e^{Bt} - I)E\tilde{B}^{-1}\tilde{A} + \text{T.c.}\Big). \tag{4.67}$$

Substituting K_o (4.61) in the solution provides,

$$-\Big((AB^{-1} + K)B^{-1}(I - e^{-Bt})E\tilde{B}^{-1}\tilde{A} + \text{T.c.}\Big). \tag{4.68}$$

To determine the last integral in (4.66), the eigenbasis of B also has to be used, but this time it remains explicit in the solution,

$$(K_o + AB^{-1})P\Big[\int_0^t e^{\mathbb{B}t'}P^{-1}E\tilde{P}^{-1}e^{\mathbb{B}t'}dt'\Big]\tilde{P}(\tilde{K}_o + \tilde{B}^{-1}\tilde{A}), \tag{4.69}$$

and K_o (4.61) can already be substituted,

$$(AB^{-1} + K)P\left[e^{-\mathbb{B}t}\Big[\int_0^t e^{\mathbb{B}t'}P^{-1}E\tilde{P}^{-1}e^{\mathbb{B}t'}dt'\Big]e^{-\mathbb{B}t}\right]\tilde{P}(\tilde{B}^{-1}\tilde{A} + \tilde{K}). \tag{4.70}$$

Here we used the manipulation, $\ldots e^{-Bt}P\big[\ \ldots\ \Rightarrow\ \ldots e^{-P\mathbb{B}P^{-1}t}P\big[\ \ldots\ \Rightarrow\ \ldots P\big[e^{-\mathbb{B}t}\ \ldots$, and its T.c.. We further define a matrix which combines the eigenvector matrix of B with E,

$$E_p = P^{-1}E\tilde{P}^{-1}, \tag{4.71}$$

and solve the centre part of (4.70) as,

$$e^{-\mathbb{B}t}\Big[\int_0^t e^{\mathbb{B}t'}E_p e^{\mathbb{B}t'}dt'\Big]e^{-\mathbb{B}t} = \sum_{ij}\hat{\imath}\otimes\hat{\jmath}\frac{e_{p\,ij}}{\mathrm{b}_{ii}+\mathrm{b}_{jj}}(1-e^{-(\mathrm{b}_{ii}+\mathrm{b}_{jj})t}), \tag{4.72}$$

since the $e^{\mathbb{B}t'}$ on the left of E_p applies to it row-wise, whereas the one on the right applies column-wise. The outer product of unit vectors $\hat{\imath},\hat{\jmath}$ produces a matrix with all zeros, except for a 1 at position ij; $\mathrm{b}_{ii},\ \mathrm{b}_{jj}$ are the diagonal elements of $\mathbb{B}$.

(iii) We therefore write the full solution of our characteristics equation (4.52) as

$$\begin{aligned} g = g_o(K_o)\exp\Bigg[& ct - DAB^{-1}t + AB^{-1}E\tilde{B}^{-1}\tilde{A}t \\ &+ D(AB^{-1}+K)B^{-1}(I-e^{-Bt}) \\ &- \Big((AB^{-1}+K)B^{-1}(I-e^{-Bt})E\tilde{B}^{-1}\tilde{A} + \text{T.c.}\Big) \\ &+ (AB^{-1}+K)P\Big[\sum_{ij}\hat{\imath}\otimes\hat{\jmath}\frac{e_{p\,ij}}{\mathrm{b}_{ii}+\mathrm{b}_{jj}}(1-e^{-(\mathrm{b}_{ii}+\mathrm{b}_{jj})t})\Big]\tilde{P}(\tilde{B}^{-1}\tilde{A}+\tilde{K})\Bigg], \end{aligned} \tag{4.73}$$

with $e_{p\,ij}$ being the elements of E_p (4.71). The initial condition, g_o, is obtained by placing u_o (4.26), (C.2) in two modes, in the reciprocal space,

$$\begin{aligned} g_o(K_o) &= \int e^{-iK_o\cdot(\mathbf{n}-\mathbf{n}^l)}n_1 P_{(n_1,n_2,..)}d^i n \\ &= \left(\int e^{-iK_o\cdot\mathbf{n}}n_1 P_{(n_1,n_2,..)}d^i n\right)\exp(iK_o\cdot\mathbf{n}^l), \end{aligned} \tag{4.74}$$

where we shifted by the linearization point, $\mathbf{n}' = \mathbf{n}-\mathbf{n}^l$, such that g_o is consistent with the remainder of the solution.

Obtaining $\mathbf{g^{(1)}}(\tau)$

Finally, the solution we seek corresponds to $g(K)$, given by (4.73), evaluated at $K(\tau) = 0$,

$$\int e^{-\mathrm{i}\sum_i n_i' k_i}u(\tau)\ d^i n'\Big|_{k_i=0} = \int u(\tau)\ d^i n' = g^{(1)}(\tau). \tag{4.75}$$

This turns (4.73) into

$$g^{(1)}(\tau) = g_o(\tau)\exp\big[c\tau + \zeta(\tau) + \xi(\tau)\big] \tag{4.76}$$

with, the term from the first integral, (4.65),

$$\zeta(\tau) = -DAB^{-1}\tau + DAB^{-1}B^{-1}(I - e^{-B\tau}), \tag{4.77}$$

the term from the second integral, (4.66 $\rightarrow$ 4.68, 4.70, 4.72),

$$\xi(\tau) = AB^{-1}\left[E\tau - \Big(B^{-1}(I - e^{-B\tau})E + \text{T.c.}\Big) + P\Big[\sum_{ij}\hat{\imath}\otimes\hat{\jmath}\frac{E_{p\,ij}}{\mathbb{B}_{ii}+\mathbb{B}_{jj}}(I - e^{-(\mathbb{B}_{ii}+\mathbb{B}_{jj})\tau})\Big]\tilde{P}\right]\tilde{B}^{-1}\tilde{A}, \tag{4.78}$$

and $g_o(\tau)$ being (4.74) evaluated at,

$$K_o' = -AB^{-1}(I - e^{-B\tau}), \tag{4.79}$$

the value of K_o (4.61) on the characteristic for which $K(\tau)$ at time τ is zero.

In evaluating (4.76), the coefficients, Eqs. (4.45−4.49), can be obtained analytically, while the diagonalization of B ($\mathbb{B}, P$), which remains explicit in (4.78), and the integral in $g_0(\tau)$ (4.74), are performed numerically.

Figure 4.2 shows how the first order coherence function obtained from the Fokker-Planck approach compares with the direct numerical solution for the two-mode case; they are in good agreement. Looking more closely, the best fit occurs in the ridge case, when interactions dominate the form of the decay (Fig. 4.2D, $\kappa, \eta = 0.005$). The interaction energy is bigger in this case than in the independent case due to larger population fluctuations in the initial conditions. The worst prediction also occurs in the ridge case, when the interactions are small (Fig. 4.2D, $\kappa, \eta = 0.0005$). This time the large fluctuations take the distribution further away from the linearization point and make the one-point approximative scheme less accurate. We also show how our method compares with the Kubo form in [Whit09], (Fig. 4.2B, blue dotted line). Overall, the analytically convenient Kubo expression has lower accuracy than the Fokker-Planck approach developed here. Appendix C.2 gives further comparisons of the Kubo formulas with our Fokker-Planck approach.

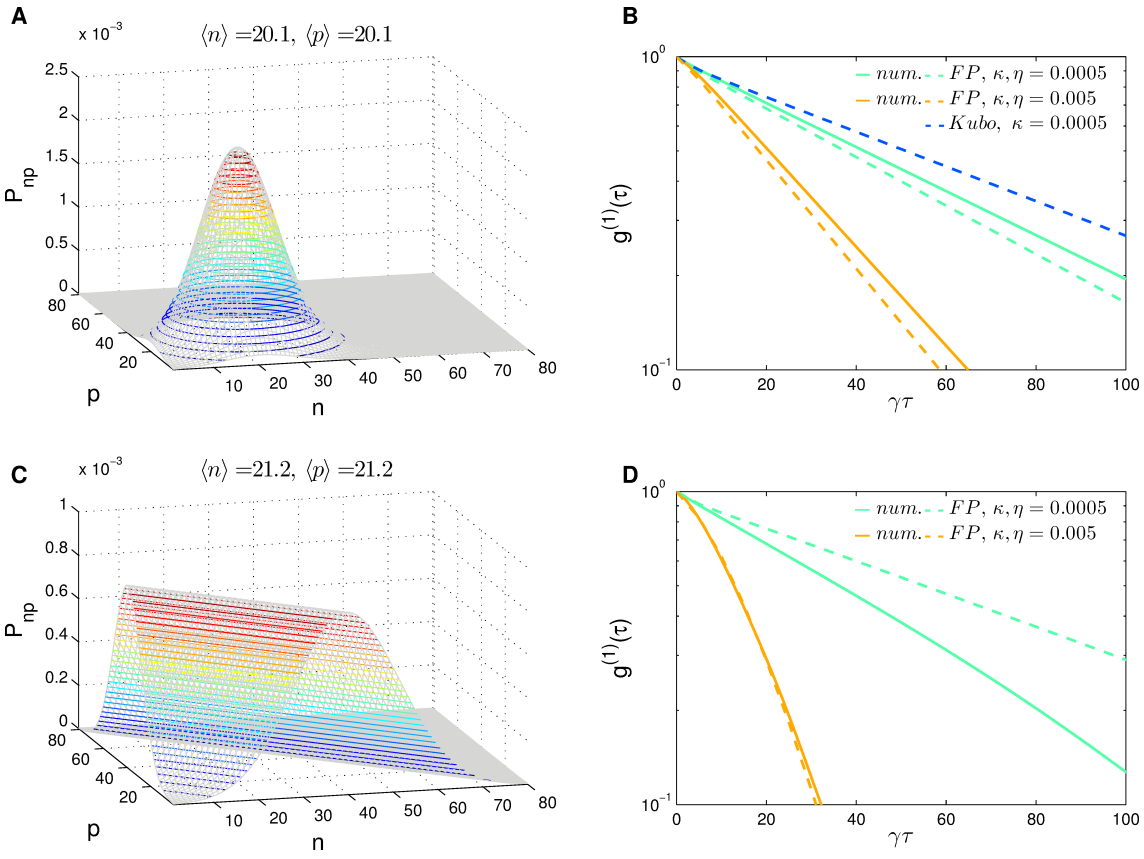

Figure 4.2: (A,C) Population distributions for two modes pumped by two reservoirs, with $\alpha_{11,22} = 1$, $\alpha_{12,21} = 0$ (independent pumping), and $\alpha_{ij} = 0.5$ (ridge), for $n_s = 50$, $n_c = 70$. (B,D) Comparison of first order coherence functions obtained numerically (solid lines) or with the Fokker-Planck approach (dashed lines) for the independent and ridge case. The interactions are either weak, $\kappa, \eta = 0.0005$, or stronger, $\kappa, \eta = 0.005$. With small interactions and in the independent case, in (B), we compare the Fokker-Planck approach with the Kubo form of [Whit09] (blue dashed line). The Fokker-Planck approach agrees well with the numerical solution, particularly when the interactions are strong and the population fluctuations are large, as seen in the ridge case.

4.3.2 Static Limit

A second approximative approach we consider is to evaluate $g^{(1)}$ in the static limit. This is cruder than the Fokker-Planck approach but also simpler to implement. For sufficiently small timescales, we can neglect the dynamics due to gain and loss processes. In such a situation we can therefore calculate $g^{(1)}$ by considering only the interaction Hamiltonian for the condensate. Formally, the static limit entails two approximations. The first is to assume that the evolution of the system is strictly due to interactions, $\dot{\rho} \simeq \mathcal{L}'\rho = -i[H, \rho]$, with the H from Sec. 2.5, while the second is to assume that n_1 does not vary across the distribution $\int n_1 P_{n_1..}.. \approx \langle n_1 \rangle \int P_{n_1..}.. $. With these, $\langle A^\dagger(\tau)A(0)\rangle$ (4.14), is turned into a integral transform with integration kernel related to $\sqrt{n_1}\langle ... - i[H, \rho']..\rangle$, (4.24). We show a general derivation here for $g^{(1)}$.

We start with

$$g_s^{(1)}(\tau) = \frac{1}{\langle n_1 \rangle} \langle a_1^\dagger e^{i\mathcal{L}'\tau} a \rangle, \tag{4.80}$$

and use,

$$\rho = \sum_{n1,n_2..} P_{n_1 n_2..} |n_1, n_2, ..\rangle\langle n_1, n_2..| \tag{4.81}$$

$$H = \sum_i \kappa_1 (a_i^\dagger a_i)^2 + \frac{1}{2} \sum_{i \neq j} \eta_{ij} a_i^\dagger a_i a_j^\dagger a_j, \tag{4.82}$$

to further write,

$$g_s^{(1)}(\tau) = \frac{1}{\langle n_1 \rangle} \sum_{n_{(i)}, n_{(j)}} \langle n_{(i)} | a_1^\dagger \mathrm{e}^{-iH\tau} a_1 P_{n_1 n_2} | n_{(j)} \rangle\langle n_{(j)} | \mathrm{e}^{iH\tau} | n_{(i)} \rangle \tag{4.83}$$

$$= \frac{1}{\langle n_1 \rangle} \sum_{n_{(i)}, n_{(j)}} \langle n_1\text{-}1, n_{(i\neq 1)} | \sqrt{n_1} \mathrm{e}^{-iH\tau} \sqrt{n_1} P_{n_1 n_2} | n_1\text{-}1, n_{(j\neq 1)} \rangle\langle n_{(j)} | \mathrm{e}^{iH\tau} | n_{(i)} \rangle \tag{4.84}$$

$$= \frac{1}{\langle n_1 \rangle} \mathrm{Tr}\Big[\mathrm{e}^{-i[\kappa_1 (n_1\text{-}1)^2 + \sum_{j\neq 1} \eta_{1j} (n_1\text{-}1) n_j \ ..]\tau} n_1 P_{n_1 n_2} \mathrm{e}^{i[\kappa_1 n_1^2 \tau + \sum_{j\neq 1} \eta_{1j} n_1 n_j \ ..]\tau} \Big], \tag{4.85}$$

where we have kept explicit in the exponentials, $e^{\mp iH\tau}$, only the terms which do not cancel. The factor $\frac{1}{2}$ in H disappears with $\sum_{i\neq j} \to \sum_{j\neq 1}$. This further simplifies as,

$$g_s^{(1)}(\tau) = \frac{1}{\langle n_1 \rangle} \sum_{n_1, n_{(j\neq 1)}} n_1 \mathrm{e}^{i[\kappa_1 (2n_1\text{-}1) + \sum_j \eta_j n_j]\tau} P_{n_1 n_2..} \tag{4.86}$$

$$\approx \sum_{n_1, n_{(j\neq 1)}} \mathrm{e}^{i[2\kappa n_1 + \sum_j \eta_j n_j]\tau} P_{n_1 n_2..}. \tag{4.87}$$

In the last step we have made use of the second approximation, i.e. we assumed n_1 constant across the distribution. We also simplified, $\kappa_1 = \kappa$, $\eta_{1j} = \eta_j$, as we have done before (4.24).

The general integral (4.87) has to be performed numerically. Appendix C.3 shows, in two modes, how the static limit can be calculated analytically for independent ($\beta_{o,1} = 1, 0$) and ridge ($\beta_{o,1} = 0.5$) distributions. In the ridge case, the integral is performed by changing basis, $u = \frac{1}{\sqrt{2}}(n-p)$, $v = \frac{1}{\sqrt{2}}(n+p)$.

Figure 4.3 shows how first order coherence functions obtained in the static limit compare with direct numerical solutions for the two-mode case. The static limit solution corresponds to the numerical solution, at early times, when the interaction is strong. In these cases, decoherence is rapid and occurs on a time-scale for which the dynamics of the population are negligible. The best fit is obtained in the ridge case since the larger population fluctuation makes the interaction broadening larger. The

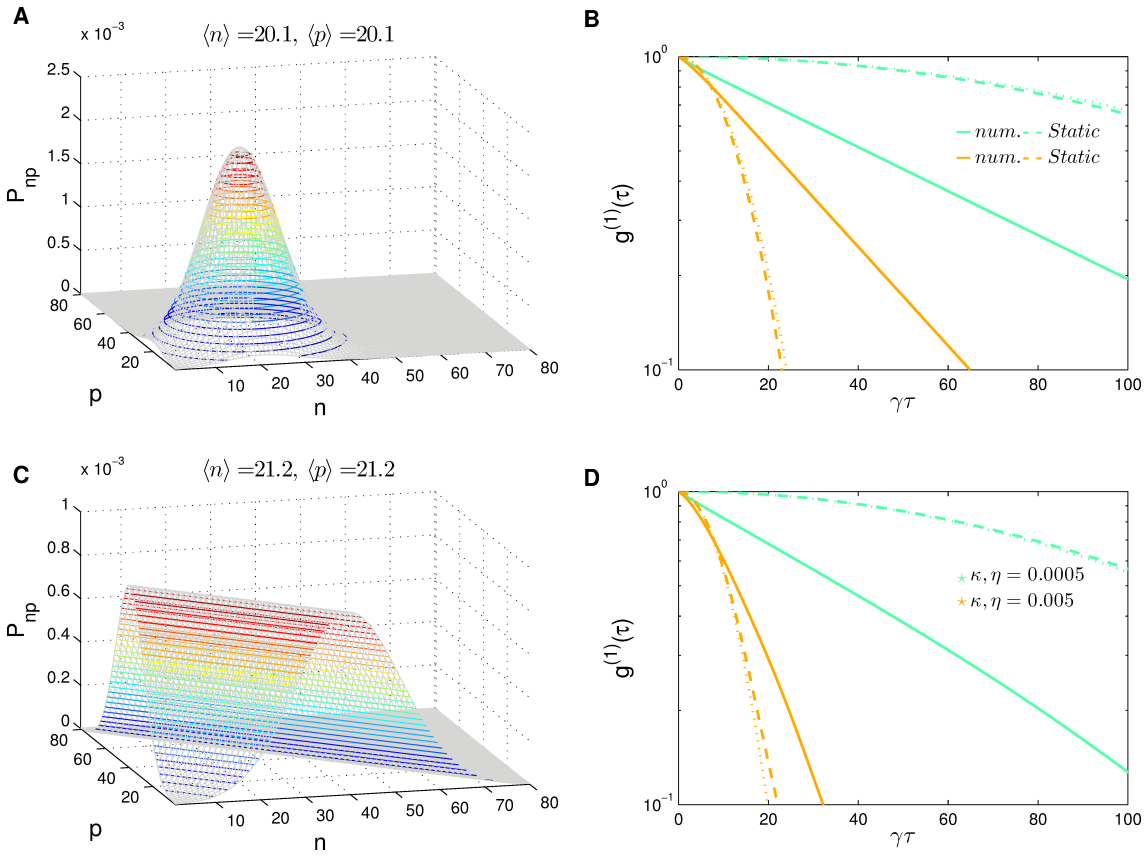

Figure 4.3: (A,C) Population distributions for two modes pumped by two reservoirs, with $\alpha_{11,22} = 1$, $\alpha_{12,21} = 0$ (independent pumping), and $\alpha_{ij} = 0.5$ (ridge), for $n_s = 50$, $n_c = 70$. (B,D) Comparison of first order coherence functions obtained numerically (solid lines) or with the static limit approximation (dashes lines) for the independent and ridge case. The interactions are either small, $\kappa, \eta = 0.0005$, or stronger, $\kappa, \eta = 0.005$. The static limit approximation improves when the interaction becomes stronger. The ridge case shows a better approximation due to the population fluctuations being stronger and therefore having stronger interaction broadening. The faint dotted line is with $\int n_1 P_{n_1..}..$ rather than $\approx \langle n_1 \rangle \int P_{n_1..}..$; this simplification does not affect the results significantly.

faint dotted lines show the static limit calculated without assuming that n_1 is constant across the distribution (4.86), (C.20) in two modes. Neglecting the multiplier n_1 does not have much effect. This is also true when the system is at mean threshold, $n_c = n_s$, where the variation of n_1 along the distribution is the largest.

4.3.3 Static Limit – Three Modes

The simplicity of the static limit approach allows to perform calculations that are either prohibitive with the full numerical or quite involved with the Fokker-Planck approach. Here we combine the analytical expression we obtained for the population distribution (3.29) with the static limit approach (4.87) to calculate the coherence functions of three-mode condensates, Fig. 4.4. We present results for the independent case Fig.

4.4A,C,E and the ridge case Fig. 4.4B,D,F. In three modes, the interaction strengths κ, η become κ, η_2, η_3. We present static limit calculations with η_2 and η_3 being switched on successively and compare the results with those of the two-mode case.

The parameter values we choose for n_c, n_s are 10400, 10000, the same as what we chose to show the three mode population in Sec. 3.2.3. We let $\beta_{0,1,2}$ be either 1,0,0 to form independent modes, Fig. 4.4A, or $\frac{1}{3}, \frac{1}{3}, \frac{1}{3}$ and form the ridge, Fig. 4.4B. In the independent case, the marginal population distribution, Fig. 4.4C, is no different from the population distribution of the two-mode case (e.g. Fig. 4.3A). Since the modes do not bear any correlation, the probability distribution of any of them do not depend on the others. This is not the case for the marginal probability distribution of the ridge, Fig. 4.4D. Compared with the two-mode ridge (e.g. Fig. 4.3C), the marginal distribution has a probability which goes down to zero since the particles can all be in the mode that is marginalized. We see through this that population fluctuations are therefore much larger in the ridge case when a third mode is introduced.

Looking at the static limit results, we see that in the independent case, Fig. 4.4D, the coherence time steadily decreases as η_2 and η_3 are being switched on. The effect of introducing intermode interactions is simply to increase the fluctuation energy and to therefore reduce the coherence time. We also see that the case where $\kappa, \eta_2, \eta_3 = g, g, 0$ provides the same coherence decay curve as in the two-mode case with $\kappa, \eta = g, g$. The marginal probability distribution of the three independent modes condensate being the same as for the two-mode independent distribution, the fluctuation energy when interactions only involve two modes is also identical, hence the same decay curve.

In Fig. 4.4D, the coherence decay curves for the three mode ridge follow a different trend. The cohence time increases slightly when the interaction due to η_2 is introduced and increases further when both η_2, η_3 are switched on. This is due to the same effect which was pointed out when discussing the numerical results (Fig. 4.1). Fluctuations between the modes being anticorrelated, introducing η_2 adds some energy fluctuations which cancels those due to κ, but only when both η_2 and η_3 are switched on do we see the intercorrelation effect between the three modes acting in a concerted manner and producing a significant increase in coherence time. Another way to interpret this result is to consider the vector in the kernel of the static limit integral transform (4.87). As we introduce the interactions η_2, η_3 the kernel vector points closer to the direction normal to the main axis of the ridge, i.e. the narrowest cut through it, Fig. 4.4B. The decay time is inversely proportional to this effective width of the ridge and therefore becomes longer as the integral is performed along an axis where the distribution is narrower. The independent modes distribution being isotropic the orientation of the

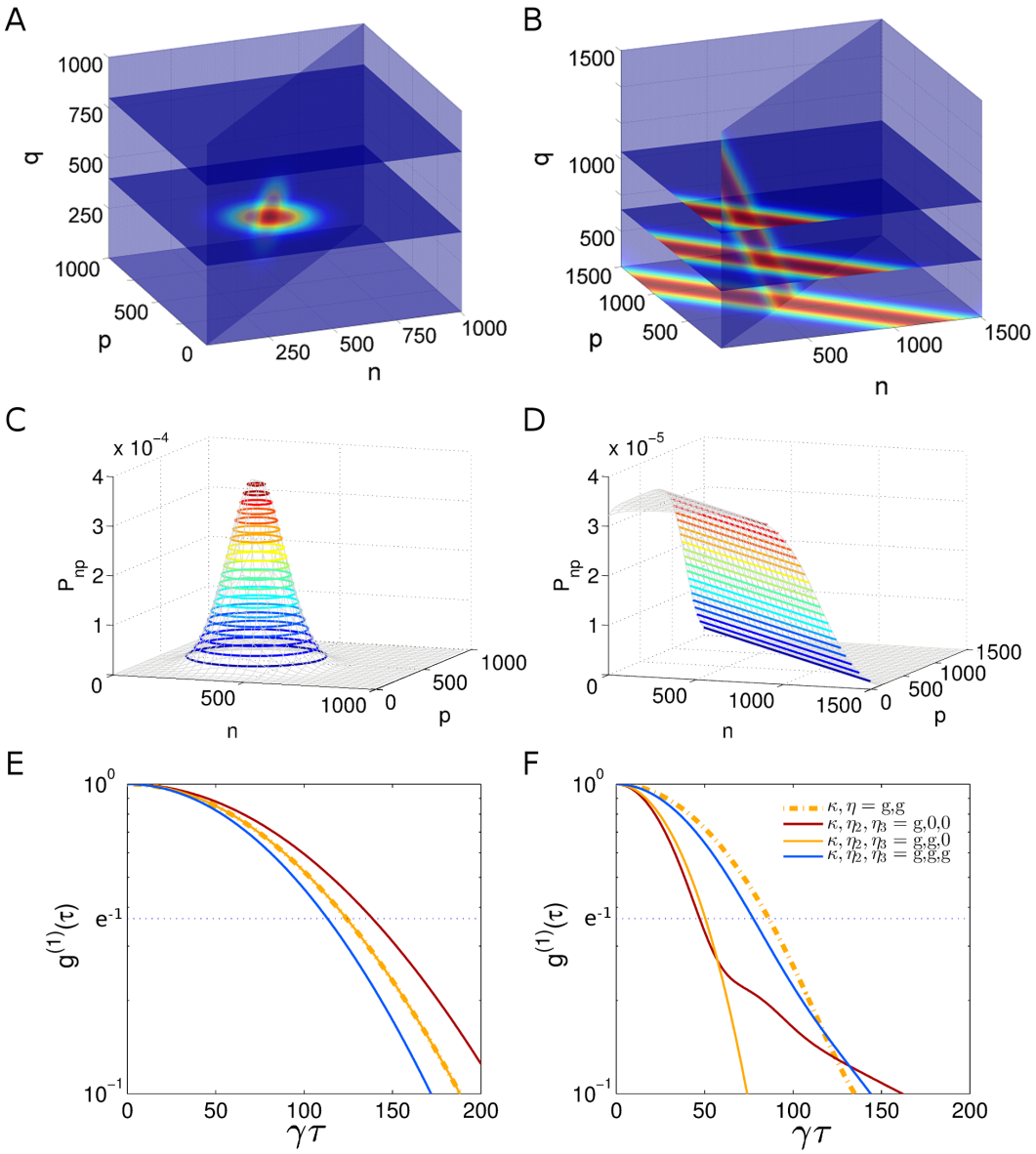

Figure 4.4: (A,B) Three mode joint population distributions, $P_{(n,p,q)}$, with $n_c, n_s = 10400, 10000$ in the independent case $\beta_{0,1,2} = 1, 0, 0$ and in the ridge case $\beta_{0,1,2} = \frac{1}{3}, \frac{1}{3}, \frac{1}{3}$. (C,D) Marginal population distribution $P_{(n,p)} = \int P_{(n,p,q)} dq$. The independent population distribution being isotropic, its marginal distribution takes the same form as the independent population distribution in two modes. In the ridge case, the particles can all be in the marginalized mode and the marginal distribution goes all the way down to zero, and thereby exhibits larger population fluctuations than the two mode ridge distribution. (E,F) Static limit results with $g = 5e-5$, $\kappa = g$ and η_2, η_3 being either 0 or g. Also shown is the static limit result in two modes with $\kappa, \eta = g, g$. In the independent case, only the magnitude of the total interaction strength influences the decay time. With $\kappa, \eta_2, \eta_3 = g, g, 0$ the decay curve is the same as the one in two modes with $\kappa, \eta = g, g$. In the ridge case, the anticorrelation in the population fluctuations cause the decay time to increase as η_2, η_3 are being switched on. Larger population fluctucations in the marginal distribution explain why the decay time is smaller in three modes than in two modes for the same interaction strengths.

kernel vector does not have an influence, only its magnitude.

Finally we compare the decay curves of the three mode ridge and of the two mode ridge when $\kappa, \eta_2, \eta_3 = g, g, 0$ and $\kappa, \eta = g, g$. For identical interaction strengths, the decay time for the three mode condensate is shorter for the two mode one. This can be explained by the fact that the marginal probability distribution contains larger fluctuations than the two mode distributions and that the energy fluctuations are therefore larger, hence the shorter decay time.

4.4 Second Order Correlation – Dephasing time of Josephson (Intensity) Oscillations.

Above we have shown how our theory can be used to calculate the first order coherence function, and hence the linewidth of the optical emission from the polariton condensate. We now show how it may be used to calculate a higher-order coherence function. In particular we shall develop a differential equation analogous to (4.25), in two modes (C.1), for a field distribution u, which allows us to compute the time-dependent second order coherence function $\langle a_1^\dagger(\tau) a_2(\tau) a_2^\dagger a_1 \rangle$. We focus on this specific coherence function because it corresponds to the oscillations in the emission intensity, which would arise in a multimode condensate due to beating between the different emission frequencies, i.e. it is a multimode phenomenon. Such intensity oscillations are similar to those of the a.c. Josephson effect [Jose 62], which has recently been observed for the polariton condensate in a double-well potential [Lago 10]. Our theory will allow to study the dephasing of these oscillations. We will find that because the condensate modes are coupled, this dephasing is not, in general, simply related to the decay of first order coherence. Thus measurements of these intensity oscillations provide information beyond that of the emission spectrum and could provide insight into the coupling between the condensates.

4.4.1 Intensity Oscillations

To motivate the consideration of the intensity-intensity coherence function, we consider for definiteness a double-well potential, as studied in [Lago 10] and discussed further in Chapter 5. We suppose that there are two relevant orbitals, $a_{L,R}$, localized in the left and right well (see Fig. 4.5), with some tunneling between them.

The single-particle states for this double well are in general a superposition of these left and right orbitals, $a_{1,2} = \frac{c_1}{c_1^2 - c_2^2} a_{L,R} + \frac{c_2}{c_2^2 - c_1^2} a_{R,L}$, and therefore overlap in space. The

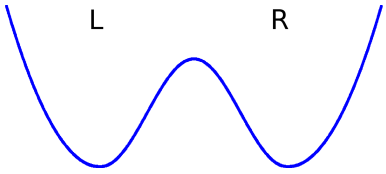

Figure 4.5: Schematic of a double well potential. In general, single-particle states, a_1, a_2, in a double well potential are superpositions of the relevant left and right orbitals, a_L, a_R.

intensity on the left is

$$\begin{aligned}\hat{I}_L &= a_L^\dagger a_L \\ &= (c_1^* a_1^\dagger + c_2^* a_2^\dagger)(c_1 a_1 + c_2 a_2) \\ &= |c_1^2| a_1^\dagger a_1 + |c_2^2| a_2^\dagger a_2 + c_1^* c_2 a_1^\dagger a_2 + c_2^* c_1 a_2^\dagger a_1.\end{aligned} \tag{4.88}$$

We treat the operators $a, a^\dagger$ as the classical, complex amplitudes of the electric field (order parameter of the condensate) to show how, semiclassically, the intensity on the left or right oscillates,

$$\begin{aligned}\langle \hat{I}_L \rangle &= |c_1^2| \langle a_1^\dagger \rangle \langle a_1 \rangle + |c_2^2| \langle a_2^\dagger \rangle \langle a_2 \rangle + c_1^* c_2 \langle a_1^\dagger a_2 \rangle + c_2^* c_1 \langle a_2^\dagger a_1 \rangle \\ &= |c_1^2| n_1 + |c_2^2| n_2 + 2\,\mathrm{Re}[c_1^* c_2 \sqrt{n_1 n_2} \mathrm{e}^{i(\omega_1 - \omega_2)t}]\end{aligned} \tag{4.89}$$

where $\omega_{1,2}$ are the frequencies of the condensate orbitals in each mode and $n_{1,2}$ the densities in the modes. The final term in (4.89) is the beating of the intensity between the oscillators corresponding to the single-particle orbitals.

The intensity oscillations are non-zero in the semiclassical theory because we assumed a particular phase for the order parameter(s), which could physically arise from spontaneous symmetry breaking[Pita 03]. However, our theory does not include any terms which fix this (relative) phase, so that the ensemble averaged intensity will not oscillate, $\langle a_1^\dagger(\tau) a_2(0) \rangle = 0$, as shown in Sec. 4.2.3. We interpret this within the semiclassical theory by noting that the phase of the oscillating component will fluctuate between members of an ensemble (e.g. different runs of an experiment); our theory is an average over many such phases. However, we can study how the oscillations in each member behave, for example considering the intensity-intensity correlation function, $\langle I(\tau) I(0) \rangle$, and in particular the components relating to the semiclassical oscillation, $\langle a_1^\dagger(\tau) a_2(\tau) a_2^\dagger a_1 \rangle$. We will see that these components decay so that the oscillating part of the intensity-intensity correlation, averaged over different runs, decays.

Experimentally, an oscillating emission from a condensate has indeed been observed for a double-well potential[Lago 10]; the results were shown in Figure 1.12. However we

note one important difference: the experimental data is an average over many runs and still reveals oscillations, showing that there are processes which fix the relative phase of the condensate orbitals, i.e., the origin of the intensity oscillations. Such a relative phase could be established by the Josephson-like terms, which we neglect in the strong-trapping regime, as discussed in section 2.5. Thus the experiment may not be entirely in this regime, although it is in principle accessible. We observe that these intensity oscillations are non-harmonic, contrary to the expectation based on the beating of different modes. Finally note that different regimes of a Josephson junction are possible; the physics discussed above applies to that of a conventional junction deep in the Rabi regime (where interaction effects are negligible), [Legg01]. Closer to our theory are the coherently pumped Rabi regime experiments performed in [Abba13], where the phase of the oscillations in the double well is fixed by the pumping laser.

4.4.2 Coherence Function and Static Limit Expressions

Having determined the form of the Josephson correlation function, $\langle a_1^\dagger(\tau)a_2(\tau)a_2^\dagger a_1\rangle$, we now proceed to obtain the distribution for it, u^J, and the static limit expression which approximates it. In Liouville form, the correlation function reads

$$g^J(\tau) = \langle a_1^\dagger a_2 e^{\mathcal{L}\tau} a_2^\dagger a_1 \rho_o\rangle. \tag{4.90}$$

We define

$$\rho'(\tau) = e^{\mathcal{L}\tau} a_1 a_2 \rho_o \qquad \Rightarrow \qquad \rho'_{nnpp} = \sqrt{p}\sqrt{n+1}\,\rho_{n+1np-1p}, \tag{4.91}$$

and

$$u^J_{np} = \sqrt{n}\sqrt{p+1}\,\rho'_{n-1np+1p}(\tau) \tag{4.92}$$

such that

$$u^J_{np}(0) = \sqrt{n}\sqrt{p+1}\,(\sqrt{p+1}\sqrt{n}\,\rho_{nnpp}) = n(p+1)\,P^{ss}_{np}. \tag{4.93}$$

And, following the same steps as in (4.22–4.25), we reach,

$$\begin{aligned}\dot{u}^J_{np} = \gamma \sum_i n_i^c \Bigg[& \frac{\alpha_{i1} n}{\alpha_{i1}(n-\frac{1}{2}) + \alpha_{i2}(p+\frac{3}{2}) + n_i^s} u^J_{n-1p} \\ & + \frac{\alpha_{i2}(p+1)}{\alpha_{i1}(n+\frac{1}{2}) + \alpha_{i2}(p+\frac{1}{2}) + n_i^s} u^J_{np-1} \\ & - \frac{\alpha_{i1}(n+\frac{1}{2}) + \alpha_{i2}(p+\frac{3}{2})}{\alpha_{i1}(n+\frac{1}{2}) + \alpha_{i2}(p+\frac{3}{2}) + n_i^s} u^J_{np} \Bigg] \\ + \gamma & \Big[n u^J_{n+1p} + (p+1) u^J_{np+1} - \big(n+p\big) u^J_{np} \Big] \\ + i & \Big(\kappa(2n-1) - \kappa(2p+1) + \eta(-n+p+1) \Big) u^J_{np},\end{aligned} \tag{4.94}$$

The static limit can be calculated in the same fashion as above (Sec. 4.3.3) and gives the expression,

$$g^J_s(\tau) \propto \iint P_{(n,p)} e^{i(2\kappa-\eta)(n-p)\tau} \, \mathrm{d}n \, \mathrm{d}p. \tag{4.95}$$

Both (4.94) and (4.95) are solved numerically. Example solutions will be shown in Chapter 5.

4.4.3 Factorization of the Josephson Coherence Function

In Chapter 3, we presented how the natural variable to describe the ridge is $u = \frac{1}{\sqrt{2}}(n+p)$, Eq. (3.13), i.e. a combination of the occupancy in n and p, and that the zero-particle cutoff adds features along the soft mode. On the contrary, with independent pumping, the population distribution highlights the fact that the modes are completely independent. In this section these observations are considered in the context of coherence functions. We examine the factorization of the correlation function for Josephson oscillations

$$\langle a_1^\dagger(\tau) a_2(\tau) a_2^\dagger a_1 \rangle \stackrel{?}{=} \langle a_1^\dagger(\tau) a_1 \rangle \langle a_2(\tau) a_2^\dagger \rangle. \tag{4.96}$$

We know that for any given time, two mode operators commute, e.g $[a_2^\dagger, a_1] = 0$, but it is not necessarily the case at two different time points $[a_2^\dagger(\tau), a_1]$. Moreover, we know that $[a_1^\dagger(\tau), a_1] \neq 0$ and that the two correlation functions above, $\langle a_1^\dagger(\tau) a_1 \rangle$ and $\langle a_2(\tau) a_2^\dagger \rangle$, correspond to the emission spectrum of the first mode and the absorption spectrum of the second mode[Glau 63], respectively.

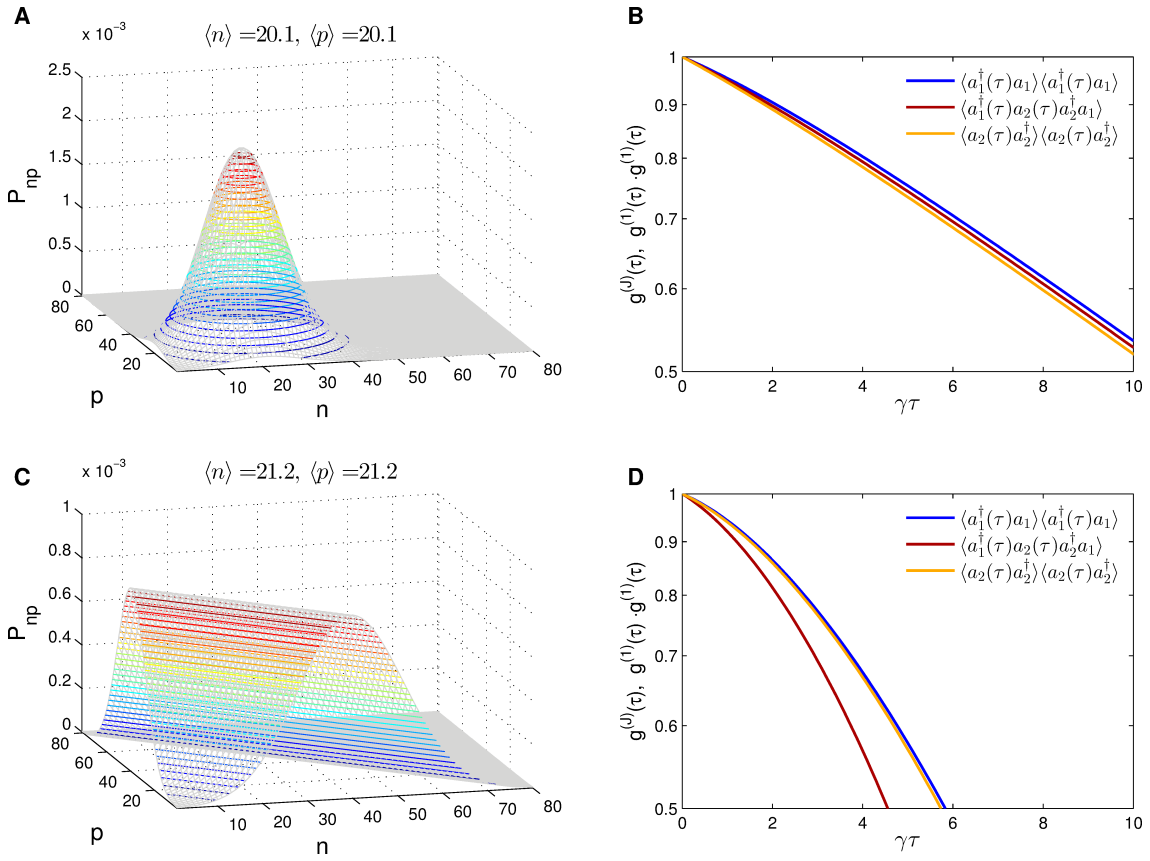

Figure 4.6: (A, C) Independent, $\alpha_{11,22} = 1$, $\alpha_{12,21} = 0$, and ridge, $\alpha_{ij} = 0.5$, population distribution with $n_s = 50,\ n_c = 70$. (B, D) Comparison of first order coherence function with Josephson coherence function with $\kappa = 0.005, \eta = 0$. In the independent case the Josephson coherence function factorizes $\langle a_1^\dagger(\tau)a_2(\tau)a_2^\dagger a_1\rangle = \langle a_1^\dagger(\tau)a_1\rangle\langle a_2(\tau)a_2^\dagger\rangle$. It is not the case however with common reservoirs.

We ran the numerical calculation of the Josephson, first mode emission and second mode absorption correlation functions, both for the ridge and the independent cases (Fig. 4.6). We plotted Josephson correlation function together with the square of the two first order correlation functions. In the independent case, (Fig. 4.6B), the correlation time for the absorption spectrum (squared) is longer than for the emission spectrum. Simply expressed, this difference to the energy difference of adding an extra particle in the initial condition. The Josephson correlation falls exactly in between the two first order correlations, indicating that it factorizes verifies the hypothesis above (4.96). In the ridge case (Fig. 4.6D) the emission absorption correlation also decays faster than the one for emission. But the Josephson coherence decays much faster than the square of either first order function. The Josephson correlation function does not factorize in the ridge case, due to the coupling between the modes in $\mathcal{L}_p$.

4.5 Discussion

We have shown how our theory can be applied to calculate coherence functions. We presented an exact numerical solution and two approximate approaches. Our full quantum theory can be exploited to study the effects on the emission linewidth of fluctuations in the population distribution which are not accessible with semi-classical approaches, i.e. mean-field theories[Wout 07, Keel 08]. We also show how these enter into the calculation of higher order correlation functions by calculating the dephasing in the beating of the intensity – Josephson oscillations.

The Fokker-Planck approach provides a way to transform u into a form where an integral can be performed analytically. This reduces the effective dimensionality of the problem quite significantly while also providing reasonable accuracy. The integral transform approach for calculating $g^{(1)}$ or static limit, although much simpler, is valid only when the decoherence is dominated by the interaction-induced energy fluctuations.

Chapter 5

Application and Results

The theory developed so far makes very little reference to the specific form of the multi-mode condensate. We defined a mode with single particle wavefunction, ϕ_j, associated with a bosonic operator, a_j. We incorporated pumping of this mode by an arbitrary number of saturable reservoirs, $\mathcal{L}_p$, (2.73), parametrized by the quantities $n_i^c, n_i^s, \alpha_{ij}$; as well as a decay of the mode into vacuum, $\mathcal{L}_d$, (1.44); and interactions, H (2.91). This provided the theory with flexibility in its application, making it a useful tool for describing, at a quantum level, non-equilibrium condensation with different potentials, interaction, and kinetic terms.

This chapter serves a dual purpose. On one hand, we give a flavor for how the theory can used to describe an actual multi-mode polariton condensate (Secs. 5.1, 5.2) with a realistic set of parameters (Sec. 5.3). The application model we employ is the double-well potential which formed the basis for the demonstration of Josephson oscillations in polariton condensates[Lago 10]. We use the theory to calculate the population distributions (Sec. 5.4.1), emission linewidths (Sec. 5.4.2), and decay of Josephson oscillations (Sec. 5.4.3). One the other hand, the Chapter also serves to discuss the population distributions (Chapters 3) and to expose and contrast the full numerical solutions, with the Fokker-Planck and static limit approximations (Chapter 4) in a realistic physical context.

5.1 The Double-Well : Application of the Theory

We derive the properties of condensates residing in a double well potential[Weis 91] (Fig 5.1), in the regime where particle non-conserving terms in the condensates Hamiltonian

can be neglected, following the criteria discussed in Sec. 2.5. The description we use,

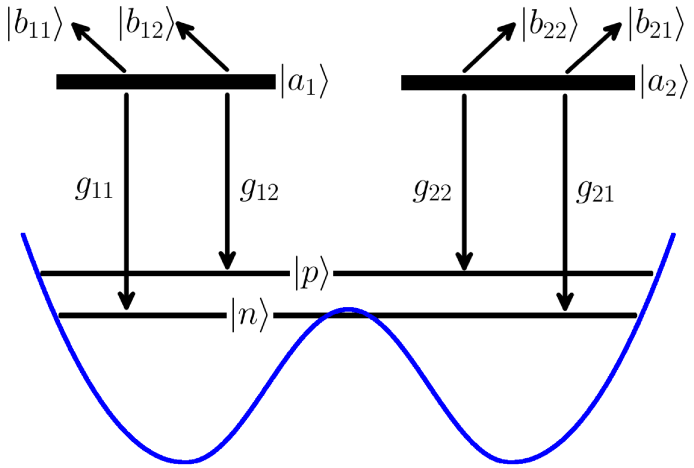

Figure 5.1: Schematic of the application of the theory to a double-well. Localized left-right pumping reservoirs, $|a_1\rangle, |a_2\rangle$, pump, with matrix elements g_{ij}, two delocalized modes, $|n\rangle$, $|p\rangle$. The modes are a linear combinations of left and right tight-binding orbitals with weight varying with detuning between the wells, $\Delta\epsilon$, and hopping parameter, t. This scheme allows to eliminate the hopping terms, e.g. $a_L^\dagger a_R$, in the condensates Hamiltonian (H_{LR}, (5.1) $\rightarrow H$, (5.3)).

shown in Fig. 5.1, is the tight-binding model of a double-well; isolated left and right well orbitals with operators, a_L, a_R, are combined to form an approximate solution of the double-well potential. Our solution retains only eigenvalues and matrix elements. It is parametrized by the detuning between the wells, $\Delta\epsilon$, and the hopping between left and right wells, t. The tight binding Hamiltonian is,

$$H_{LR} = \Delta\epsilon(a_R^\dagger a_R - a_L^\dagger a_L) - t(a_R^\dagger a_L + a_L^\dagger a_R) + H_{LR(NL)}. \tag{5.1}$$

We assume that interactions, $H_{LR(NL)}$, only occur within the localized orbitals condensates, and the wavefunction overlap between the left and right modes is negligible. Thus,

$$H_{LR(NL)} = g((a_L^\dagger a_L)^2 + (a_R^\dagger a_R)^2), \tag{5.2}$$

where for simplicity we take the localized orbitals to have identical wavefunctions and terms of the from $a_L^\dagger a_L a_R^\dagger a_R$ are absent due to the overlap being negligible. To describe the pumping we assume there are two non-coherent, thermalized (Sec. 2.1) reservoirs localized over each well (Fig 5.1).

Having defined our model system, we shall proceed with diagonalizing the hopping term, $t(a_R^\dagger a_L + a_L^\dagger a_R)$, in new modes ($a_1$, a_2, Sec. 5.2) which, for $\Delta\epsilon = 0$, correspond to the symmetric and anti-symmetric eigenstates of a double-well. Two delocalized modes are thereby obtained. We then determine (Sec. 5.2.1) how each one receives pumping

from the two localized left-right reservoirs. The next step is to map the left-right tight-binding interaction term of the condensate, (5.2), onto our condensate's interactions, $H_{(NL)}$, (5.13), preserving only the particle conserving terms, κ, η (Sec. 5.2.2).

Once this exercise has been done, we establish physically relevant parameters to be used (Sec. 5.3) and we study the population distributions, coherence decay and Rabi regime Josephson coherence decay (Sec. 5.4).

5.2 Left-Right Well to Delocalized Representation

Here the left-right Hamiltonian (5.1) is mapped onto the delocalized modes representation, a_1, a_2,

$$H = \Delta E(a_2^\dagger a_2 - a_1^\dagger a_1) + H_{(NL)}, \tag{5.3}$$

with the use of intermediate variable θ and the unitary transformation ansatz,

$$\begin{pmatrix} a_L^\dagger & a_R^\dagger \end{pmatrix} = \begin{pmatrix} a_1^\dagger & a_2^\dagger \end{pmatrix} \begin{pmatrix} \cos(\theta) & -\sin(\theta) \\ \sin(\theta) & \cos(\theta) \end{pmatrix} \tag{5.4}$$

and its Hermitian conjugate (H.c.).

In this transformation, the linear component of H_{LR} (5.1) reads,

$$\begin{aligned} H_{LR(0)} = \Delta\epsilon\big[&\big(a_1^\dagger \sin(\theta) + a_2^\dagger \cos(\theta)\big)\big(a_1 \sin(\theta) + a_2 \cos(\theta)\big) \\ &- \big(a_1^\dagger \cos(\theta) - a_2^\dagger \sin(\theta)\big)\big(a_1 \cos(\theta) + a_2 \sin(\theta)\big)\big] \\ -t\big[&\big(a_1^\dagger \sin(\theta) + a_2^\dagger \cos(\theta)\big)\big(a_1 \cos(\theta) - a_2 \sin(\theta)\big) + \text{H.c.}\big]. \end{aligned} \tag{5.5}$$

We isolate the off-diagonal components in (5.5) and require that they vanish,

$$\begin{aligned} 0 =& 2\Delta\epsilon \sin(\theta)\cos(\theta)(a_1^\dagger a_2 + a_2^\dagger a_1) \\ &+ t\big[\sin(\theta)^2 a_1^\dagger a_2 - \cos(\theta)^2 a_2^\dagger a_1\big] + t\big[\sin(\theta)^2 a_2^\dagger a_1 - \cos(\theta)^2 a_1^\dagger a_2\big]. \end{aligned} \tag{5.6}$$

The solution must have each component, $a_1^\dagger a_2$, $a_2^\dagger a_1$, cancel separately, and we obtain,

$$2\Delta\epsilon \sin(\theta)\cos(\theta) + t(\sin(\theta)^2 - \cos(\theta)^2) = 0, \tag{5.7}$$

giving

$$\Delta\epsilon \sin(2\theta) = t\cos(2\theta) \quad \text{or} \quad \tan(2\theta) = \frac{t}{\Delta\epsilon}. \tag{5.8}$$

The ratio of hopping over detuning, $\frac{t}{\Delta\epsilon}$, is the key control parameter in our double-well representation. A value of $t/\Delta\epsilon = 0$ is the limit case for large detuning between the two wells. This makes $\theta = 0$, so the transformation (5.4) is diagonal and the modes map directly to the left and right well. The other limit is $t/\Delta\epsilon \to \infty$, which makes $\theta = \pi/4$ and means the modes are the fully distributed symmetric and anti-symmetric superposition of the left and right orbitals.

The remaining terms of the linear Hamiltonian in (5.5) must be equivalent to the form in (5.3),

$$\begin{aligned}\Delta E(a_2^\dagger a_2 - a_1^\dagger a_1) =& \Delta\epsilon(\sin(\theta)^2 a_1^\dagger a_1 + \cos(\theta)^2 a_2^\dagger a_2 - \cos(\theta)^2 a_1^\dagger a_1 - \sin(\theta)^2 a_2^\dagger a_2)) \\ &- 2t\sin(\theta)\cos(\theta)(a_1^\dagger a_1 - a_2^\dagger a_2) \\ =& \Delta\epsilon\cos(2\theta)(a_2^\dagger a_2 - a_1^\dagger a_1) + t\sin(2\theta)(a_2^\dagger a_2 - a_1^\dagger a_1),\end{aligned} \tag{5.9}$$

giving,

$$\begin{aligned}\Delta E &= \Delta\epsilon\cos(2\theta) + t\sin(2\theta) \\ &= \frac{\Delta\epsilon^2 + t^2}{\sqrt{\Delta\epsilon^2 + t^2}}.\end{aligned} \tag{5.10}$$

5.2.1 Left-Right Pumping of Delocalized Condensates

The modes now being in a delocalized representation, a_1, a_2, will receive pumping from both the left and the right reservoirs (Fig 5.1) based on the fraction of the mode that is subtended by each reservoir. One can read from the mapping ansatz (5.4) established above, the fraction of the pumping which is received from either reservoir. We simply use the function, $\sin(\theta)$, $\cos(\theta)$ to trace back the fraction of each mode lying on the left and on the right.

We recall that matrix elements, $g_{1,2}$, parametrize amplitude interactions, H_p (2.51) and that they appear as density parameters, $\alpha_{12} = g_{12}^2/(g_{12}^2 + g_{22}^2)$, in our pumping superoperator, $\mathcal{L}_p$ (2.73). We therefore read the density fractions on the left and on the right as the square of the transformation functions in (5.4),

$$\alpha_{11} = \alpha_{22} = \cos^2(\theta) = \tfrac{1}{2} + \frac{\Delta\epsilon}{2\sqrt{\Delta\epsilon^2 + t^2}} \tag{5.11}$$

$$\alpha_{12} = \alpha_{21} = \sin^2(\theta) = \tfrac{1}{2} - \frac{\Delta\epsilon}{2\sqrt{\Delta\epsilon^2 + t^2}}, \tag{5.12}$$

where we also used trigonometric manipulations to show how α_{ij} relate to $t, \Delta\epsilon$. For

large detuning, $\Delta\epsilon \gg t$, the modes become localized and the cross-pumping, α_{12}, α_{21}, vanishes.

5.2.2 Mapping of the Interaction Terms

The last step in establishing this example application of the theory is to map the non-linear coefficients of (5.2) into

$$H_{(NL)} = \kappa(a_1^\dagger a_1)^2 + \kappa(a_2^\dagger a_2)^2 + \eta a_1^\dagger a_1 a_2^\dagger a_2. \tag{5.13}$$

To do this, we place (5.4) and its H.c. into (5.2),

$$\begin{aligned} H_{LR(NL)} = g\Big[&\big((a_1^\dagger a_1)^2 + (a_2^\dagger a_2)^2\big)(\sin(\theta)^4 + \cos(\theta)^4) + 4a_1^\dagger a_1 a_2^\dagger a_2 \sin(\theta)^2\cos(\theta)^2 \\ &+ \big((a_1^\dagger a_1 - a_2^\dagger a_2)(a_1^\dagger a_2 + a_2^\dagger a_1) + (a_1^\dagger a_2 + a_2^\dagger a_1)(a_1^\dagger a_1 - a_2^\dagger a_2)\big)\times \\ &\quad (\sin(\theta)^2 - \cos(\theta)^2)\sin(\theta)\cos(\theta) \\ &+ 2(a_1^\dagger a_2 + a_2^\dagger a_1)^2 \sin(\theta)^2\cos(\theta)^2\Big] \\ = g\Big[&\big((a_1^\dagger a_1)^2 + (a_2^\dagger a_2)^2\big)(\sin(\theta)^4 + \cos(\theta)^4) \\ &+ \big(8a_1^\dagger a_1 a_2^\dagger a_2 + 2a_1^\dagger a_1^\dagger a_2 a_2 + 2a_2^\dagger a_2^\dagger a_1 a_1 - a_1^\dagger a_1 - a_2^\dagger a_2\big)\sin(\theta)^2\cos(\theta)^2 \\ &+ \big(a_2^\dagger a_2^\dagger a_2 a_1 - a_1^\dagger a_1^\dagger a_1 a_2 + a_1^\dagger a_2^\dagger a_2 a_2 - a_2^\dagger a_1^\dagger a_1 a_1\big)\tfrac{1}{2}\sin(4\theta)\Big]. \end{aligned} \tag{5.14}$$

The terms present in (5.14) but not in (5.13), which describe interaction processes with transfer of particles between single particle orbitals, will be neglected. As discussed in (Sec. 2.5), this is valid when the energy separation between orbitals $\Delta\epsilon$ is large compared with the interaction energy $g\langle n_{1,2}\rangle$. We identify that the self interaction, $\kappa = \kappa_1 = \kappa_2$, and the density-density interaction, $\eta = \frac{1}{2}(\eta_{12} + \eta_{21})$, terms in (2.91) are

$$\kappa = g(\sin(\theta)^4 + \cos(\theta)^4) = g\big(\tfrac{1}{2} + \tfrac{1}{2}\cos(2\theta)^2\big) = \frac{g}{2}\big(1 + \frac{\Delta\epsilon^2}{\Delta\epsilon^2 + t^2}\big) \tag{5.15}$$

$$\eta = 8g\sin(\theta)^2\cos(\theta)^2 = 2g\sin(2\theta)^2 = \frac{2g\,t^2}{\Delta\epsilon^2 + t^2}, \tag{5.16}$$

when translated in our model application.

5.3 Choice of Parameters

In the following, we adopt parameters which are physically realistic and yet also computationally accessible. We make $\gamma = \tau_o^{-1}$, the inverse of the polariton lifetime, and we adopt a value of $\tau_o = 2$ps, [Whit09]. This sets the unit of time and energy ($\hbar = 1$).

We then make the interaction strength between each tight-binding orbital, $g = 4 \times 10^{-5}\gamma$, which sets the values of κ and η (5.15, 5.16). This is consistent with previous values used in single mode mean field[East 08] and density matrix studies[Whit 09] which were parametrized with linewidth experiments. It depends both on the underlying exciton-exciton interaction[Tass 99] and the size of the single-particle orbitals which appears as a field mode normalizing factor. Averaging over Hopfield coefficients and Stokes vectors[Deng 10] is implied.

For simplicity, the pump power, n_c, and gain saturation, n_s, parameters are made equal for both reservoirs. While $n_s = 25000, n_c = 25500$ have been taken for condensates significantly above threshold earlier[Whit 09], this generates population distributions, $\sigma \propto \sqrt{n_c}$, and average populations, $\langle n \rangle \propto \bar{n} = n_c - n_s$, which in two modes are difficult to handle in the numerical coherence calculations: $\left(4 \times \max(\sigma, \bar{n})\right)^2 \sim 4 \times 10^6$ equations to solve. We therefore settle for a slightly reduced system. Earlier we showed numerical results in a reduced exploratory system where g was modified (Sec 4.2.2). Its non-linear effect on coherence time, especially in the motional narrowing regime, precludes the scaling of g in our physically grounded approach.

We settle for $n_s = 5000$, and $n_c = 5000, 5200$ which correspond to values at mean field threshold $\bar{n} = 0$ and above threshold $\bar{n} = 200$. This will generate a maximum of $800^2 = 640\,000$ equations to solve. Physically this corresponds to a system with smaller gain medium, which gets depleted for a smaller n with respect to n_s. It will also have a narrower population distribution, σ, which means that for g being the same, the interaction broadening will be smaller. This will place our system in a motional narrowing regime rather than in a static limit (Sec. 1.2.4).

We shall see in Sec. 5.4.2 that this choice of parameters is also advantageous when comparing the methods of Chapter 4. It shows the limit of validity of the static limit approximation in the motional narrowing regime where Fokker Planck and full numerics still capture the physics.

5.4 The Double-Well : Results

Now that the theory has been related to a specific model of a two-mode condensate, we present results for the population distributions, first-order coherence functions, and the decay of Josephson oscillations.

Beside the two values of $n_c = 5000, 5200$ mentioned above, we also vary the ratio $t/\Delta\epsilon$. The sets of parameters we shall focus on are presented in Table 5.1.

n_c	$t/\Delta\epsilon$	α_{11}, α_{22}	α_{12}, α_{21}	κ	η	Figures
5000	0	1	0	4×10^{-5}	0	5.2D,5.3A, 5.5A
5200	0	1	0	4×10^{-5}	0	5.2A,5.3, 5.4B,5.5
5200	*1*	*0.85*	*0.15*	*3 × 10^{-5}*	*4 × 10^{-5}*	*5.4B*
5200	3	0.66	0.33	–	–	5.2B
5200	∞	0.5	0.5	2×10^{-5}	8×10^{-5}	5.2C,5.3, 5.4B,5.5

Table 5.1: Summary of sets of values used throughout ($n_s = 5000,\ g = 4 \times 10^{-5},\ \gamma = 1$).

5.4.1 Population Distributions of the Condensate

In this section we shall describe the population distribution obtained in our double-well model, Fig. 5.2. These will allow to resolve discontinuities in mode occupancies which are pointed out by a nonequilibrium phase boundary in mean-field theories[East 08] (Sec. 1.3). The additional information they provide is also key to the calculation of coherence functions[Whit 09] (Sec. 4.2.1). We point out features in the distribution which will have an important effect on coherence.

The population distributions for different values of $t/\Delta\epsilon$ (Table 5.1) are presented in Fig. 5.2A-C. Fig. 5.2A is for $t/\Delta\epsilon = 0$, where the two modes are pumped independently and we see that the population distribution is indeed formed out of two independent Gaussian; it factorizes, $P_{np} = P_n P_p$.

Fig. 5.2C is for $t/\Delta\epsilon = \infty$, where the two modes are fully delocalized between the left and the right wells and are equally pumped by the left and right reservoirs. The population distribution takes the form $P_{np} = (P_{n+p})|_{n,p\geq 0}$. A Gaussian form is still present but this time its shape is dictated by the unique variable $n+p$. The n and p variables are present independently only in the zero particle cut-off. One could have expressed the population distribution with a single variable were it not of the zero

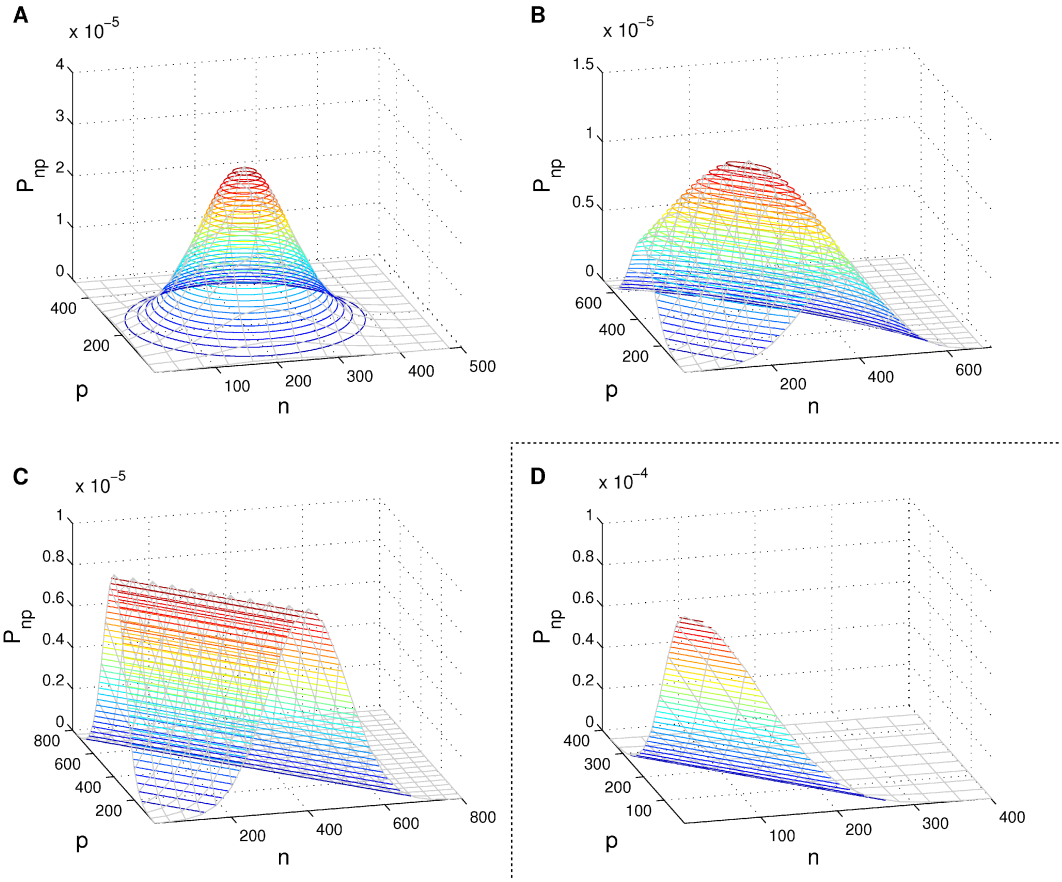

Figure 5.2: (A-C) Populations with left-right reservoir pumping of modes n, p above threshold $n_c = 5200$, $n_s = 5000$ with the reservoir to mode coupling varying as $\alpha_{11} = \alpha_{22} = 1$, 0.66, 0.5, $\alpha_{12} = \alpha_{21} = 0$, 0.33, 0.5. The relevant quantities evolves from n, p to $n+p$ as the modes become pumped indiscriminately by the left and right reservoirs. (D) Population at mean field threshold $n_c = n_s = 5000$ and $\alpha_{11} = \alpha_{22} = 1$, $\alpha_{12} = \alpha_{21} = 0$.

particle cut-off. We suggest that the n and p picture is partly overcomplete and that the modes take a distribution where they are mostly unique but also preserve some independence through the zero particle cut-off. This population corresponds to the transition point between the single-mode and the two-mode solutions in the mean-field, approach presented in [East08]. Linearizing the mean field version of the population equation (**??**) and mapping the parameter notation ($2\gamma_{\text{eff}} = \sum_i \frac{\gamma n_c \alpha_{ij}}{n_s} - \gamma$, $2\Gamma\eta_j = \sum_i \frac{\gamma n_c \alpha_{ij}^2}{n_s^2}$, $4\Gamma\beta = \sum_i \frac{\gamma n_c \alpha_{i1}\alpha_{i2}}{n_s^2}$) indeed shows that the ridge solution corresponds to the discontinuity in [East08].

Fig. 5.2B shows how these two pictures, independent versus partly unique, merge for an intermediate value of $t/\Delta\epsilon = 3$, $0 < 3 < \infty$. At the mean field threshold, Fig. 5.2D, the dominant feature is the zero particle cutoff.

We shall also mention how some interplay between the modes is embedded in the

distribution. This in turn influences coherence decays (Sec. 5.4.2, 5.4.3). In the independent case, $P_{np} = P_n P_p$, there is no inter-dependence in the mode distributions and the interplay between the modes, when studying the decay of coherence, can only be due to condensate interactions. In the other limit, $P_{np} = (P_{n+p})|_{n,p\geq 0}$, our distributions point out the correlation of the population distribution in the diagonalized single-particle basis, and the decay of coherence will be impacted not only by the interactions but also by these correlations.

5.4.2 Decay of First-Order Coherence

We now present and discuss our results for the decay of the first-order coherence function of one mode of the condensate. This subsection plays the dual role of describing the physics determining this quantity, and discussing the three approaches to its calculation developed in this thesis from a technical point of view. On the physics side, we shall mention coherence times, modes interplay and interactions, and the static and motional narrowing regimes. The technical side compares the full numerical solution of Sec. 4.2.2, with the Fokker-Planck (Sec. 4.3.1) and the static limit (Sec. 4.3.3) approximations.

The full numerical solution is considered to be "the gold standard", the static limit is the "back of the envelope" calculation. The Fokker-Planck approach is in between, more involved than the static limit, but much more direct than the numerical solution. Nonetheless we shall see that it is in good agreement with full numerics. We first discuss our best picture of the physical phenomena, the full numerical solution.

Figure 5.3A presents the numerical calculation of the coherence decay at mean-field threshold ($n_c = n_s$, thin dark blue line, with P_{np}^{ss} corresponding to Fig.5.2D) and above threshold (thick dark blue lines, with P_{np}^{ss} corresponding to Fig.5.2A-solid line, C-dotted line). These results are obtained by direct numerical solution of u (4.25), for the present two-mode, two-reservoir case (C.1). In all cases, we see a straight line on the semilog plot, representative of the motional narrowing regime (Sec. 1.2.4). The model would present the static regime only with wider population distribution (larger $\sqrt{n_c}$) or stronger interaction (larger g) which both induce larger interaction energy. The coherence increases as we go from mean field threshold to significantly above threshold; the linewidth reflects the ratio of the fluctuations ($\propto \sqrt{n_c}$) to the total density ($\propto \bar{n}$), so that larger populations give larger coherence times. We also see that the coherence time for zero detuning, $t/\Delta\epsilon = \infty$, where the modes are a symmetric and antisymmetric superpositions (dotted line), is shorter than that for large detuning,

$t/\Delta\epsilon = 0$, where they form independent condensates (solid line), although intricate interplay between interactions and population distributions adds an additional level to this observation. We will discuss this with Figure 5.4 below. For now, we simply say that in the symmetric-antisymmetric configuration, the modes are more distributed and therefore experience less interaction within themselves ($\kappa = 2 \times 10^{-5}$ vs 4×10^{-5}) but overlap much more with each other ($\eta = 8 \times 10^{-5}$ vs 0). The combined effect of these interactions and the changes in population distributions is a more rapid loss of coherence ($t_c = 265\gamma$ vs 435γ) in the ridge case.

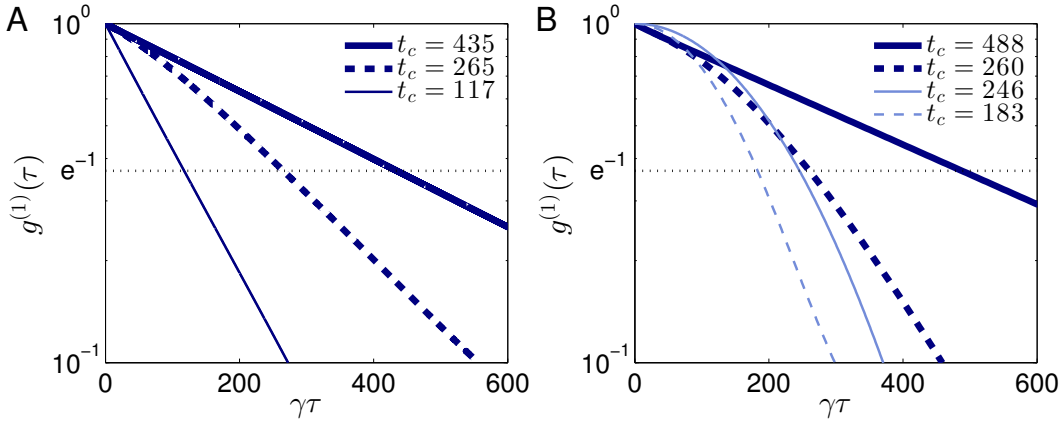

Figure 5.3: A - Coherence decays with $\kappa, \eta = \mathrm{f}^{\kappa,\eta}(g)$, $n_s = 5000$ and $n_c = 5000$-*thin line*, 5200-*thick lines*. The solid lines are for independent pumping (vanishing tunneling), while the dotted line is with modes equally pumped by either reservoirs (vanishing detuning). B - Equivalent decays in the static limit (*light blue*) and from the Fokker-Planck approach (*dark blue*.)

Figure 5.3B (thick lines) shows the Fokker-Planck calculations with the same above-threshold parameters as in 5.3A. The Fokker-Planck solution is in good agreement with full numerics both in terms of magnitude and shape.

On the technical side, we discuss two features of the Fokker-Planck solution, one general, and the other linked with the loss of precision due to the linearization (Sec. 4.3.1). (i) In independent modes, t_c is slightly overestimated with respect to the numerics ($t_c = 488\gamma$ vs 429γ). (ii) This effect is overshadowed however in the symmetric-antisymmetric configuration by the fact that the population is distributed further away (5.2C vs 5.2A) from the linearization points, $\frac{\langle n^2 \rangle}{\langle n \rangle}$, $\frac{\langle np \rangle}{\langle n \rangle}$, and the Fokker-Planck solution looses its precision. The loss in precision is reflected in the Gaussian aspect of the thick dotted line in Fig. 5.3B. These two features are also reflected in Fig. 5.4B below.

Figure 5.3B (thin lines) also shows the static limit results with its characteristic Gaussian shape, quadratic on a semilog plot. It gives the correct orders of magnitude and presents the faster decoherence of the symmetric-antisymmetric case compared with the independent (5.2C vs 5.2A). As expected, the static limit results also show

shorter coherence times than the other approaches because all forms of motional damping (dynamical averaging of the fluctuations) have been neglected.

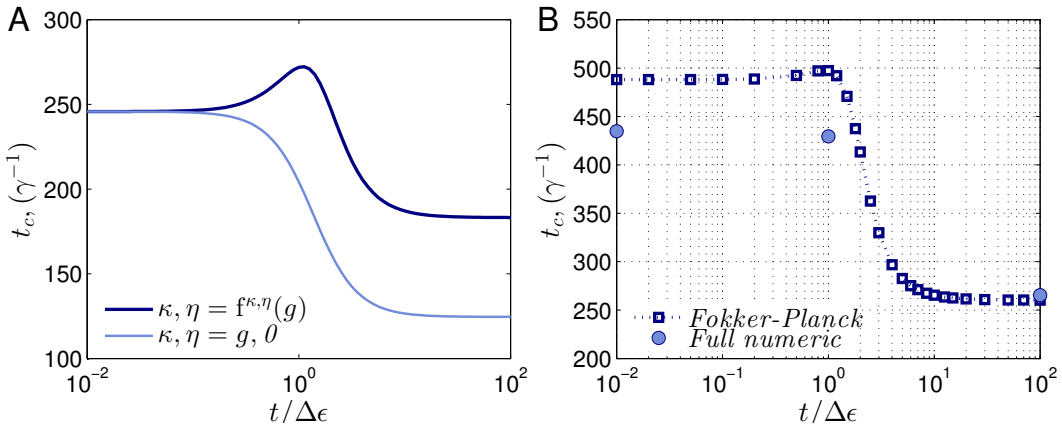

Figure 5.4: (A) Effect on the coherence time, t_c, of the correlations in the population distribution, in the static limit. When the energy interaction terms included, $\kappa, \eta = \mathrm{f}^{\kappa,\eta}(g)$, (5.15, 5.16), the fact that they are anticorrelated in the $t/\Delta\epsilon > 0$ population distributions prolongs the coherence time compared with them being rigid, $\kappa, \eta = g, 0$. (B) This effect, albeit damped, is also present in the motional narrowing regime as seen in the Fokker-Planck and full numeric results.

We now turn to Figure 5.4, which shows the coherence time as a function of detuning or tunneling at a fixed above-threshold pumping, $n_c = 5200$, and discuss the effect of correlations in the distribution mentioned above. We shall do so with Figure 5.4A, which presents static limit results, in conjunction with Figure 5.2C, the symmetric-antisymmetric population. As we noted already, the relevant variable in this population distribution is $n + p$ which implies that within the distribution an increase in n corresponds to a decrease in p and vice-versa. The energy fluctuations associated with the population distribution will therefore be anticorrelated since they either depend on self $\times$ self (κ) or self $\times$ other (η) and the latter contributions are anticorrelated with the former. This is most obviously seen in the static limit as shown in Figure 5.4A. If we eliminate this effect by including only a constant (rigid) interaction within each mode, $\kappa = g, \eta = 0$, the increasingly wider population distribution as we sweep $t/\Delta\epsilon$ from 0 to ∞ causes t_c to decrease monotonically. In contrast, letting the inter-mode interaction increase as the modes overlap maintains t_c larger even though, at $t/\Delta\epsilon = \infty$, the total interactions are stronger than in the rigid case (see Table 5.1). What is more, the effect destroys the monotonicity when κ and η are of approximately the same strength, $t/\Delta\epsilon = 1$; giving a peak in the coherence time when the modes partially overlap. The numerical and Fokker-Planck coherence times results in Figure 5.4B show that this effect is still present but is less pronounced in the motional narrowing regime.

5.4.3 Decay of Josephson (Density) Oscillations

In Section 4.4 we saw how the equation of motion for multi-mode condensates can be used to study the dephasing of the beating between two modes and that the corresponding coherence function which describes it is $\langle a_1^\dagger(\tau)a_2(\tau)a_2^\dagger a_1\rangle$. Here we apply our numerical and static limit solutions of it to the double-well model (Fig. 5.5).

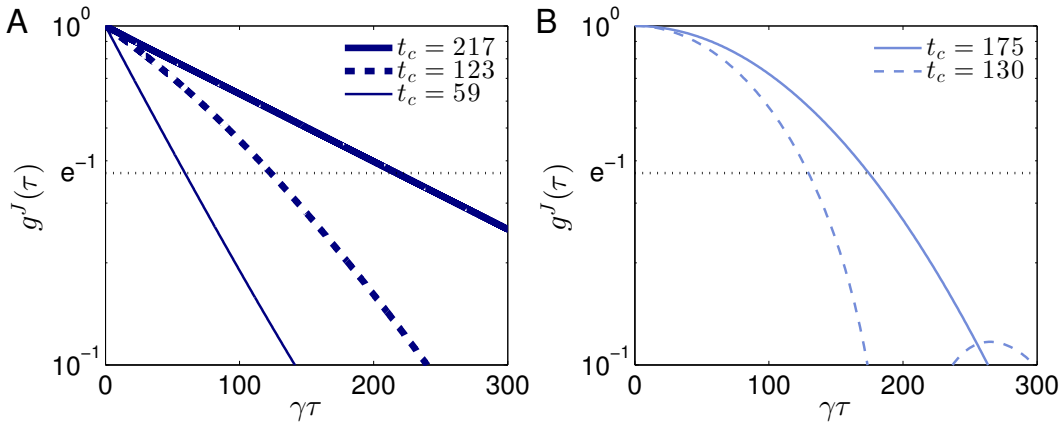

Figure 5.5: (A) Full numeric and (B) static limit Rabi regime Josephson coherence decays with same parameters as for the coherence decay results (Fig. 5.3).

With the numerical calculations (Fig.5.5A), we see that the decay follows an exponential form (linear on a semilog plot); the motional narrowing regime is reflected in this calculation as well. A comparison of the beat coherence decay times, $(t_c)^J$, (Fig.5.5A), with the decay time of the first-order coherence, t_c, (Fig.5.3A), shows that the values of $(t_c)^J$ are slightly more than half those of t_c. As we saw in Section 4.4.3, the Josephson beats correlation function factors into the product of two coherence decay calculations only when the modes are independent ($t/\Delta\epsilon = 0$).

Figure 5.5B shows the static limit calculation. As in the first-order calculations above, motional narrowing of the fluctuations is neglected in the static limit and the correlation times obtained are smaller than in full numerics. It is worth highlighting the coherence revival which arises, from a mathematical point of view, from the Fourier transform of the zero particle cutoff in the population distribution (Fig. 5.2C). The interactions can indeed rebuild the phase of the order parameter in the correlation function although it is unlikely that this can be observed experimentally due to other sources of noise which come into play as $t > t_c$.

Given the interaction terms included in the Hamiltonian, the Rabi regime Josephson oscillations are being considered here[Legg01]. As discussed in Section 4.4.1, other non-particle conserving interaction terms would have to be introduced in order to be

used in the Josephson regime[Lago 10]. These additional terms provide the pulse to pulse synchronization observed in the measurement. In order to perform experiments close to threshold and in the Rabi regime, while still having incoherent pumping, synchronization would have to be provided by a probe beam with pulse to pulse coherence time longer than the coherence we wish to measure. The coherent pumping experiments presented in [Abba13] show Josephson oscillations in the Rabi regime.

5.5 Discussion

We exposed how the theory can be applied to a specific physical system, used relevant parameters, and obtained the population, linewidth and Josephson coherence decay. These results were used to discuss the strengths and weaknesses of the tools developed in Chapter 4. We also uncovered a multimode effect with our theory. The correlations which appears in the ridge population distribution when two modes share common reservoirs enhance the coherence time of the condensate. Josephson oscillation coherence decay is the first example of the usage of the many-mode quantum theory beyond population distributions and first order coherence decays. The theory shows how population distributions provide additional information with respect to mean field theory. It would be interesting to investigate further, in light of non-locality in quantum mechanics, the fact that in the symmetric-antisymmetric distribution, beside for the zero particle cutoff, $n + p$ becomes the relevant parameter, rather than the individual occupations.

Chapter 6

Conclusion and Future Work

We conclude this thesis by, on one hand, summarizing the theory work that has been done, suggesting novel experiments and drawing further links with the current field of polariton condensation (Sec. 6.1). On the other hand, we discuss how the theory could be expanded by adding the treatment of non-particle conserving terms in the condensate Hamiltonian (Sec. 6.2).

6.1 Summary and Further Applications

In summary, we have developed a model for the nonequilibrium dynamics of polaritons in an incoherently pumped microcavity, incorporating gain due to scattering from multiple reservoirs, and resonant polariton-polariton interactions. We innovate from previous works addressing condensates formed with a single macroscopically-occupied orbital by having several such states coexist, i.e., multimode polariton condensates. We used the theory to determine the steady state population distributions of the modes. We have also used it to predict the quantum statistics, revealed for example via the linewidths, and shown how these quantities are affected by interactions between the condensates. We predict that the populations of the modes can be anticorrelated due to their coupling to a common reservoir, leading to a narrowing of the emission lines and a prolongation of the coherence time. We have also demonstrated theoretically a dephasing mechanism for intensity oscillations, and shown that, for realistic parameters, their coherence decay provides a useful probe of correlation effects.

Novel expirements can be envisaged with the theory. The first would be to observe the enhancement in coherence time due to anticorrelations in the population fluctu-

ations as $t/\Delta\epsilon$ is being swept from zero to infinity, Fig. 5.4A (see also Figs. 4.1C, 4.4F). To see the enhancement effect on the linewidth, one would have to ensure that the system is in the static regime. Another experiment which could be proposed and would help in parametrizing the coupling strengths, α_{ij}, is to compare the first-order decay time, t_c, with the dephasing time of Josephson oscillations, $(t_c)^J$. As we saw in Sections 5.4.3, 4.4.3, the Josephson coherence decay function factorizes into two first-order decay functions, with $(t_c)^J = t_c/2$, only when the pumping is independent. By comparing the two coherence times one could establish how much each mode shares the same reservoir and therefore parametrized α_{ij}.

Although we have focused on the specific example of condensation in a double-well potential, our theory can be applied to a range of many-condensate systems now being considered [Lago 10, Masu 12, Tosi 12, Galb 12], once they have been decomposed into the appropriate single particle orbitals. Each such orbital comprises a possible condensate mode in our theory, with gain and loss characterized by a few phenomenological parameters. In general the decoherence of the condensate depends on the structure of the single particle orbitals, so our theory allows for the study and optimization of coherence properties of polariton condensates across the geometries now being developed, including wires, photonic molecules, and photonic crystals [Masu 12]. With respect to superfluidity studies [Caru 13], the condensate in-plane reference frame does not have to be fixed to that of the laboratory, i.e. the condensate Hamiltonian can have a term to accommodate in-plane flow [Hive 12, Bali 07]. More speculatively, the model could provide a basis for studying spontaneous vortex lattices [Keel 08], beyond the mean-field level, and also for treatments of polariton dynamics in the quantum correlated regime [Caru 13]. Pulsed experiments could also be accommodated by providing a time evolution to the pumping strength parameter, $n_c^i \to n_c^i(t)$, as long as the Hamiltonian, H_p, can be assumed to remain time independent.

One notable feature in experiments is the presence of a large repulsive interaction with the reservoir excitons [Tosi 12, Wout 08c]. We have omitted this from our discussion, because it can be included on average as an effective potential, and hence a redefinition of the orbitals. Fluctuations in the reservoir occupation can broaden the emission line, i.e., lead to decoherence of the condensate, but this is negligible compared with the intrinsic linewidth provided pump laser noise is eliminated [Love 08].

Macroscopic quantum objects are ideally suited for the study of entanglement [Brau 05]. The multimode polariton condensate, treated beyond mean-field theory, could be used as a model to study entanglement [Liew 11]. In the two mode problem that we studied in this thesis, the modes are treated as local orthogonal and continuous observables [Zhan 13].

Reservoir polaritons do not distinguish in which mode they end up and can be thought of being in any of the modes to which they couple, with a probability given by the coupling coefficient, α_{ij}. This lends itself to the exploration of entanglement between modes.

6.2 Extension of the Theory

An important theoretical extension of our work would be to allow the treatment of non-particle conserving terms, both in the condensate Hamiltonian, H, and in the decay term, $\mathcal{L}_d$. The inclusion of nonresonant interaction terms between the modes, in particular terms such as $a_1^\dagger a_1^\dagger a_2 a_2$, become significant beyond the strong-trapping regime. The non-resonant interaction terms lead to the equivalent Bogoliubov spectrum for a homogeneous single-mode condensate, and hence are implicated in superfluidity, while at the semiclassical level they cause nonlinear mixing and synchronization in the multimode case[East 08]. We suggest a generalization of our theory would allow the impact of quantum and nonequilibrium fluctuations on such phenomena to be explored, in complex geometries where many condensates coexist. Another example is the spin. The modes will have, in addition to the spatial structure emphasized here, a polarization structure, which could be incorporated as an additional degree of freedom to the single-particle orbitals[Shel 10, Read 10]. This would also allow to include spin flip and polarization dependent mechanisms[Glaz 13, Magn 10]. With respect to density oscillations, the non-resonant terms would allow to study the phenomenon beyond the Rabi regime, i.e. in interaction dominated Josephson phenomena[Legg 01, Abba 13].

The Lindblad decay form we used also assumes a particle conserving form, because we provided a reservoir for each mode (Sec.1.2.2). With a common decay reservoir for all the modes, terms such as $\langle a_2^\dagger\, b\, b^\dagger a_1\rangle$ would provide another mechanism for particle exchange between the modes. Interference effects due this mechanism have been suggested in [Alei12].

In Fock space, the Liouville evolution of non-particle conserving terms generates a recursive dependence on all the elements within the density matrix. This contrasts with having to solve for the diagonal elements in the case of steady-state population distributions or the one off-diagonal terms for linewidth and Josephson coherence functions. We suggest that these interactions could be included by generalizing the Fokker-Planck approach to apply to the full density operator, rather than the distributions u or P, i.e., by assuming ρ_{mnpq} is smooth, so that Eq. (1.45) becomes a partial differential

equation. Such an approach would be similar in spirit to those based on the classical limit Wigner representation for ρ, as discussed by Wouters and Savona[Wout 09] among others. The smoothness of ρ_{mnpq} would have to be asserted.

Alternatively, the problem could also be approached without consideration of the classical limit of quantum electrodynamics. The Fokker-Planck approach could be generalized to the entire density matrix, as mentioned above. We draw a parallel with the approach in Chapter 4 for the remaining steps. In our expansion in Chapter 4, once the Kramer-Moyal expansion had been done, we performed a double-side Laplace transform which interchanged linear terms with differential operators and turned the second-order derivatives into quadratic terms. The equation became a first order differential equation. This allowed for integrals to be done analytically and we were left with doing the transform of the initial conditions, u_o, and diagonalizing a coefficient matrix, B, rather than evolving matrix elements. We suggest that a transform could be performed on a linearized Kramer-Moyal expansion of the full density matrix in order to reach both a steady state for the population distribution and calculate coherence functions. The transform to be used might be related to the Mellin transform[Erde 54],

$$\begin{aligned} \mathcal{F}(s) &= \mathcal{M}\{f(x); s\} \\ &= \int_0^\infty f(x) x^{s-1} dx \end{aligned} \tag{6.1}$$

in relation to fractional calculus[Saba 07, Das 11], to deal with square root terms which arise from having to deal with amplitudes, e.g. $a|n\rangle = \sqrt{n}|n-1\rangle$ since

$$\begin{aligned} \mathcal{M}\{n^a \rho_{(n,m,p,q)} : \mathbf{s}\} &= \mathcal{P}(s_n + a, s_m, s_p, s_q) \\ &\approx \mathcal{P}(\mathbf{s}) + a\, \partial_n \mathcal{P}(\mathbf{s}). \end{aligned} \tag{6.2}$$

We note also that while our expansion was at most linear when combined with differential operators, there is no limitation with the order of the derivative when the coefficient is a constant. We also note that while the dimensionality of the problem would remain quite large, it will only be so in the intermediate steps if the initial conditions are to be reached with this method also. The intermediate steps would largely remain analytical; in the Fokker Planck approach, we evaluated our solution at $K = 0$ and we were left with only one variable which is time.

Another approach, more numerically-driven, is the cumulant expansion technique used in [Magn 10] which may also lead to a way to deal with the non-resonant terms. Since the population distribution is also non-diagonal with particle non-conserving

terms, the moments use in the cumulant expansion may have to be obtained thought adiabatic evolution or perturbative schemes in order to reach the steady state.

Appendix A

Topics Related to Cavity Polariton Condensation

A.1 Thermal BEC

We derive here the expressions whereof the emergence of thermal BEC can be seen, with particular attention to the features of Bose statistics and dimentionality which give rise to thermal BEC in 3D. The derivation follows that of Pitaevskii and Stringari [Pita03] and Annett [Anne04].

A.1.1 Derivation of Bose-Einstein Statistics

The key component of thermal Bose-Einstein condensation is the Bose distribution. We derive it here, starting with the grand canonical partition function which highlights the important fact that every state is summed over occupation numbers running to infinity,

$$Z = \sum_{n_0=0}^{\infty} (e^{\beta(\mu-\epsilon_0)})^{n_0} \cdot \sum_{n_1=0}^{\infty} (e^{\beta(\mu-\epsilon_1)})^{n_1} \dots \tag{A.1}$$

where ϵ_i is the single-particle state energy, μ is the chemical potential of the particle ensemble and β is Boltzmann constant times the temperature, $k_B T$. The grand canonical potential is then obtained, with the individual sums being taken and the multiplication over each energy states now turning into a sum,

$$\Omega = -k_B T \ln Z = k_B T \sum_i \ln(1 - e^{\beta(\mu-\epsilon_i)}). \tag{A.2}$$

An implicit expression relating the chemical potential, μ, to the total number of particles, N, follows as

$$N = -\frac{\partial \Omega}{\partial \mu} = \sum_i \frac{1}{e^{\beta(\epsilon_i - \mu)} - 1}. \tag{A.3}$$

and we obtained the Bose-Einstein distribution. We note that in the factor

$$\frac{1}{e^{\beta(\epsilon_o - \mu)} - 1} \tag{A.4}$$

the chemical potential, μ, cannot take a value larger than ϵ_o since this would correspond to having a negative number of particles in that state. As $\mu \to \epsilon_o$, the occupation of the lowest level becomes very large. This is the mechanism of Bose-Einstein condensation.

A.1.2 The Emergence of BEC

Having obtained the key equation for Bose statistics (A.3), we now determine in which circumstances it saturates and do not allow further particles within the distribution. This is the criteria for the emergence of thermal BEC. We first label the single particle state energy with its wavevector, $\epsilon_i \to \epsilon_{\mathbf{k}}$, and we let sum over the states become an integral, $\sum_i \to \frac{V}{(2\pi)^3} \int d^3\mathbf{k}$,

$$N = \frac{V}{(2\pi)^3} \int_{\epsilon_o}^{\infty} \frac{d^3\mathbf{k}}{e^{\beta(\epsilon_{\mathbf{k}} - \mu)} - 1}, \tag{A.5}$$

or, working with the particle density, $n = \frac{N}{V}$,

$$n = \frac{1}{(2\pi)^3} \int_{\epsilon_o}^{\infty} \frac{d^3\mathbf{k}}{e^{\beta(\epsilon_{\mathbf{k}} - \mu)} - 1}. \tag{A.6}$$

We wish to perform this integral in terms of energy. In 3D, the energy degeneracy of the momentum space provides the following relationship between increments in energy and in wavevector,

$$d\epsilon = 4\pi k^2 dk, \tag{A.7}$$

where we used spherical coordinates and k is now a scalar. By using the dispersion relation of our Bose particles, $\epsilon = \frac{\hbar^2 k^2}{2m}$, we can write

$$k = \sqrt{\frac{2m\epsilon}{\hbar^2}}, \qquad dk = \sqrt{\frac{m}{2\hbar^2 \epsilon}} d\epsilon, \tag{A.8}$$

and rewrite terms in (A.6, A.7) as a function of the energy variable

$$\begin{aligned} g(\epsilon)d\epsilon &= \frac{4\pi}{(2\pi)^3}\frac{2m\epsilon}{\hbar^2}\sqrt{\frac{m}{2\hbar^2\epsilon}}d\epsilon \\ &= \frac{m^{3/2}\epsilon^{1/2}}{\sqrt{2}\pi^2\hbar^3}d\epsilon, \end{aligned} \tag{A.9}$$

where $g(\epsilon)$ is the density of states. Our integral (A.6) becomes

$$n = \int_{\epsilon_o}^{\infty} \frac{g(\epsilon)d\epsilon}{e^{\beta(\epsilon-\mu)}-1}. \tag{A.10}$$

The next few steps involve some algebraic manipulations. We let $x = \beta(\epsilon_k - \epsilon_o)$ and $z = e^{\beta(\mu-\epsilon_o)}$, and rewrite (A.10) in dimensionless form

$$\begin{aligned} n &= \frac{m^{3/2}}{\sqrt{2}\pi^2\hbar^3}\frac{1}{\beta^{3/2}}\int_{0^+}^{\infty}\frac{x^{1/2}dx}{e^x z^{-1}-1} \\ &= \frac{(mk_BT)^{3/2}}{\sqrt{2}\pi^2\hbar^3}\int_{0^+}^{\infty} x^{1/2}\frac{ze^{-x}}{1-ze^{-x}}dx. \end{aligned} \tag{A.11}$$

The integral can be expanded into a series and further manipulated

$$\begin{aligned} \int_{0^+}^{\infty} x^{1/2}\frac{ze^{-x}}{1-ze^{-x}}dx &= \int_{0^+}^{\infty} x^{1/2}ze^{-x}(1+ze^{-x}+z^2e^{-2x}+\dots)dx \\ &= \int_{0^+}^{\infty} x^{1/2}\sum_{p=1}^{\infty} z^p e^{-px}dx \\ &= \sum_{p=1}^{\infty} z^p \int_{0^+}^{\infty} x^{1/2}e^{-px}dx \\ &= \sum_{p=1}^{\infty} z^p \frac{1}{p^{3/2}}\int_0^{\infty} y^{1/2}e^{-y}dy \\ &= \sum_{p=1}^{\infty} z^p \frac{1}{p^{3/2}}\frac{\sqrt{\pi}}{2}. \end{aligned} \tag{A.12}$$

We can now write (A.11) as

$$n = \left(\frac{mk_BT}{2\pi\hbar^2}\right)^{3/2} g_{3/2}(z). \tag{A.13}$$

The function $g_{3/2}(z) = \sum_{p=1}^{\infty}\frac{z^p}{p^{3/2}}$ is plotted between zero and one in Figure A.1. The ratio test of convergence shows that the series converges when $|z| < 1$ and diverges if

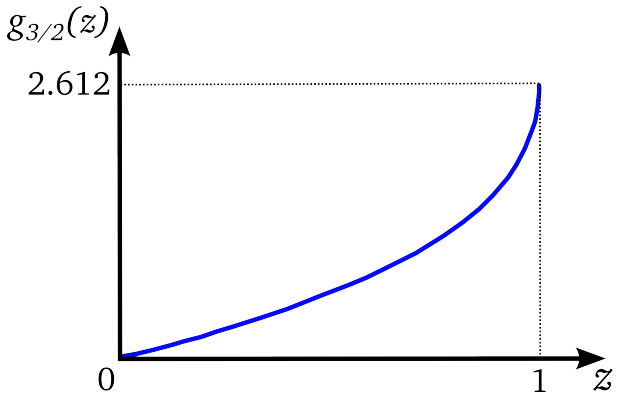

Figure A.1: Plot of the function $g_{3/2}(z)$ between zero and one. At $z = 1$, the function is finite but its derivative is infinite (reproduced from [Anne04]).

$|z| > 1$. For $z = 1$, the series is just convergent,

$$g_{3/2}(1) = \sum_{p=1}^{\infty} \frac{1}{p^{3/2}} = 2.612. \tag{A.14}$$

Going back to the definition $z = e^{\beta(\mu-\epsilon_o)}$, we see from the partition function (A.1) that μ cannot take a value larger than ϵ_o ($z > 1$) since this would make it diverge (also pointed out in the Bose factor, A.4). We are therefore limited to $\mu \leq \epsilon_o$ or $z \leq 1$. When z reaches one ($\mu = \epsilon_o$) the Bose distribution saturates, no more particle can be accommodated. For any density n there therefore is a critical temperature

$$n = \left(\frac{mk_BT_c}{2\pi\hbar^2}\right)^{3/2} 2.612 \quad \rightarrow \quad T_c = \frac{2\pi\hbar^2}{k_Bm}\left(\frac{n_{sat}}{2.612}\right)^{2/3} \tag{A.15}$$

below which the excess number of particle cannot be accommodated with Bose statistics. All exceeding particles, $N_o = N - Vn_{sat}$, end up in the ground state, forming a massive coherent state – the Bose Einstein condensate. At zero temperature, the trivial solution of having all particles in the ground state, $n_{sat} = 0$, is obtained.

A.2 Semi-infinite Bragg Mirrors

To illustrate the physics of Bragg mirrors, which allow to confine the photonic components of polaritons, we derive the reflectivity and stop band characteristics of a semi-infinite Bragg mirror[Felb98, East10, Kavo07]. This derivation is the Bragg mirror equivalent to the use of Snell's law in a simple dielectric interface[Jack98], from which the total internal reflection angle can be determined.

One period of the Bragg mirror is composed of two layers with thickness $d = d_1 + d_2$,

and refractive indices $n_1, n_2 \in \mathbb{R}_{>1}$.

We denote $k_o = \omega/c$ the wavevector incident at angle θ from the normal, and $k_{1,2} = n_{1,2}k_o$, the wavevectors inside the two layers of a Bragg mirror period. Maxwell's equations ($\nabla \times H = \dot{D}$ for a transverse-magnetic (TM) wave or $\nabla \times E = -\dot{B}$ for a transverse-electric (TE) wave) oblige the wavevector component parallel to the surface, $k_o \sin(\theta) = k_{\|o} = k_{\|1,2} \equiv k_\|$, to remain conserved throughout. We therefore have, along the z-axis,

$$\beta_o = (k_o^2 - k_\|^2)^{1/2} \tag{A.16}$$
$$\beta_1 = (n_1^2 k_o^2 - k_\|^2)^{1/2} \tag{A.17}$$
$$\beta_2 = (n_2^2 k_o^2 - k_\|^2)^{1/2}. \tag{A.18}$$

We define the fields

$$\mathbf{E} = \hat{\mathbf{e}} E(z) e^{ik_\| \cdot r_\|} e^{-i\omega t} \quad \text{for TE}, \quad \mathbf{B} = \hat{\mathbf{e}} B(z) e^{ik_\| \cdot r_\|} e^{-i\omega t} \quad \text{for TM} \tag{A.19}$$

And we solve for $U(z) = E(z), B(z)$, inside the mirror with the wave equation, $\nabla^2 \mathbf{E} = \frac{n(z)^2}{c^2}\ddot{\mathbf{E}}$, $\nabla^2 \mathbf{B} = \frac{n(z)^2}{c^2}\ddot{\mathbf{B}}$, $(\nabla^2 = \partial_z^2 + \nabla_\|^2)$,

$$0 \le z \le nd : \frac{d^2}{dz^2} U(z) + \Big(\frac{\omega^2}{c^2} n(z) + k_\|^2\Big) U(z) = 0 \tag{A.20}$$

and at the boundary conditions,

$$\begin{aligned} z \le 0 \quad &: U(z) = e^{i\beta_o z} + re^{-i\beta_o z}. \\ z \ge Nd &: U(z) = te^{i\beta_o z}. \end{aligned} \tag{A.21}$$

Eq. (A.20) can be solved piecewise with the transfer matrices for which we introduce the vector

$$\phi(z) = \begin{pmatrix} U(z) \\ \frac{-i}{k_o} \frac{dU(z)}{dz} \end{pmatrix}. \tag{A.22}$$

We rewrite the problem as

$$T^n \phi(0) = \phi(z_{Nd}) \tag{A.23}$$

where $T = T_2 T_1$ is the transfer matrix accross one period of the Bragg mirror. The transfer matrices for each layer are

$$T_i = \begin{pmatrix} \cos(\beta_i d_i) & -\frac{k_o}{i\beta_i} \sin(\beta_i d_i) \\ \frac{i\beta_i}{k_o} \sin(\beta_i d_i) & \cos(\beta_i d_i) \end{pmatrix}. \tag{A.24}$$

Substituting (A.21, A.22) into (A.23), we get

$$T^n \begin{pmatrix} 1+r \\ \frac{\beta_o}{k_o}(1-r) \end{pmatrix} = \begin{pmatrix} t \\ \frac{\beta_o}{k_o}t \end{pmatrix}. \tag{A.25}$$

We recognize that $\det T_i$ is unity and so is $\det T = \det T_1 \det T_2$. The characteristic equation for T therefore is

$$\lambda^2 - \operatorname{Tr} T\lambda + \det T = \lambda^2 - \operatorname{Tr} T\lambda + 1 = 0, \tag{A.26}$$

for which the roots multiply to one,

$$\lambda_1\lambda_2 = \left(\tfrac{\operatorname{Tr} T}{2} + \sqrt{\tfrac{(\operatorname{Tr} T)^2}{4} - 1}\right)\left(\tfrac{\operatorname{Tr} T}{2} - \sqrt{\tfrac{(\operatorname{Tr} T)^2}{4} - 1}\right) = \tfrac{(\operatorname{Tr} T)^2}{4} - \tfrac{(\operatorname{Tr} T)^2}{4} + 1 = 1 \tag{A.27}$$

and take the following form,

$$\begin{aligned} &\tfrac{1}{2}|\operatorname{Tr} T| < 1 : \lambda_{1,2} = e^{\pm i\phi} \text{ are imaginary.} \\ &\tfrac{1}{2}|\operatorname{Tr} T| \geq 1 : \lambda_1 = \lambda_2^{-1} \text{ are real; we pick } |\lambda_1| \leq 1. \end{aligned} \tag{A.28}$$

The eigenvalues follow from the boundary conditions to be satisfied and the wave nature of the phenomena but not the detailed nature of the waves (E vs B field, TE vs TM). They are kinematic (only depends on the wave nature of the field) as opposed to dynamic properties (depends on the specifics of EM waves), [Jack98]. With $\lambda_{1,2}$ imaginary, the incident wave can be placed in the eigenbasis of T, $U(0) = a\,\mathbf{e}_1 + b\,\mathbf{e}_2$, and will take an additional phase at each layer

$$U(ld) = ae^{il\phi}\mathbf{e}_1 + b\,e^{-il\phi}\mathbf{e}_2; \tag{A.29}$$

the wave will propagate through the structure. With $\lambda_{1,2}$ real, the solution can only be proportional to the eigenvector associated with λ_1,

$$\phi(0) \propto \mathbf{e}_1 = \begin{pmatrix} a \\ ib \end{pmatrix}, \tag{A.30}$$

since any component in $\mathbf{e}_2$ would grow indefinitely by λ_2 in each layer ($\mathbf{e}_{1,2}$ take the form above when $\lambda_{1,2}$ are real). The transmission as $N \to \infty$ is therefore $t = 0$ and

$$\begin{pmatrix} 1+r \\ \frac{\beta_o}{k_o}(1-r) \end{pmatrix} \propto \begin{pmatrix} a \\ ib \end{pmatrix} \tag{A.31}$$

from which we obtain

$$\frac{1+r}{\frac{\beta_o}{k_o}(1-r)} = \frac{a}{ib} \quad \rightarrow \quad r = \frac{\beta_o a - ik_o b}{\beta_o a + ik_o b} \tag{A.32}$$

and therefore $|r| = 1$. An evanescent wave decays as

$$\lambda_1 = e^{-d/\gamma} \quad \rightarrow \quad \gamma = -d/\log|\lambda_1|, \tag{A.33}$$

inside the structure.

The criteria (A.28) when related to (A.24) provides us with where the stop bands are in the Bragg mirror. Reflectivity outside the stop band cannot be calculated in a semi-infinite mirror since the lhs. of (A.25) is undetermined.

A.3 Quality Factor

The notion of quality factor is crucial to the trapping of light and strong coupling. Here we derive the expression for it, starting from its definition

$$Q = \frac{w_o}{\delta\omega}, \tag{A.34}$$

where $\delta\omega$ is the full-width at half maximum of a resonance with energy ω_o. We begin with the expression for a driven oscillator that is homogeneously damped

$$\ddot{x} + \gamma\dot{x} + \omega_o^2 x = Ae^{i\omega t} \tag{A.35}$$

The frequency response, $f(\omega) = |x(t)|^2/A^2$, for it is

$$f(\omega) = \frac{1}{(\omega_o^2 - \omega^2)^2 + \omega^2\gamma^2}, \tag{A.36}$$

which has a maximum at resonance $f(\omega_o) = 1/\gamma^2\omega_o^2$. We are looking for ω at half-maximum,

$$f(\omega = \omega_o \pm \tfrac{\delta\omega}{2}) = \frac{1}{2\gamma^2\omega_o^2} = \frac{1}{(\omega_o^2 - \omega^2)^2 + \gamma^2\omega^2}, \tag{A.37}$$

which can be manipulated into,

$$(2\omega_o^2 - \omega^2)\gamma^2 = (\omega_o^2 - \omega^2)^2 \quad \text{or} \quad (\omega_o^2 \pm \tfrac{\delta\omega^2}{4})\gamma^2 = (\omega_o^2 - (\omega_o \pm \tfrac{\delta\omega}{2})^2)^2. \tag{A.38}$$

This leads to the approximation

$$\omega_o^2\gamma^2 = (\mp 2\omega_o\frac{\delta\omega}{2})^2 \quad \rightarrow \quad \gamma = \delta\omega \tag{A.39}$$

since $\gamma, \omega_o \gg \frac{\delta\omega}{2}$. We therefore reach

$$Q = \frac{\omega_o}{\gamma}. \tag{A.40}$$

In microcavities, photonic (homogeneous) decay dominates over excitonic (inhomogeneous) decay[Skol98] and this description is therefore a useful one to understand the physics of microcavity polaritons.

Appendix B

Code for Numerical Solution of $g^{(1)}(\tau)$

Certain subtleties in obtaining the numerical solution for u_{np} are easily pointed out by presenting core code elements. We ran the code using Matlab for up to a week on a Linux desktop. Matlab allows to represent u_{np} (4.25) directly in matrix from,

$$\dot{u}_{np} = [Au_{n-1p}+Bu_{np-1}+Cu_{np}+Du_{np}]+[Eu_{n+1p}+Fu_{n+1p}+Gu_{np}+Hu_{np}]+Iu_{np}, \quad \text{(B.1)}$$

and to use elementwise (`A.*u`) multiplication. We define matrices, formed by outer products of vectors, which increment in the direction of the quantity they describe,

```
n_mat = (0:n_max)'*ones(1,p_max_ind);
p_mat = ones(n_max_ind,1)*(0:p_max);
```

We initialize $u_{np}(t)$ according to (4.26),

```
u = n_mat.*P_norm;
u_dot = zeros(n_max_ind, p_max_ind);
```

The coefficients are then generated (`./` is elementwise division), paying close attention to the factors ± 0.5, ± 1 in order to obtain the right dynamics,

```
A1 = gm*n_c1 * alpha11*n_mat ./ ( alpha11*(n_mat -0.5) + alpha12*(p_mat +1) +n_s2);
A2 = gm*n_c2 * alpha21*n_mat ./ ( alpha21*(n_mat -0.5) + alpha22*(p_mat +1) +n_s2);
A = A1+A2;
B1 = gm*n_c1 * alpha12*p_mat ./ ( alpha11*(n_mat +0.5) + alpha12*p_mat +n_s1);
B2 = gm*n_c2 * alpha22*p_mat ./ ( alpha21*(n_mat +0.5) + alpha22*p_mat +n_s2);
B = B1+B2;
C1 = gm*n_c1 * alpha11*(n_mat +0.5) ./ ( alpha11*(n_mat +0.5) + alpha12*(p_mat +1) +n_s1);
C2 = gm*n_c2 * alpha21*(n_mat +0.5) ./ ( alpha21*(n_mat +0.5) + alpha22*(p_mat +1) +n_s2);
C = C1+C2;
D1 = gm*n_c1 * alpha12*(p_mat +1) ./ ( alpha11*(n_mat +0.5) + alpha12*(p_mat +1) +n_s1);
D2 = gm*n_c2 * alpha22*(p_mat +1) ./ ( alpha21*(n_mat +0.5) + alpha22*(p_mat +1) +n_s2);
```

```
D = D1+D2;
E = gm * n_mat;
F = gm * (p_mat +1);
G = gm * (n_mat -0.5);
H = gm * p_mat;
I = i*(kappa*(2*n_mat -1) + eta*p_mat);
CDGHI = -C-D-G-H+I;
```

The time consuming part of the code is to evolve u_{np} according to the Euler method, with very small time steps, 0.0001γ. It is the weighted difference between values of neighboring matrix elements which induces the evolution of $u_{n_1 n_2}$. Making the time step larger will not allow for the changes to "propagate" through the matrix correctly and it will start to evolve garbage values. Another point is to treat the natural and artificial boundary conditions properly. We eliminate certain terms at the natural boundary conditions, $n, p = 0$, and we clamp $\dot{u}_{np}$ to zero at the artificial boundary conditions (`n_max_ind, p_max_ind`),

```
step_size = 0.0001*gm;
while g1 >= 0.08 && t <= 6000001
    % n,p=0, discard A,B,G and H to maintain dynamic balance.
    u_dot(1,1) =
        - C(1,1)*u(1,1) - D(1,1)*u(1,1) + E(1,1)*u(2,1) + F(1,1)*u(1,2) + I(1,1)*u(1,1);
    % n=0, discard A and G to maintain dynamic balance.
    u_dot(1,2:p_max_ind-1) =
        B(1,2:p_max_ind-1).*u(1,1:p_max_ind-2) - C(1,2:p_max_ind-1).*u(1,2:p_max_ind-1) ...
        - D(1,2:p_max_ind-1).*u(1,2:p_max_ind-1) + E(1,2:p_max_ind-1).*u(2,2:p_max_ind-1) ...
        + F(1,2:p_max_ind-1).*u(1,3:p_max_ind) - H(1,2:p_max_ind-1).*u(1,2:p_max_ind-1) ...
        + I(1,2:p_max_ind-1).*u(1,2:p_max_ind-1);
    % p=0, discard B and H to maintain dynamic balance.
    u_dot(2:n_max_ind-1,1) =
        A(2:n_max_ind-1,1).*u(1:n_max_ind-2,1) - C(2:n_max_ind-1,1).*u(2:n_max_ind-1,1) ...
        - D(2:n_max_ind-1,1).*u(2:n_max_ind-1,1) + E(2:n_max_ind-1,1).*u(3:n_max_ind,1) ...
        + F(2:n_max_ind-1,1).*u(2:n_max_ind-1,2) - G(2:n_max_ind-1,1).*u(2:n_max_ind-1,1) ...
        + I(2:n_max_ind-1,1).*u(2:n_max_ind-1,1);
    % n,p>0, center elements
    u_dot(2:n_max_ind-1,2:p_max_ind-1) =
        A(2:n_max_ind-1,2:p_max_ind-1).*u(1:n_max_ind-2,2:p_max_ind-1) ...
        + B(2:n_max_ind-1,2:p_max_ind-1).*u(2:n_max_ind-1,1:p_max_ind-2) ...
        + E(2:n_max_ind-1,2:p_max_ind-1).*u(3:n_max_ind  ,2:p_max_ind-1) ...
        + F(2:n_max_ind-1,2:p_max_ind-1).*u(2:n_max_ind-1,3:p_max_ind  ) ...
        + CDGHI(2:n_max_ind-1,2:p_max_ind-1).*u(2:n_max_ind-1,2:p_max_ind-1);
    % outer edges, clamp to zero
    u_dot(n_max_ind,1:p_max_ind-1) = 0;
    u_dot(1:n_max_ind-1,p_max_ind) = 0;
    u_dot(n_max_ind,p_max_ind) = 0;

    if mod(t-1,1000) == 0 %record g1 every 1000 increments (0.1*gm)
        g1_(index1) = abs(sum(sum(u))/pop_n);
        index1 = index1 +1;
    end
    u = u + step_size*u_dot;
    t = t +1;
end
```

Appendix C

First Order Coherence Approximations – One and Two Modes Analytical Specifics

C.1 Fokker-Planck Approach – Two Modes

Although we derived the Fokker-Planck approach in the general case, the full solution has only been implemented in two modes. Here we present the two-mode formalism as well as the linearized coefficients A to E, appearing in (4.45−4.49).

The two-mode equation (cf. 4.25) we wish to solve is

$$\begin{aligned}\dot{u}_{n,p} = \gamma \sum_{i=1,2} n_i^c \Big[& \frac{\alpha_{i1} n u_{n-1p}}{\alpha_{i1}(n-\frac{1}{2}) + \alpha_{i2}(p+1) + n_i^s} + \frac{\alpha_{i2} p u_{n-1p}}{\alpha_{i1}(n+\frac{1}{2}) + \alpha_{i2} p + n_i^s} \\ & - \frac{\alpha_{i1}(n+\frac{1}{2}) + \alpha_{i2}(p+1)}{\alpha_{i1}(n+\frac{1}{2}) + \alpha_{i2}(p+1) + n_i^s} u_{np} \Big] \\ & + \gamma \big[n u_{n+1p} + (p+1) u_{np+1} - \big((n-\frac{1}{2}) + p\big) u_{np} \big] + i(\kappa(2n-1) + \eta p) u_{np}.\end{aligned} \tag{C.1}$$

We use the initial conditions (cf. 3.29, 4.26),

$$u_o(n,p) = n \exp\left(- \begin{pmatrix} n & p \end{pmatrix} \cdot \begin{pmatrix} \frac{\beta_0^2+\beta_1^2}{2n_c} & \frac{\beta_0\beta_1}{n_c} \\ \frac{\beta_0\beta_1}{n_c} & \frac{\beta_0^2+\beta_1^2}{2n_c} \end{pmatrix} \cdot \begin{pmatrix} n \\ p \end{pmatrix} + \begin{pmatrix} \frac{n_c-n_s}{n_c} & \frac{n_c-n_s}{n_c} \end{pmatrix} \cdot \begin{pmatrix} n \\ p \end{pmatrix} \right) \tag{C.2}$$

with $\beta_0 = \alpha_{11}, \alpha_{22}$ and $\beta_1 = \alpha_{12}, \alpha_{21}$.

Placing (C.2) in the form $\dot{u}_{(np)}$ (4.32) provides the following prefactor functions,

$$g_n(n,p) = \gamma n_c\Big(\frac{\beta_o(n+1)}{\beta_o(n+\frac{1}{2})+\beta_1(p+1)+n_s} + \frac{\beta_1(n+1)}{\beta_1(n+\frac{1}{2})+\beta_o(p+1)+n_s}\Big) \tag{C.3}$$

$$g_p(n,p) = \gamma n_c\Big(\frac{\beta_1(p+1)}{\beta_o(n+\frac{1}{2})+\beta_1(p+1)+n_s} + \frac{\beta_o(p+1)}{\beta_1(n+\frac{1}{2})+\beta_o(p+1)+n_s}\Big) \tag{C.4}$$

$$r_n(n,p) = \gamma(n-1) \tag{C.5}$$

$$r_p(n,p) = \gamma\, p \tag{C.6}$$

$$h(n,p) = \frac{\gamma}{2} n_c\Big(\frac{\beta_o}{\beta_o(n+\frac{1}{2})+\beta_1(p+1)+n_s} + \frac{\beta_1}{\beta_1(n+\frac{1}{2})+\beta_o(p+1)+n_s}\Big) - \frac{\gamma}{2} \tag{C.7}$$

$$s(n,p) = i(\kappa(2n-1)+\eta p), \tag{C.8}$$

The Taylor expansion of the prefactors (cf. 4.45−4.49) around the mean of the initial conditions,

$$n_l = \frac{\langle n u_o\rangle}{\langle u_o\rangle}, \quad p_l = \frac{\langle p u_o\rangle}{\langle u_o\rangle}, \tag{C.9}$$

gives the following coefficients (cf. 4.45-4.49),

$$A = -i\nabla(h+s)|_{n_l,p_l} \tag{C.10}$$

$$B = \begin{pmatrix}\nabla(r_n - g_n)\\ \nabla(r_p - g_p)\end{pmatrix}\Big|_{n_l,p_l} \tag{C.11}$$

$$c = h|_{n_l,p_l} \tag{C.12}$$

$$D = i\big(r_n - g_n + \frac{1}{2}\partial_n(r_n+g_n), r_p - g_p + \frac{1}{2}\partial_p(r_p+g_p)\big)\big|_{nl,pl} \tag{C.13}$$

$$E = -\frac{1}{2}\begin{pmatrix} r_n+g_n & 0\\ 0 & r_p+g_p\end{pmatrix}\Big|_{n_l,p_l}. \tag{C.14}$$

As mentioned in Chapter 4, the coefficients (C.10−C.14) can be obtained analytically but the eigenbasis of B used in $g^{(1)}(\tau)$, (4.76) as well as the initial condition, g_o, (4.79, 4.74) used with (C.2, C.9), which appear in the result require the last steps to be numerical.

C.2 Fokker-Planck Approach – One Mode

We compare the solution developed in this thesis, in one mode, with the one developed by Whittaker and Eastham[Whit 09]. The approach in this thesis gives the following characteristic equation in one mode (cf. 4.42)

$$\dot{g} + \left(2\kappa + \gamma k + \frac{2\gamma n_c\big(i-(2n_s-1)k\big)}{(1+2n_s+2n_l)^2}\right)\frac{\mathrm{d}g}{\mathrm{d}k} = \gamma\Bigg[-\frac{1}{2} + i(n_l-\frac{1}{2})k - \frac{1}{2}(n_l-1)k^2 + \frac{n_c}{1+2n_l+2n_s}\Big(1-2(n_l+1)k + \frac{(2n_c-1)k}{1+2n_l+2n_s} + (n_l+1)k^2\Big)\Bigg]g. \tag{C.15}$$

We note that the interaction (κ), originating from the s term (4.33, 4.45, C.15, C.10), appears only in the characteristics.

Once the one-mode version of (C.1) is linearized around $n_l = \bar{n} + \frac{n_c}{\bar{n}}$, $\bar{n} = n_c - n_s$, the Kubo form of [Whit 09] arises from the characteristic equation,

$$\dot{g} + \Big(2\kappa + \frac{i\gamma}{2n_c} + \gamma\frac{n_c-n_s}{n_c}k\Big)\frac{\mathrm{d}g}{\mathrm{d}k} = \gamma\Big[\frac{-1}{2(n_c-n_s)} - (n_c-n_s)k^2\Big]g, \tag{C.16}$$

This simpler from is obtained by manipulating and dropping terms that are small when $n_s = [1000, 4000]$, $\bar{n} = 200$. It is solved, along with the shifted (Gaussian) steady state population which, once expressed with the characteristics k_o for $k(\tau) = 0$, reads,

$$g_o = \exp\left[-2n_c\Big(\kappa + \frac{i\gamma}{4n_c}\Big)^2\,\frac{1-2e^{-\bar{\gamma}\tau}+e^{-2\bar{\gamma}\tau}}{\bar{\gamma}^2}\right], \tag{C.17}$$

where $\bar{\gamma} = \gamma\bar{n}/n_c$. This gives the form[Whit],

$$g^{(1)}(\tau) = \exp\left[-4n_c\Big(\kappa + \frac{i\gamma}{4n_c}\Big)^2\,\frac{e^{-\bar{\gamma}\tau}+\bar{\gamma}\tau-1}{\bar{\gamma}^2}\right]\exp\Big(\frac{-\gamma\tau}{2\bar{n}}\Big), \tag{C.18}$$

$$|g^{(1)}(\tau)| = \exp\Big[\frac{-4n_c\kappa^2}{\bar{\gamma}^2}(e^{-\bar{\gamma}\tau}+\bar{\gamma}\tau-1)\Big]\exp\Big[\frac{n_c}{4\bar{n}^2}(e^{-\bar{\gamma}\tau}-\bar{\gamma}\tau-1)\Big]. \tag{C.19}$$

In C.19, the exponential which contains the interactions κ corresponds to the form derived by Kubo for the spectrum of a transition whose frequency is fluctuating (Sec.

1.2.4) [Kubo54, Hamm05]. The steps to reach this expression combine elegant manipulations which we have not been able to generalize in the multimode theory. Furthermore the cutoff needs to be included, even far above threshold, in the multimode case (Sec. 4.3).

C.3 Static Limit – Analytic Solutions

Here we show how an analytic expressions for the static limit in the ridge case can be obtained.

In a continuous occupation and for two modes Eq. (4.86) reads,

$$g_s^{(1)}(\tau) = \frac{1}{\langle n \rangle} \iint n P_{(np)} \mathrm{e}^{i(\kappa(2n+1)+\eta p)\tau} \mathrm{d}n \, \mathrm{d}p, \tag{C.20}$$

while the fully formed expression (4.87) is

$$g_s^{(1)}(\tau) = \int_0^\infty \int_0^\infty P_{(np)} \mathrm{e}^{i(2\kappa n+\eta p)\tau} \mathrm{d}n \, \mathrm{d}p, \tag{C.21}$$

with (3.29), (3.34) in two modes,

$$P_{(n,p)} = \frac{1}{Z} \exp\left(- \begin{pmatrix} n & p \end{pmatrix} \cdot \begin{pmatrix} \frac{\beta_o^2+\beta_1^2}{2n_c} & \frac{\beta_1\beta_o}{n_c} \\ \frac{\beta_1\beta_o}{n_c} & \frac{\beta_o^2+\beta_1^2}{2n_c} \end{pmatrix} \cdot \begin{pmatrix} n \\ p \end{pmatrix} + \begin{pmatrix} \frac{n_c-n_s}{n_c} & \frac{n_c-n_s}{n_c} \end{pmatrix} \begin{pmatrix} n \\ p \end{pmatrix} \right). \tag{C.22}$$

Independent Case

In the independent case, $\beta_{o,1} = 1, 0$, the integral gives,

$$\begin{aligned} g_s^{(1)}(\tau) =& \frac{1}{Z} \cdot \frac{n_c \pi}{2} \, e^{(\frac{n_c-n_s+2in_c\kappa\tau}{\sqrt{2n_c}})^2 + (\frac{n_c-n_s+in_c\eta\tau}{\sqrt{2n_c}})^2} \times \\ & \left[1 + \mathrm{erf}\big(\frac{n_c-n_s+2in_c\kappa\tau}{\sqrt{2n_c}}\big)\right] \cdot \left[1 + \mathrm{erf}\big(\frac{n_c-n_s+in_c\eta\tau}{\sqrt{2n_c}}\big)\right] \end{aligned} \tag{C.23}$$

which factorizes with respect to κ, η, as expected.

Ridge Case

In the ridge case, $\beta_{o,1} = 0.5$, also has an analytic solution. It is obtained by performing, the following transformation

$$u = \frac{1}{\sqrt{2}}(n-p) \tag{C.24}$$

$$v = \frac{1}{\sqrt{2}}(n+p) \tag{C.25}$$

$$\Rightarrow \begin{cases} 2\kappa n + \eta p = \frac{1}{\sqrt{2}}(2\kappa - \eta)u + \frac{1}{\sqrt{2}}(2\kappa + \eta)v \\ \int_0^\infty \int_0^\infty \mathrm{d}n\,\mathrm{d}p \to \int_0^\infty \mathrm{d}v \int_{-v}^{v} \mathrm{d}u \end{cases}, \tag{C.26}$$

So that

$$g_s^{(1)}(\tau) = \frac{1}{Z} \cdot \frac{\sqrt{\pi n_c}}{i(2\kappa-\eta)\tau} \times \left[e^{\frac{(n_c - n_s + 2in_c\kappa\tau)^2}{n_c}} \left(1 + \mathrm{erf}\left(\frac{n_c - n_s + 2in_c\kappa\tau}{\sqrt{n_c}}\right)\right) - e^{\frac{(n_c - n_s + in_c\eta\tau)^2}{n_c}} \left(1 + \mathrm{erf}\left(\frac{n_c - n_s + in_c\eta\tau}{\sqrt{n_c}}\right)\right) \right]. \tag{C.27}$$

The factor $1/i(..)\tau$ is reminiscent of the denominator in a Sinc function and occurs due to the cutoff. The normalization, Z, is given by the $g_s^{(1)}(0)$. The error functions can be neglected far above threshold.

For the intermediate cases, the integrals (C.21) have to be performed numerically.

Bibliography

[Abba13] M. Abbarchi, A. Amo, V. G. Sala, D. D. Solnyshkov, H. Flayac, L. Ferrier, I. Sagnes, E. Galopin, A. Lemaître, G. Malpuech, and J. Bloch. "Macroscopic quantum self-trapping and Josephson oscillations of exciton polaritons". *Nat. Phys.*, Vol. 9, pp. 275–279, 2013.

[Alei12] I. L. Aleiner, B. L. Altshuler, and Y. G. Rubo. "Radiative coupling and weak lasing of exciton-polariton condensates". *Phys. Rev. B*, Vol. 85, p. 121301, 2012.

[Alle38] J. F. Allen and A. D. Misener. "Flow of liquid helium II". *Nature*, Vol. 141, p. 75, 1938.

[Altl10] A. Altland and B. D. Simons. *Condensed matter field theory.* Cambridge University Press, 2010.

[Anne04] J. F. Annett. *Superconductivity, Superfluids, and Condensates.* Oxford University Press, 2004.

[Aski11] A. Askitopoulos, L. Mouchliadis, I. Iorsh, G. Christmann, J. J. Baumberg, M. A. Kaliteevski, Z. Hatzopoulos, and P. G. Savvidis. "Bragg polaritons: Strong coupling and amplification in an unfolded microcavity". *Phys. Rev. Lett.*, Vol. 106, No. 7, p. 076401, 2011.

[Bagn91] V. Bagnato and D. Kleppner. "Bose-Einstein condensation in low-dimensional traps". *Phys. Rev. A*, Vol. 44, pp. 7439–7441, 1991.

[Bali07] R. Balili, V. Hartwell, D. Snoke, L. Pfeiffer, and K. West. "Bose-Einstein condensation of microcavity polaritons in a trap". *Science*, Vol. 316, No. 5827, p. 10071010, 2007.

[Ball13] D. Ballarini, M. D. Giorgi, E. Cancellieri, R. Houdré, E. Giacobino, R. Cingolani, A. Bramati, G. Gigli, and D. Sanvitto. "All-optical polariton transistor". *Nature Communications*, Vol. 4, p. 1778, 2013.

[Bany00] L. Bányai, P. Gartner, O. M. Schmitt, and H. Haug. "Condensation kinetics for bosonic excitons interacting with a thermal phonon bath". *Phys. Rev. B*, Vol. 61, pp. 8823–8834, 2000.

[Brau05] S. L. Braunstein and P. van Loock. "Quantum information with continuous variables". *Rev. Mod. Phys.*, Vol. 77, pp. 513–577, 2005.

[Brow57] R. H. Brown and R. Twiss. "Interferometry of the intensity fluctuation on light. I. Basic theory: The correlation between photons in coherent beams of radiation". *Proc. of the Royal Society of London. Series A, Mathematical and Physical Sciences*, Vol. 242, No. 1230, pp. 300–324, 1957.

[Call51] H. B. Callen and T. A. Welton. "Irreversibility and generalized noise". *Phys. Rev.*, Vol. 83, No. 1, p. 3440, 1951.

[Carm74] H. J. Carmichael and D. F. Walls. "Modifications to the Scully-Lamb laser master equation". *Phys. Rev. A*, Vol. 9, pp. 2686–2697, 1974.

[Caru13] I. Carusotto and C. Ciuti. "Quantum fluids of light". *Rev. Mod. Phys.*, Vol. 85, p. 299, 2013.

[Chri07] S. Christopoulos, G. B. H. von Högersthal, A. J. D. Grundy, P. G. Lagoudakis, A. V. Kavokin, J. J. Baumberg, G. Christmann, R. Butté, E. Feltin, J.-F. Carlin, and N. Grandjean. "Room-Temperature Polariton Lasing in Semiconductor Microcavities". *Phys. Rev. Lett.*, Vol. 98, p. 126405, Mar 2007.

[Comb07] M. Combescot, O. Betbeder-Matibet, and R. Combescot. "Exciton-exciton scattering: Composite boson versus elementary boson". *Phys. Rev. B*, Vol. 75, No. 17, p. 174305, 2007.

[Corz93] S. W. Corzine, R.-H. Yan, and L. A. Coldren. "Optical Gain in III-V Bulk and Quantum Well Semiconductor". In: P. S. Zory, Ed., *Quantum Well Lasers*, Chap. 1, p. 17, Academic Press, 1993.

[Dang98] L. S. Dang, D. Heger, R. André, F. Bœuf, and R. Romestain. "Stimulation of polariton photoluminescence in semiconductor microcavity". *Phys. Rev. Lett.*, Vol. 81, No. 18, pp. 3920–3923, 1998.

[Das11] S. Das. *Functional Fractional Calculus*. Springer, 2011.

[Demi14] S. Demirchyan, I. Chestnov, A. Alodjants, M. Glazov, and A. Kavokin. "Qubits based on Polariton Rabi Oscillators". *arXiv:1401.3509*, 2014.

[Demo06] S. O. Demokritov, V. E. Demidov, O. Dzyapko, G. A. Melkov, A. A. Serga, B. Hillebrands, and A. N. Slavin. "Bose-Einstein condensation of quasi-equilibrium magnons at room temperature under pumping". *Nature*, Vol. 443, p. 430, 2006.

[Deng03] H. Deng, G. Weihs, D. Snoke, J. Bloch, and Y. Yamamoto. "Polariton lasing vs. photon lasing in a semiconductor microcavity". *PNAS*, Vol. 100, No. 26, pp. 15318–15323, 2003.

[Deng10] H. Deng, H. Haug, and Y. Yamamoto. "Exciton-polariton Bose-Einstein condensation". *Rev. Mod. Phys.*, Vol. 82, pp. 1489–1537, 2010.

[East01] P. R. Eastham and P. B. Littlewood. "Bose condensation of cavity polaritons beyond the linear regime: The thermal equilibrium of a model microcavity". *Phys. Rev. B*, Vol. 64, p. 235101, 2001.

[East08] P. R. Eastham. "Mode locking and mode competition in a nonequilibrium solid-state condensate". *Phys. Rev. B*, Vol. 78, p. 035319, 2008.

[East10] P. Eastham. *Nanophotonics I: Quantum theory of microcavities*. Lecture notes, Trinity College Dublin, 2010.

[Elli57] R. J. Elliott. "Intensity of optical absorption by excitons". *Phys. Rev.*, Vol. 108, pp. 1384–1389, 1957.

[Erde54] A. Erdélyi, W. Magnus, M. F. Oberhettinger, and F. G. Tricomi. *Tables of Integral Transforms, 2 vols.* McGraw-Hill, 1954.

[Faur08] S. Faure, T. Guillet, P. Lefebvre, T. Bretagnon, and B. Gil. "Comparison of strong coupling regimes in bulk GaAs, GaN, and ZnO semiconductor microcavities". *Phys. Rev. B*, Vol. 78, No. 23, p. 235323, 2008.

[Felb98] D. Felbacq, B. Guizal, and F. Zolla. "Wave propagation in one-dimentional photonic crystals". *Optics Communications*, Vol. 152, pp. 119–226, 1998.

[Galb12] M. Galbiati, L. Ferrier, D. D. Solnyshkov, D. Tanese, E. Wertz, A. Amo, M. Abbarchi, P. Senellart, I. Sagnes, A. Lemaître, E. Galopin, G. Malpuech,

and J. Bloch. "Polariton condensation in photonic molecules". *Phys. Rev. Lett.*, Vol. 108, p. 126403, 2012.

[Gard98] C. W. Gardiner and P. Zoller. "Quantum kinetic theory. III. Quantum kinetic master equation for strongly condensed trapped systems". *Phys. Rev. A*, Vol. 58, pp. 536–556, 1998.

[Gasi74] S. Gasiorowitcz. *Quantum Physics.* John Wiley & Sons, 1974.

[Glau63] R. J. Glauber. "Coherent and incoherent states of the radiation field". *Phys. Rev.*, Vol. 131, pp. 2766–2788, 1963.

[Glaz13] M. M. Glazov, M. A. Semina, E. Y. Sherman, and A. V. Kavokin. "Spin noise of exciton polaritons in microcavities". *Phys. Rev. B*, Vol. 88, p. 041309, 2013.

[Hake75] H. Haken. "Cooperative phenomena in systems far from thermal equilibrium and in nonphysical systems". *Rev. Mod. Phys.*, Vol. 47, pp. 67–121, 1975.

[Hake86] H. Haken. *Light, Laser light dynamics, Volume II.* North Holland, 1986.

[Hamm05] P. Hamm. *Principles of nonlinear optical spectroscopy: A practical approach.* Lectures of the Virtual European University on Lasers, U. of Zurich, 2005.

[Haug12] H. Haug, T. D. Doan, H. T. Cao, and D. B. T. Thoai. "Temporal first- and second-order correlations in a polariton condensate". *Phys. Rev. B*, Vol. 85, p. 205310, 2012.

[Henr82] C. H. Henry. "Theory of the linewidth of semiconductor lasers". *IEEE J. Quantum Electronics*, Vol. 18, No. 2, p. 259, 1982.

[Hive12] R. Hivet, H. Flayac, D. D. Solnyshkov, D. Tanese, T. Boulier, D. Andreoli, E. Giacobino, J. Bloch, A. Bramati, G. Malpuech, and A. Amo. "Half-solitons in a polariton quantum fluid behave like magnetic monopoles". *Nature Phys.*, Vol. 8, No. 10, pp. 724–728, 2012. Times Cited: 4.

[Hohe67] P. C. Hohenberg. "Existence of long-range order in one and two dimensions". *Phys. Rev.*, Vol. 158, pp. 383–386, 1967.

[Hopf58] J. J. Hopfield. "Theory of the contribution of excitons to the complex dielectric constants of crystals". *Phys. Rev.*, Vol. 1, No. 11, pp. 427–428, 1958.

[Jack98] J. D. Jackson. *Classical electrodynamics, Third edition*. Wiley, 1998.

[Jose62] B. Josephson. "Possible new effect in superconductive tunneling". *Physics Letters*, Vol. 1, No. 7, p. 251, 1962.

[Kamp07] N. V. Kampen. *Stochastic processes in physics and chemistry, third edition (North-Holland Personal Library)*. North Holland, 2007.

[Kasp06] J. Kasprzak, M. Richard, S. Kundermann, A. Baas, P. Jeambrun, J. M. J. Keeling, F. M. Marchetti, M. H. Szymanska, R. Andre, J. L. Staehli, V. Savona, P. B. Littlewood, B. Deveaud, and L. S. Dang. "Bose-Einstein condensation of exciton polaritons". *Nature*, Vol. 443, No. 7110, pp. 409–414, 2006.

[Kasp08] J. Kasprzak, M. Richard, A. Baas, B. Deveaud, R. André, J.-P. Poizat, and L. S. Dang. "Second-order time correlations within a polariton Bose-Einstein condensate in a CdTe microcavity". *Phys. Rev. Lett.*, Vol. 100, p. 067402, 2008.

[Kavo07] A. Kavokin, J. J. Baumberg, G. Malpuech, and F. P. Laussy. *Microcavities (Series on Semiconductor Science and Technology)*. Oxford University Press, USA, 2007.

[Keel07] J. Keeling, F. M. Marchetti, M. H. Szymanska, and P. B. Littlewood. "Collective coherence in planar semiconductor microcavities". *Semicond. Sci. Technol.*, Vol. 22, No. 5, p. R1R26, 2007.

[Keel08] J. Keeling and N. G. Berloff. "Spontaneous rotating vortex lattices in a pumped decaying condensate". *Phys. Rev. Lett.*, Vol. 100, No. 25, p. 250401, 2008.

[Kett08] W. Ketterle and M. W. Zwierlein. "Making, probing and understanding ultracold Fermi gases". In: M. Ingusci, W. Ketterle, and C. Salomon, Eds., *Ultracold Fermi Gases, Proceedings of the International School of Physics "Enrico Fermi, Course CLXIV, Varenna, 20 - 30 June 2006*, IOS Press, Amsterdam, 2008.

[Koya88] F. Koyama, S. Kinoshita, and K. Iga. "Room temperature CW operation of GaAs vertical cavity surface emitting laser". *IEICE Transactions*, Vol. E71, p. 1098, 1988.

[Kubo54] R. Kubo. "Note on the stochastic theory of resonance absorption". *J. Phys. Soc. Jpn.*, Vol. 9, p. 535, 1954.

[Lago10] K. G. Lagoudakis, B. Pietka, M. Wouters, R. André, and B. Deveaud-Plédran. "Coherent oscillations in an exciton-polariton Josephson junction". *Phys. Rev. Lett.*, Vol. 105, p. 120403, 2010.

[Lai07] C. W. Lai, N. Y. Kim, S. Utsunomiya, G. Roumpos, H. Deng, M. D. Fraser, T. Byrnes, P. Recher, N. Kumada, T. Fujisawa, and Y. Yamamoto. "Coherent zero-state and p-state in an exciton-polariton condensate array". *Nature*, Vol. 450, pp. 529–533, 2007.

[Lang02] W. Langbein and J. M. Hvam. "Elastic scattering dynamics of cavity polaritons: Evidence for time-energy uncertainty and polariton localization". *Phys. Rev. Lett.*, Vol. 88, p. 047401, 2002.

[Lang99] W. Langbein, J. M. Hvam, and R. Zimmermann. "Time-resolved speckle analysis: A new approach to coherence and dephasing of optical excitations in solids". *Phys. Rev. Lett.*, Vol. 82, pp. 1040–1043, 1999.

[Laus04] F. P. Laussy, G. Malpuech, A. Kavokin, and P. Bigenwald. "Spontaneous coherence buildup in a polariton laser". *Phys. Rev. Lett.*, Vol. 93, p. 016402, 2004.

[Lax60] M. Lax. "Fluctuations from the nonequilibrium steady state". *Rev. Mod. Phys.*, Vol. 32, pp. 25–64, 1960.

[Lax63] M. Lax. "Formal theory of quantum fluctuations from a driven state". *Phys. Rev.*, Vol. 129, pp. 2342–2348, 1963.

[Legg01] A. J. Leggett. "Bose-Einstein condensation in the alkali gases: Some fundamental concepts". *Rev. Mod. Phys.*, Vol. 73, No. 2, p. 307356, 2001.

[Liew11] T. C. H. Liew and V. Savona. "Multipartite polariton entanglement in semiconductor microcavities". *Phys. Rev. A*, Vol. 84, p. 032301, 2011.

[Li12] F. Li, L. Orosz, O. Kamoun, S. Bouchoule, C. Brimont, P. Disseix, T. Guillet, X. Lafosse, M. Leroux, J. Leymarie, M. Mexis, M. Mihailovic,

F. Réveret, D. Solnyshkov, J. Zuniga-Perez, and G. Malpuech. "ZnO-based polariton laser operating at room temperature: From excitonic to photonic condensate". *arXiv:1207.7172*, 2012.

[Lind83] C. Lindblad. *Non-equilibrium entropy and irreversibility (Mathematical Physics Studies)*. D. Reidel Publishing Company, 1983.

[Love08] A. P. D. Love, D. N. Krizhanovskii, D. M. Whittaker, R. Bouchekioua, D. Sanvitto, S. A. Rizeiqi, R. Bradley, M. S. Skolnick, P. R. Eastham, R. André, and L. S. Dang. "Intrinsic decoherence mechanisms in the microcavity polariton condensate". *Phys. Rev. Lett.*, Vol. 101, No. 6, p. 067404, 2008.

[Lu12] T.-C. Lu, Y.-Y. Lai, Y.-P. Lan, S.-W. Huang, J.-R. Chen, Y.-C. Wu, W.-F. Hsieh, and H. Deng. "Room temperature polariton lasing vs. photon lasing in a ZnO-based hybrid microcavity". *Optics Express*, Vol. 20, No. 5, pp. 5530–5537, 2012.

[Magn10] E. B. Magnusson, H. Flayac, G. Malpuech, and I. A. Shelykh. "Role of phonons in Josephson oscillations of excitonic and polaritonic condensates". *Phys. Rev. B*, Vol. 82, p. 195312, 2010.

[Maha00] G. D. Mahan. *Many-Particle Physics (Physics of Solids and Liquids)*. Springer, 2000.

[Malp03] G. Malpuech, Y. G. Rubo, F. P. Laussy, P. Bigenwald, and A. V. Kavokin. "Polariton laser: thermodynamics and quantum kinetic theory". *Semicond. Sci. Technol.*, Vol. 18, pp. S385–S669, 2003.

[Mand95] L. Mandel and E. Wolf. *Optical Coherence and Quantum Optics*. Cambridge University Press, 1995.

[Masu12] N. Masumoto, N. Y. Kim, T. Byrnes, K. Kusudo, A. Löffler, S. Höfling, A. Forchel, and Y. Yamamoto. "Exciton–polariton condensates with flat bands in a two-dimensional kagome lattice". *New J. Phys.*, Vol. 14, No. 6, p. 065002, 2012.

[Mosk00] S. A. Moskalenko and D. W. Snoke. *Bose-Einstein Condensation of Excitons and Biexcitons: And Coherent Nonlinear Optics with Excitons*. Cambridge University Press, 2000.

[Mosk62] S. Moskalenko. "Reversible optico-hydrodynamic phenomena in a nonideal exciton gas". *Fiz. Tverd. Tela [Sov. Phys. Solid State]*, Vol. 4, No. 1, p. 276 [199], 1962.

[Pasc13] R. Paschotta. *Derivation of the SchawlowTownes linewidth*. RP Photonics Consulting GmbH, 2013.

[Penr51] O. Penrose. "On the quantum mechanics of helium II". *Phil. Mag.*, Vol. 42, pp. 1373–1377, 1951.

[Piko01] A. Pikovsky, M. Rosenblum, and J. Kurths. *Synchronization, A universal concept in nonlinear sciences*. Cambridge University Press, 2001.

[Pita03] L. Pitaevskii and S. Stringari. *Bose-Einstein condensation*. Vol. 116 of *International Series of Monographs on Physics*, Oxford University Press, 2003.

[Porr02] D. Porras, C. Ciuti, J. J. Baumberg, and C. Tejedor. "Polariton dynamics and Bose-Einstein condensation in semiconductor microcavities". *Phys. Rev. B*, Vol. 66, No. 8, p. 085304, 2002.

[Porr03] D. Porras and C. Tejedor. "Linewidth of a polariton laser: Theoretical analysis of self-interaction effects". *Phys. Rev. B*, Vol. 67, p. 161310, 2003.

[Pres07] W. H. Press, S. A. Teukolsky, W. T. Vetterling, and B. P. Flannery. *Numerical Recipes 3rd Edition: The Art of Scientific Computing*. Cambridge University Press, 2007.

[Puri01] R. R. Puri. *Mathematical methods of quantum optics (Springer Series in Optical Sciences)*. Springer, 2001.

[Read10] D. Read, Y. G. Rubo, and A. V. Kavokin. "Josephson coupling of Bose-Einstein condensates of exciton-polaritons in semiconductor microcavities". *Phys. Rev. B*, Vol. 81, p. 235315, 2010.

[Rich05] M. Richard, J. Kasprzak, R. André, R. Romestain, L. S. Dang, G. Malpuech, and A. Kavokin. "Experimental evidence for nonequilibrium Bose condensation of exciton polaritons". *Phys. Rev. B*, Vol. 72, p. 201301, 2005.

[Roch00] G. Rochat, C. Ciuti, V. Savona, C. Piermarocchi, A. Quattropani, and P. Schwendimann. "Excitonic Bloch equations for a two-dimensional system

of interacting excitons". *Phys. Rev. B*, Vol. 61, No. 20, pp. 13856–13862, 2000.

[Rodr13] A. S. Rodrigues, P. G. Kevrekidis, J. Cuevas, R. Carretero-Gonzalez, and D. J. Frantzeskakis. "Symmetry-breaking effects for polariton condensates in double-well potentials". *Progress in Optical Science and Photonics*, Vol. 1, pp. 509–529, 2013.

[Saba07] J. Sabatier, O. Agrawal, and J. T. Machado. *Advances in Fractional Calculus: Theoretical Developments and Applications in Physics and Engineering*. Springer, 2007.

[Savo07] V. Savona. "Effect of interface disorder on quantum well excitons and microcavity polaritons". *J. Phys.: Condens. Matter*, Vol. 19, No. 29, p. 295208, 2007.

[Savo95] V. Savona, L. Andreani, P. Schwendimann, and A. Quattropani. "Quantum well excitons in semiconductor microcavities: Unified treatment of weak and strong coupling regimes". *Solid State Commun.*, Vol. 93, pp. 733–739, 1995.

[Scha58] A. L. Schawlow and C. H. Townes. "Infrared and optical masers". *Phys. Rev.*, Vol. 112, pp. 1940–1949, 1958.

[Schw08] P. Schwendimann and A. Quattropani. "Statistics of the polariton condensate". *Phys. Rev. B*, Vol. 77, p. 085317, 2008.

[Schw10] P. Schwendimann, A. Quattropani, and D. Sarchi. "Stationary and time-dependent correlations in polariton condensates". *Phys. Rev. B*, Vol. 82, p. 205329, 2010.

[Scul97] M. O. Scully and M. S. Zubairy. *Quantum Optics*. Cambridge University Press, 1997.

[Shel10] I. A. Shelykh, A. V. Kavokin, Y. Rubo, T. Liew, and G. Malpuech. "Polariton polarization-sensitive phenomena in planar semiconductor microcavities". *Semicond. Sci. Technol.*, Vol. 25, p. 013001, 2010.

[Sing80] S. Singh and M. S. Zubairy. "Quantum theory of a two-mode laser with coupled transitions". *Phys. Rev. A*, Vol. 21, pp. 281–292, 1980.

[Skol98] M. S. Skolnick, T. A. Fisher, and D. M. Whittaker. "Strong coupling phenomena in quantum microcavity structures". *Semicond. Sci. Technol.*, Vol. 13, No. 7, pp. 645–669, 1998.

[Swai81] S. Swain. "Master equation derivation of quantum regression theorem". *Journal of Physics A: Mathematical and General*, Vol. 14, No. 10, p. 2577, 1981.

[Szym07] M. H. Szymańska, J. Keeling, and P. B. Littlewood. "Mean-field theory and fluctuation spectrum of a pumped decaying Bose-Fermi system across the quantum condensation transition". *Phys. Rev. B*, Vol. 75, p. 195331, 2007.

[Tass00] F. Tassone and Y. Yamamoto. "Lasing and squeezing of composite bosons in a semiconductor microcavity". *Phys. Rev. A*, Vol. 62, p. 063809, 2000.

[Tass97] F. Tassone, C. Piermarocchi, V. Savona, A. Quattropani, and P. Schwendimann. "Bottleneck effects in the relaxation and photoluminescence of microcavity polaritons". *Phys. Rev. B*, Vol. 56, pp. 7554–7563, 1997.

[Tass99] F. Tassone and Y. Yamamoto. "Exciton-exciton scattering dynamics in a semiconductor microcavity and stimulated scattering into polaritons". *Phys. Rev. B*, Vol. 59, pp. 10830–10842, 1999.

[Thom02] L. K. Thomsen and H. M. Wiseman. "Atom-laser coherence and its control via feedback". *Phys. Rev. A*, Vol. 65, p. 063607, 2002.

[Thon09] S. M. Thon, M. T. Rakher, H. Kim, J. Gudat, W. T. M. Irvine, P. M. Petroff, and D. Bouwmeester. "Strong coupling through optical positioning of a quantum dot in a photonic crystal cavity". *Appl. Phys. Lett.*, Vol. 94, p. 111115, 2009.

[Tosi12] G. Tosi, G. Christmann, N. G. Berloff, P. Tsotsis, T. Gao, Z. Hatzopoulos, P. G. Savvidis, and J. J. Baumberg. "Sculpting oscillators with light within a nonlinear quantum fluid". *Nature Phys.*, Vol. 8, No. 3, pp. 190–194, 2012.

[Tred95] A. Tredicucci, Y. Chen, V. Pellegrini, M. Börger, L. Sorba, F. Beltram, and F. Bassani. "Controlled exciton-photon interaction in semiconductor bulk microcavities". *Phys. Rev. Lett.*, Vol. 75, No. 21, pp. 3906–3909, 1995.

[Vaha03] K. Vahala. "Optical microcavities". *Nature*, Vol. 424, pp. 839–846, 2003.

[Verg06] A. Verger, C. Ciuti, and I. Carusotto. "Polariton quantum blockade in a photonic dot". *Phys. Rev. B*, Vol. 73, p. 193306, 2006.

[Vern98] D. W. Vernooy, A. Furusawa, N. P. Georgiades, V. S. Ilchenko, and H. J. Kimble. "Cavity QED with high-Q whispering gallery modes". *Phys. Rev. A*, Vol. 57, No. 4, pp. R2293–R2296, 1998.

[Wall10] D. Walls and G. J. Milburn. *Quantum Optics*. Springer, 2010.

[Weis] E. W. Weisstein. "Wiener-Khinchin theorem". MathWorld – A Wolfram Web Resource.

[Weis91] C. Weisbuch and B. Vinter. *Quantum semiconductor structures: Fundamentals and applications*. Academic Press, 1991.

[Weis92] C. Weisbuch, M. Nishioka, A. Ishikawa, and Y. Arakawa. "Observation of the coupled exciton-photon mode splitting in a semiconductor quantum microcavity". *Phys. Rev. Lett.*, Vol. 69, No. 23, pp. 3314–3317, 1992.

[Whit] D. Whittaker. "Notes obtained from D. Whittaker". U. of Sheffeild, private communication.

[Whit09] D. M. Whittaker and P. R. Eastham. "Coherence properties of the microcavity polariton condensate". *EPL*, Vol. 87, No. 2, p. 27002, 2009.

[Wout07] M. Wouters and I. Carusotto. "Excitations in a nonequilibrium Bose-Einstein condensate of exciton polaritons". *Phys. Rev. Lett.*, Vol. 99, p. 140402, 2007.

[Wout08a] M. Wouters. "Synchronized and desynchronized phases of coupled nonequilibrium exciton-polariton condensates". *Phys. Rev. B*, Vol. 77, p. 121302, 2008.

[Wout08b] M. Wouters, I. Carusotto, and C. Ciuti. "Spatial and spectral shape of inhomogeneous nonequilibrium exciton-polariton condensates". *Phys. Rev. B*, Vol. 77, p. 115340, 2008.

[Wout08c] M. Wouters, I. Carusotto, and C. Ciuti. "Spatial and spectral shape of inhomogeneous nonequilibrium exciton-polariton condensates". *Phys. Rev. B*, Vol. 77, p. 115340, 2008.

[Wout09] M. Wouters and V. Savona. "Stochastic classical field model for polariton condensates". *Phys. Rev. B*, Vol. 79, p. 165302, 2009.

[Yang62] C. N. Yang. "Concept of off-diagonal long-range order and the quantum phases of liquid He and of superconductors". *Rev. Mod. Phys.*, Vol. 34, pp. 694–704, 1962.

[Zhan13] C. Zhang, S. Yu, Q. Chen, and C. H. Oh. "Detecting and Estimating Continuous-Variable Entanglement by Local Orthogonal Observables". *Phys. Rev. Lett.*, Vol. 111, p. 190501, 2013.